Changes in bitumen due to thermal conversion affecting the description of coke formation

by

Lina Maria Yañez Jaramillo

A thesis submitted in partial fulfillment of the requirements for the degree of

Doctor of Philosophy

in

Chemical Engineering

Department of Chemical and Materials Engineering
University of Alberta

Abstract

At the heart of heavy oil and bitumen upgrading, thermal conversion technologies are found. One such process is visbreaking where bitumen is thermally converted into lighter materials. However, the conversion by visbreaking is limited by the onset of the formation of solid carbonaceous materials (coke). The formation of coke has been explained by two pathways: (i) The formation of a mesophase (or a second liquid phase) that will eventually lead to coke, and (ii) Asphaltenes as precursors of coke formation due to increasing insolubility.

The objective of this work was to better understand the changes that bitumen and bitumen-related materials undergo in thermal conversion from the perspective of the change in the nature of the species. The results were employed to provide a better understanding of the onset of coke formation in visbreaking, and a different point of view about the process leading to coke formation which results from highlighting potential misconceptions within this field.

Considering the first pathway used to explain the origin of coke, mesophase formation follows from an increase in the aromatic character of the material as the first step. Hydrogen transfer and aromatization reactions are examples of reactions occurring in thermal conversion that could contribute to an increase in the aromatic hydrogen and carbon content. It was found that there was not a fixed relationship between aromatic hydrogen and aromatic carbon content. It was further found that changes in aromatic hydrogen content do not necessarily describe the changes in aromatic carbon content after visbreaking. The formation of aromatic structures as an early step of coke formation would imply an increase in the aromatic content, but the aromatic carbon and coke content of the thermally converted products only had a weak relationship.

The second pathway describes coke formation as a progression of insolubility where asphaltenes are considered precursors. As a result, it was expected to observe a relationship between coke and asphaltenes content in thermally converted samples. Contrary to the expectation, the visbroken products did not show a relationship between coke and asphaltenes content and did not provide evidence of asphaltenes being an intermediate step in coke formation.

The study also made other minor contributions to the field through work on water removal from emulsified bitumen and showing that there might be a relationship of free radical concentration in unconverted petroleum materials that is consistent with the composition continuum proposed by Boduszynski. This study has opened the possibility to further investigations that could address some of the hypotheses in this work and provide valuable inputs into the role of free radical species in coke formation during thermal conversion.

Preface

(Mandatory due to collaborative work)

Chapter 5 of this thesis was published as "Yañez Jaramillo, L.M.; Link, F.; De Klerk, A Relationship between Aromatic Hydrogen and Aromatic Carbon in Straight Run and Converted Oils. *Fuel* **2022**, *327*, p.124414". I was responsible for concept formation, experimental design, data collection and analysis as well as manuscript composition. Diana Tulegenova provided some of the samples used in this study. Felix Link collaborate with manuscript editing. Arno de Klerk acted as the supervisory author and was involved in the concept formation, data interpretation and manuscript composition.

Chapter 6 of this thesis was published as "Yañez Jaramillo, L.M.; de Klerk, A. Is Solubility Classification a Meaningful Measure in Thermal Conversion? *Energy and Fuels* **2022**, *36*: 8649 - 8662". I was responsible for concept formation, experimental design, data collection and analysis as well as manuscript composition. Arno de Klerk acted as the supervisory author and corresponding author, and was involved in the concept formation, data interpretation and manuscript composition.

Chapter 7 of this thesis was partially revised and edited by Dr. Joy Tannous from the United Arab Emirates University.

Dedicated to women and science

Acknowledgements

I would like to thank my supervisor, Arno de Klerk, for his patience during my Ph.D. journey. I don't think there are enough words to thank you for your guidance and support. You always believed in me, even when I was losing hope.

I would like to thank my mom, and my aunt for their support. I don't think I would have ever imagined pursuing a Ph.D. if it wasn't for you. Thank you for never stopping me to ask questions, or being curious, and for always encourage me.

I would also thank my husband, Akash, for his support, for being the ray of light when everything seemed to be dark, for his patience and love. Thank you for always inspiring me to do/be better.

I would also like to thank my friends and colleagues (especially, Nata, Jose, Yoha, Sima, Giselle, Joy, Cibele, Shirley, Kaushik, Felix, Garima, Diana, Nuvaid, Felipe, Priscila, Sowmya) from De Klerk's research group for all the joy and learnings during this journey; and my supervisor (Nestor) and colleagues (Fredy and Thiago) at CNOOC International for all their support and teaching. I think I am extremely fortunate for meeting so many wonderful people during my Ph.D. studies.

I would like to thank CNOOC International, NSERC, Alberta Innovates, the University of Alberta and the Ministerio de Ciencia, Tecnología e Innovación de Colombia for all the financial support during my Ph.D. program.

To Canada, thank you for giving me the opportunity to explore the world.

Table of Contents

List of Tables

xiii

List of Figures

xix

1. Introduction

1.1. Background

The research that will be presented deals with Canadian oilsands bitumen. Canadian oilsands bitumen has its origin in the Western Canada Sedimentary Basin formed in the Lower Cretaceous, shaped by the Rocky Mountains that allowed the migration of oil and gas through limestone to the deposits in the Fort McMurray area [1]. Due to its exposure that caused the volatile material to be lost over time, it is an unconventional oil resource, which is in a near solid state both in the oilsands deposit and after recovery [2].

The extraction of bitumen from the oil sand deposit can be achieved by mining in shallow deposits or by subsurface (in situ) technologies such as Steam-Assisted Gravity Drainage (SAGD). Either of these methods require further processing to recover oil from the emulsions resulting from the extraction processes. Due to the lack of low boiling material, bitumen characteristically has a high heteroatom content (nitrogen-, sulfur-, and oxygen-containing compounds), high density, and high viscosity. To facilitate pipeline transport of the bitumen, the material has to be diluted with low viscosity material or upgraded in some way to reduce its viscosity [3].

Depending on the extent of upgrading, processes are referred to either as full upgrading, or partial upgrading [4]. The use of a mild thermal cracking process, visbreaking, as a part of a partial upgrading technology results in an economic benefit due to its lower capital cost compared to hydroconversion or catalytic cracking where hydrogen and catalysts are employed. Visbreaking is no panacea and in the context of partial upgrading there are several limitations to consider [5]. One of these limitations is the limit on vacuum residue conversion.

Visbreaking involves the thermal cleavage of some molecular bonds and the reactions proceed by free radical mechanism. The cracking of the bitumen to lower boiling products is necessary to reduce its viscosity. However, the vacuum residue conversion that can be achieved by this technology is limited at about 30 % [6] due to the formation of carbonaceous deposits. The

formation of deposits in the furnace coils and downstream equipment with time on stream decreases heat transfer efficiency and eventually requires the unit to be shut down for cleaning. The conversion limit is related to the extent of deposit formation and its impact on the time period of on-stream availability between shutdowns for cleaning. This is pointed out to indicate the potential benefit that could be realised by decreasing the extent of deposit formation at constant conversion.

The formation of deposits in visbreaking are in the form of coke, or carbon-rich material. This has been explained as the formation, or the separation, of a second phase that has a higher concentration of aromatic structures [7].

Two descriptions have been forwarded for explaining development of deposits during thermal conversion. The first one is related to the formation of an ordered structure (i.e. mesophase) which starts by the stacking of planar aromatic molecules that will grow and coalesce until it separates from the system. The second description is related to a solubility class, asphaltenes that becomes insoluble in the converted product. The asphaltenes are generally characterized as having abundant polynuclear aromatic structures [3] with a high amount of free radicals [8]. The high persistent free radical content can lead to free radical addition reactions and the formation of an insoluble product.

To make an advance in such as mature field as the study of thermal conversion by visbreaking, or in the upgrading of oilsands bitumen in general, is challenging. The approach that was followed, was to take a step back from the application of visbreaking of bitumen and look more closely at the materials, as well as the claims made in literature about thermal conversion leading to second phase formation, aromatics formation, and the relationship between properties.

1.2. Objective

The objective of this work was to better understand the changes bitumen and bitumen-related materials undergo in thermal conversion from the perspective of the change in the nature of the

species. The specific aim was to provide a better understanding of the onset of coke formation in visbreaking.

1.3. Scope of Work

Chapter 2 reviews the available literature in the topics involved in this thesis. The extraction of bitumen from the oil sands is a unique process for which two main technologies have been used over the last decades. The characteristics of the produced emulsions and the technology sequence used to produce and upgrade bitumen were briefly discussed. One technology is of particular interest, visbreaking, as the formation of a carbonaceous solid limits its conversion. The description of how the second phase forms and their connections with free radical mechanisms have been covered. Additionally, the nature of mesophase was explored and how it may relate to second phase formation.

Chapter 3 presents the experimental methodology followed in this work. The description of the materials used in this study as well as the analytical techniques employed are discussed in this chapter. Results are organized in a more comprehensive way, and they will be discussed in each of the subsequent sections.

Chapter 4 discusses different laboratory techniques removing water from a water-in-oil emulsion obtained from SAGD process. The performance of each technique was discussed, as well as the challenges encountered in the separation process and the characterization of the resulting samples. This work was a necessary prerequisite for dealing with industrially obtained materials in the rest of the study.

Chapter 5 studies the changes in aromatic hydrogen and carbon content in thermally converted products. Cookson et al. [9] proposed a relationship between the aromatic hydrogen (H_{Ar}) and carbon (C_{Ar}) content. The purpose of this work was to determine whether C_{Ar} and H_{Ar} had a fixed relationship in bitumen and in converted bitumen. Experimental data generated as part of this thesis was employed in conjunction with data from literature. It was found that the values of H_{Ar} and C_{Ar} for petroleum and coal derived materials did not follow a narrowly defined relationship

3

but a band. Similarly, a fixed relationship between these two values in thermally converted products was not observed suggesting that the conversion process affected the way changes take place in H_{Ar} and C_{Ar}.

Chapter 6 investigates the concept of solubility classification as a meaningful descriptor of thermal conversion. Asphaltenes, a solubility class defined in this work as *n*-heptane insolubles, was considered to be a precursor of coke formation, defined as material insoluble in carbon disulfide, as suggested in the literature. However, no relationship was found between the two solubility classifications. Additionally, *n*-heptane asphaltenes were poorly related to properties that could be used in reaction chemistry (e.g., aromatic carbon and hydrogen content, density). A relationship between free radical content and refractive index were observed, which led to the next topic of study.

Chapter 7 explores the relationship of free radical content with different bulk properties in straight-run materials. The persistent free radical content increases with the boiling point which suggest an apparent agreement with the Boduszynski continuum [10]. Although the question about the exclusive dependency of free radical content with boiling point distribution was not answer, a potential path for exploring the contribution of compositional properties to the free radical content has been proposed. The evaluation of free radical concentration in solubility classes such as asphaltenes is also discussed, aiming to understand the high amount of free radical species in the solubility class.

Chapter 8 discusses the main findings in this work and how it advanced understanding in this field. Recommendations for future work are proposed.

References

[1]   Strausz, O. P.; Lown, E. M. *The Chemistry of Alberta Oil Sands, Bitumens and Heavy Oils*; Alberta Energy Research Institute: Calgary, AB, 2003.

[2]   De Klerk A. Unconventional Oil: Oilsands. In *Future Energy: Improved, Sustainable and Clean Options for our Planet*; Letcher, T. M., Ed.; Elsevier: Amsterdam; 2020; 3ed, p. 49 - 65.

[3]   Gray, M. R. *Upgrading Oilsands Bitumen and Heavy Oil.* University of Alberta Press: Edmonton, Canada, 2015.

[4]   Gray, M. R. Fundamentals of Partial Upgrading of Bitumen. *Energy and Fuels* **2019**, *33*: p. 6843 - 6856.

[5]   De Klerk, A. Processing Unconventional Oil: Partial Upgrading of Oilsands Bitumen. *Energy and Fuels* **2021**, *35*: p. 14343 - 14360.

[6]   Speight, J.G. *The Chemistry and Technology of Petroleum*. 5th ed. CRC Press: Boca Raton, FL, 2014.

[7]   Wiehe, I.A. A Phase-Separation Kinetic Model for Coke Formation. *Industrial and Engineering Chemistry Research* **1993**, *32*: p. 2447 - 2454.

[8]   Tannous, J. H.; De Klerk, A. Quantification of the Free Radical Content of Oilsands Bitumen Fractions. *Energy and Fuels* **2019**, *33*: p. 7083 - 7093.

[9]   Cookson, D. J.; Lloyd, C. O.; Smith, B. A Novel Semi-Empirical Relationship between Aromaticities Measured from ^{1}H and ^{13}C N.M.R. Spectra. *Fuel* **1986**, *65*: p. 1247 - 1253.

[10]   Altgelt, K.H.; Boduszynski, M.M. *Composition and Analysis of Heavy Petroleum Fractions*. Marcel Dekker: New York, NY, 1994.

2. Literature Review

2.1. Introduction

Petroleum is of great importance in everyday life; its products are basically divided into two categories [1]: petrochemical, which includes the cosmetics, textiles and plastics industries; and fuels which it is translated into the transportation and power generation industries. Up to 2019, the total world petroleum consumption reached 100.37 million barrels per day [2].

Since this thesis deals with oil sands bitumen, the scope is narrowed from petroleum in general to oil sands bitumen in particular.

Canada accounts for about 10 % of the total proven oil reserves in the world, where 96 % corresponds to oil sand deposits. Oil sands are defined as a complex mixture which contains sand, clays, salts, fines, bitumen and water. There are two main technologies used to extract bitumen from oil sands formations: mining and subsurface recovery techniques such as Steam-Assisted Gravity Drainage (SAGD). The recovered material will have certain characteristics that require further processing to produce bitumen. A brief overview of the production process will be described here to provide context for the thesis before narrowing the scope further to deal with topics central to the research in the thesis.

2.2. Bitumen production: from the well to the pipeline

2.2.1. Bitumen extraction

The Western Canadian Sedimentary Basin (WCSB) covers a great extent of Western Canada and displays an amazing geological history [3]. Three oil sands deposits can be found: Peace Lake, Cold Lake, and Athabasca. The latter has a reservoir bed between 0 to 500 m [4] below the ground, making it accessible to develop mining and subsurface (in situ) extraction processes.

6

2.2.1.1. Mineable bitumen recovery

The mining extraction process is used in reservoirs whose usual depth is about 30 m [5]. The maximum commercially viable depth depends on ore quality due to the cost associated with the removal of the overburden. The product from mining is oil sands ore and to liberate the bitumen, the bitumen must be separated from the mineral matter in the ore.

To explain the main features of the bitumen extraction process, only one of several industrially employed extraction designs will be used. Schramm and Mikula [6] presented a diagram of the commercial extraction operation shown in **Figure 2-1**. The process starts by removing the ore from the deposits; the lumps will be crushed and sieved into pieces of around 5 cm in diameter. Hot water and caustic soda (in some cases) are added to the lumps facilitating bitumen liberation from the minerals and keeping the pH of the slurry at around 8.5 to promote sand surface cleaning. The slurry is hydrotransported, which helps breaking the lumps further by shear forces. Up to this point, the mixture contains mostly water and solids (50 and 43 wt. %, respectively [6]).

The slurry is moved into a separation unit (often called primary separation vessel) where aeration of bitumen takes place. This is a froth flotation separation, and the materials are divided into a froth that contains the bitumen, middlings and tailings that contains most of the mineral matter. The middlings will move into a secondary separation stage (e.g., additional flotation cells) where more bitumen will be recovered. The typical composition of the froth produced at this secondary separation stage contains about 59 wt.% water, 17 wt.% solids, and 24 wt.% bitumen [6]. The combined froth obtained from the primary and secondary separation vessels usually contains about 50 – 55 wt.% bitumen.

The resulting froth contains a high volume of entrained air (e.g., small bubbles) that impacts the buoyancy of the bitumen, which is beneficial for gravity separation. The presence of air can affect the pumpability of the froth and substantially increase the volumetric flow rate, making it necessary to deaerated it. After removing enough air, the froth will move the froth treatment unit, where a diluent is added to reduce the viscosity of the bitumen. One of two different types of

solvents is used depending on the process, naphtha or light paraffins. The process in **Figure 2-1** makes use of naphtha, but due to the relevance to this thesis, both solvents are discussed:

- *Naphtha*: The addition of naphtha to the froth is reported to rapidly separate most of the water and solids from the emulsion [7]. However, an interface between the aqueous phase and the bitumen phase is formed and it is stabilized by different components in both phases. Typically, the diluted bitumen will contain between 3.5 to 5.5 wt.% of water, and 0.5 to 1.2 wt.% of solids [5].

- *Paraffinic solvents*: Mainly composed of pentanes, hexanes, and heptanes [7] will promote partial asphaltenes precipitation when added in sufficient quantities. Asphaltenes flocs will be able to trap most of the water and solids present in the bitumen, producing a bitumen product that meets pipeline specification for basic sediment and water (BS&W) of < 0.5 %. The amount of paraffinic solvent employed is three times the amount used in the naphtha treatment.
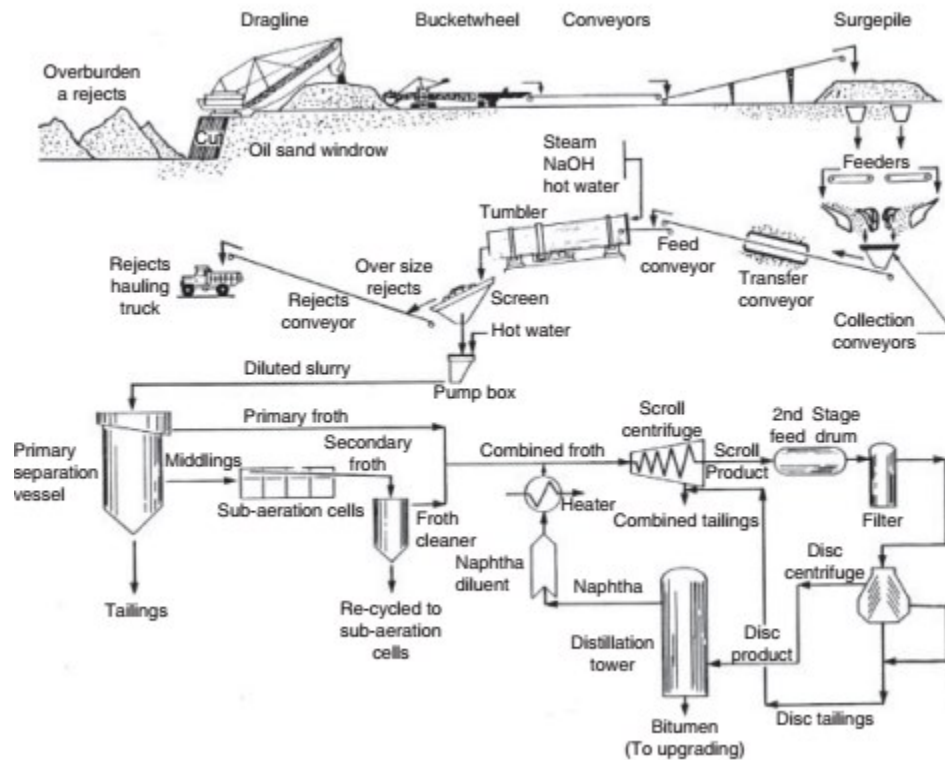
Figure 2-1. Example of a commercial bitumen extraction process from mined oil sands ore. Reprinted from [6] with permission of John Wiley and Sons.

8

2.2.1.2. Subsurface bitumen recovery

Deeper deposits require other extraction strategies, many of which employ steam as a heat carrier to facilitate subsurface production. In the 1970s, Butler and his colleagues at Imperial Oil proposed the continuous injection of steam to extract bitumen from the oil sands formation called Steam-Assisted Gravity Drainage [8,9]. The extraction process consists of two horizontal wells 5 meters apart (vertically) from each other [10]; the top well will be used to inject steam into the reservoir, and the bottom well will be used to collect the flowing bitumen [11]. The steam forms a heated chamber (approximately 200 ºC) and transfers enough heat to the surrounding bitumen reservoir. The steam condensate and heated bitumen will flow towards the producer well by gravity, and the formed steam chamber expands vertically and horizontally [12]. The SAGD scheme is shown in **Figure 2-2**. Currently, different variations of the process proposed by Butler are available [5].
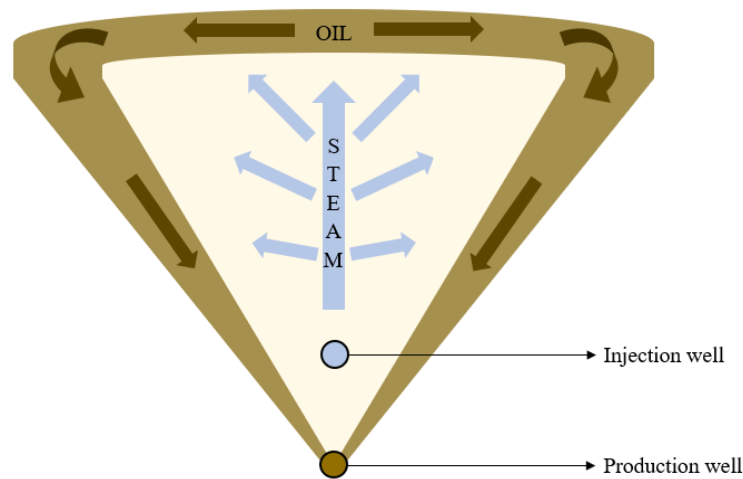
Figure 2-2. Diagram showing cross-section of SAGD wells to illustrate how bitumen is produced from the subsurface oil sands deposit.

The recovered liquid from the reservoir consists predominantly of a free water phase, a water-in-oil (bitumen is the continuous phase and water is the dispersed phase), and oil phase for a short time in the early stages of SAGD production [13]. Velayati mentions that heated oil can encapsulate condensate steam droplets which is facilitated by the higher temperatures used in

SAGD production. The produced emulsion contains natural emulsifiers such as fine solids (e.g., clays) and surface-active compounds (e.g., species with polar groups present in the asphaltenes) that promote emulsion stability. Once the produced fluid reaches the surface, it will undergo different separation processes to remove water and solids from the emulsion to produce bitumen. One example of a process to illustrate how the separation is performed is shown in **Figure 2-3**, which produces diluted bitumen as product.
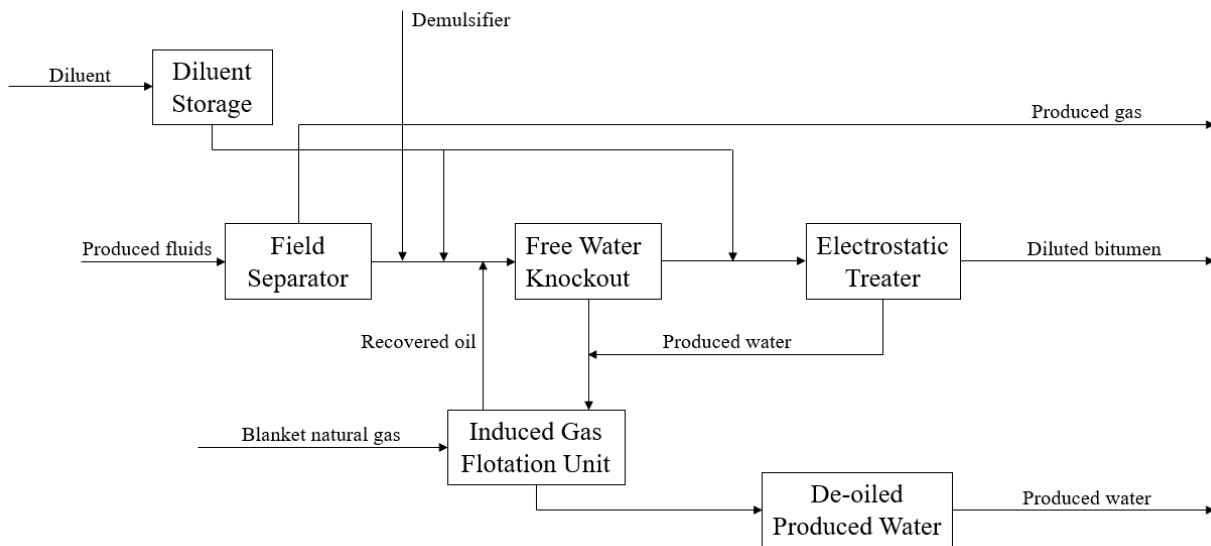
Figure 2-3. Example of a separation process associated with subsurface production to recover bitumen from the produced fluids. Redrawn from [5].

2.2.2. *Bitumen Processing*

The preceding description of bitumen production highlighted the two aspects that are relevant to subsequent processing. First, the bitumen is recovered in association with water and mineral matter, and the separation of water and mineral matter from the bitumen is an involved process. This was also a challenge faced in this study and explains the need for the work in **Chapter 4**. Second, straight-run bitumen is invariably a material that was exposed to some additional processing, which may affect downstream bitumen processing.

The composition of bitumen includes a wide variety of compounds such as aliphatic, naphthenic and aromatic species and heteroatom-containing compounds (oxygen-, sulfur-, and nitrogen-containing compounds). Bitumen is often characterized by its high viscosity (over 10^3 Pa·s at 20 °C [14]), a semi-solid appearance and a low H/C ratio compared to conventional crude oils. Typical values for the Athabasca bitumen are shown in **Table 2-1**.

Table 2-1. Typical values for Athabasca bitumen characterization.

Property	Values
Refractive Index at 20 °C [nD] [15-18]	1.5752 – 1.5840
Density at 20 °C [kg/m3] [14]	991 – 1010
Elemental composition [wt.%] [5]	
C	83.1 – 83.9
H	10.5 – 10.6
N	0.4
S	1.0 – 1.1
O	4.2 – 4.8
Aromatic hydrogen [%] [15,16]	5.3 – 6.0
Aromatic carbon [%] [5,16,19]	28.4 - 32
Free radical content [spins/g] [20]	$0.9 – 1.1 \times 10^{18}$
n-heptane asphaltenes [wt.%] [19,21,22]	15 – 17.4

Practically, because of these properties, oil processing and transportation become hard, and in the case of oil transport, improvement of some properties is required (e.g., viscosity). One of the simplest strategies is to dilute the bitumen with material that decreases the viscosity, and some of the bitumen is diluted and sold as a diluted bitumen (Dilbit) mixture [23]. An alternative strategy is to process the bitumen to improve the bitumen properties, which is the bitumen processing strategy that is relevant to this study.

2.2.2.1.   Separation Processes

Over the years, different separation technologies have been developed in order to improve oil characteristics. There are two important front-end separation processes that may be considered for improving the properties of bitumen before or during upgrading / refining.

- *Desalting* [5,24]: The aim is to separate emulsified material from bitumen, created by the presence of dissolved brine (water, salts, and fine particles). This is removed to reduce corrosion [25] damage such material can cause, as well as catalyst deactivation. The operating conditions (e.g., temperature, volume of wash water, pH, etc.) at which this treatment is carried out will depend on the oil properties. A traditional procedure involves oil being water washed to then separate the water used for washing. The use of electric potential fields (e.g., 16 – 35 kV) has been beneficial for the separation in heavy oil systems. This is possible because the voltage allows the coalescence of water.

- *Solvent Deasphalting (SDA)*: The aim of this process is to remove asphaltenes (a solubility class) from the feed before it is processed. The separation takes place by mixing the feed with a paraffinic solvent (usually lower alkanes, e.g., propane to heptane or low-boiling paraffin mixture) in a ratio that varies from 3:1 to 10:1. The remaining fraction from the separation is called Deasphalted Oil (DAO). The separation conditions are determined by desired characteristics of the DAO in relation to the cost of solvent recovery. Examples of technologies [18,26] available for this process are Low Energy Deasphalting (LEDA), Demex, MDS, Residuum Oil Supercritical Extraction (ROSE), Solvahl, and Lube Deasphalting.

As is conventional for petroleum refining processes, the bitumen is further separated by distillation into different boiling fractions, which directs each boiling fraction to an appropriate processing pathway. This separation is performed only when the bitumen is further upgraded or refined.

- *Distillation* [5]*:* This process separates the crude oil into compounds based on their molecular size and boiling-point ranges. It can be divided into **atmospheric distillation**

and **vacuum distillation.** The first one is used to fractionate the crude at temperatures ranging between 343 to 399 ºC and at atmospheric pressure. On the other hand, **vacuum distillation** uses pressures ranging between 25 to 40 mm Hg and an outlet temperature of 388 to 454 ºC. Lower pressures are used since at the temperature in which atmospheric distillation occurs can lead to the cracking of the materials.

2.2.2.2.   Upgrading Processes

Upgrading is defined as the combination of conversion processes where bitumen is transformed into a lighter and higher quality crude oil and includes processes such as thermal cracking, catalytic cracking and hydroconversion [5]. Based on the intensity of the upgrading, the upgrading processes are divided into "full" upgrading processes and "partial" upgrading processes.

Upgrading could be "full" when bitumen is converted into synthetic crude oil (SCO) and other high-quality products and at present, represents all of the industrially employed upgrading processes. On the other hand, it could also be "partial" upgrading [23,27-29], which refers to ideally lower cost and lower intensity processing to convert bitumen into a lower viscosity oil to facilitate oil transport. Although there are no "partial" upgrading processes in industrial operation, the work in this study was in support of the development of one such technology (discussed in **Section 2.3**).

By converting material in the residue fraction, it results in most of the gain that can be made to improve oil properties and decrease viscosity. The residue fractions are the products leaving the bottom of the distillation towers. Conversion technologies that are employed to convert residue fractions are:

- *Visbreaking*: A technology available for many decades that mainly focuses on reducing the viscosity of bitumen to meet fuel oil specifications. Visbreaking conventionally operating temperatures vary between 430 – 490 ºC at the coil outlet [30] and pressures between 0.4 and 1.4 MPa [31], which makes it to be considered a mild thermal cracking process. Visbreaking can reach up to 30 % conversion of vacuum residue to lighter

products [32].   Coil and coil-and-soaker visbreakers are the two process variants available.

- *Coking* [24,32,33]: This process uses higher temperatures and longer residence times compared to visbreaking. The objective is to produce coke and lighter products (e.g., gases, naphtha, and distillate). Some of the advantages of coking are related to a higher H:C ratio and lower heteroatoms and metal content in the liquid products. Delayed coking, flexi-coking, and fluid coking are the different process variants available for this process.

- *Catalytic Cracking:* Widely used refinery process to convert heavy oils into more valuable lighter products (i.e., olefinic material and naphtha range material). The catalyst used could belong to one of these three groups: acid-treated alumino-silicates, amorphous synthetic silica-alumina combinations, and crystalline synthetic silica-alumina (zeolites or molecular sieves). This is not a process used for upgrading of bitumen, although it is encountered in refineries that process bitumen.

- *Residue hydroconversion* [5,24,32-34]*:* This process uses higher temperatures to promote bond breakage. The production of coke is suppressed due to the hydrogen addition by a hydrotreating catalyst. Additionally, hydrotreating is useful for stabilizing the petroleum products by saturating olefins and removing sulfur and nitrogen.

2.3. BituMax™ Partial Upgrader Process

As previously mentioned, bitumen requires processing after extraction to recover the bitumen from the oil sands ore and to make it suitable for pipeline transportation. The primary aim of a "partial" upgrading process is to keep the cost of upgrading low while at the same time to produce a product that ideally meets pipeline specifications (**Table 2-2**).

14

Table 2-2. Alberta's Pipeline Specifications

Property	Specification
Viscosity [cSt]	350[a]
Density at 15.6 °C [kg/m^3]	<940
Gravity °API	>19
Bottom Solids and Water [vol. %]	<0.5
Olefin Content [wt. %][b]	<1

[a] At pipeline temperature
[b] 1-decene equivalent measured by 1H-NMRThis is the integrated area of olefinic hydrogen in the NMR spectrum relative to the area corresponding to the indicated wt. % equivalent of 1-decene that would give the same integrated area of olefinic hydrogen.

In 2015, the National Partial Upgrading Program (NPUP) was created to identify partial upgrading technologies that would upgrade bitumen just enough to meet the pipeline specification at a low cost [23]. One of those technologies is BituMax™, which was proposed by CNOOC International Ltd (former Nexen Energy ULC) [35]. A block flow diagram of the BituMax™ technology is shown in **Figure 2-4**.

BituMax™ is a technology for an integrated facility, which involves the SAGD recovery of bitumen in tight integration with a process to improve the bitumen quality to meet the specification target in **Table 2-2**. The process has a primary separation step (solvent deasphalting) that comes directly from the SAGD unit. This step intends to remove asphaltenes, metals and other impurities found in bitumen since these materials are often considered coke precursors. The next step is thermal cracking (visbreaking) of DAO, which will produce a partially upgraded bitumen. However, the product after visbreaking does not meet the olefin content specification in **Table 2-2**. This leads to the olefin treating unit (olefin-aromatic alkylation), which enables the technology to reduce the olefin content without the need for hydrogen or hydrotreating as part of the process.
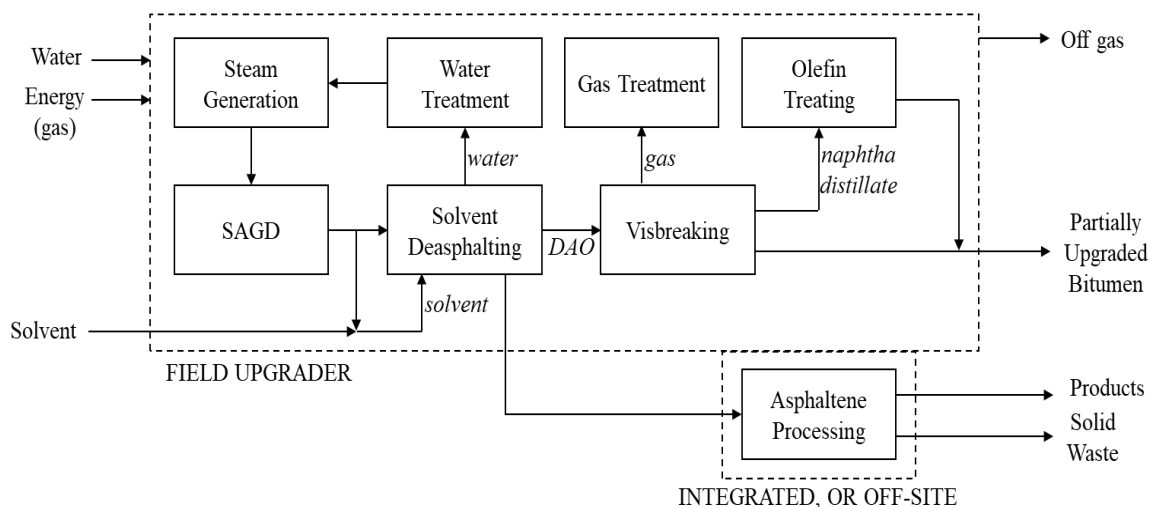
Figure 2-4. BituMax™ Field Upgrader Block Flow Diagram. Redrawn from [35].

This study deals with the visbreaking unit in the BituMax™ technology. As can be seen from **Figure 2-4**, the visbreaking unit is the only conversion unit that performs residue conversion to lighter products. The ability of this technology to meet the viscosity specification in **Table 2-2** depends partly on the removal of asphaltenes by solvent deasphalting, but mostly on the cracking of the residue fraction to lower boiling, lower viscosity products.

Herein lies one of the biggest challenges when processing bitumen, which is the formation of carbonaceous materials. When performing visbreaking, as suggested in the design, it is possible to form such materials due to the extent of cracking conversion that is required. The formation of carbonaceous deposits is a side reaction when performing thermal and/or catalytic cracking. In the case of catalytic cracking, the technology is designed to enable continuous catalyst regeneration to remove the carbonaceous deposits from the catalyst [36]. However, in thermal cracking, such as visbreaking, the buildup of carbonaceous deposits affects the efficiency and proper operation of the system, leading to equipment shutdown.

Speight [37] extolled the virtues of visbreaking as a process for upgrading bitumen, but the fact remains that the extent of conversion by visbreaking is limited by the onset of coking, and the formation of carbonaceous deposits. Many studies have explored different approaches in an attempt to understand how to suppress or reduce carbonaceous deposit formation. Previous works

have found [38-40] that performing visbreaking at lower temperatures could upgrade the visbroken products to meet pipeline specifications (e.g., viscosity reduction) with less production of solid carbonaceous materials. However, this advantage comes with a disadvantage. By reducing the treatment's temperature, more time will be required in order to achieve a similar level of conversion. Both, reaction time and reaction temperature are dependent on each other [41]. For partial upgrading the challenge that remains is to find a way to increase vacuum residue conversion without the use of hydrogen and without triggering the onset of coking.

2.4. Coke Formation during thermal conversion

Visbreaking usually operates at coke yields of 1 wt.% or less than that in accordance with the operating conditions (i.e., temperature and residence time) [42]. This is an economically motivated threshold since there is a trade-off between coke yield and the frequency with which the unit has to be shut down for cleaning. Coke formation is explained as the development of a second phase [15], and descriptions of onset of coking in visbreaking are often refer to the asphaltenes content in the feed material, because it refers to material that is separated by causing it to form a second phase. This is a topic that is explored in **Chapter 6**.

Coke, in this chapter, is defined as a carbonaceous material, carbon-rich and with a high hydrogen deficiency. However, it is important to note that other definitions based on solubility classification also exist. A material insoluble in a solvent like toluene [42-46] or carbon disulfide [46-48] is often referred to as coke. The composition of coke will depend on variables such as the feed composition and the operating reaction conditions [49].

2.4.1. Asphaltenes in coke formation

Asphaltenes are a solubility class defined as insoluble material in paraffinic solvents, usually *n*-pentane or *n*-heptane, but soluble in aromatic solvents like toluene. The definition of this solubility class in terms of structure and properties has been controversial. While they have been described as polynuclear aromatic structures [50] with a high concentration of heteroatoms and metals; the presence of alkyl, cycloalkyl or aryl chains [51-53] has to be mentioned as they could be found as

side chains in condensed aromatic groups [54], or as bridges between polynuclear aromatic structures [55]. It is then unavoidable to use this description to refer to the main structures proposed in literature for asphaltenes: island and archipelago. Island structure consists of a multinuclear aromatic core (seven or more rings) with aliphatic chains as substituents in the periphery. On the other hand, archipelago structure contains small multinuclear aromatic cores (up to four rings) that could be connected through aliphatic chains [56]. The coexistence of both structures has been reported by [57-59].

Several authors [43,44,60-62] have studied the impact of asphaltenes in coke formation, considering them as precursors [43,63-65]. Based on experimental results, Wiehe [43] developed a kinetic model that could describe the conversion of asphaltenes in the entire conversion range. This was the preamble of the pendant-core model [68,69] in which petroleum fractions are shown in terms of *pendant* (volatile when cracked from the residua molecule) and *core* (nonvolatile when cracked from the residua molecule) blocks. Asphaltenes are shown as molecules built mostly from core blocks with some pendants attached. This description of the molecular structure is not universally accepted [68,69].

In industry, the use of Carbon Conradson Residue (CCR) has been widely used as it is a standard measure of the tendency of a feed to form coke. Wiehe was able to use the pendant-core model to describe the chemical mechanisms in the Carbon Conradson Residue and its linear relationship with the hydrogen content in a sample. It was shown that high CCR was linked to low hydrogen content. Polynuclear aromatic structures influence the thermal stability and the strong attractive forces in petroleum; hence, the coke propensity and the solubility parameter of these materials are a function of the hydrogen content [67,70].

It has been suggested that asphaltenes are surrounded by resins (a solubility class considered to resemble the characteristics of asphaltenes but of smaller size, lower aromaticity and double bond equivalent, or DBE, and lower heteroatoms content but higher H/C ratio [71-73]) and other hydrocarbon materials which stabilize them ("peptized") [74-76]. This allows such structures to remain dispersed in the oil, but it could imply the presence of two phases. This description agrees with the one given by Hirschberg [77], the importance of the resin component is considered crucial

for the stability of the system. A change in the oil's composition affects the stability of the suspended resin/asphaltene structures, facilitating the "collision" of asphaltenes as there are no resins around them. This process will lead to a phase separation in the system, as it is shown in **Figure 2-5**. This is called the steric-stabilization model by Cimino et al. [78], which could find similarities with a lyophobic colloidal system.
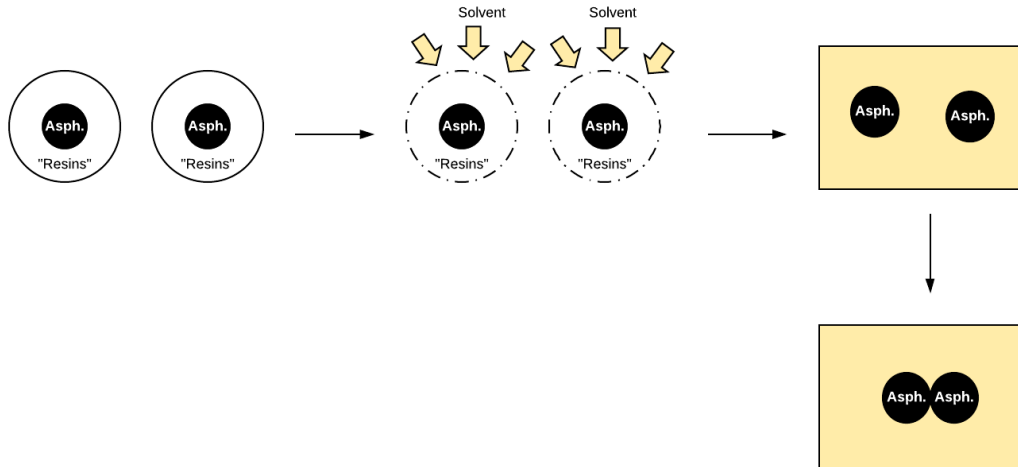
Figure 2-5. Asphaltene aggregation proposed by Hirschberg.

On the other hand, Cimino, et al. [78] and Tompa and Heithaus [79] have suggested the exact opposite description for the separation process. The asphaltenes would not be the ones separating but rather the solvent (i.e., the oil matrix, resins). This agrees with the lyophilic colloid theory. Instead of having a dispersed phase, the system behaves just as one phase, with material from the oil phase being dissolved into the solvent-rich phase that separates. The aggregation process takes place because the characteristics of the medium change, and the paraffin-soluble material partitions between the phases. This partitioning of material between the phases causes the oil-rich phase to be depleted from paraffin-soluble material to a point where the oil-rich phase becomes a solid phase due to the nature of the material that remains.

2.4.2. *Mesophase leading to the formation of coke*

The formation of coke has been explained as the result of the development of a mesophase where a long-range crystallographic order is observed, exhibiting an optical texture (anisotropic) that

allows its identification. On the other hand, it is possible that coke is a consequence of a second liquid phase formation with a small-scale crystallographic order and that it does not display optical texture (isotropic) as the mesophase does. Because of this, either the anisotropic or isotropic phase are considered precursor materials in coke formation [43].

Whether the material passes through a mesophase (liquid crystal phase) or not is related to the nature of the oil. When two liquid phases are formed, and the material partitions between the two phases, the phase that becomes depleted in lower boiling material may approach a point where its most stable phase at the prevailing conditions is no longer an isotropic liquid. In such a case, the phase transition that takes place may be a phase transition to an ordered liquid phase. However, since the liquid is a mixture, there is a further possibility that only a fraction of the species would engage in the phase transition.

There is high crystallographic order in the mesophase, i.e., liquid crystal behavior. However, it is important to note that for this to take place, molecules should exhibit a certain degree of planarity [80-83] in order to prevent any steric barrier that may cause instability of the liquid crystal system. The size of the molecules, the concentration of those molecules and the fluidity of the system are also factors that have an impact on the coke formation process. Even though reaction temperature and reaction time are not part of the system's characteristics, they play an important role in the formation of a second phase.

The coke formation process [80,84] has been described, and the following steps have been proposed to describe its sequence:

1. Molecular weight and molecular size increment (mesogens);
2. Larger molecules start the mesophase formation (mesogens self-assembly)
3. The critical concentration of larger molecules is exceeded, and the transition to the liquid crystal phase starts (mesogens coalescence);
4. The increase of molecular weight reduces the mobility of molecular species;
5. The thermal process has created reactive species that will allow the polymerization reactions to take place even after the thermal treatment is stopped;

20

6.   The liquid crystal system transitions into a solid phase.

One could rephrase the same steps without reference to species as mesogens to describe the formation of a second isotropic phase within the system that will undergo a direct phase transition into a solid. It should be pointed out that the mesophase refers to an optical texture resulting from a planar aromatic stacking mechanism within a certain orientational range. Hence, the absence of an optical texture does not invalidate the description of a phase transition (i.e., isotropic to second isotropic phase and/or isotropic to solid phase).

Marsh and Menendez [85] have suggested the isotropic phase results from molecules that are macromolecular in nature whereas the anisotropic structure originates from a mixture of polynuclear aromatic systems. However, there is some discrepancy with this distinction since it has also been suggested by Greinke [86] and Singer [87] that the isotropic phase is richer in smaller molecules compared to the anisotropic phase (mesophase). Nevertheless, it is agreed that these types of reactions (besides many others) are taking place [88]:

- *Cracking:* The objective is to reduce the carbon number by breaking carbon-carbon bonds. And the hydrogen required for saturation will be provided by the second type of reaction. Riggs and Diefendorf [89] believed that cracking reactions preceded the mesophase   formation.
  The energy required to break a carbon-carbon bond or a carbon-hydrogen bond will depend on the type of structure present in the system. The homolytic bond dissociation energy required to break C-C or C-H bonds depends on their position in the molecular structure. For example, Billaud et al. [90] explained this using cracking of dodecylbenzene to illustrate the differences. Breaking a bond in an aromatic ring (or structure) requires more energy than in an aliphatic group since it has high resonance energy that stabilizes the ring.

- *Aromatization and Addition reactions:* The dehydrogenation of saturated rings and the recombination of aromatic groups can lead to an increase in aromatic ring structures. This allows the hydrogen to be released or transferred. The previous "definitions" for

coke are commonly used; however, it is noteworthy to mention that the aromatic hydrogen content in samples that have been subject to different conditions (i.e., temperature and reaction time) did not show a big change [85,86].

In summary, the literature suggested that mesophase formation was not due to macromolecular structures per se but due to macromolecular polynuclear aromatic systems that exhibit a degree of planarity. This focused specific attention on the research on the development of aromatic content and the work reported in **Chapter 5**.

2.4.3.   Free radical reactions

Free radicals are species characterized by the presence of an unpaired electron, which makes them reactive compared to other molecules. It has been known bitumen naturally contains such free radical species, and the reason for their persistence despite their reactivity was explained in terms of dynamic association-dissociation reactions [91]. It was shown that asphaltenes (a solubility class) contain the highest free radical content in bitumen [20]. Zhang et al. [68] proposed different "prototypical" molecules that contain free radical species and ranked them based on their stability, suggesting that an island asphaltene motif could favor radical stability and hence, persistence.

In thermal cracking as well as in the description of reactions that may lead to mesophase formation given at the end of **Section 2.4.2**, free radical reactions play an important role. The formation of free radicals during thermal cracking, is often described with the general reaction sequence [26,32,92], starting with the initiation step described in **Equation (2-1)**:

<u>Initiation</u> $$R\!-\!R' \xrightarrow{\ k_{in}\ } R\!\cdot\ +\ R'\cdot \qquad\qquad (2\text{-}1)$$

The formation of free radical species implies that a certain amount of energy is applied to the system for bond homolysis to take place. Due to the nature of bitumen and bitumen-related systems, it was pointed out that due to the presence of native free radical species, an initiation step is not strictly speaking required [30]. A different type of initiation that is also possible is molecule-induced homolysis. This type of initiation requires a species that can act as a hydrogen donor and

a species that can act as a hydrogen acceptor. Initiation by this type of reaction does not involve thermolysis but a concerted hydrogen transfer.

The propagation step can involve different "types" of free radical reactions. Some of them are the free radical abstraction (e.g., hydrogen abstraction, **Equation (2-2)**, inter- and intramolecular transfers (e.g., hydrogen transfer and free radical isomerization, respectively), fragmentation (e.g., β – scission, **Equation (2-3)**, addition reactions – **Equation (2-4)** – (e.g., cyclization), and rearrangements [93].

Propagation

- Hydrogen abstraction

$$\beta_j^{\bullet} + R_jH \xrightarrow{\ k_{ij}\ } \beta_jH + R_j^{\bullet} \qquad (2\text{-}2)$$

- β - Scission

$$R^{\bullet}\!-\!C\!-\!C\!-\!\beta_j \xrightarrow{\ k_i\ } R\!-\!C\!=\!C\!-\!\beta_j^{\bullet} \qquad (2\text{-}3)$$

- Radical Addition

 (2-4)
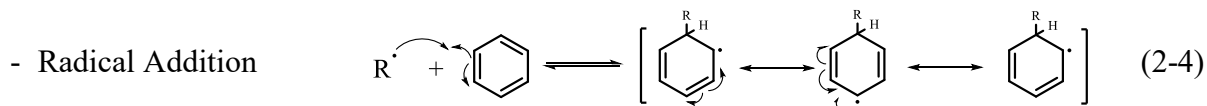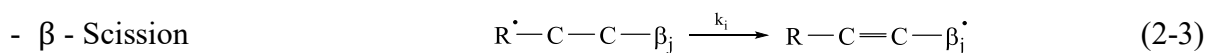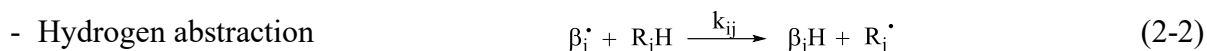
Different propagation reactions can take place during a thermal treatment, De Klerk [30] has discussed the impact of the operating temperature in terms of kinetics and thermodynamics of the free radical reactions. It was noted that a thermal treating operating at lower temperatures could favor a relatively higher rate of transfer reactions compared to cracking reactions. However, it should be kept in mind that all the reaction rates will be decreased by a decrease in temperature. Thermodynamically, systems are generally driven to lower their Gibbs free energy; reducing the operating temperature will increase the driving force of free radical addition reactions compared to cracking reactions.

The termination step in free radical reactions refers to the formation of a product obtained from the reaction of two radical species. There are two mechanisms in which this step can be completed: recombination (e.g., radical addition, **Equation (2-5)**, and disproportionation (e.g., hydrogen transfer, **Equation (2-6)**).

Termination

- Recombination

$$R\cdot \ + \ R'\cdot \ \xrightarrow{k_t} \ R-R' \qquad (2\text{-}5)$$

- Disproportionation

$$R-\underset{H}{\overset{H}{C}}-\underset{H}{\overset{H}{C}}-R \ + \ R-\underset{H}{\overset{H}{C}}-\underset{H}{\overset{H}{C}}-R \ \xrightarrow{Disproportionation} \ R-CH=CH-R \ + \ R-CH_2CH_2-R \qquad (2\text{-}6)$$
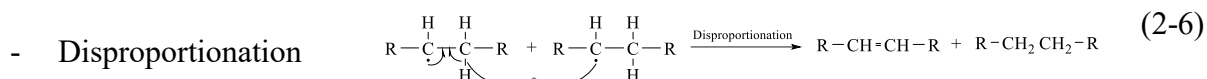
In thermal conversion, the word termination does not necessarily mean that the resulting products will not undergo another reaction. Instead, they can go through another initiation step, and that is why every product in thermal conversion could be considered an intermediate product.

The development of a second phase, which may be a mesophase, can then be explained by the radical reactions leading to an increase in the molecular mass of the products compared to the reagents. Free radical reactions such as addition (which may also be referred to as polymerization or condensation reactions in the petroleum literature) make it possible for an increase in the molecular weight of some species to take place. This is considered as the first step leading to second phase formation. The implication is that the macromolecular species have a higher probability of being insoluble in the bulk liquid, which may lead to coking [43,67].

2.5. Changes in the nature of species during thermal conversion

The changes a material undergoes during thermal conversion can be studied and tracked in-line, or they can be studied by analyzing the resulting products offline. It has been discussed up to this point how the conversion in visbreaking is limited by the coke formation. The development of this material, coke, has been explained. Two origins were suggested in the literature, which are not necessarily mutually exclusive: a) Asphaltenes as precursors of phase separation with phase separation taking place due to change in the bulk liquid properties causing the asphaltenes to phase separate. b) Formation of a second phase that could be a mesophase as a consequence of reactions forming heavier macromolecules, which may be concomitant with an increase in multinuclear aromatic species.

To understand and study the changes a material is experiencing during thermal treating or has experienced, different methodologies and techniques have been used by investigators.

The study of the mesophase and its formation have been studied using optical microscopy. Brooks and Taylor [94] have summarized the work previously done by Ramdohr, Marshall, Mackowsky and Stach. They have first reported the use of optical microscopy to study the formation of anisotropic phases. These regions could be identified using polarized light microscopy, where the ordered structures, the anisotropic phases, show different colors such as light purple, blue, or yellow. Whereas the isotropic regions will display a purple color independent of the rotation's angle. Since then, several authors [80,95-99] have reported the use of optical microscopy (polarized light) as a powerful tool to study and understand the formation of the mesophase. However, optical microscopy exhibits a size limitation when referring to the formation of the anisotropic phase since values could be smaller than the power of the microscope, as it is noted by Marsh and Walker [80]. In addition, a second phase can be formed and not be an anisotropic structure. In such cases, microscopy cannot be used to determine a second isotropic phase.

Other techniques can also indicate the formation or the presence of a second phase. When dealing with crystalline structures, the use of x-ray diffraction could provide an indication of the presence of a mesophase and its position [100]. Changes in interlamellar spacing (d_C) and stacking height of lamellae (L_C) during the early conversion stages of a coal-tar pitch and naphtha-tar pitch were reported by Honda [101,102]. A mesophase, or simply a second phase, could also be observed in a thermogram as the phase transition [100] that will generate an exothermic event [103]. This technique has been widely used in polymer science, and it could provide good insights into the formation process of a second phase. Similarly, the use of viscosity has been reported to study the mesophase formation [104], and also phase separation [75,105], suggesting a rapid increase in the viscosity of the material with the increase in temperature as a potential result of higher molecular weight and/or proximity to a phase transition.

Coke formation is the result of various and different changes bitumen and bitumen-related materials undergo during thermal conversion. The compositional [106] and structural [107] changes can be studied by measuring properties such as density, refractive index and molecular

weight. Kurtz and Ward [107] studied different types of hydrocarbons by measuring the density and refractive index at different temperatures. They found that each type of hydrocarbon was associated to a refractivity intercept (b in y = mx + b), an observation corroborated by Rivolta [108]. The first derivatives of both refractive index and density with respect to temperature also give information about the changes a material has experienced in visbreaking, since they vary inversely proportional with molecular weight [109,110].

Refractive index values are also used to determine changes in nature a material might experience in visbreaking. An increment is often associated with an increase in aromatic content in a sample [108,111], but it can also mean a change in the polarity of the system [112].

Thanks to the electromagnetic theory, it is possible to understand how such changes are able to have an impact on the refractive index of a sample (i.e., electric and magnetic dipole). Changes in the aromatic nature of the samples could be tracked by using both ^{13}C and ^{1}H Nuclear Magnetic Resonance (NMR). Several authors [87,113-116] have used the understanding of these changes to develop potential reaction pathways that could provide some guidance about how the reactions led to coke formation. This cannot be considered without also considering free radical mechanisms [117]. It was mentioned earlier that bitumen naturally contains free radical species [20,91] and that they are heavily involved in thermal conversion. Lewis [118] proposed a typical free radical mechanism as the initial development of a second phase. At the same time and in agreement with the mechanism proposed, it was suggested that a higher content of free radicals is often associated with a rapid increase in molecular weight [119,120], potentially as a result of addition reactions.

It is the aim of this work to provide a fundamental and practical understanding of the changes that bitumen and bitumen-related products undergo during visbreaking. The complexity of the system is well known, which poses many challenges for its extraction, processing, and transportation. The knowledge and relationships developed in the literature review hopefully show a muster point in the understanding of different processes during thermal conversion.

References

[1] Canadian Association of Petroleum Producers. Uses for Oil. https://www.capp.ca/oil/uses-for-oil/ (accessed March 23, 2021).

[2] EIA. Oil and Petroleum Products Explained, Use of Oil. https://www.eia.gov/energyexplained/oil-and-petroleum-products/use-of-oil.php (accessed October 18, 2022).

[3] MacKay, P.; Pedersen, P.K. The Western Canada Sedimentary Basin: A confluence of science, technology, and ideas. *AAPG Bulletin* **2022**, *106*: p. 655 - 676.

[4] Zhou, S.; Huang, H.; Liu, Y. Biodegradation and Origin of Oil Sands in the Western Canada Sedimentary Basin. *Petroleum Science*, **2008**, *5*: p. 87 - 94.

[5] Gray, M.R. *Upgrading Oilsands Bitumen and Heavy Oil*. University of Alberta Press: Edmonton, Canada, 2015.

[6] Schramm, L.L., Mikula, R.J. Froth Flotation of Oil Sand Bitumen. In: *Foam Engineering: Fundamentals and Applications*, Stevenson, P., Ed.; Wiley-Blackwell: Chichester, UK, 2012; p. 530.

[7] Tipman, R. Froth Treatment. In: *Handbook on theory and practice of bitumen recovery from Athabasca oil sands. Vol. II. Industrial practice*, Masliyah, J.; Xu, Z.; Dabros, M., editor. Kingsley Knowledge Publishing, 2013, p. 211 - 253.

[8] Butler, R.M., Stephens, D.J. The Gravity Drainage of Steam-Heated Heavy Oil to Parallel Horizontal Wells. *Journal of Canadian Petroleum Technology* **1981**, *April-June*, p. 90 - 96.

[9] Butler, R.M. SAGD Comes of Age! *Journal of Canadian Petroleum Technology* **1998**, *37*: p. 9 - 12.

[10] Schramm, L.L., Isaacs, E.E. Development on in-situ Oil Sands and Heavy Oil Reservoirs in Canada. In: *Handbook on theory and practice of bitumen recovery from Athabasca oil sands. Vol. II. Industrial practice,* Masliyah, J.; Xu, Z.; Dabros, M., editor. Kingsley Knowledge Publishing, 2013, p. 603 - 635.

[11] Ansari, S., Sabbagh, R., Yusuf, Y., Nobes, D.S. The Role of Emulsions in Steam-Assisted-Gravity-Drainage (SAGD) Oil Production Process: A Review. *SPE Journal*, **2020**, *25*: p. 969 - 989.

[12]   Albahlani, A.M., Babadagli, T. A Critical Review of the Status of SAGD: Where Are We and What Is Next? In: *SPE Western Regional and Pacific Section AAPG Joint Meeting*, Bakersfield, CA, March 29 – April 2, 2008; p. SPE 113283.

[13]   Velayati, A., Nouri, A. Emulsification and Emulsion Flow in Thermal Recovery Operations with a Focus on SAGD Operations: A Critical Review. *Fuel* **2020**, *267*: p. 117141.

[14]   Strausz, O. P.; Lown, E. M. *The Chemistry of Alberta Oil Sands, Bitumens and Heavy Oils*; Alberta Energy Research Institute: Calgary, AB, 2003.

[15]   Yan, Y.; De Klerk, A.; Prado, G. H. C. Visbreaking of Vacuum Residue Deasphalted Oil: New Asphaltenes Formation. *Energy and Fuels* **2020**, *34*: p. 5135 - 5147.

[16]   Yañez Jaramillo, L.M.; Link, F.; De Klerk, A. Relationship between Aromatic hydrogen and Aromatic Carbon in Straight Run and Converted Oils. *Fuel* **2022**, *327*: p. 124414.

[17]   Taylor, S.D.; Czarnecki, J.; Masliyah, J. Refractive Index Measurements of Diluted Bitumen Solutions. *Fuel* **2001**, *80*: p. 2013 - 2018.

[18]   Turuga, A.S.S. Effect of Solvent Deasphalting Process on the Properties of Deasphalted Oil and Asphaltenes from Bitumen. M.Sc. Thesis, University of Alberta, 2017.

[19]   Suzuki, T.; Itoh, M.; Takegami, Y.; Watanabe, Y. Chemical Structure of Tar-sand Bitumens by ^{13}C and ^{1}H N.M.R. Spectroscopic Methods. *Fuel* **1982**, *61*: p. 402 - 410.

[20]   Tannous, J. H.; De Klerk, A. Quantification of the Free Radical Content of Oilsands Bitumen Fractions. *Energy and Fuels* **2019**, *33*: p. 7083 - 7093.

[21]   Clarke, P.F.; Pruden, B.B. Asphaltene Precipitation from Cold Lake and Athabasca Bitumen. *Petroleum Science and Technology* **1998**, *16*, p. 287 - 305.

[22]   Alboudwarej, H.; Akbarzadeh, K.; Beck, J.; Svrcek, W.Y.; Yarranton, H.W. Regular Solution Model for Asphaltene Precipitation from Bitumens and Solvents. *AIChE Journal* **2003**, *49*: p. 2948 - 2956.

[23]   Jacobs Consultancy. Bitumen Partial Upgrading (Whitepaper). Calgary, Canada, 2018.

[24]   Kaiser, M.J.; de Klerk, A.; Gary, J.H.; Handwerk G.E. *Petroleum refining: technology, economics, and markets*. Sixth edit. CRC Press: Boca Raton, FL, 2020.

[25]   Gruse, W.A.; Stevens, D.R. *Chemical Technology of Petroleum*. McGraw-Hill: New York,NY, 1960.

[26]   Speight, J.G. *Fouling in Refineries*. Gulf Professional Publishing: Amsterdam, Netherlands, 2015.

[27]   Gray, M.R. Fundamentals of Partial Upgrading of Bitumen. *Energy and Fuels* **2019**, *33*, p. 6843 - 6856.

[28]   Gholami, R.; Alvarez-Majmutov, A.; Ali, M.; Chen, J. Understanding Bitumen Partial Upgrading through Process Modelling and Simulation. *The Canadian Journal of Chemical Engineering* **2021**, *99:* p. 222 - 234.

[29]   Winter, J.; Goodday, V.; Fellows, K. Enabling Partial Upgrading in Alberta: A review of the Regulatory Framework and Opportunites for Improvement. *The School of Public Policy Publications* **2019**, *12:* p. 1 - 47.

[30]   De Klerk, A. Thermal Conversion Modeling of Visbreaking at Temperatures below 400 °C. *Energy and Fuels* **2020**, *34*: p. 15285 - 15298.

[31]   Speight, J.G. *The Chemistry and Technology of Petroleum*. 5th ed. CRC Press: Boca Raton, FL, 2014.

[32]   Ancheyta Juárez, J. *Modeling of Processes and Reactors for Upgrading of Heavy Petroleum*. CRC Press: Boca Raton, FL, 2013.

[33]   *Bitumen, Asphalts and Tar Sands*. Chilingarian, G.V.; Yen, T.F., Eds.; Elsevier Scientific Publishing Company: Amsterdam, Netherlands,1978.

[34]   Ancheyta Juárez, J.; Speight, J.G. *Hydroprocessing of Heavy Oils and Residua*. CRC Press: Boca Raton, FL, 2007.

[35]   De Klerk, A.; Zerpa Reques, N. G.; Xia, Y.; Omer, A.A. Integrated Central Processing Facility (CPF) in Oil Field Upgrading (OFU). CA2837345A1, 2014.

[36]   Ancheyta Juárez, J.; Trejo, F.; Rana, M.S. *Asphaltenes: Chemical Transformation during Hydroprocessing of Heavy Oils*. CRC Press: Boca Raton, FL, 2009.

[37]   Speight, J.G. Visbreaking: A technology of the past and the future. *Scientia Iranica* **2012**, *19*: p. 569 - 573.

[38]   Wang, L. Low temperature visbreaking. MSc Thesis, Edmonton: University of Alberta, 2013.

[39]   Zachariah, A. Low temperature pyrolysis and its application in bitumen processing. MSc Thesis, University of Alberta, 2014.

[40] Yañez Jaramillo, L.M. Visbreaking of Oilsands Bitumen between 150 and 300 ºC. M.Sc. Thesis, University of Alberta, 2016.

[41] Leprince, P. *Petroleum Refining.* Leprince, P., Ed.; Editions Technip: Paris, France, 2001; Vol. 3, Conversion Processes.

[42] Yan, T. Y. Characterization of Visbreaker Feeds. *Fuel* **1990**, *69*: p. 1062 - 1064.

[43] Wiehe, I.A. A Phase-Separation Kinetic Model for Coke Formation. *Industrial and Engineering Chemistry Research* **1993**, *32*: p. 2447 - 2454.

[44] Rahmani, S.; McCaffrey, W.; Gray, M.R. Kinetics of solvent interactions with asphaltenes during coke formation. *Energy and Fuels* **2002**, *16*: p. 148 - 154.

[45] Rahimi, P.M.; Teclemariam, A.; Taylor, E.; DeBruijn, T.; Wiehe, I.A. Thermal Processing Limits of Athabasca Bitumen during Visbreaking Using Solubility Parameters. *ACS Symposium Series* **2005**, *895*: p. 183 - 196.

[46] Speight, J.G. Resids. In: *Handbook of Alternative Fuel Technologies*, 1st. ed.; S., Lee; Speight, J.G.; Loyalka, S.K., Eds.; Taylor & Francis Group: Boca Raton, FL, p. 171 - 196.

[47] Marafi, M.; Stanislaus, A.; Furimsky, E. Spent Unconventional Hydroprocessing Catalysts. In: *Handbook of Spent Hydroprocessing Catalysts*; Elsevier B.V: Amsterdam, Netherlands, 2017, p. 357 - 374.

[48] Wen, C.S.; Chilingarian, G. V.; Yen, T.F. Properties and Structure of Bitumens. In: *Bitumen, Asphalts and Tar Sands*. Chilingarian, G.V.; Yen, T.F., Eds.; Elsevier Scientific Publishing Company: Amsterdam, Netherlands,1978, p. 162.

[49] Guisnet, M.; Magnoux, P. Organic Chemistry of Coke Formation. *Applied Catalysis A: General* **2001**, *212*: p. 83 - 96.

[50] Sheremata, J.M.; Gray, M.R.; Dettman, H.D.; McCaffrey, W.C. Quantitative Molecular Representation and Sequential Optimization of Athabasca Asphaltenes. *Energy and Fuels* **2004**, *18*: p. 1377 - 1384.

[51] Podgorski, D.C.; Corilo, Y.E.; Nyadong, L.; Lobodin, V.V.; Bythell, B.J.; Robbins, W.K.; McKenna, A.M.; Marshall, A.G.; Rodgers, R.P. Heavy Petroleum Composition. 5. Compositional and Structural Continuum of Petroleum Revealed. *Energy and Fuels* **2013**, *27*: p. 1268 - 1276.

[52]   Chacón-Patino, M.L.; Rowland, S.M.; Rodgers, R.P. Advances in Asphaltene Petroleomics. Part 2: Selective Separation Method That Reveals Fractions Enriched in Island and Archipelago Structural Motifs by Mass Spectrometry. *Energy and Fuels* **2018**, *32*: p.314 - 328.

[53]   McKenna, A.M.; Marshall, A.G.; Rodgers, R.P. Heavy Petroleum Composition. 4. Asphaltene Compositional Space. *Energy & Fuels* **2013**, *27*: p. 1257 - 1267.

[54]   Mullins, O.C. The Modified Yen Model. *Energy and Fuels* **2010**, *24*: p. 2179 - 2207.

[55]   McKenna, A.M.; Chacón-Patino, M.L.; Weisbrod, C.R.; Blakney, G.T.; Rodgers, R.P. Molecular-Level Characterization of Asphaltenes Isolated from Distillation Cuts. *Energy and Fuels* **2019**, *33*: p. 2018 - 2029.

[56]   Rodriguez Leon, S.L. The Stability of Visbroken Heavy Oil Against Asphaltene Precipitation. MSc Thesis, University of Calgary, 2018.

[57]   Gray, M.R.; Tykwinski, R.; Stryker, J.; Tan, A. Supramolecular Assembly Model for Aggregation of Petroleum Asphaltenes. *Energy and Fuels* **2011**, *25*: p. 3125 - 3134.

[58]   Mullins, O.; Sabbah, H.; Pomerantz, A.E; Andrews, A.B.; Ruiz-Morales, Y.; Mostow, F.; Mcfarlane, R.; Goual, L.; Lepkowicz, R.; Cooper, T.; Orbulescu, J.; Leblanc, R.M.; Edwards, J.; Zare, R.N. Advances in Asphaltene Science and the Yen − Mullins Model. *Energy and Fuels* **2012**, *26*: p. 3986 - 4003.

[59]   Chacón-Patiño, M.L.; Gray, M.R.; Rüger, C.; Smith, D.F.; Glattke, T.J.; Niles, S.F.; Neumann, A.; Weisbrod, C.R.; Yen, A.; McKenna, A.M.; Giusti, P.; Bouyssiere, B.; Barrere-Mangote, C.;Yarranton, H.; Hendrickson, C.L.; Marshall, A.G.; Rodgers, R.P. Lessons Learned from a Decade-Long Assessment of Asphaltenes by Ultrahigh-Resolution Mass Spectrometry and Implications for Complex Mixture Analysis. *Energy and Fuels* **2021**, *35*: p. 16335 - 16376.

[60]   Gonçalves, M.L.A.; Ribeiro, D.A.; Teixeira, A.M.R.F.; Teixeira, M.A.G. Influence of Asphaltenes on Coke Formation during the Thermal Cracking of Different Brazilian Distillation Residues. *Fuel* **2007**, *86*: p.619 - 623.

[61]   Magaril, R.Z.; Aksenova, E.I. Study of the Mechanism of Coke Formation in the Cracking of Petroleum Resins. *International Chemical Engineering* **1968**, *8*: p. 727 - 729.

[62]   Magaril, R.Z.; Ramazaeva, L.F.; Aksenova, E.I. Kinetics of the Formation of Coke in Thermal Processing of Crude Oil. *International Chemical Engineering* **1971**, *11*: p. 250 - 251.

[63]   Rahimi, P.; Gentzis, T.; Dawson, W.H.; Fairbridge, C.; Khulbe, C.; Chung, K.; Nowlan, V.; DelBianco, A. Investigation of Coking Propensity of Narrow Cut Fractions from Athabasca Bitumen using Hot-Stage Microscopy. *Energy and Fuels* **1998**, *12*: p. 1020 - 1030.

[64]   Rahimi, P.; Gentzis, T.; Taylor, E.; Carson, D.; Nowlan, V.; Cotté, E. The Impact of Cut Point on the Processability of Athabasca Bitumen. *Fuel* **2001**, *80*: p. 1147 - 1154.

[65]   Wiehe, I.A.; Kennedy, R.J. Oil compatibility model and crude oil incompatibility. *Energy and Fuels* **2000**, *14*: p.56 - 59.

[66]   Wiehe, I.A. The Pendant-Core Building Block Model of Petroleum Residua. *Energy and Fuels* **1994**, *8*: p. 536 - 544.

[67]   Wiehe, I.A. *Process Chemistry of Petroleum Macromolecules*. CRC Press: Boca Raton, FL, 2008.

[68]   Zhang, Y.; Siskin, M.; Gray, M.R.; Walters, C.C.; Rodgers, R.P. Mechanisms of Asphaltene Aggregation: Puzzles and a New Hypothesis. *Energy and Fuels* **2020**, *34*: p. 9094 - 9107.

[69]   Rueda-Velásquez, R.I.; Freund, H.; Qian, K.; Olmstead, W.N.; Gray, M.R. Characterization of Asphaltene Building Blocks by Cracking under Favorable Hydrogenation Conditions. *Energy and Fuels* **2013**, *27:* p. 1817 - 1829.

[70]   Wiehe, I.A. The Chemistry of Coke Formation from Petroleum: A Tutorial. In: *Preprint National Meeting - American Chemical Society Division of Petroleum Chemistry* **1998**, p. 612 - 615.

[71]   Acevedo, S.; Mendez, B.; Rojas, A.; Layrisse, I.; Rivas, H. Asphaltenes and Resins from the Orinoco Basin. *Fuel* **1985**, *64*: p. 1741 - 1747.

[72]   Fakher, S.; Ahdaya, M.; Elturki, M.; Imqam, A. Critical Review of Asphaltene Properties and Factors impacting its Stability in Crude Oil. *Journal of Petroleum Exploration and Production Technology* **2020**, *10*: p. 1183 - 1200.

[73]   *Structures and Dynamics of Asphaltenes; Mullins, O.C., Sheu, E.Y., Eds.;* Springer Science+Business Media: New York, 1998.

[74] Park, S.J.; Mansoori, G.A. Aggregation and Deposition of Heavy Organics in Petroleum Crudes. *Energy Sources* **1988**, *10*: p. 109 - 125.

[75] Escobedo, J.; Mansoori, G.A. Viscometric Determination of the Onset of Asphaltene Flocculation: A Novel Method. *SPE Production and Facilities* **1995**, *10*: p. 115 - 118.

[76] Nellesteyn, F.J. The Constitution of Asphalt. *Journal of the Institute of Petroleum* **1924**, *10*: p. 311 - 325.

[77] Hirschberg, A.; de Jong, L.N.J.; Schipper, B.A.; Meijer, J.G. Influence of Temperature and Pressure on Asphaltene Flocculation. *Society of Petroleum Engineers Journal* **1984**, *24*: p. 283 - 293.

[78] Cimino, R.; Correra, S.; Del Bianco, A.; Lockhart, T. P. Solubility and Phase Behavior of Asphaltenes in Hydrocarbon Media. In *Asphaltenes. Fundamentals and applications*; Sheu, E. Y., Mullins, O. C. Eds.; Plenum Press: New York, 1995, p. 97 - 130.

[79] Heithaus, J.J. Measurement and Significance of Asphaltene Peptization. *Journal of the Institute of Petroleum* **1962**, *48*: p. 45.

[80] Marsh, H.; Walker, P.L. The Formation of Graphitizable Carbons via Mesophase: Chemical and Kinetic considerations. In: *Chemistry and Physics of Carbon*; Walker, P.L.; Thrower, P.A., Eds.; Marcel Dekker Inc: New York, NY, 1979; vol. 15, p. 230 - 286.

[81] Hurt, R.H.; Hu, Y. Thermodynamics of Carbonaceous Mesophase. *Carbon* **1999**, *37*: p. 281 - 292.

[82] Mochida, I.; Inoue, S.-I.; Maeda, K.; Takeshita, K. Carbonization of Aromatic Hydrocarbons VI. Carbonization of Heterocyclic Compounds Catalyzed by Aluminum Chloride. *Carbon* **1977**, *15*: p. 9 - 16.

[83] Singer, L.S.; Lewis, R.T. Orientation of Mesophase in a Magnetic Field: Optical and Electron Spin Resonance Studies. *Carbon* **1973**, *11*: p. 675.

[84] Santamaría-Ramírez, R.; Romero-Palazón, E.; Gómez-de-Salazar, C.; Rodríguez-Reinoso, F.; Martínez-Saez, S.; Martínez-Escandell, M.; Marsh, H. Influence of Pressure Variations on the Formation and Development of Mesophase in a Petroleum Residue. *Carbon* **1999**, *37*: p. 445 - 455.

[85]   Marsh, H.; Menendez, R. Mechanisms of Formation of Isotropic and Anisotropic Carbons. In: *Introduction to Carbon Science*; Marsh, H., Ed.; Butterworths: London, UK, 1989; p. 37 - 73.

[86]   Greinke, R.A. Kinetics of Petroleum Pitch Polymerization by Gel Permeation Chromatography. *Carbon* **1986**, *24*: p. 677 - 686.

[87]   Greinke, R.A.; Singer, L.S. Constitution of Coexisting Phases in Mesophase Pitch during Heat Treatment: Mechanism of Mesophase Formation. *Carbon* **1988**, *26*: p. 665 - 670.

[88]   Loison, R.; Foch, P.; Boyer, A. *Coke: Quality and Production.* 2nd Edition; Butterworth & Co: London, UK, 1989.

[89]   Riggs, D.M.; Diefendorf, R.J. Effect of Heat Treatment on the Molecular Characteristics of Mesophase Forming Material. In: *Extended Abstracts 14th Biennial Conference of Carbon* **1979**, p. 413 - 414.

[90]   Billaud, F.; Chaverot, P.; Berthelin, M.; Freund, E. Thermal Decomposition of Aromatics Substituted by a Long Aliphatic Chain. *Industrial and Engineering Chemistry Research* **1988**, *27*: p. 1529 - 1536.

[91]   Alili, A.S.; Siddiquee, M.N.; De Klerk, A. Origin of Free Radical Persistence in Asphaltenes: Cage Effect and Steric Protection. *Energy and Fuels* **2020**, *34*: p. 348 - 359.

[92]   Gray, M. R.; McCaffrey, W. Role of Chain Reactions and Olefin Formation in Cracking, Hydroconversion, and Coking of Petroleum and Bitumen Fractions. *Energy and Fuels* **2002**, *16*: p.756 - 766.

[93]   Parsons, A.F. Radical Reactions. In: *Introduction to Free Radical Chemistry.* Blackwell Science: Oxford, UK, 2000, p. 61 - 95.

[94]   Brooks, J. D.; Taylor, G.H. The Formation of some Graphitizing Carbons. *Chemistry and Physics of Carbon* **1969**, *4*: p. 243 - 286.

[95]   Gasparoux, H. Carbonaceous Mesophase and Disc-like Nematic Liquid Crystals. *Molecular Crystals and Liquid Crystals* **1981**, *63*: p. 213 - 248.

[96]   Brooks, J.D.; Taylor, G.H. The Formation of Graphitizing Carbons from the Liquid Phase. *Carbon* **1965**, *3*: p. 185 - 193.

[97]   Marsh, H.; Latham, C.S. The Chemistry of Mesophase Formation. In: *Petroleum-Derived Carbons;* ACS Symposium Series: Washington, DC, 1986; p. 1 - 27.

[98]   Evans, S.; Marsh, H. The Chemistry of Formation of Semi-Cokes from Aromatic Systems using Mass Spectrometer - I. *Carbon* **1971**, *9*: p. 733 - 746.

[99]   Ihnatowicz, M.; Chiche, P.; Deduit, J.; Pregermain, S.; Tournant, R. Formation de la Texture des Cokes de Houilles et de Brais Etudiée par Solubilité et par Microscopie. *Carbon* **1966**, *4:* p. 41 - 50.

[100]   Collings, P.J.; Hird, M. *Introduction to Liquid Crystals: Chemistry and Physics*. Taylor & Francis Group: Boca Raton, FL, 2009.

[101]   Monthioux, M.; Oberlin, M.; Oberlin, A.; Bourrat, X.; Boulet, R. Heavy Petroleum Products: Microtexture and Ability to Graphitize. *Carbon* **1982**, *20*: p. 167 - 176.

[102]   Honda, H.; Kimura, H.; Sanada, Y.; Sugawara, S.; Furuta, T. Optical Mesophase Texture and X-ray Diffraction Pattern of the Early-Stage Carbonization of Pitches. *Carbon* **1970**, *8*: p. 181 - 182.

[103]   Lewis, I.C.; Edstrom, T. Thermal Reactivity of Polynuclear Aromatic Hydrocarbons. *The Journal of Organic Chemistry* **1963**, *28*: p. 2050 - 2057.

[104]   Rand, B. The Pitch-Mesophase-Coke Transformation as Studied by Thermal Analytical and Rheological Techniques. In: *Petroleum Derived Carbons*; ACS Symposium Series: Washington, DC, 1986, p.45 - 61.

[105]   Escobedo, J.; Mansoori, G.A. Viscometric Principles of Onsets of Colloidal Asphaltene Flocculation in Paraffinic Oils and Asphaltene Micellization in Aromatics. *SPE Production and Facilities* **1997**, *12*: p. 116 - 122.

[106]   Liu, Y.; Daum, P.H. Relationship of Refractive Index to Mass Density and Self-Consistency of Mixing Rules for Multicomponent Mixtures like Ambient Aerosols. *Journal of Aerosol Science* **2008**, *39*: p. 974 - 986.

[107]   Kurtz, S.S.; Ward, A.L. The Refractivity Intercept and the Specific Refraction Equation of Newton. I. Development of the Refractivity Intercept and Comparison with Specific Refraction Equations. *Journal of the Franklin Institute* **1936**, *222*: p. 563 - 592.

[108]   Rivolta, A.A. Molar Refractivity and Oxygen Solubility. MSc Thesis, University of Alberta, 2020.

[109]   Wen, Q.; Shen, J.; Gieleciak, R.; Michaelian, K.H.; Rohling, J.H.; Astrath, N.G.C.; Baesso, M.L. Temperature Coefficients of the Refractive Index for Complex Hydrocarbon Mixtures. *International Journal of Thermophysics: Journal of Thermophysical Properties and Thermophysics and its Applications* **2014**, *35*, p. 930 - 941.

[110]   Lipkin M.R; Kurtz, S.S. Temperature Coefficient of Density and Refractive Index for Hydrocarbons in the Liquid State. *Industrial and Engineering Chemistry – Analytical Edition* **1941**, *13*: p. 291 - 295.

[111]   Sachanen, A.N. *The Chemical Constituents of Petroleum*. Reinhold Publishing Corporation: New York, NY, 1945.

[112]   Dunstan, A.E. *The Science of Petroleum*. Oxford University Press: London, UK, 1938.

[113]   Pugmire, R.J.; Grant, D.M.; Zilm, K.W.; Anderson, L.L.; Oblad, A.G.; Wood, R.E. Carbon-13 Magnetic Resonance of Coal-Derived Liquids. *Fuel* **1977**, *56*: p. 295 - 301.

[114]   Mochida, I.; Nakamura, E.-I.; Maeda, K.; Takeshita, K. Carbonization of Aromatic Hydrocarbons IV. Reaction Path of Carbonization Catalyzed by Alkali Metals. *Carbon* **1976**, *14*: p. 123 - 129.

[115]   Bartle, K.D.; Martin, T.G.; Williams, D.F. Chemical Nature of a Supercritical-Gas Extract of Coal at 350 ºC. *Fuel* **1975**, *54*, p. 226 - 235.

[116]   Greinke, R.A. Quantitative Influence of Dealkylation and Polymerization Reactions on Mesophase Formation. *Carbon* **1990**, *28*: p.701 - 706.

[117]   Lewis, I.C.; Singer, L.S. Electron Spin Resonance and the Mechanism of Carbonization. *Chemistry and Physics of Carbon* **1984**, *17*: p. 1 - 79.

[118]   Lewis, I.C.; Singer, L.S. Electron Spin Resonance of Stable Aromatic Radical Intermediates in Pyrolysis. *Carbon* **1969**, *7*: p. 93 - 99.

[119]   Lewis, I.C.; Kovac, C.A. The Role of Free Radicals and Molecular Size in Mesophase Pitch. *Carbon* **1978**, *16*: p. 425 – 429.

[120]   Singer, L.S.; Lewis, I.C. ESR Study of the Kinetics of Carbonization. *Carbon* **1978**, *16*: p. 417 - 423.

3. Methodology

3.1. Introduction

It was explained in the introductory chapter (**Chapter 1**) that the study is focused on thermal conversion, as applied in visbreaking processes. It was also explained that the study would look more closely at the materials and changes in the materials with conversion. To facilitate the study, a series of thermal conversion experiments were performed that were designed to generate data that could be useful across all of the themes, namely, second phase formation, formation of aromatics, and relationships between properties as thermal conversion progresses.

The purpose of this chapter is to provide detail on the experimental methods used and that were applied to generate the materials used for the studies presented in **Chapters 5**, **6**, and **7**. A summary of the rationale behind those chapters is provided to give context to the methodology that is described in this chapter.

The formation of coke has been described as the result of the development of a mesophase (a phase with long-range crystallographic order) or a second phase. These structures can be considered the result of several types of reactions that take place during thermal conversion, but two of them are particular importance: cracking and aromatization/condensation [1]. The working hypothesis was that the thermally induced changes leading to coking would involve an increase in aromatic content in the visbroken products. Cookson et al. [2] proposed a relationship to determine the aromatic carbon content of a material by using its aromatic hydrogen content. It was of interest to determine whether this relationship applied to thermally converted materials, because hydrogen transfer is an important free radical reaction (see **Chapter 2**), and such a relationship would then provide a direct link between hydrogen transfer reactions and the formation of aromatics. This will be discussed in **Chapter 5**.

Several studies have linked the presence of a solubility class, asphaltenes, to the formation of coke [3-6] as they are considered to be precursors [7-10]. Nevertheless, there could be several factors

impacting coke formation other than a solubility class, those could include the reaction severity, the metal and heteroatoms content, the molecules' structure, and the thermolysis of weak bonds. Determining whether there is a relationship between coke content and asphaltene content in the visbroken samples could provide a description for the separation of a second phase at reaction condition. This will be discussed in **Chapter 6**. It will be noticed from the methodology, that asphaltenes content in the feed materials used for thermal conversion was a manipulated variable.

Kucora, et al. [11] described the formation of coke in a steam cracker unit employing light hydrocarbon fractions such as naphtha (<190 °C boiling) as feed material. This cut contains most of the light species in petroleum and it is considered to be asphaltene-free and coke-free. At the same time, as thermal conversion progresses the cracked naphtha is enriched in unsaturated molecules [12] that are susceptible to free radical addition reactions. Thus, coke can be formed even from light, asphaltene-free, and coke-free feed materials. Visbreaking, like steam cracking, is a thermal conversion process that involves free radical reactions. The cracking of molecules that are present in bitumen during thermal treatment forms unsaturated molecules. The combination of unsaturated molecules and free radicals appears to be the common denominator leading to coke formation. As a consequence, establishing relationships between the free radical content in the unconverted and thermally converted materials and their bulk properties could insights about the changes in nature of the species involved in thermal conversion and radical formation. This will be discussed in **Chapter 7**.

3.2. Experimental

3.2.1. Materials

A water-in-oil emulsion (W/O) obtained from CNOOC International (former Nexen Energy ULC) Long Lake Upgrader facility in the Anzac region, Alberta, Canada was used as raw feed material for this study. The characterization of the emulsion, as well as the procedure to remove water is described in **Chapter 4**.

After removing water from the emulsion, nearly water-free Athabasca bitumen was obtained. A sub-sample of the Athabasca bitumen was separated into two solubility fractions using *n*-heptane as solvent, with the maltenes being *n*-heptane soluble material and the asphaltenes being *n*-heptane insoluble material. The solubility fractions were obtained following a procedure based on the ASTM D3279-19 [13], but not following this standard test method. The separation was performed using a ratio of 1:60 (g/vol) of bitumen and *n*-heptane. They were both placed in a flask and stirred for one hour at 250 rpm and room temperature (approximately 20 ºC). The mixture was left in a fumehood for a contact time of 24 hours. Afterwards, the sample was filtered using a vacuum system with a 0.22 μm nitrocellulose filter paper. The filter paper was previously weighed in an aluminum pan, and both were weighed after filtration. The collected solids (asphaltenes) were placed in a fumehood for 48 hours for drying. The recovered liquid resulting from the filtration was collected in a round flask and placed into the rotary evaporator for four hours at 50 ºC and 12 kPa absolute pressure to recover the maltenes as nearly *n*-heptane free product. The characterization of the Athabasca bitumen, and its *n*-heptane solubility fractions is shown in **Table 3-1**.

Table 3-1. Athabasca bitumen and n-heptane solubility fractions characterization.

Property	Bitumen		Maltenes		Asphaltenes	
	x^a	s^a	x^a	s^a	x^a	s^a
Material Balance	100	0.6	81.4	0.6	18.6	0.6
Water content [wt. %]	0.6	0.1	-	-	-	-
Density [kg/m^3]						
20 ºC	1014.2	2.1	956.3	2.36	1145.0[b]	-
40 ºC	1001.6	2.2	944.4	0.25	1134.8[b]	-
60 ºC	988.6	2.6	931.0	0.26	1125.4[b]	-
Viscosity [Pa.s]						
20 ºC	2461.0	26.4	1.5	0.0	-	-
Refractive Index [nD]						
20 ºC	1.5791	0.0001	1.5391	0.0007	1.9210[b]	-
40 ºC	1.5716	0.0002	1.5327	0.0013	1.7839[b]	-
60 ºC	1.5641	0.0002	1.5282	0.0027	1.7104[b]	-
Elemental analysis [wt. %][c]						
Carbon	83.0	0.1	83.4	0.1	79.6	1.4
Hydrogen	10.3	0.0	10.9	0.1	8.0	0.2
Nitrogen	0.5	0.0	0.4	0.0	1.2	0.0
Sulfur	5.2	0.3	4.4	0.1	8.6	0.0
Oxygen[d]	1.0	0.2	1.0	0.2	2.6	1.6
Free Radical Content [spins/g][c,e]	1.6×10^{18}	-	1.1×10^{18}	-	3.4×10^{18}	-
Aromatic hydrogen content [%][c,f]	5.3	-	4.5	-	7.2	-
Aromatic carbon content [%][c,g]	28.4	-	23.3	-	43.4	-

[a] x denotes the average value of the measurements and s refers to the standard deviation of the measurements performed.
[b] Calculated from measurements performed on asphaltenes dissolved in toluene.
[c] Analysis performed on a single sample.
[d] Calculated by difference.
[e] On the basis of ESR calibration with 2,2-diphenyl-1-picrylhydrazyl (DPPH).
[f] Based on ^{1}H NMR analysis where aromatic H is defined as shift values higher than 6.3 ppm.
[g] Based on ^{13}C NMR analysis where aromatic C is defined as shift values higher than 120 ppm.

Several chemicals, cylinder gases, and calibration materials were employed to characterize and perform some of the experiments in this work and the list of materials is presented in **Table 3-2**.

Table 3-2. Materials used in this work.

Compound	Formula	CASRN	Mass fraction purity[a]	Supplier
Chemicals				
n-Heptane	C_7H_{16}	142-82-5	0.997[b]	Fisher Scientific
Carbon Disulfide	CS_2	75-75-0	0.9999[b]	Fisher Scientific
Deuterated Chloroform	$CDCl_3$	865-49-6	0.998[b]	Acros Organic
Toluene	C_7H_8	108-88-3	0.998[b]	Fisher Scientific
Chloroform	$CHCl_3$	67-66-3	0.998 [b]	Fisher Scientific
Methylene Chloride	CH_2Cl_2	75-09-2	$\geq$0.995 [b]	Fisher Scientific
Methanol	CH_3OH	67-56-1	0.999 [b]	Fisher Scientific
Cyclohexane	C_6H_{12}	110-82-7	$\geq$0.99[b]	Fisher Scientific
Tetrahydrofuran	C_4H_8O	109-99-9	$\leq$ 0.999[b]	Fisher Scientific
Hydranal® composites 1	-	-	-	Fluka
Chromium (III) acetylacetonate	$C_{15}H_{21}CrO_6$	21679-31-2	0.999[b]	Aldrich
Cylinder gases				
Nitrogen	N_2	7727-37-9	0.99999[b]	Praxair
Helium	He	7440-59-7	0.99999[b]	Praxair
Air	O_2/N_2 mix	13229-10-0		Praxair
Calibration Materials				
Reference Material 5010	-	-	-	Supelco
Polywax 655	-	-	-	Agilent

[a]Purity of the material guaranteed by the supplier.
[b]Mole fraction purity.

3.2.2. Reactions

Visbreaking reactions were performed in a Swagelok 316 stainless steel microbatch reactor (Outside Diameter – OD - 0.025 m and 0.16 m length). To discard any effect from the reactor's wall in the reaction, a glass vial (OD 0.02 m and 0.15 m long) was inserted into the reactor. The

reactor had a pressure gauge with a reading range of 0 to 35,000 kPa. The reaction setup used in this work is shown in **Figure 3-1a**, additional details about the reactor (i.e., dimensions) are shown in **Figure 3-1b**.
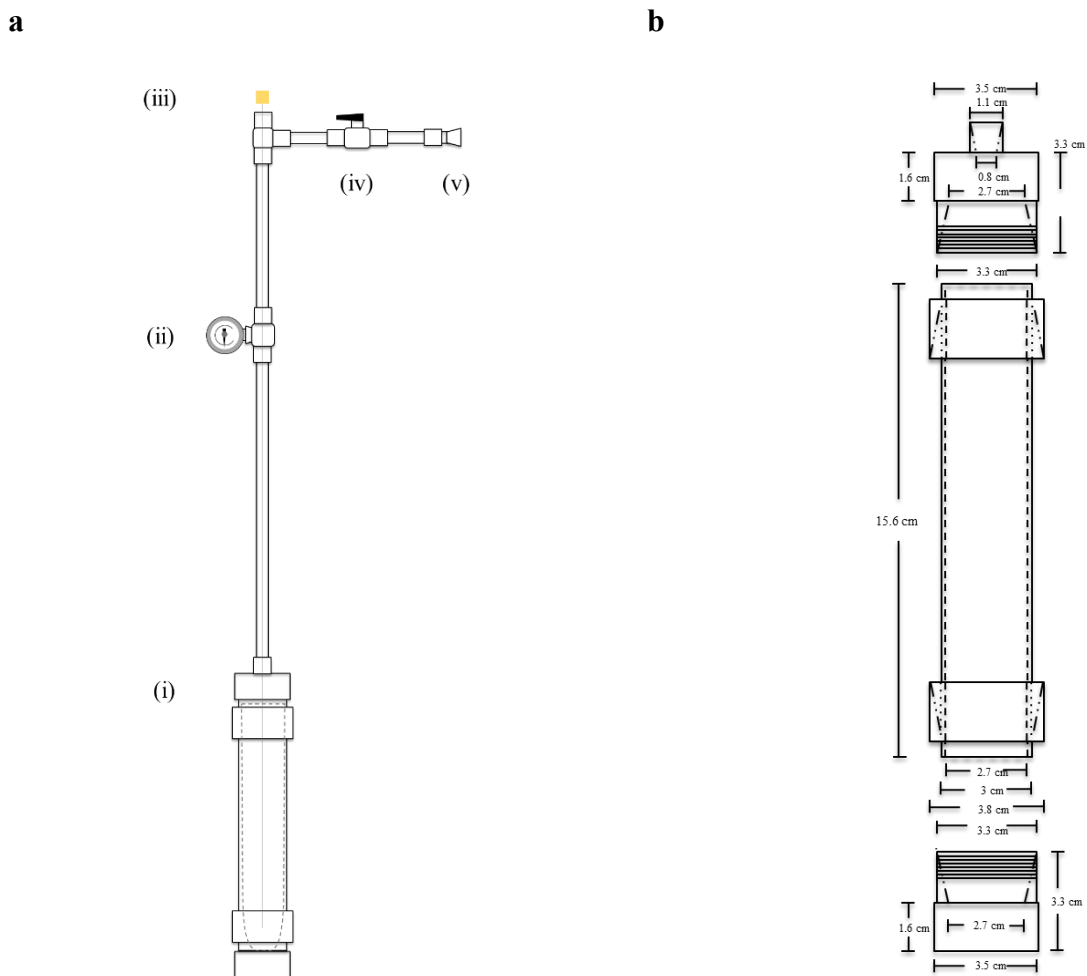
Figure 3-1. Thermal conversion reaction setup (a): Numbered elements correspond to: (i) Reactor, (ii) Pressure gauge, (iii) Thermocouple, (iv) Ball valve, (v) Quick-connector; reactor's dimensions (b), redrawn from [14].

To evaluate the effect of *n*-heptane insolubles (asphaltenes) on visbreaking, feed materials with different concentrations of asphaltenes were used. The feed materials were prepared from one or more of the bitumen-derived materials listed in **Table 3-1**. The feed materials and how they were prepared, are summarized in **Table 3-3**. It is worth noting that the 0 wt. % concentration of

asphaltenes refers to maltenes. On the other hand, the concentration of 18.6 wt. % asphaltenes corresponds to bitumen.

Table 3-3. Feed materials used for thermal conversion in this study.

Asphaltene Concentration [wt. %]	Bitumen [wt.%]	Asphaltenes [wt.%]	Maltenes [wt.%]
0	0	0	100
9	0	9	91
18.6	10	0	0
28	89	11	0

When mixtures were used (i.e., maltenes + asphaltenes, and bitumen + asphaltenes), the feed material was sonicated for 30 minutes to guarantee better dispersion of the asphaltenes in the maltenes or bitumen.

In a typical thermal conversion experiment, the total amount of sample added to a glass vial using a spatula for each reaction was approximately 12 g. The glass vial was weighed before and after adding the sample to it. The balance used was a Mettler Toledo XS 105 with a capacity of 120 g and 0.0001 g readability in the mass range used. The reactor was weighed empty and then the glass vial containing the sample was placed inside the reactor. The reactor was weighed one more time, the weights at each step were recorded. The reactor was closed and pressurized with nitrogen at 2 MPa gauge to ensure that there were no leaks in the system. The pressure was released and the process of pressurizing and depressurizing the reactor was repeated three times to purge the reactor of most of the oxygen. The reactor was then pressurized one more time with nitrogen at 2 MPa gauge and its weight was recorded. The weights involving the reactor were obtained using a Mettler Toledo MS6001S balance with a capacity of 6,200 g and a readability of 0.1 g in the mass range used.

To carry out the reactions, the pressurized reactor was placed inside a fluidized sand bath heater (Omega fluidized bath FSB-3) that was preheated at the desired reaction temperature (380 ºC). The reactor's inside temperature was monitored using a thermocouple and a thermocouple reader.

Once the reactor reached 380 ºC, the reaction time was started. To evaluate the effect of reaction time, 5 different reaction times were considered, i.e., 0 min, 5 min, 10 min, 47 min, and 146 min. After the reaction time was completed, the reactor was removed from the sand bath and cooled down to room temperature. The temperature during the entire process (heating, isothermal reaction and cooling step) was recorded in intervals of 30 seconds in order to obtain the temperature profile with respect to time over the duration of the experiment. The time-dependent temperature profile was employed to calculate an equivalent residence time at 380 °C (see **Section 3.2.4.1**). The pressure inside the reactor was monitored using the pressure gauge, the internal pressure at reaction temperature was recorded.

Once the reactor reached room temperature, the reactor's weight was again recorded. At this temperature, the gaseous products resulted from the visbreaking reaction were then collected using a gas bag. The gaseous samples were analyzed using a gas chromatograph (Agilent 7820A). The results of these analyses (**Appendix A**) were not considered trustworthy, because of potential condensation in of some of the gas bags. These were not critical to the study since the focus was placed on the liquid products and the quantification of any resulted solids. No further effort was made to resolve the issues with the gas analyses.

The weight of the depressurized reactor was recorded. After this, the reactor was opened inside the fumehood to recover the visbroken product. 100 mL of CS_2 were used to recover material from the reactor. A small quantity of the specified amount of carbon disulfide was used to rinse the inside of the reactor. No visible material was remaining inside the reactor or the glass vial after transferring the resulted liquid into a glass container. Carbon disulfide was chosen as solvent due to its higher solubility parameter (20.3 MPa$^{0.5}$ [15]) compared to *n*-heptane (15 MPa$^{0.5}$ [15]), which is beneficial for the solubility separation of coke. In addition, coke can be further classified into carbenes (material soluble in CS_2) and carboids (insoluble material in CS_2), which was of interest as a separate solubility class.

In order to separate the liquid and solid products, a vacuum filtration setup was used. An aluminum pan and a filter paper (0.22 μm Millipore nitrocellulose membrane filter) were weighed. The system was prepared by placing a filter paper in the glass frit membrane support. Once the

separation was completed, the filter paper was removed from the filtration system and placed back into the aluminum pan. The solid material collected in the filter paper was left inside the fumehood for 48 hours to allow the evaporation of any remaining solvent. After that period, the aluminum pan containing the filter paper and the solid material were then weighed. The liquid product was heated using a rotary evaporator under 0.04 MPa, 40 °C and 50 rpm for 50 minutes. Every step in the process involved weighing and recording weight of the sample and the elements to collect the different samples.

SAFETY NOTE

The flashpoint of CS_2 is -30 °C, and its autoignition temperature is 100 °C [16]. *Hence, special care should be taken to keep the carbon disulfide from any potential ignition source and to guarantee a proper temperature control.*

The characterization of the visbroken products is detailed in **Chapters 5** and **0**. The description of the techniques used to characterize the visbroken products is found in **Section 3.2.3**.

3.2.3. *Analyses*

3.2.3.1. Asphaltene content

The asphaltene solubility fraction of the visbroken samples was determined using the procedure described in **Section 3.2.1**. The same procedure was applied for asphaltenes separation of thermally converted samples.

3.2.3.2. Density measurements

Density measurements were performed using an Anton Paar Model DMA 4500M. The equipment was calibrated with ultra pure water (standard provided by Anton Paar) and its temperature uncertainty was 0.01 °C. The liquid samples were injected into the equipment using a

polypropylene syringe (Luer-Lok syringe). For the cases where the sample was too viscous, the material was heated up to 60 ºC for about 15 minutes. The sample was then fluid enough to be injected into the density meter.

Density measurements were performed at three different temperatures: 20, 30, 40, and 60 ºC. This was done to enable the calculation of the temperature dependence of density.

In the case of asphaltenes that were solids at ambient conditions, the sample was diluted in toluene. Different concentrations of asphaltenes in toluene were prepared and the density of each mixture was measured. The calculation used to estimate the density of the asphaltenes from the measurement of the diluted samples is shown in **Equation (3-1)**. These calculations assumed that the volume of the asphaltenes and the volume of toluene were additive [17]. The application of regular solution theory is then possible when the additional assumption is made that the excess volume is zero.

$$\frac{1}{\rho_{Asph+S}} = \frac{w_S}{\rho_S} + \frac{w_{Asph}}{\rho_{Asph}} \tag{3-1}$$

Where ρ_{Asph} is the density of the asphaltenes in kg/m^3, w_{Asph} and w_S are the mass fractions of asphaltenes and solvent, respectively, ρ_{Asph+S} is the density of the diluted asphaltenes (measured) in kg/m^3, and ρ_S is the density of the solvent (toluene) in kg/m^3.

The density of toluene at the indicated temperatures (20, 30, 40, and 60 ºC) was measured and it is reported in **Table 3-4**. These measurements were for the toluene used for dilution.

Table 3-4. Measured density of toluene at different temperatures.

Temperature [ºC]	Density [kg/m^3]
20	866.91
30	857.63
40	848.26
60	829.25

3.2.3.3. Refractive index measurements

The refractive index was measured using an Anton Paar Abbemat 200 that uses the sodium D-line (589 nm). The equipment's calibration was checked through an air-check test. The visbroken samples were placed into the equipment using a spatula, making sure the sample was covering the prism. Similar to density measurements, refractive index of asphaltenes was determined by diluting the asphaltene sample in toluene at different concentrations. The measurements were performed at three different temperatures: 20, 30, 40, and 60 °C with an uncertainty of 0.05 °C.

Similar to what was done in **Section 3.2.3.2**, asphaltenes were diluted in toluene as they are solids at ambient conditions. Different concentrations were prepared, and the refractive index of each mixture was measured. The calculation of the refractive index of the asphaltenes was performed using **Equation (3-2)**. These calculations assumed that the volume of the asphaltenes and the volume of toluene were additive [17]. As it was assumed that no significant change in volume took place, the refractive index of the mixture was considered to be approximated the refractive index function [18].

$$RI_{Asph+S} = \left[\left(RI_S \cdot \frac{w_S}{\rho_S} \right) + \left(RI_{Asph} \cdot \frac{w_{Asph}}{\rho_{Asph}} \right) \right] \cdot \rho_{Asph+S} \tag{3-2}$$

Where RI_{Asph+S} is the refractive index of the diluted asphaltenes (measured), RI_S and RI_{Asph} are the refractive index of the solvent and the asphaltenes, respectively; w_S and w_{Asph} are the mass fractions of the solvent and the asphaltenes, respectively; ρ_{Asph+S} is the density of the diluted asphaltenes (measured) in kg/m³, and ρ_S and ρ_{Asph} are the density of the solvent (toluene) and the asphaltenes, respectively in kg/m³.

As employed, the implication is that RI can be sufficiently well approximated by the refractive index instead of using a refractive index function, such as that of Eykman or Lorenz–Lorentz. A further assumption inherent in **Equation (3-2)** is that the volume fractions calculated from the mass fractions are representative of the molar volume fractions.

The refractive index of toluene was measured at different temperatures (20, 30, 40, 60 ºC) and the values are shown in **Table 3-5**.

Table 3-5. Measure refractive index of toluene at different temperatures.

Temperature [ºC]	Refractive index [nD]
20	1.4970
30	1.4913
40	1.4856
60	1.4741

3.2.3.4. Electron Spin Resonance (ESR)

ESR measurements were carried out in an Active Spectrum Micro-ESR. The samples were prepared by dissolving 20 mg of sample into 600 µL of toluene. The mixture was transferred to a 5 mm diameter PQ quartz tube. The parameters of the equipment to perform the analysis were 9.6×10^9 Hz, microwave power of 15 mW, 1.2 Gauss coil amplitude and a digital gain of 12 dB. The analysis was conducted at room temperature ($\sim$ 20 ºC). The instrument has a detection limit of 10^{16} spins/g and a quantification limit of 3×10^{16} spins/g.

In order to quantify the amount of free radicals in the sample, a calibration curve was prepared with a mixture of 2,2-diphenyl-1-picrylhydrazyl (DPPH) and toluene. The equation obtained from the calibration (**Equation (3-3)**) and used to determine the free radical content in the samples was the same as reported in [19].

$$C_{Free\ radical} = a \cdot A_{ESR\ double\ integral} + b \qquad (3\text{-}3)$$

Where C is the concentration of free radicals in µmol/mL, A is the area of the double integral obtained from the ESR spectrum, a and b are constants associated with calibration using DPPH (1.99×10^{12}, and 3.37×10^{16}, respectively).

3.2.3.5. Nuclear Magnetic Resonance (NMR)

^{1}H NMR and ^{13}C NMR analyses used an Agilent/Varian Innova 400 MHz spectrometer equipped with a 9.395 Tesla magnet. The spectra were recorded at 400 MHz for hydrogen, and at 100.58 MHz for carbon. The difference in resonance frequencies employed affects the resolution. These analyses were performed at the Chemistry Department of the University of Alberta.

For ^{1}H NMR, the samples were prepared with 0.15 g of sample dissolved into 0.70 mL of deuterated chloroform. Once the sample was dissolved, it was placed in 5 mm diameter NMR tubes. Each spectrum was obtained by performing 16 scans per sample between −1 and 11 ppm. The aliphatic region in this study was set within 0.4 to 3.6 ppm, and the aromatic region 6.0 to 9.0 ppm to match the values used by Cookson, et al. [2], which is explained in **Chapter 5**.

The sample preparation for ^{13}C NMR required that 0.35 mL of the oil sample and 0.35 mL of a 0.2 mM chromium (III) acetylacetonate solution in deuterated chloroform. The use of a paramagnetic relaxation agent such as chromium (III) acetylacetonate ($Cr(acac)_3$) [20] is a common practice to reduce all of the spin-lattice relaxation times and level all of the NOE (nuclear Overhauser effect) factors, leading to a more quantitative spectrum [21] and accelerate the relaxation process. Once the sample was homogeneous, it was transferred to a 5 mm diameter NMR tube. Each sample was scanned 2000 times within −10.0 to 270.0 ppm with an acquisition time of 0.5 s and a relaxation time of 2 s. The relaxation times were considered to be sufficient based on the characteristics of the sample determined by the NMR facility at the University of Alberta. In addition, it was observed from the Free Induction Decay (FID) of the samples that 0.5 s for the acquisition time is an appropriate value for recording the generated signal for this type of sample (i.e., bitumen and bitumen-related samples). The aliphatic and aromatic region were defined as 2.5 to 60.0 ppm, and 110 to 160 ppm, respectively. These values were selected to match the values used by Cookson, et al. [2], which is explained in **Chapter 5**.

3.2.3.6. Simulated Distillation

Simulated distillation was used to obtain the boiling point distribution of the feed and the visbroken products. The instrument employed was an Agilent 7890B high temperature gas chromatograph equipped with a flame ionization detector (FID) and a DB-HT SimDis column (5 m × 0.53 mm × 0.15 μm, length × inner diameter × film thickness). The procedure followed was in accordance with the ASTM D7169 standard method [22].

In a 10 mL volumetric flask, about 0.1 g of sample were added and dissolved in 10 mL of carbon disulfide. The weights of the volumetric flask, the sample and the solvent were obtained using a Mettler Toledo XS 105 balance (capacity of 120 g and 0.0001 g readability in the mass range used) and recorded. Reference material 5010 and Polywax 655 were used to determine the detector response factor and the retention time calibration, respectively. A blank (carbon disulfide) was run after each standard or sample to guarantee that there was no carryover from previous samples.

3.2.3.7. Elemental analysis

Elemental analyses were performed by the Analytical and Instrumentation Laboratory at the Chemistry Department at the University of Alberta using a Thermo Flash CHNS-O analyzer. In a typical analysis, the sample is placed in a tin (Sn) cup and then dropped into a vertical quartz tube (combustion reactor) maintained at 1000 °C with helium flowing continuously as carrier gas. The quartz tube is filled with an oxidation catalyst (WO_3 on alumina) at the top and reduced copper wires at the bottom. Then, a small and fixed volume of oxygen is added to the carrier gas (Helium). The combustion takes place, and the carbon, hydrogen, nitrogen and sulfur are quantitatively converted into CO_2, H_2O, and SO_x that are swept through the chromatographic column (Porapak QS, 4 mm ID, 2 m long) by the carrier gas. NO_x was decomposed and swept by the carrier gas. The Thermal Conductivity Detector (TCD) detects the individual gases and the conversion of the output signal into a chromatogram is achieved using Eager Xperience software. A calibration curve is obtained from organic analytical standards which is used to quantify the gases of the analysis. Calibration is carried out every four samples to monitor the accuracy of the analysis.

3.2.4. Calculations

3.2.4.1. Equivalent Residence Time (ERT)

The concept of ERT, as employed by Yan [23], was used to express the severity of the thermal treatment (visbreaking) process. The modified expression to calculate ERT [24] accounts for all the temperature segments involved during the reaction (i.e., heat-up, isothermal, and cool-down). **Equation (3-4)** shows the expression used to calculate the ERT.

$$ERT_{at\ T_{ref}} = \sum_{i=1}^{n} \Delta t_i \cdot exp\left[\left(-\frac{E_a}{R}\right)\left(\frac{1}{T_i} - \frac{1}{T_{ref}}\right)\right] \tag{3-4}$$

Where the reference temperature T_{ref} can be selected as appropriate; a reference temperature of 380 °C was employed. The activation energy E_a is 209,500 J/mol, which is the value used by Yan [23], and the constant R is 8.314 J/(mol · K). Where n refers to the temperature segment (i.e., heating, cooling and isothermal), Δt_i, in seconds, represents the time at the temperature segment, and T_i is the temperature at the time segment in K. Both ERT and $t_{residence}$ are in seconds.

As it was mentioned, **Equation (3-4)** is a modified version of the one employed by Yan [23] since it was necessary to account for the non-isothermal segments of the reaction. It was discussed in [24] that the feed experiences changes during the heating up and cooling down periods. It is important to note at the reaction temperature used in this study, the applicability of the expression is at its threshold [25]. Nevertheless, the calculations were done using the above-mentioned expression due to the lack of an alternate strategy to account for the non-isothermal segments.

3.2.4.2. Material balance

The material balance of the visbroken products were determined by the difference between the initial mass (feed) and the final mass (product) of the reaction. The material balance was reported in terms of percentages.

As it was indicated in **section 3.2.2**, weights were recorded at every step of the reaction process. The initial mass (*i*) for each experiment was defined as the sum of the feed material mass loaded into the reactor (m_{feed}) and the mass of nitrogen used to pressurize the reactor ($m_{nitrogen}$). For the cases where a mixture was used as feed material (maltenes + asphaltenes, and bitumen + asphaltenes), the sum of both components was considered m_i.

On the other hand, the final mass (*f,r*) was defined as the sum of the masses of the resulted product (m_p) and the gas (nitrogen and any gaseous material resulting from the reaction), m_g after opening the reactor. Hence, the material balance after reaction is reported in **Table B-1** (**Appendix B**) and it can be expressed as **Equation (3-5)**:

$$\left(m_{feed} + m_{nitrogen}\right)_i = \left(m_p + m_g\right)_{f,r} \tag{3-5}$$

To recover the liquid products from the reactor, the samples were diluted with 100 mL of carbon disulfide. The solvent was also used to rinse the thermocouple that was inserted into the reactor, as a small amount of sample was on it. The diluted sample was then filtered to recover the solid material in the sample (m_s). The filtered liquid was placed in the rotary evaporator to remove the carbon disulfide and obtained the resulted liquid product (m_l). By measuring the weight of the sample flask, the extent of solvent removal from the diluted sample was monitored. It was found that all the solvent could be removed. Additionally, the characteristic smell of the solvent was absent from samples after the solvent was removed. These values were considered to calculate the material balance closure for each reaction was using **Equation (3-6)**. The values were reported in **Chapter 6**, and they are also summarized in **Table B-1**.

$$Material\ balance\ closure\ [\%] = \frac{\left(m_l + m_s + m_g\right)_f}{\left(m_{feed} + m_{nitrogen}\right)_i} * 100 \tag{3-6}$$

For example, for the thermal conversion reaction using maltenes as feed (0 wt. % of asphaltenes) performed at 380 ºC and 0 minutes (nominal residence time), it is noted in **Table B-2** (**Appendix B**) that the initial mass is 13.03 g and the final mass is 12.90 g. The calculation for material balance

closure using **Equation (3-6)** gives 99 % as a result. The reactor's pressure during visbreaking reactions is also included in **Table B-2**.

References

[1]   Loison, R.; Foch, P.; Boyer, A. *Coke: Quality and Production.* 2nd Edition; Butterworth & Co: London, UK, 1989.

[2]   Cookson, D.J.; Lloyd, C.O.; Smith B. E. A Novel Semi-Empirical Relationship between Aromaticities Measured from ^{1}H and ^{13}C N.M.R. Spectra. *Fuel* **1986**, *65*: p. 1247 - 1253.

[3]   Rahimi, P.; Gentzis, T.; Dawson, W.H.; Fairbridge, C.; Khulbe, C.; Chung, K.; Nowlan, V.; DelBianco, A. Investigation of Coking Propensity of Narrow Cut Fractions from Athabasca Bitumen using Hot-Stage Microscopy. *Energy and Fuels* **1998**, *12*: p. 1020 - 1030.

[4]   Rahimi, P.; Gentzis, T.; Taylor, E.; Carson, D.; Nowlan, V.; Cotté, E. The Impact of Cut Point on the Processability of Athabasca Bitumen. *Fuel* **2001**, *80*: p. 1147 - 1154.

[5]   Wiehe, I.A. A Phase-Separation Kinetic Model for Coke Formation. *Industrial and Engineering Chemistry Research* **1993**, *32*: p. 2447 - 2454.

[6]   Wiehe, I.A.; Kennedy, R.J. Oil compatibility model and crude oil incompatibility. *Energy and Fuels* **2000**, *14*: p. 56 - 59.

[7]   Rahmani, S.; McCaffrey, W.; Gray, M.R. Kinetics of solvent interactions with asphaltenes during coke formation. *Energy and Fuels* **2002**, *16*: p. 148 - 154.

[8]   Gonçalves, M.L.A.; Ribeiro, D.A.; Teixeira, A.M.R.F.; Teixeira, M.A.G. Influence of Asphaltenes on Coke Formation during the Thermal Cracking of Different Brazilian Distillation Residues. *Fuel* **2007**, *86*: p. 619 - 623.

[9]   Trejo, F.; Ancheyta, J.; Noyola, A.; Sámano, V. Cracking of Maya Crude Asphaltenes. *Petroleum Science and Technology* **2014**, *32*: p. 2592 - 2598.

[10]   Maity, S.K.; Centeno, G.; Ancheyta, J. Experimentation with Heavy Oil in Batch Reactors. In *Experimental Methods for Evaluation of Hydrotreating Catalysts*; Ancheyta, J., Ed; Wiley: Hoboken, NJ, 2020, p. 97 - 119.

[11]   Kucora, I.; Paunjoric, P.; Tolmac, J.; Vulovic, M.; Speight, J.G.; Radovanović, L.Z. Coke Formation in Pyrolysis Furnaces in the Petrochemical Industry. *Petroleum Science and Technology* **2017**, *35*: p. 213 - 221.

[12]   Reyniers, G.C.; Froment, G.F.; Kopinke, F.D.; Zimmermann, G. Coke Formation in the Thermal Cracking of Hydrocarbons. 4. Modeling of Coke Formation in Naphtha Cracking. *Industrial and Engineering Chemistry Research* **1994**, *33*: p. 2584 - 2590.

[13]   *ASTM D3279: Standard Test Method for n-Heptane Insolubles*; ASTM International: West Conshohocken, PA, 2019.

[14]   Yañez Jaramillo, L.M. Visbreaking of Oilsands Bitumen between 150 and 300 ºC. M.Sc. Thesis, University of Alberta, 2016.

[15]   Wiehe, I.A. *Process Chemistry of Petroleum Macromolecules*; CRC Press: Boca Raton, FL, 2008.

[16]   Hawley, G.G. *The Condensed Chemical Dictionary*. 8th Edition. Van Nostrands Reinhold: New York, NY, 1971.

[17]   Guan, J. G.; Kariznovi, M.; Nourozieh, H.; Abedi, J. Density and Viscosity for Mixtures of Athabasca Bitumen and Aromatic Solvents. *Journal of Chemical Engineering Data* **2013**, *58*: p. 611 - 624.

[18]   Wattana, P.; Wojciechowski, D.J.; Bolaños, G.; Fogler, H.S. Study of Asphaltene Precipitation using Refractive Index Measurement. *Petroleum Science and Technology* **2003**, *21*: p. 591 - 613.

[19]   Tannous, J. H.; De Klerk, A. Quantification of the Free Radical Content of Oilsands Bitumen Fractions. *Energy and Fuels* **2019**, *33*: p. 7083 - 7093.

[20]   Shoolery, J.N. Some Quantitative Applications of ^{13}C NMR Spectroscopy. *Progress in Nuclear Magnetic Resonance Spectroscopy* **1977**, *11*: p. 79 - 93.

[21]   Silverstein, R.M.; Webster, F.X.; Kiemle, D.J. *Spectrometric identification of organic compounds.* 7th Edition; John Wiley & Sons: Hoboken, NJ, 2005.

[22]   *ASTM D7169: Standard test method for boiling point distribution of samples with residues such as crude oils and atmospheric and vacuum residues by high temperature gas chromatography*; ASTM International: West Conshohocken, PA, 2020.

[23]   Yan, T. Y. Characterization of Visbreaker Feeds. *Fuel* **1990**, *69*: p. 1062 - 1064.

[24]   Yan, Y.; De Klerk, A.; Prado, G. H. C. Visbreaking of Vacuum Residue Deasphalted Oil: New Asphaltenes Formation. *Energy and Fuels* **2020**, *34*: p. 5135 - 5147.

[25]   De Klerk, A. Thermal Conversion Modeling of Visbreaking at Temperatures below 400 °C. *Energy and Fuels* **2020**, *34*: p. 15285 - 15298.

4. Comparison of laboratory techniques for recovering oilsands bitumen from bitumen-and-water emulsions

4.1. Introduction

The geological origin and the geographical conditions give to Canadian Oilsands reservoirs very particular characteristics. Due to the nature of these deposits, the extraction process could be primarily through mining (oilsands deposit near to the surface) or in situ subsurface recovery such as steam-assisted gravity drainage as discussed in **Chapter 2**. Irrespective of the method of recovery, processing of the oilsands involves water, leading to the formation of an emulsion phase. These emulsions tend to be highly stable, usually due to the presence of natural stabilizers such as fine solids and surface-active organic species in asphaltenes that retard or prevent the coalescence of water droplets and the subsequent water separation from the emulsion [1].

During the separation process, the formation of a layer at the oil-water interface is frequently observed. This layer may contain emulsified water and/or oil, asphaltenes, ions, clays, and other mineral solids [2]. The presence of a solvent that increases the asphaltenes mobility will create a less rigid interface and hence the emulsion will be less stable [3]. Industrially the addition of a solvent to assist with separation is employed in processes such as froth treatment and solvent deasphalting [4,5] (see **Chapter 2**).

Strong bitumen-and-water emulsions also present a challenge to those conducting laboratory investigations, since industrial samples are seldom free of water. The present study is aimed at this community for whom water removal from bitumen-and-water emulsions might be the first practical hurdle to overcome, as it was in this thesis.

In order to recover bitumen from a bitumen-and-water emulsion, different separation techniques were evaluated. Methods investigated included centrifugation, centrifugation with solvents, liquid–liquid extraction, and rotary evaporation. The advantages, disadvantages, and practical considerations associated with each method will be discussed.

4.2. Experimental

4.2.1. Materials

The feed material used is a bitumen-and-water emulsion industrially produced at the Long Lake SAGD (Steam-Assisted Gravity Drainage) facility, located near Anzac, Alberta in the Athabasca Oilsands region. The characterization of the emulsion is shown in **Table 4-1**. The material contains 20.3 ± 2.9 wt% of emulsified water measured 7 times using a Karl Fischer titrator; the value agrees with the 20.5 wt. % obtained by thermogravimetric analysis (TGA) as internal check. The typical emulsion obtained from a SAGD operation contains between $8 - 33$ wt.% of water [6]. These values for the material employed in this study were therefore within the range of typical SAGD operation.

Table 4-1. Characterization of the emulsion.

Property	Emulsion	
	x	s
Water Content by Karl Fischer titration [wt.%]	20.3	2.9
Water Content by TGA [wt.%][a]	20.5	-
nC$_5$ insolubles [wt.%][b,c]	17.2	3.4
nC$_7$ insolubles [wt.%][b,c]	15.4	2.3
Free Radical Content [spins/g][a]	1.2×10^{18}	-
H$_{Ar}$ [%][a]	1.7	-
Refractive Index[a]		
20	1.5709	-
40	1.5625	-
60	1.5544	-
dn/dT [1/K]	-4.1×10^{-4}	-
Density [kg/m^3][a]		
20	1006.1	-
40	995.0	-
60	983.4	-
dρ/dT [kg/m^3.K]	-0.6	-
Mineral Matter [wt.%][a]	5.1	-

[a] Analysis performed to a single sample
[b] wt.% = mass of asphaltenes per mass of emulsion
[c] Analysis performed to three samples

Other materials employed in this study were the solvents toluene (99.8%), chloroform (99.8%), methylene chloride (≥ 99.5%), methanol (99.9%), cyclohexane (≥ 99%), and tetrahydrofuran (≥ 99.9%). They were obtained commercially from Fischer Scientific. Additionally, Hydranal® composite 5 obtained from Fluka was used in the determination of water content by Karl Fischer titration.

4.2.2. Methods

4.2.2.1. Centrifugation

Centrifugation is one of the methods suggested to remove water from bitumen-and-water emulsions [7,8]. To evaluate this method an Eppendorf 5430 centrifuge was used. The amount of emulsion placed in each centrifugation tube (polyethylene terephthalate tube with conical shape at the bottom, outside diameter of 17 mm and l9 mm of length) was approximately 5.1 g. To avoid imbalance during centrifugation, the difference in weight between tubes was maximum 0.1 g, and tubes were placed across each other in the sample holder. The conditions for the separation that were evaluated included different rotational speeds, 1000, 2500, and 4100 revolutions per minute (rpm), and centrifugation times, 15, 30, 60, and 90 min. The centrifugation was performed at room temperature (21 °C). After centrifugation the separated water phase was removed from the centrifugation tube using a glass pipet. The water content of the bitumen-containing phase after centrifugation was determined by a volumetric Karl Fischer titration. As described in the analysis section, the Karl Fischer titration employed a modification for bitumen [9], which employed a different solvent than normally used. The measurements were performed four times. All phases were weighed using a Mettler Toledo XS105 dual range analytical balance with a readability of 0.01 mg. Water balance closure was calculated and thermogravimetric analysis (TGA) was performed as internal check.

4.2.2.2. Centrifugation + solvent

Adding solvent to the emulsion to reduce the viscosity of the bitumen-containing phase may help breaking it, although it would add an additional step for solvent removal once the water has been removed. Including this step to the centrifugation process may facilitate the water removal during centrifugation. A mixture of bitumen-and-water emulsion and solvent (i.e., cyclohexane, toluene, methylene chloride, chloroform, and methanol) at different solvent concentrations were prepared in a centrifugation tube. The centrifugation tube characteristics were given in the previous section. The mixtures were placed on an Eppendorf 5430 centrifuge to separate the emulsion. The amount of sample was approximately 5 g, with solvent concentrations of 5, 10, and 25 wt. %. The

maximum weight difference between tubes was 0.1 g. The separation took place at 2500 rpm for 90 min at room temperature. Similarly, the water content was measured using a Karl Fischer titrator and TGA measurements were done as internal check.

4.2.2.3. Liquid-liquid extraction

This separation process relies on the solvent solubility of water in the solvent used. This is another strategy to attempt the water separation from the emulsion. Two different solvents were used in order to achieve the bitumen-and-water emulsion separation. They were chosen based on their solubility, methanol is characterized for its low miscibility in oil [10] (in this case, bitumen), and cyclohexane was selected due to its low miscibility in water [11]. Solvent and emulsion were added in equal quantities (approximately 103 g of each component) to the glass separating funnel, the mixture was in contact for 24 hours. No agitation was involved. After this time, the resultant phases were separated, collected and weighed to determine the degree of separation achieved. Additionally, water content was measured using a Karl Fischer titrator and TGA measurements were done as internal check.

4.2.2.4. Rotary evaporation

The bitumen-and-water emulsion separation was performed in a rotary evaporator (rotovap) Heidolph Hei-VAP advantage. The operating principle of the equipment is based on a single equilibrium stage vapor-liquid separation. The low pressure (vacuum) used in the rotovap lead to a lowering of the boiling point temperature of the solvent. The temperature of the oil bath was set at 110 ºC and the vacuum pressure was set at 0.04 MPa absolute. The condenser temperature was 4 ºC with continuous cooling liquid (1:1 mixture of water and ethylene glycol) circulation using a Julabo heater/chiller attached to this equipment. The rotation of the evaporating flask was set at 75 rpm, the rotation increases the surface area of the liquid–vapor interface and helps to increase the evaporation rate. The maximum amount of sample that was placed in the flask was 200 g. The duration of each experiment was on average 82 hours. At the end of this period the vacuum was broken and the evaporating flask was removed to collect the oil extracted from the emulsion. Then the condenser was removed to recover the water from the separation process. The two phases were

weighed and the water content in the bitumen phase after separation was determined using a Karl Fischer titrator and as internal check TGA measurements were performed.

4.2.3. Analyses

The water content in the system was determined by Karl Fischer titration using a Karl Fischer Titrator (Mettler Toledo KF titrator V20S) with a DM-143 SC electrode. The measurements were performed using a modified methodology [9] to measure water content in bitumen and vacuum residua with THF as solvent. The equipment is filled with the solvent (THF) and later neutralized it with Hydranal composite 5. The measurement of the water content of samples was preceded by a blank measurement, which consisted of adding 1 mL of THF to the system. The titration then starts by adding Hydranal composite 5. The equipment will provide two values which will be compared with the next duplicates of this procedure or until the values is the same (~0.05 %). This is repeated every four samples in order to improve the accuracy of the results.

The sample is prepared by dissolving the bitumen into THF with a ratio of 1:20. After this, an aliquot is taken from the solution and dissolved again into THF with a ratio of 1:4. Once this step is completed, 0.6 mL of the resultant mixture is added to the equipment and the titration starts. The equipment will give a value for the water content in the diluted sample. The calculation for the water content in the diluted samples can be done with the following expressions (**Equations (4-1)** to **(4-4)**):

$$Dilution\ factor\ 1_{sample} = \frac{(Wt_{sample}Wt_{THF})}{Wt_{sample}} \qquad (4\text{-}1)$$

$$Dilution\ factor\ 2_{THF} = \frac{(Wt_{sample}Wt_{THF})}{Wt_{THF}} \qquad (4\text{-}2)$$

$$Water\ content_{THF}(\%) = \%\ water\ content_{blank} * Dilution\ factor\ 2_{THF} \qquad (4\text{-}3)$$

$$Water\ content_{sample}(\%) = (\%\ water\ content_{mixture} - \%\ water\ content_{THF}) * Dilution\ factor\ 1_{sample} \qquad (4\text{-}4)$$

A Mettler Toledo TGA/DSC-1 was used to determine the water content in the samples. The equipment has a LF1100 furnace, and an internal balance MX5 with a capacity of 5 g and a readability of 1 µg. Additionally, it is equipped with a sample robot and a Mettler Toledo gas controller GC10, which help to set the gas flow at the desired flow rate. In general, the alumina crucible (70 µL capacity) was filled with approximately 10 mg of sample. The temperature program started at 25 ºC up to 900 ºC at a heating rate of 10 ºC/min and remained at that temperature for 30 minutes. The nitrogen flow rate into the furnace was set at 50 mL/min.

4.2.4. Calculations

The water content in the samples was also determined by performing a simultaneous TGA/DSC analysis, as the mass loss event in the TGA curve could be associated with a transition observed in the DSC curve. **Figure 4-1** shows the results obtained after analyzing a water and a water-in-oil (W/O) emulsion sample with a TGA/DSC equipment.
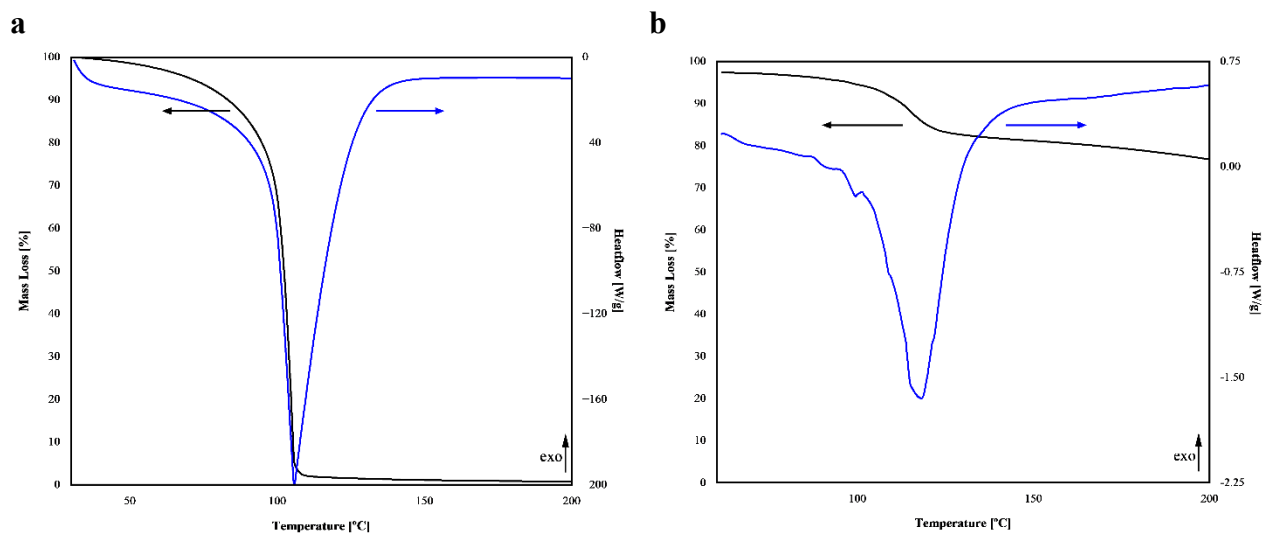
Figure 4-1. TGA (black) and DSC (blue) analysis performed to a) distilled water, and b) water-in-oil (bitumen) emulsion.

The boiling point of water and solvents used in this study were estimated using Antoine's equation (**Equation (4-5)**), the values of the constants used in the equation were obtained from different

studies reported by the National Institute of Standards and Technology, NIST. The average atmospheric pressure at the University of Alberta was obtained from the data provided by the Earth and Atmospheric Science Weather Station, the value during the measurements was 92.4 kPa (0.92 bar).

$$\log_{10}(P^v) = A - \frac{B}{T + C} \qquad\qquad (4\text{-}5)$$

Where P^v is the vapor pressure of the solvent in bar, T is the boiling temperature of the solvent in K. The constants A, B, and C are specific to each material [12], the values are displayed in **Table 4-2**. The boiling temperature was estimated from **Equation (4-5)**, as the vapor pressure of the solvents was assumed to be the same as the atmospheric pressure (92.4 kPa or 0.92 bar).

Table 4-2. Antoine's equation parameters, enthalpy of vaporization [12] and estimated boiling point of water and solvents used in this study.

Material	Antoine Equation Parameters			$T_{boiling}$ [°C]
	A	B	C	
Water	4.6543	1435.264	-64.848	97.69
Cyclohexane	4.13983	1316.554	-35.581	78.05
Toluene	4.07827	1343.943	-53.773	107.26
Methylene Chloride	3.97323	1016.865	-56.623	37.09
Chloroform	4.20772	1233.129	-40.953	58.37
Methanol	5.20409	1581.341	-33.500	62.12

It is observed the boiling temperature of water at 92.4 kPa using steam tables suggest that the boiling temperature is about 97.43 °C. On the other hand, at the same atmospheric pressure, the boiling temperature was found to be about 97.69 °C using Antoine's equation. Both values seem to agree and it is noted they properly described the onset temperature in **Figure 4-1a**. On the other hand, the onset temperature in **Figure 4-1b** appears to be higher which could have diverse explanations such as the characteristics of the system (e.g., one or two phase, concentration) and inherent limitations and uncertainty associated to the thermogravimetric analysis (e.g.,

transportation, experimental error). This finding was not explored as the purpose of the thermogravimetric analysis was to determine water removal from the W/O emulsion.

4.3. Results

4.3.1. Centrifugation

Different centrifugation speeds and centrifugation times were investigated as way to evaluate the stability of the emulsion. Water content of the centrifuged samples (bitumen phase) was measured via Karl Fischer titration and Thermogravimetric Analysis and reported in **Table 4-3**. The amount of water that was physically separated and recovered is also reported in **Table 4-3**.

Table 4-3. Measured water content after centrifugation.

Centrifugation			Measured water content			
rpm	time [min]	emulsion [g]	Karl Fischer $[g_{water}/g_{sample}]$ [a]		TGA $[g_{water}/g_{sample}]$ [a]	Physically separated water $[g_{water}]$
			x [b]	s [b]		
1000	15	5.036	0.17	0.01	0.17	0.000
	30	5.055	0.23	0.01	0.11	0.154
	60	5.055	0.25	0.00	0.14	0.351
	90	5.068	0.28	0.00	0.11	0.115
2500	15	5.150	0.14	0.00	0.15	0.329
	30	5.117	0.16	0.00	0.07	0.363
	60	5.028	0.16	0.00	0.11	0.448
	90	5.123	0.17	0.00	0.15	0.443
4100	15	4.928	0.15	0.01	0.21	0.271
	30	5.145	0.15	0.00	0.17	0.379
	60	5.007	0.17	0.01	0.17	0.424
	90	5.342	0.21	0.00	0.09	0.362

[a] The measurement is the water content in the bitumen-containing sample recovered after centrifugation and it is based on the mass of the bitumen-containing sample recovered after centrifugation.
[b] Measurement performed 4 times.

The measured values in **Table 4-3** were employed to calculate the extent of water removal. For calculations the water content of the emulsion feed was assumed to be the average concentration

measured by Karl Fischer titration in **Table 4-1**, i.e., 0.20 $g_{water}/g_{emulsion}$. The challenge with this calculation is that the amount of water physically separated after centrifugation left a small amount of water in contact with the bitumen at the interface that could not be cleanly recovered. Irrespective of whether the results are expressed on a bitumen basis, or an emulsion basis, the calculation requires material balance and an assumption about how one should deal with the interface layer that is finite, but difficult to quantify.

Since the amount of physically separated water was always <10 % of the emulsion, the implied error was less to assume that the material at the interface was part of the sample that was analysed by Karl Fischer and TGA. Using this assumption, the water recovery could be calculated from the measurements in **Table 4-3**, and the results are presented in **Table 4-4**.

Table 4-4. Water recovery from the bitumen emulsion after centrifugation of the water-in-bitumen emulsion that was calculated from different measurements reported in **Table 4-3**.

Centrifugation		Water recovery from water-in-bitumen emulsion after centrifugation [%]		
RPM	**time [min]**	**Karl Fischer Titration**	**TGA**	**Physical separation**
1000	15	14	18	0
	30	-10	47	15
	60	-13	34	34
	90	-36	47	11
2500	15	35	29	31
	30	28	70	35
	60	27	49	44
	90	26	33	43
4100	15	29	4	27
	30	34	21	36
	60	24	22	42
	90	2	59	33

4.3.2. Centrifugation + solvent

Different solvents were used in an attempt to increase the water removal from the water-and-oil emulsion using centrifugation. The solvents were selected mainly based on their low solubility in water. The solubility of cyclohexane in water at 25 ºC is 0.05 g/L [13]; toluene solubility in water at 25 ºC has been found to be between 0.5 – 0.6 g/L [13,14]; chloroform's solubility in water at 25 ºC is 8 g/L [13]; and the solubility of dichloromethane in water at 25 ºC is 17.3 g/L [13]. In contrast, the previously mentioned solvents have a high solubility in oil. On the other hand, methanol is miscible in water at 25 ºC [15] but has poor solubility in bitumen [16].

The solvents mentioned used in this study were added in different concentrations to the emulsion (5, 10, 25 wt.%, and 50 wt.% for methanol only). After centrifugation, no water was recovered from the samples where cyclohexane, toluene, methylene chloride, or chloroform was added. However, water was recovered from the centrifuged samples where methanol was added to the emulsion.

The water content in the centrifuged samples was determined using a Karl Fischer titrator and by TGA. It is noted that the analyzed samples contain certain amount of solvent; it is not expected that the solvents interfere with the measurement of the water content via Karl Fischer titration [17]. Most of the solvents, except toluene, have their boiling point below 100 ºC. To estimate the amount of water in the sample, it was assumed that any mass loss below 100 ºC (except in the case of toluene) was associated to the solvent evaporation. For the case of toluene, it is assumed that any mass loss below 110 ºC is due to the evaporation of both water and toluene. The further assumption was made that all of the solvent would be removed when conducting TGA.

The results of the centrifugation experiment where solvents were used are shown in **Table 4-5**. It is observed that the amount of water determined by Karl Fischer titration and by TGA does not show an agreement in any of the datasets. The most straightforward explanation for this is that the indicated assumptions for the interpretation and treatment of the TGA mass loss with temperature data were not valid.

Table 4-5. Measured water content after centrifugation at 2500 rpm and 90 minutes using different solvent concentration.

Solvent	Emulsion [g]	Solvent Concentration [wt.%][a]	Karl Fischer Titration [g_{water}/g_{sample}]		TGA [g_{water}/g_{sample}]	Physically Separated [g_{water}]
			x[b]	s[b]		
	4.751	5	0.12	0.01	0.08	0.00
Cyclohexane	4.501	10	0.13	0.01	0.10	0.00
	3.752	25	0.14	0.01	0.10	0.00
	4.749	5	0.21	0.01	0.16	0.00
Toluene	4.546	10	0.25	0.02	0.12	0.00
	3.749	25	0.26	0.01	0.07	0.00
	4.749	5	0.08	0.00	0.31	0.20
Methylene Chloride	4.503	10	0.13	0.01	0.28	0.00
	3.751	25	0.09	0.00	0.39	0.00
	4.748	5	0.16	0.01	0.28	0.00
Chloroform	4.501	10	0.16	0.01	0.21	0.00
	3.751	25	0.07	0.00	0.16	0.00
	4.752	5	0.09	0.00	0.19	0.01
	4.502	10	0.07	0.00	0.13	0.13
Methanol	3.749	25	0.07	0.00	0.14	0.17
	2.518	50	0.03	0.00	0.09	0.15

[a] Solvent concentration [wt.%] = $g_{solvent}/g_{emulsion+solvent}$
[b] Measurement performed 4 times.

It is interesting the high values obtained in both, Karl Fischer titration and TGA when chloroform was used. Samples containing toluene also exhibit high values in the Karl Fischer titration results.

No water was removed from centrifuged samples containing cyclohexane, toluene, methylene chloride and chloroform. However, water was removed from the methanol-added centrifuged samples. The values shown in **Table 4-5** were used to estimate water removal from the samples using the water content value reported in **Table 4-1** (0.20 $g_{water}/g_{emulsion}$). The assumption for calculating the water recovery of methanol-added centrifuged samples is no amount of methanol was dissolved into the emulsion. The water recovery calculation using the results in **Table 4-5** are shown in **Table 4-6**.

Table 4-6. Water recovery from the bitumen emulsion after centrifugation of the water-in-bitumen emulsion that was calculated from different measurements reported in **Table 4-5**.

Solvent	Solvent Concentration [wt.%]	Water recovery from water-in-bitumen emulsion after centrifugation [%]		
		Karl Fischer Titration	**TGA**	**Physical separation**
Cyclohexane	5	39	61	0
	10	38	53	0
	25	33	49	0
Toluene	5	-4	23	0
	10	-22	43	0
	25	-27	68	0
Methylene Chloride	5	59	-55	0
	10	38	-40	0
	25	54	-93	0
Chloroform	5	21	-39	0
	10	20	-2	0
	25	63	19	0
Methanol	5	57	9	1
	10	64	36	14
	25	67	36	23
	50	85	59	29

It is observed that even though no water was recovered from samples containing cyclohexane, toluene, methylene chloride, and chloroform as solvents, there are samples showing recovery values different from what was expected. Additionally, it should be pointed out the instances where recovery values were negative as it was the case of samples containing toluene. No explanations were found to explain these results; all the precautions taken during the analyses are discussed in **Section 4.4.2**.

4.3.3. *Liquid-liquid extraction*

The third strategy studied in the removal of water from the bitumen-and-water emulsion was to perform a liquid-liquid extraction using two different solvents that differ in the solubility in water, one that is miscible in water (methanol) and another one that has low solubility in water (cyclohexane). The extractions were performed at room temperature without any agitation involved.

Cyclohexane is considered a good solvent to extract bitumen [18]. In this experiment, the cyclohexane was added to the emulsion in a ratio of 1:1 approximately. After 24 hours of settling, the mixture of emulsion and solvent show three distinguishable phases as shown in **Figure 4-2**. The top phase is a mixture of bitumen and solvent, the second phase is known as rag layer (oil-water-sediment interface), and the bottom phase is most likely a mixture of water and sediments.

Figure 4-2. Set up of liquid-liquid extraction process using cyclohexane.

Different from what was observed in the cyclohexane extraction, the experiment using methanol did not exhibit three phases, meaning the solvent did not dissolve into the emulsion. The initial two phases, constituted by the W/O emulsion and the methanol, remained fairly stable through the time of this experiment. The same procedure used in the cyclohexane experiment, was followed with a solvent/emulsion ratio of 1:1 without any agitation and a 24-hour settling period.

The water content of the samples was determined using Karl Fischer titration and thermogravimetric analysis and it is shown in **Table 4-7**. Some water was recovered from both of the solvent extraction experiments; the amount of water remaining on the sample is estimated based on the amount of water that was recovered. The last column of the table reports the estimated water content based on the average water content of the emulsion based on the Karl Fischer titration and TGA of the emulsion.

Table 4-7. Measured water content from samples after the liquid-liquid extraction process using cyclohexane and methanol.

Sample	Emulsion [g]	Solvent	Karl Fischer Titration $[g_{water}/g_{sample}]$ x^d	s^d	TGA $[g_{water}/g_{sample}]$	Physically Separated $[g_{water}]$
				Measured water content		
Mixture[a]			1.5×10^{-3}	0.00	0.07	
	104.38	Cyclohexane				4.89
Rag Layer[b]			0.27	0.00	0.16	
Bitumen[c]			0.19	0.02	0.15	
	101.64	Methanol				0.00
Recovered liquid			0.15	0.00	0.22	

[a] Bitumen and cyclohexane mixture
[b] Interface between oil and water, containing cyclohexane
[c] Emulsion sample recovered from the methanol solvent extraction
[d] Measurement performed 4 times.

The calculation of water recovery from these experiments is shown in **Table 4-8**. Water was not recovered from the methanol extraction experiment; the recovered liquid was considered to be a mixture of methanol and water. On the other hand, it was possible to recovered waster from the cyclohexane extraction. It was assumed that this material was predominantly water for the calculation in **Table 4-8**. Similar to previous sections, the water content measured to the emulsion by Karl Fischer titration was 0.20 $g_{water}/g_{emulsion}$ (**Table 4-1**).

Table 4-8. Water recovery from the liquid-liquid extraction experiments based on the measurements reported in **Table 4-7**.

Emulsion [g]	Solvent	Water recovery from water-in-bitumen emulsion after liquid-liquid extraction [%]		
		Karl Fischer Titration	TGA	Physically Separated
104.38	Cyclohexane	35	47	23
101.64	Methanol	18	6	0

4.3.4. *Rotary evaporation*

Based on the data given by the rotary evaporator manufacturer, it was expected to remove water from the emulsion at 50 ºC and 0.002 MPa. However, no water was recovered at these conditions. In contrast, the rotary evaporation was performed at 110 ºC and 0.04 MPa during 82 hours with some agitation (75 rpm) in order to remove water from the emulsion. It was found after performing the rotary evaporation 10 times that the average water removal from the emulsion is 99 wt.%.

The water content in the resulted bitumen was determined via Karl Fischer titration and TGA, the results are shown in **Figure 4-3**. The Karl Fischer result gives a 0.6 wt.% $\pm$ 0.2 wt.% of water content whereas the TGA result was approximately 0.46 wt.%.
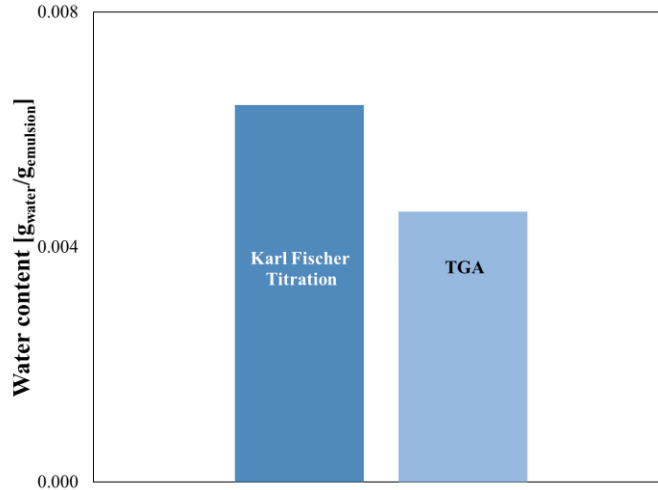
Figure 4-3. Water content in bitumen sample after 82 hours in the rotary evaporator and 99 wt.% water removal.

4.4. Discussion

4.4.1. Emulsion separation: Importance of the emulsion type and stability

Emulsions can be divided in terms of the continuous and dispersed phases. An emulsion where the oil is the continuous phase and eater is the dispersed phase is known as a water-in-oil (W/O) emulsion. This type of emulsion is predominantly produced in SAGD; however, a reverse emulsion (water is the continuous phase and oil is the dispersed phase, O/W) has also been observed in the field [19]. The formation of an emulsion requires for various factors to take place [20]:

- Difference in solubility of the liquids, enough that they are immiscible,

- Presence of materials that are partially soluble in both phases (e.g., amphiphiles), and

- Applied energy (e.g., mixing) to the system.

Additional classifications have been proposed in order to understand the behaviors of the emulsions in the petroleum industry. For example, Kokal [21] presents three different categories

based on the kinetic stability of an emulsion which refers to the extent of time an emulsion remains. If water can be removed from the emulsion within:

- A few minutes, it is called *loose*,
- Ten minutes or longer, it is known *medium*,
- Hours or longer, it is considered *tight*.

This classification is closely related to the droplet size of water and the interfacial films that forms around them [21], which are some of the different factors that contribute to the stability of an emulsion [22]. On the other hand, Rao and Liu [23] reported three categories based on the size distribution in a bitumen diluted system presented in the experimental study developed by Long et al. [6]: (i) emulsified water with a droplet size smaller than 10 μm and cannot be removed unless coalescence or aggregation takes place (ii) dispersed water where the droplet size varies between 10 and 60 μm which requires centrifugation to be removed, and (iii) free water with a droplet size higher than 60 μm that settles under the influence of gravity.

The relevance of the previous information lies in the challenges faced during the water removal of the W/O emulsion used in this study. Different processes are known to be employed in the oilsands industry used to remove water and solid materials up to specification level; incline plate settlers, centrifuges, cyclones and the use of solvents are examples of them [24]. The use of centrifugation only, as described in **Section 4.3.1**, showed that at the conditions explored in this study was not enough to completely remove the water from the emulsion. This might suggest (qualitatively) the average droplet size is smaller, hence this could be a tight emulsion based on the classification reported by Kokal [21], and it is possible that the viscosity of the system prevented water droplets from coalescence or aggregation [6]. However, it is important to note that other components present in the emulsion (i.e., solids [25,26] and asphaltenes [3,25,27]) could play an important role in the stabilization of the emulsion.

The addition of a solvent was considered as the addition of a non-paraffinic solvent [22] might contribute to the destabilization of the emulsion to ease the water separation and reduce the viscosity of the system. Long et al. [28] mentioned in their work that the nature of the solvent used

to dilute a bitumen emulsion sample will play an important role in the stability of the system and provided examples with toluene and *n*-hexane. It was shown that at a solvent-to-bitumen ratio (S/B) of 0.7, both solvents had a similar behavior. The toluene-diluted bitumen emulsion sample displayed water and solids dispersed in the oil phase; however, by increasing the S/B to 1.5 for the *n*-hexane, the diluted system showed zone settling where water, solids and any precipitated asphaltenes formed large clusters.

In this work, the solvents were selected based on their solubility with bitumen, except for methanol. After performing centrifugation with the solvent at different concentrations and different times, it was surprising to find that no separation was achieved. One potential reason to explain the results in **Section 4.3.2** is that the S/B ratios used in this study were low compared to what has been used in the literature (0.6 – 2.0) [29]. This could mean that the viscosity of the system was not sufficiently reduced and the density difference between the phases was not significantly increased by the solvent addition. The results could indicate that the system, in fact, contains emulsified water, which cannot be removed unless the size of the water droplets increase via coalescence or aggregation, based on the classification developed by Long et al. [6].

In contrast to the experiments performed in **Section 4.3.2**, the liquid-liquid extraction attempt had a S/B of approximately 1 which falls within the range reported in the literature (0.6 – 2.0) [29]. As cyclohexane is soluble in bitumen, it was expected for the viscosity to decrease and the density difference to increase. As a result, it was possible to observe the phase separation as shown in **Figure 4-2**. The formation of the rag layer reduces the dewatering capabilities [30], and hence affect the water removal process. On the other hand, the use of methanol as solvent in both **Section 4.3.2** and **4.3.3** did not provide the necessary conditions for water removal as it is not soluble in bitumen resulting in no changes to the viscosity of the system or density of the bitumen-containing phase.

The viscosity of the system can also be changed with temperature. The rotary evaporation at the conditions used was able to: (i) reduce the viscosity by increasing the temperature of the system, and (ii) provide the required conditions for water droplets to coalesce, although water removal was by evaporation. The emulsified water in the W/O emulsion used in this study will impact the

evaporation rate. The work of Aranberri et al. [31] discussed how the water evaporation rate should account for the presence of an oil. The fact that the water droplet size seems to be smaller (< 10 μm) could relate to the work developed by Flint et al. [32] where W/O microemulsions were studied as it was found that the water evaporation rate in the microemulsion was slower compared to pure water. In addition, it is shown in the same work that the water evaporation rate is also dependant on the water concentration in the emulsion. This shows that the water evaporation rate is then dependent on the water droplet size, the water concentration in the emulsion and the diffusion coefficient of water in the oil.

4.4.2. Water content determination

The water content in a sample can be determined using a Karl Fischer titration [17,33-35]. The quantification of water content is based on the following reaction **Equations (4-6)** to **(4-8)**:

$$2ROH + SO_2 \longrightarrow RSO_3^+ + ROH_2^- \tag{4-6}$$

$$RSO_3^+ + ROH_2^- + R'N \longrightarrow (R'NH^+) \cdot SO_3R^- + ROH \tag{4-7}$$

$$(R'NH^+) \cdot SO_3R^- + I_2 + H_2O + 2R'N \longrightarrow (R'NH^+) \cdot SO_4R^- + 2(R'NH^+)I^- \tag{4-8}$$
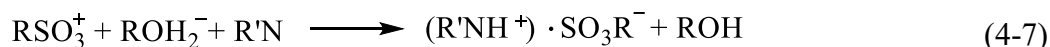
An alcohol (ROH), usually methanol or 2-(2-ethoxyethoxy) ethanol reacts with the sulfur dioxide (SO_2) and the base (R'N) neutralizes the acidic ester to form an intermediate compound, alkyl sulfite ([R'NH$^+$] $\cdot$ SO$_3$R$^-$). The intermediate compound is oxidized by iodine and forms alkyl sulfate ([R'NH$^+$]SO$_4$R$^-$) while water is consumed during the oxidation reaction.

The water determination using Karl Fischer titration is based on the consumption of water and iodine in a ratio of 1:1 by the oxidation reaction. The electrode inserted in the titrator measures the excess of iodine voltametrically. When all of the water in the sample has been converted following **Equations (4-6)** to **(4-8)**, iodine will remain unconverted due to the absence of water in the sample. This marks the end of the titration. To quantify the amount of water in the sample, the concentration of iodine in the Karl Fischer titrating reagent and the consumed amount of Karl Fischer reagent are considered.

There are reactions that might interfere with the Karl Fischer titration [36], different side reactions have been reported by different authors. Chen and Wang [37] presented a compilation of common undesired side reactions, from there side reactions relevant to bitumen and bitumen emulsions (based on compound classes found in bitumen [38]) are mentioned below:

- *Ketones* [34,35]: The formation of ketals ($R_2C=O + 2ROH \rightarrow R_2C(OR)_2 + H_2O$) releases water which can overestimate the water measurement as 1 mole of ketone could produce 1 mole of water. This reaction is equilibrium limited and requires excess of alcohol and acid media. Methanol is the most reactive alcohol with ketones, the reactivity and the reaction rate decrease with the increase of chain length [17]. Strausz and Lown [38] reported an estimated concentration of ketone (e.g., fluorenone) in oilsands bitumen of 0.3 %. Due to the limitations related to this equilibrium reaction ($K_{eq} = 10^{-7}$ for fluorenone [17]), it is estimated that for ketones to interfere with the Karl Fischer titration the concentration should be at least 70 times what has been reported for Athabasca bitumen. However, quinones can interact with the reactants and could liberate iodine resulting in a lower reported water content than what actually is present [39].

- *Thiols (mercaptans)* [17,37,39]: These compounds are oxidized by iodine ($2RSH + I_2 \rightarrow$ RSSR + 2HI) which increases the consumption of iodine, giving an erroneous higher water content in the sample. Concentrations of mercaptans higher than 2.5×10^{-7} moles of mercaptan per g of sample [40] will interfere with the titration. The ASTM standard test method [36] indicates that for 1 mole of mercaptan, 0.5 moles of apparent water are measured. The amount of thiols (mercaptans) could be estimated from the information provided about the sulfur groups found in Athabasca bitumen [38,41-43]. Based on the data reported in the cited works the sulfur containing compound classes reported are sulfides (1.25 wt.% [41]), thiophenes (3 wt.% [42] - suggested to be 60 - 80 % of the total sulfur), sulfoxides (0.7 wt.% [43]), thiolane (traces [38]), thiane (traces, [38]), and thiols (calculated by difference). The calculation of thiols by difference is problematic considering that the total sulfur content is not a singular value but spans a range. Using a total sulfur content of 5 wt% for a bitumen sample, the concentration of thiols will be

around 2.5×10^{-6} moles of mercaptan per g of sample, which is an order of magnitude higher than the threshold reported in [36,40] and could represent a source of uncertainty in the Karl Fischer measurement. Nevertheless, 4.0×10^{-4} moles of water per g of sample are required to alter the measurement. This means that about 8.0×10^{-4} moles of mercaptan per g of sample will be required to impact the Karl Fischer titration.

- *Minerals (e.g., carbonates, hydroxides and oxides)* [34,35]: Salt formation can take place while producing water at the same time, this can result in erroneous water measurement. Basic oxides, hydroxides and carbonates consume 1 mole of iodine per mole of oxide/hydroxide/carbonate, resulting in an apparent mole of water [39,44]. Examples of reactions in each category were described in [39]. For oxides, a common example is: $CaO + I_2 + SO_2 + ROH \rightarrow CaI_2 + HSO_4R$. The reaction involving hydroxides can be described as: $NaOH + I_2 + SO_2 + ROH \rightarrow NaI + HI + HSO_4R$. Finally, for carbonates, the proposed reaction is: $K_2CO_3 + I_2 + SO_2 + ROH \rightarrow 2KI + CO_2 + HSO_4R$. The reactions mentioned are just examples to provide a better understanding of the mechanisms, and it does not imply that these are the only reactions that take place. Although some oxides/hydroxides/carbonates can be found in the emulsion, the most representative compound could be alumina (Al_2O_3) which has been reported not to react during the Karl Fischer measurement. Additionally, the pH measured (5.4 – 7.3) of the aqueous phase of a water-in-oil emulsion [45] indicate that the measurement takes place within the pH range (4 - 8) where the KF titration reaction takes place [17].

- *Salts that can be reduced*: There are salts that can be potentially reduced, which may be present in the form of hydrates. An example of a metal ion in a salt that can be reduced due to its electrode potential is iron (III) chloride 6-hydrate where Fe^{3+} that can be reduced to Fe^{2+} while consuming only 5.5 moles of I_2, giving a false result [34]. In an Athabasca bitumen sample, Jacobs and Filby [46] reported the concentration of Fe ions of less than 200 ppm. It is estimated that less than 20 ppm of Fe^{3+} could affect the water measurement. However, the presence of Fe^{3+} will require the pH of the system to be greatly acidic, as shown by Brezonik and Arnold [47] making unlikely for the Fe^{3+} to be observed.

In an attempt to minimize errors that could affect the determination of water content via Karl Fischer titration, the following factors were considered:

- The use of 2-(2-ethoxyethoxy) ethanol ($C_6H_{14}O_3$), solvent in Hydranal composite 5, is beneficial as it is not prone to ketal formation that can occur in the presence of methanol. Additionally, as solvent it is known for dissolving a wide range of hydrophilic and lipophilic material [48].
- It is important to guarantee the homogeneity of the sample, THF was used for this purpose. An aliquot of the solution was used to determine the water content of the samples and the calculation accounted for any water present in the solvent as it was titrated prior to the sample's analysis.
- Freshness of the solvent is important as it could contribute to inconsistency in the results. To guarantee the solvency power of the solvent, it should be changed in the titration vessel after every sample. In addition, the THF in the solvent vessel was ensured to be fresh before starting the measurements as some degradation can take place leading to moisture adsorption and ketones formation via autoxidation.
- A calibrated syringe (Hamilton glass syringe, 1 mL) was used for the analysis to have a higher degree of accuracy. Once filled, the syringe was inspected to check whether air bubbles were present. This is relevant as it would affect the actual weight of the injected sample and, although is a small quantity, it adds environmental moisture.

Each of the discussed items will contribute to the overall uncertainty associated to the Karl Fischer measurement. For instance, all the instruments (e.g., titrator, balance) used during the analysis have an uncertainty. After taking into consideration the uncertainties from the calibrated syringe (±1 %, given by Hamilton Company), the titrator (±0.05 %, given by Mettler Toledo), the balance (±0.00004 %, given by Mettler Toledo) and the purity of the chemicals used in the analysis (±1 % for THF and ±0.02 % for Hydranal, given by the manufacturer), it was estimated that the overall uncertainty of the measurement was about ±1.4 %. This suggests that after considering all the sources of error, the obtained results are valid. To calculate the overall uncertainty, **Equation (4-9)** was used.

$$Overall\ uncertainty\ (\%) = \sqrt{\sum_i x_i^2} \qquad (4\text{-}9)$$

The calculated uncertainty of measurement excludes the uncertainty derived from reactions of species present in the bitumen that affect the iodometric titration of water. The potential side reactions previously described, if occurring, will result in an overestimation of water content.

Water content can also be determined by Thermogravimetric Analysis, this technique measures the weight of a sample as a function of the sample's temperature or time. A small amount of sample is placed in a crucible, which will be introduced into the furnace chamber equipped with a balance and atmosphere control. The sample will be subjected to a temperature program where the weight of the sample is recorded at all times during the analysis.

Different bitumen samples have shown different temperature onsets for mass loss. For an Athabasca bitumen sample, Murugan et al. [49] evaluated different heating rates and under nitrogen environment. The heating rate can have an impact on the observed onset temperature for mass loss due to transport effects [50], as opposed to the invariance of onset temperature to heating rate in scanning calorimetry. For that reason, only the result of a single heating rate, 10 ºC/min, as employed in Murugan's work was considered.

It is observed that for the Athabasca bitumen sample, the mass loss associated with the bitumen started at around 150 ºC. This could be used as an indication that the results observed in this work might suggest that any mass loss below 150 ºC is indeed related to water evaporation.

Based on the study developed by Jha et al. [51], the potential contribution of gas evolution from bitumen due to low temperature thermolysis was neglected in the TGA analysis. The evolution rate of gas due to thermolysis increases exponentially with temperature; however, in the time-temperature range of interest, the amount of "volatile" materials generated from the sample during the temperature program is low. Jha et al. [51] reported values in the range of a 4×10^{-11} moles/s per g bitumen. The mass loss rate observed in an Athabasca bitumen sample is about 3×10^{-4} g/h

per g of bitumen, which is lower compared to that measured in this study (4×10^{-3} g/h per g of emulsion).

Although many considerations were taken into account to perform the TGA analysis (i.e., heating rate [52-56] and crucible selection), different factors could play a role in the results of this analysis. Some of them are:

- *Water droplets*: Mura et al. [57] discussed in their work the relationship between the water droplet size and the metastability (an apparent equilibrium or pseudo equilibrium with the possibility of reaching a more stable state) of water by using the nucleation theory ($j = N_l*(3\gamma/\pi m)^{1/2}*\exp(-E_b/kT)$ where is N_l the mass of water, γ is the surface tension, m is the molar mass of water, E_b is the energetic limit from critical vapor radius, k is the Boltmann's constant and T is the temperature), the smaller water droplet size diameters were linked to higher metastability. At the same time, the authors mentioned that an increase in the metastability results in an increase in the vaporization temperature. In addition to the droplet size, a non-uniform distribution of water within the emulsion could also affect the evaporation onset temperature [55]. As a result, it is possible to observe evaporation onset temperatures above 150 ºC in a water-in-oil emulsion.

- *Mass transfer*: Viscosity as the resistance of a fluid to flow could impact the mobility of water droplets and bubbles within the emulsion, representing a mass transfer barrier. As temperature increases during the TGA program, viscosity of the continuous media reduces. This results in a higher mobility of vapor bubbles, allowing them to reach the interface faster (than at lower temperatures). However, the effect of mobility in overall mass loss will be reflected in TGA measurements only if the vapor bubbles are able to overcome the interfacial tension and leave the emulsion.

- *Interfacial tension*: The two points previously discussed (water droplet size diameters and a potential mass transfer barrier) are affected by the interfacial tension. A higher value will imply that a higher amount of energy will be required to create a new interface between any two phases. This could prevent water molecules from leaving the water droplet and

81

transition into vapor phase during the TGA program. Friberg [58] suggested that for water bubbles to move toward the interface, a surface tension imbalance will be required. An important note should be made in regard to the presence of natural surfactants (e.g., asphaltenes [59]) that will further stabilize the emulsion, affecting the phase transition of liquid water into vapor.

- *Thermal lag (ΔT)*: The design of the TGA equipment used in this study has its temperature sensors (thermocouples) located in a way where a thermal lag can take place [60] (one place in the furnace and another in the sample holder). The sample temperature is assumed based on the measurement done by the thermocouples placed at the sample holder and the furnace. This results in variations and not an accurate display of the real temperature of the sample or at which a thermal event takes place within the time frame of the program as shown in [61]. The ΔT at a heating rate of 10 ºC/min can be within the order of 4.8 ºC, as described in the work of Czajka [63] where evaluated the thermal lag of cellulose pyrolysis at different heating rates including 10 ºC/min. This could result in a slightly lower estimate of the temperature at which the mass loss event takes place, leading to underestimation of water content.

- *Vapor pressure*: The transition of water droplets into vapor requires the chemical potential of both phases to be equal. At the same time, the vapor pressure of water needs to be higher than the external pressure of the system for the phase transition to take place.

To minimize errors that could affect the determination of water content via TGA, the following aspects were considered:

- To guarantee the temperature sensors in the sample holder will provide an accurate measurement, the equipment's chamber was cleaned using a temperature program reaching up to 1000 ºC under air and staying at that temperature for 24 hours.
- The heating rate used in the thermogravimetric analysis was consistently set at 10 ºC/min as it could affect the results (i.e., onset temperature for evaporation). Values ranging

between 2 ºC/min and 10 ºC/min have been previously reported in the literature [52-56] for water content determination.

The factors previously discussed will have an impact to the overall uncertainty associated to the TGA measurement, as well as the instrument itself. To put into perspective, the measurement has an associated uncertainty of ±3.4 %, given in the documentation provided by the manufacturer (Mettler Toledo). The equipment has an uncertainty of ±0.05 %, given by Mettler Toledo, which results in an overall uncertainty (**Equation (4-9)**) of ±3.4 %. The estimated value excludes the uncertainty derived from the potential limitations previously described (i.e., droplet size, mass transfer, interfacial tension, thermal lag, vapor pressure) that affect the measurement, if taking place, it will result in the underestimation of water content as evaporation mass loss can occur outside the temperature threshold used in this study.

The discrepancy between the water determination using Karl Fischer titration and other techniques has previously noted in different works. For example, Xu [63] compared the results obtained using Karl Fischer titration and Dean Stark method in a high-solids froth sample with a deviation of about 7 wt.%. In this study, the Dean Stark method provided a higher water content in comparison to the Karl Fischer titration. Penaloza [64] compared the water content through three methods: (i) Karl Fischer, (ii) through oxygen content determined by elemental composition, and (iii) a gravimetric approach in a washed Cold Lake bitumen sample. A discrepancy of 10 wt.% was found between approaches (i) and (ii) and of almost 20 wt.% between approaches (i) and (iii). The water content using approach (iii) showed a higher value compared to the other two approaches. Karl Fischer titration, approach (i), gave the lowest value for water content. Penaloza suggested that a source of discrepancy between the techniques could be related to the sample size, since it was difficult to ensure collection of a representative sample with a smaller sample size. Karl Fischer titration used a small amount of sample (0.5 g) compared to the gravimetric method that used a larger amount of sample (20 g).

In the present study, the situation is as disparate when Karl Fischer analysis is compared to the analysis performed with a TGA where the average amount of sample was 0.01 g.

Referring to the results shown in **Section 4.3**, it is noted that the water concentration obtained from the thermogravimetric analysis, in general, is lower than that measured by Karl Fischer titrations. This might provide support to the suggestion of water content being underestimated while using TGA; this could be due to the characteristics of the system (e.g., composition, viscosity, interfacial forces) and also the factors affecting each technique. On the other hand, the potential side reactions that could take place during Karl Fischer titration of a W/O emulsion can result in an overestimation of water content. After considering the outcomes of this section, the water content determined by Karl Fischer titration seem to provide a more reliable result and be a more suitable method for this system. The potential sources of errors were discussed, and the effect of side reactions were found to be negligible.

4.5. Conclusions

This study explored different separation techniques to remove water from a bitumen-and-water emulsion. After completing all the separation experiments, it was found that:

a. Based on the findings in this work, the water in the emulsion seems to be mostly in the form of emulsified water (i.e., < 10 μm). This was suggested based on the highly stable nature of the emulsion despite using centrifugation at different conditions (up to 4100 rpm, equivalent to 2000 G).

b. Different water removal techniques were used in order to separate water from the water-in-oil emulsion. Under the conditions explored in this study for each of the techniques, it was concluded that among them, the most effective water removal process was rotary evaporation. The conclusion is due to the removal of up to 99 wt.% of water from the W/O emulsion after 82 hours at 110 ºC and 400 mbar.

c. Underestimation of water content by TGA for such systems is potentially related to the described limitations (e.g., mass transfer, heat transfer, interfacial tension). The analysis suggests that Karl Fischer titration is a more reliable and a more suitable method compared to TGA for water quantification in W/O emulsions.

References

[1]   Rondón, M.; Pereira, J.C.; Bouriat, P.; Graciaa, A.; Lachaise, J.; Salager, J.L. Breaking of Water-in-Crude-Oil emulsions. 2. Influence of Asphaltene Concentration and Diluent Nature on Demulsifier Action. *Energy and Fuels* **2008**, *22*: p. 702 - 707.

[2]   Khatri, N.L.; Andrade, J.; Baydak, E.N.; Yarranton, H.W. Emulsion Layer Growth in Continuous Oil-Water Separation. *Colloids and Surfaces A: Physicochemical and Engineering Aspects* **2011**, *384*: p. 630 - 642.

[3]   Gafonova, O.; Yarranton, H.W. The Stabilization of Water-in-Hydrocarbon Emulsions by Asphaltenes and Resins. *Journal Colloidal and Interface Science* **2001**, *241*: p. 469 - 478.

[4]   Tipman, R. Froth Treatment. In: *Handbook on theory and practice of bitumen recovery from Athabasca oil sands. Vol. II. Industrial practice*, Masliyah, J.; Xu, Z.; Dabros, M., editor. Kingsley Knowledge Publishing, 2013, p. 211 - 253.

[5]   Ramirez-Corredores, M.M. *The Science and Technology of Unconventional Oils*. Academic Press: London, UK, 2017.

[6]   Long, Y.; Dabros, T.; Hamza, H. Selective Solvent Deasphaltene for Heavy Oil Emulsion Treatment. In: *Asphaltenes, Heavy Oils and Petroleomics*, Mullins, O., editor., Springer: New York, NJ, 2007, p. 511 - 547.

[7]   Czarnecki, J. Water-in-Oil Emulsions in Recovery of Hydrocarbons from Oil Sands. In *Encyclopedic Handbook of Emulsion Technology*; Sjöblom, J.; editor, Marcel Dekker: NY, NY 2001, p. 497 - 514.

[8]   Fingas, M. F., Fieldhouse, B. Studies of Water-in-Oil Emulsions and Techniques to Measure Emulsion Treating Agents. In: *Proceedings of the 17th Arctic and Marine Oil Spill Program (AMOP)Technical Seminar*, Environment Canada: Ottawa, CA, 1994, p. 213 - 244.

[9]   Carbognani, L.; Roa-Fuentes, L.C.; Diaz, L.; Berezinski, J.; Carbognani-Arambarri, L.; Pereira-Almao, P. Reliable Determination of Water Contents of Bitumen and Vacuum Residua via Coulometric Karl Fischer Titration using Tetrahydrofuran. *Petroleum Science and Technology* **2014**, *32*: p. 602 - 609

[10]   Davis, M.C.; Fedick, P.W.; Lupton, D.V.; Ostrom, G.S.; Quintana, R.; Woodroffe, J.D. Solubility of Hydrocarbon Oils in Alcohols (< C_6) and Synthesis of Diesel Carbonate for Degreasing. *RSC Advances* **2019**, *9*: p. 22891 - 22899.

[11]   Graziano, G. Solvation thermodynamics of cyclohexane. *The Canadian Journal of Chemistry* **2000**, *78*: p. 1233 - 1241.

[12]   Acree, W.E. Jr.; Chickos, J.S. Phase Transition Enthalpy Measurements of Organic and Organometallic Compounds. In: *NIST Chemistry WebBook, NIST Standard Reference Database Number 69*, Linstrom, P.J.; Mallard, W.G., editor.; National Institute of Standards and Technology: Gaithersburg, MD, 20899, https://doi.org/10.18434/T4D303, (accessed March 6, 2023)

[13]   Rumble, J.R., editor. Physical Constants of Organic Compounds. In: *CRC Handbook of Chemistry and Physics*, 103rd ed., CRC Press/Taylor & Francis: Boca Raton, FL, 2022.

[14]   International Union of Pure and Applied Chemistry. *Hydrocarbons with Water and Seawater*, vol. 37. Pergamon Press: Oxford, UK, 1989.

[15]   International Union of Pure and Applied Chemistry. *Alcohols with Water*, vol. 15. Pergamon Press: Oxford, UK, 1984.

[16]   He, L.; Li, X.; Du, Y.; Wu, G.; Li, H.; Sui, H. Parameters of Solvent Extraction for Bitumen Recovery from Oil Sands. *Advanced Materials Research* **2012**, *347 - 353*: p. 3728 - 3731.

[17]   Scholz, E. *Karl Fischer Determination: Titration of Water*. Springer: Berlin, 1984.

[18]   Wang, T.; Zhang, C.; Zhao, R.; Zhu, C.; Yang, C.; Liu, C. Solvent Extraction of Bitumen from Oil Sands. *Energy and Fuels* **2014**, *28*: p. 2297 - 2304.

[19]   Ansari, S., Sabbagh, R., Yusuf, Y., Nobes, D.S. The Role of Emulsions in Steam-Assisted-Gravity-Drainage (SAGD) Oil Production Process: A Review. *SPE Journal*, **2020**, *25*: p. 969 - 989.

[20]   Umar, A.A.; Saaid, I.B.M.; Sulaimon, A.A.; Pilus, R.B.M. A Review of Petroleum Emulsions and Recent Progress on Water-in-Crude Oil Emulsions Stabilized by Natural Surfactants and Solids. *Journal of Petroleum Science and Engineering* **2018**, *165*: p. 673 - 690.

[21]   Kokal, S. Crude-Oil Emulsions: A State-of-the-Art Review. *SPE Production and Facilities* **2005**, *20*: p. 5 - 13.

[22]   Yarranton, H.; Baydak, E.N. Effect of Solvents on the Stability of Water-in-Bitumen Emulsions. *Energy and Fuels* **2022**, *36*: p. 6243 - 6260.

[23]   Rao, F.; Liu, Q. Froth Treatment in Athabasca Oil Sands Bitumen Recovery Process: A Review. *Energy and Fuels* **2013**, *27*: p. 7199 - 7207.

[24]   Gray, M. R. *Upgrading Oilsands Bitumen and Heavy Oil.* University of Alberta Press: Edmonton, Canada, 2015.

[25]   Kilpatrick, P.K. Water-in-Crude Oil Emulsion Stabilization: Review and Unanswered Questions. *Energy and Fuels* **2012**, *26*: p. 4017 - 4026.

[26]   Yan, N.; Masliyah, J.H. Adsorption and Desorption of Clay Particles at the Oil-Water Interface. *Journal of Colloid and Interface Science* **1994**, *168*: p. 386 - 392.

[27]   Rocha, J.A.; Baydak, E.N.; Yarranton, H.W. What Fraction of the Asphaltenes Stabilizes Water-in-Bitumen Emulsions? *Energy and Fuels* **2018**, *32*: p. 1440 - 1450.

[28]   Long, Y.; Dabros, T.; Hamza, H. Stability and Settling Characteristics of Solvent-Diluted Bitumen Emulsions. *Fuel* **2002**, *81*: p. 1945 - 1952.

[29]   Hamza, H. Effect of Solvent Selection on Froth Treatment for Mining Operations. In: *Proceedings of the 3rd NCUT Meeting on Upgrading and Refining of Heavy Oil, Bitumen and Synthetic Crude Oil*, Edmonton, Alberta, 2003, p. 38 - 68.

[30]   Czarnecki, J., Moran, K., Yang, X. On the "Rag Layer" and Diluted Bitumen Froth Dewatering. *The Canadian Journal of Chemical Engineering* **2007**, *85*: p. 748 - 755.

[31]   Aranberri, I.; Beverly, K.J.; Binks, B.P.; Clint, J.H.; Fletcher, P.D.I. How Do Emulsions Evaporate? *Langmuir* **2002**, *18*: p. 3471 - 3475.

[32]   Clint, J.H.; Fletcher, P.D.I.; Todorov, I.T. Evaporation Rates of Water from Water-in-Oil Microemulsions. *Physical Chemistry Chemical Physics* **1991**, *1*: p. 5005 - 5009.

[33]   Kato, H. *Karl Fischer Reagents: Technical Manual*. 2004.

[34]   Bruttel, P.; Schlink, R. *Water Determination by Karl Fischer Titration*. Herisan, Switzerland, 2006.

[35]   MacLeod, S.K. Moisture Determination using Karl Fischer Titrations. *Analytical Chemistry* **1991**, *63*: p. 557A - 566A.

[36]   *ASTM E203: Standard Test Method for Water Using Volumetric Karl Fischer Titration*. ASTM International. West Conshohocken, PA 2018.

[37]   Chen, Q.; Wang, Y. Challenges in the Determination of Water Content by Karl Fischer Titration during In-Process Control. *American Pharmaceutical Review* **2009**, *12*: p. 48 - 54.

[38]   Strausz, O. P.; Lown, E. M. *The Chemistry of Alberta Oil Sands, Bitumens and Heavy Oils*; Alberta Energy Research Institute: Calgary, AB, 2003.

[39]   Mitchell, J.; Smith, D.M. Aquametry: *A Treatise on Methods for the Determination of Water (Part III)*. John Wiley & Sons, Inc.: New York, NY, Vol. 5, 1980.

[40]   Sneed, R.W.; Altman, R.W.; Mosteller, J.C. Effect of Aviation Fuel Components on the Accuracy of the Karl Fischer Electrometric Titration. *Analytical Chemistry* **1954**, *26*: p. 1018 - 1020.

[41]   Gray, M.R.; Ayasse, A.R. Kinetics of Hydrodesulfurization of Thiophenic and Sulfide Sulfur in Athabasca Bitumen. *Energy and Fuels* **1995**, *9*: p. 500 - 506.

[42]   Selucky, M.L.; Chu, Y.; Ruo, T.; Strausz, O.P. Chemical Composition of Athabasca Bitumen. *Fuel* **1977**, *56*: p. 369 - 381.

[43]   Bunger, J.W.; Thomas, K.P.; Dorrence, S.M. Compound Types and Properties of Utah and Athabasca Tar Sand Bitumens. *Fuel* **1979**, *58*: p. 183 - 195.

[44]   Mitchell, J.; Smith, D.M.; Ashby, E.C.; Bryant, W.M.D. Analytical Procedures employing Karl Fischer Reagent. IX. Reactions with Inorganic Oxides and Related Compounds. Oxidation and Reduction Reactions. *Journal of the American Chemical Society* **1941**, *63*: p. 2927 - 2930.

[45]   Peñaloza, I.M.; Chauhan, G.; De Klerk, A. Desalting Behavior of Bitumen. *Energy and Fuels* **2021**, *35*: p. 15618 - 15627.

[46]   Jacobs, F.S.; Filby, R.H. Solvent Extraction of Oil-Sand Components for Determination of Trace Elements by Neutron Activation Analysis. *Analytical Chemistry* **1983**, *55*: p. 74 - 77.

[47]   Brezonik, P.L.; Arnold, W.L. *Water Chemistry: An Introduction to the Chemistry of Natural and Engineered Aquatic Systems*. Oxford University Press: Oxford, UK, 2011.

[48]   Ha, E-S.; Lee, S-K.; Choi, D.H.; Jeong, S.H.; Hwang, S-J.; Kim, M.-S. Application of Diethylene Glycol Monoethyl Ether in Solubilization of Poorly Water-Soluble Drugs. *Journal of Pharmaceutical Investigation* **2020**, *50*: p. 231 - 250.

[49] Murugan, P.; Mani, T.; Mahinpey, N.; Dong, M. Pyrolysis Kinetics of Athabasca Bitumen using a TGA under the Influence of Reservoir Sand. *The Canadian Journal of Chemical Engineering* **2012**, *90*: p. 315 - 319.

[50] Gabbott, P. *Principles and Applications of Thermal Analysi*s. Blackwell Publications: Oxford, UK, 2008.

[51] Jha, K.N.; Montgomery, D.S.; Strausz, O.P. Chemical Composition of Gases in Alberta Bitumens and in Low-Temperature Thermolysis of Oil Sand Asphaltenes and Maltenes. In: *Symposium on Oil Sand and Oil Shale Chemistry*, Strausz, O.P.; Lown, E.M., editor.; Verlag Chemie International: 1977, p. 33 - 54.

[52] Ng, A., Ovalles, C, Benson, I.P. Asphaltenes Contribution in Emulsion Formation During Solvent-Steam Processes. In: *SPE Western Regional Meeting*, Garden Grove, CA, 2018, p. SPE-190057-MS.

[53] Kar, T. Analysis of Saturates, Aromatics, Resins, Asphaltenes (SARA), Water, and Clays in Water-Oil Emulsions for Steam-Assisted Gravity Drainage (SAGD)and Expanding Solvent- SAGD (ES-SAGD). MSc Thesis, Texas A&M University, 2015.

[54] Korošec, R.C.; Bukovec, P. Thermal Methods of Analysis as a Tool for Quantitative Composition Determination of Water-in-Oil Emulsions. In: *Explosive Materials: Classification, Composition and Properties*, Janssen, T.J., editor.; Nova Science Publishers: Hauppauge, NY, 2011, p. 125 - 144.

[55] He, G-H; Chen, G.-H. Determination of Water in W/O Emulsion by TG. *Petrochemical Technology* **2000**, *7*: p. 526 - 529.

[56] *ASTM E1131: Standard Test Method for Compositional Analysis by Thermogravimetry*. ASTM International. West Conshohocken, PA, 2020.

[57] Mura, E.; Josset, C.; Loubar, K.; Bellettre, J.; Massoli, P. Experimental Study of the Water in Oil Emulsions Features by Differential Scanning Calorimetry Analysis. *Applied Energy* **2012**, *97*: p. 834 - 840.

[58] Friberg, S.E.; Langlois, B. Evaporation from Emulsions. *Journal of Dispersion Science and Technology* **1993**, *13*: p. 223 - 243.

[59] Umar, A.A.; Saaid, I.B.M.; Sulaimon, A.A.; Pilus, R.B.M. A Review of Petroleum Emulsions and Recent Progress on Water-in-crude Oil Emulsions Stabilized by Natural

Surfactants and Solids. *Journal of Petroleum Science and Engineering* **2018** *165*: p. 673 - 690.

[60]   Stenseng, M; Jensen, A.; Dam-Johansen, K. Investigation of Biomass Pyrolysis by Thermogravimetric Analysis and Differential Scanning Calorimetry. *Journal of Analytical and Applied Pyrolysis* **2001**, *58–59*: p. 765 - 780.

[61]   Tye, R.C.; Gardner, R.L.; Maesono, A. Temperature Measurement and Control: Critical Parameters in Thermal Analysis Techniques. *Journal of Thermal Analysis* **1993**, *40*: p. 1009 - 1016.

[62]   Czajka, K.M. The Impact of the Thermal Lag on the Interpretation of Cellulose Pyrolysis. *Energy* **2021,** *236*: p. 121497.

[63]   Xu, R. Settling Behavior in the Dewatering Process for Bitumen Froth with Different Qualities. MSc Thesis, University of Alberta, 2018.

[64]   Penaloza, I. Effect of Water Chemistry on Cold Lake and Athabasca bitumen. MSc Thesis, University of Alberta, 2018.

5. Relationship between aromatic hydrogen and aromatic carbon in straight run and converted oils

5.1. Introduction

Tracking chemical changes in high boiling oil fractions that result from conversion is difficult and further complicated by the complexity of these fractions. It is for this reason that oil characterization relies mainly on the bulk characterization of the oil, employing spectrometry, measurement of macroscopic physical properties, and elemental analysis to name a few. Our interest was specifically in tracking changes that took place during thermal conversion processes, such as visbreaking, coking and thermal liquefaction; processes that are used for the conversion of oilsands bitumen [1], petroleum [2], coal [3], and biomass / organic waste materials [4]. Hence, the contribution of this work is of practical significance, it is not novel. The work clarifies the applicability of a procedure that was published in this journal and that is used by the community.

When one looks at detailed descriptions of thermal conversion chemistry [5,6], it is immediately apparent that much of it revolves around free radical formation, propagation, and termination in which the removal or addition of hydrogen plays an important role. In fact, central to thermal conversion is hydrogen disproportionation to form hydrogen-enriched products that are more aliphatic in nature, and hydrogen-depleted products that are more aromatic in nature. Tracking the changes in the nature of hydrogen and carbon is therefore valuable and proton nuclear magnetic resonance (^{1}H NMR) spectrometry and carbon-13 nuclear magnetic resonance (^{13}C NMR) spectrometry are useful for this purpose.

The application of this can be illustrated by an example where progress in thermal conversion of Athabasca oilsands bitumen oil was tracked by various means, including ^{13}C NMR [7]. The total aromatic carbon content, which could easily have been viewed as an indicator for the conversion severity, was found not to be poorly related to measures such as phase stability, toluene insoluble coke content, or *n*-heptane insoluble asphaltenes formation. The chemical information provided by ^{13}C NMR indicated that the changes in the chemical nature of the species during thermal

conversion was quite different to the changes in their solubility behavior. In this case there is a need to infer information about the change in the nature of the hydrogen from the ^{13}C NMR data to assist with a description of the hydrogen transfer reactions. In most cases the situation would be the opposite and there would be a need to infer information about the change in the nature of the carbon from ^{1}H NMR data.

The low natural abundance of ^{13}C makes ^{13}C NMR analyses more time consuming than ^{1}H NMR analyses, because longer time must be allowed to collect ^{13}C NMR spectra. Conversely, the speed at which ^{1}H NMR spectra can be collected makes it suitable for monitoring thermal conversion almost in real time. Using a combination of ^{1}H NMR and infrared analyses of coal liquids, Brown and Ladner [8] suggested that one might be able to establish a relationship between the aromatic hydrogen content and carbon content, albeit with some assumptions. Picking up on this relationship, Cookson, et al. [9] analyzed a large number of samples by ^{1}H and ^{13}C NMR and arrived at a semi-empirical relationship to relate the aromatic carbon content, C_{Ar} (ratio of aromatic carbon to total carbon), to the aromatic hydrogen content, H_{Ar} (ratio of aromatic hydrogen to total hydrogen), through **Equation (5-1)**.

$$C_{Ar} = \left[k \cdot \left(\frac{1}{H_{Ar}} - 0.01 \right) + 0.01 \right]^{-1} \tag{5-1}$$

For materials with a median boiling point temperature <320 °C a good relationship was obtained over a wide range of values for the aromatic hydrogen content using $k = 0.282$. For higher boiling materials, the goodness of fit deteriorated with increasing H_{Ar} when $k = 0.282$, but the general relationship in **Equation (5-1)** had a good fit for $k = 0.199$ [9].

The study by Cookson, et al. [9] was rigorous, and the outcome suggested that one might be able to apply **Equation (5-1)** to high boiling oils with the caveat that an appropriate value for k has to be experimentally determined beforehand.

To determine whether **Equation (5-1)** was as widely applicable as the study by Cookson, et al. [9] suggested, ^{1}H and ^{13}C NMR analyses were performed on a range of materials and was further augmented by published data sets [10-25]. Experimentally measured ^{1}H and ^{13}C NMR data sets were obtained for Athabasca bitumen, solubility fractions of bitumen, distillation fractions of bitumen, and thermally converted bitumen, as well as distillate range narrow cuts from hydrocracked wax and hydrotreated petroleum kerosene.

5.2. Experimental

5.2.1. Materials

Athabasca bitumen was obtained from a bitumen-and-water emulsion produced at the Long Lake SAGD (Steam-Assisted Gravity Drainage) facility, located near Anzac, Alberta in the Athabasca Oil Sands region. To obtain the bitumen required for the experimental work, the emulsion had to be separated. After 82 hours in a rotary evaporator at 110 ºC and 0.04 MPa using an oil bath, the water was almost completely removed. The bitumen was characterized, and the properties of the bitumen are reported in **Table 5-1**.

Table 5-1. Characterization of Athabasca bitumen and derived materials.

Property	Bitumen		n-Heptane soluble Maltenes		n-Heptane insoluble Asphaltenes	
	x^a	s^a	x^a	s^a	x^a	s^a
Material Balance	100		81.4[b]	0.6	18.6[b]	0.6
Water content [wt. %]	0.6[c]	0.1[c]				
Density [kg/m^3]						
20 ºC	1014.2[d]	2.1[d]	956.3[d]	2.4[d]	-	-
Viscosity [Pa.s]						
20 ºC	2461[d]	26[d]	1.5[d]	<0.1[d]	-	-
Free Radical Content [spins/g][e,f]	1.6×10^{18}	-	1.1×10^{18}	-	3.4×10^{18}	-
Elemental analysis [wt. %][e]						
Carbon	83.0	0.1	83.4	0.1	79.6	1.4
Hydrogen	10.3	<0.1	10.9	0.1	8.0	0.2
Nitrogen	0.5	<0.1	0.4	<0.1	1.2	<0.1
Sulfur	5.2	0.3	4.4	0.1	8.6	<0.1
Oxygen[g]	1.0	0.2	1.0	0.2	2.6	1.6

[a] x denotes the average value of the measurements and s refers to the standard deviation of the measurements performed.
[b] n-C$_7$ insoluble asphaltenes were separated 20 times.
[c] Water content was measured 10 times.
[d] Measurements were performed three times.
[e] Analysis performed on a single sample.
[f] On the basis of ESR calibration with 2,2-diphenyl-1-picrylhydrazyl (DPPH).
[g] Calculated by difference.

Solubility fractions were obtained from the Athabasca bitumen using n-heptane (n-C$_7$) using the solubility class separation procedure described in ASTM D3279-19 [26]. The resulting products were n-C$_7$ solubles (maltenes) and n-C$_7$ insolubles (asphaltenes). These solubility fractions were similarly characterized, and the properties are reported in **Table 5-1**.

Vacuum residue deasphalted oil (VR DAO) was obtained from the Long Lake Upgrader facility. This material contains straight run material from n-pentane solvent deasphalting of Athabasca

bitumen and thermally converted material from the same. A detailed description of the material and its characterization were reported [27].

Distillation fractions from Athabasca bitumen were collected from vacuum distillation using a B/R Instruments 18 CODS distillation system. The bitumen was separated into 15 narrow distillation cuts with boiling point difference of 20 °C [28].

Thermally converted bitumen was prepared from bitumen, maltenes, and asphaltenes shown in **Table 5-1**. The thermal conversion was performed in microbatch reactors with a glass insert. Thermal conversion was conducted at 380 °C for a time range between 0 and 146 min at 2 MPa initial nitrogen pressure. For each experiment, the reaction product was recovered using 100 mL of CS_2 and then filtered. The recovered liquid was placed in a rotary evaporator to remove the CS_2. (Safety notice: CS_2 has a low autoignition temperature, about 100 °C, and its explosive range in air is 1–50 %).

Distillation fractions obtained from the product of wax hydrocracking over a $Pt/SiO_2\text{-}Al_2O_3$ catalyst operated at 2 MPa was previously described [25]. Distillation fractions were prepared from hydrotreated kerosene that was obtained from Husky Energy. The distillation was performed in the same way as for the hydrocracking products. Three distillation cuts of each material were included in this study to provide a control group in the range of materials studied by Cookson, et al. [9].

Information about the chemical and solvents used in sample preparation and the analyses (this includes chemicals, cylinder gases and calibration materials) are displayed in **Table 5-2**.

Table 5-2. Chemicals and Cylinder Gases used.

Compound	Formula	CASRN	Mass fraction purity[a]	Supplier
		Chemicals		
n-Heptane	C_7H_{16}	142-82-5	0.997	Fisher Scientific
Carbon Disulfide	CS_2	75-75-0	0.9999	Fisher Scientific
Deuterated Chloroform	$CDCl_3$	865-49-6	0.998	Acros Organic
Chromium(III) acetylacetonate	$C_{15}H_{21}CrO_6$	21679-31-2	0.999	Aldrich
		Cylinder gases		
Nitrogen	N_2	7727-37-9	0.99999	Praxair

[a] Purity of the material guaranteed by the supplier.

5.2.2. Analyses

^{1}H NMR and ^{13}C NMR spectra were obtained using an Agilent/Varian Innova 400 MHz spectrometer with a 9.395 Tesla magnet in which hydrogen resonates at 400 MHz and carbon resonates at 100.58 MHz, in accordance with the gyromagnetic ratio of each element (42.5774 MHz/T for ^{1}H and 10.7084 MHz/T for [13]C [29]). Hence, they have different frequencies which is reflected on the direct impact on the resolution. These analyses were performed at the Chemistry Department of the University of Alberta.

For ^{1}H NMR, 0.15 g of sample were dissolved in 0.70 mL of deuterated chloroform; once the sample was dissolved, it was placed in 5 mm NMR tubes. For the analysis, each spectrum was obtained by performing 16 scans (per sample) within -1 to 11 ppm. The aromatic region was defined between 6.0 and 9.0 ppm, and the aliphatic region was defined between 0.4 and 3.6 ppm to be consistent with the methodology of Cookson, et al. [9].

For ^{13}C NMR, samples were prepared for analysis by adding 0.35 mL of the oil sample and 0.35 mL of 0.2 mM chromium (III) acetylacetonate in deuterated chloroform. Once the sample was completely dissolved, it was placed in a 5 mm NMR tube. For the analysis, each sample was scanned 2000 times within -10.0 to 270.0 ppm. The acquisition time was 0.5 s and the relaxation

time was 2 s. The aromatic region was defined between 110 and 160 ppm, and the aliphatic region was defined between 2.5 and 60.0 ppm to be the same as the methodology of Cookson, et al. [9]. More detailed information on the NMR procedure is given in the **Appendix C**. The pulse sequence is shown in **Figure C-1** in the supporting information.

5.3. Results

5.3.1. ^1H and ^{13}C NMR analysis of straight run bitumen and bitumen-derived materials

There were four groups of materials that consisted of mainly of straight run Athabasca bitumen, with only the VR DAO that contained some previously converted material. These materials are representative of the naturally occurring bitumen, and its sub-fractions separated based on solubility and distillation range. All of these materials were analyzed by ^1H and ^{13}C NMR spectrometry and the results are presented in **Table 5-3**. The ^1H and ^{13}C NMR spectra are shown in **Figure C-2** to **Figure C-4** in the **Appendix C**.

Table 5-3. Nature of hydrogen and carbon in an industrial vacuum residue deasphalted oil from bitumen, bitumen, and bitumen n-C$_7$ solubility fractions determined by ^1H NMR and ^{13}C NMR, respectively.

Material Description	^1H NMR				^{13}C NMR			
	Aromatic (%)		Aliphatic (%)		Aromatic (%)		Aliphatic (%)	
	x^a	s^a	x^a	s^a	x^a	s^a	x^a	s^a
VR DAO[30][b]	7.5	-	92.5	-	32.5	-	67.5	-
Athabasca bitumen	5.1	1.2	94.9	1.2	28.5	1.8	7.5	1.8
Maltenes from Athabasca bitumen	4.5	1.8	95.5	1.8	22.7	1.0	77.3	1.0
Asphaltenes from Athabasca bitumen	9.0	1.5	91.0	1.5	43.4	3.1	56.6	3.1

[a] x denotes the average value of three measurements and s refers to the standard deviation of the measurements performed.
[b] Analysis performed on a single sample.

Despite the high density of bitumen, it has a hydrogen-to-carbon (H/C) molar ratio of 1.5 (**Table 5-1**), which indicates that the aromatic content cannot be too high. The data obtained in this study shows that the H/C ratio decreases with an increment in density, following a similar trend with aromatic carbon content. In contrast, the aromaticity (aromatic carbon content) decreases with an increment in H/C ratio. The value of 28.5% aromatic carbon that was determined for bitumen (**Table 5-3**) is congruent with the H/C molar ratio and is also close to the value of 31.6% reported before [31].

A further internal consistency check was performed on the measured amounts of aromatic hydrogen and carbon in **Table 5-3**, by calculating the material balance. It was found that the material balance for aromatic hydrogen closed within 6%. The measured value for aromatic hydrogen in bitumen was 5.1% and the value calculated from the maltenes and asphaltenes measurements was 4.6%. Similarly, the material balance for aromatic carbon closed within 4%. The measured value for bitumen was 28.5% and the value calculated from the maltenes and asphaltenes measurements was 26.6%.

It is expected that the amount of *n*-alkane insoluble material (asphaltenes) decreases when the length of the aliphatic chain in a paraffinic solvent is increased as shown in previous studies [32-34]. The *n*-C_7 asphaltenes content reported in this study is 18.60 %. This is higher than what is typically reported for Athabasca bitumen *n*-C_5 asphaltenes, which is 17.2 wt. % [35]. The anomalously high value could open the discussion about errors in the separation procedure. However, the precipitation of *n*-C_7 asphaltenes was performed 20 times following the same procedure and was unusually repeatable but reaffirmed the *n*-C_7 insoluble content of the material used in this work as 18.60 ± 0.01 wt.%.

Distillation cuts prepared by vacuum distillation of Athabasca bitumen were individually analyzed by ^{1}H and ^{13}C NMR spectrometry and the results are reported in **Table 5-4**. The ^{1}H and ^{13}C NMR spectra can be found in **Figure C-5** to **Figure C-19** in the **Appendix C**.

Table 5-4. Nature of hydrogen and carbon in distillation fractions obtained from vacuum distillation of Athabasca bitumen, as determined by ^{1}H NMR and ^{13}C NMR, respectively.

Distillation range (°C) [a]	^{1}H NMR		^{13}C NMR	
	Aromatic (%)	Aliphatic (%)	Aromatic (%)	Aliphatic (%)
<150	3.7	96.3	12.6	87.4
150–170	1.9	98.1	3.1	96.9
170–190	2.1	97.9	1.3	98.7
190–210	0.4	99.6	2.3	97.7
210–230	0.9	99.1	1.2	98.8
230–250	0.8	99.2	3.3	96.7
250–270	1.0	99.0	3.0	97.0
270–290	1.8	98.2	8.9	91.1
290–310	6.1	93.9	14.8	85.2
310–330	5.6	94.4	18.0	82.0
330–350	6.7	93.3	21.9	78.1
350–370	5.9	94.1	22.3	77.7
370–390	6.0	94.0	24.1	75.9
390–410	6.6	93.4	22.0	78.0
410–430	6.5	93.5	21.3	78.7

[a] Atmospheric equivalent boiling point temperature range.

The distillation fractions in the <430 °C boiling range represents about 25 wt% of the Athabasca bitumen, with the remainder being higher boiling material. The amount of lighter material recovered by distillation was little, with the <150 °C being <0.5 wt% of the bitumen.

5.3.2. ^{1}H and ^{13}C NMR analysis of thermally converted bitumen

Thermally converted material was prepared from the Athabasca bitumen fractions shown in **Table 5-1**. A range of thermally converted products with different degrees of conversion and that had different amounts of n-C$_7$ asphaltenes present in their feed, were recovered and analyzed using [1]H

and ^{13}C NMR spectroscopy. The results are reported in **Table 5-5**. The ^{1}H and ^{13}C NMR spectra are presented in **Figure C-26** to **Figure C-45** in the **Appendix C**.

Table 5-5. Nature of the hydrogen and carbon in thermally converted products recovered after reaction at 380 °C for the indicated time period at reaction temperature, as determined by ^{1}H and ^{13}C NMR, respectively.

Asphaltenes in Feed (wt. %) [a]	Reaction Time (min) [b]	^{1}H NMR [c]		^{13}C NMR [c]	
		Aromatic (%)	Aliphatic (%)	Aromatic (%)	Aliphatic (%)
0	0	7.6	92.4	28.4	71.6
	5	9.1	90.9	28.7	71.3
	10	4.8	95.2	26.0	74.0
	47	6.5	93.5	28.7	71.3
	146	9.3	90.7	34.0	66.0
8.5	0	6.9	93.1	30.1	69.9
	5	7.1	92.9	30.4	69.6
	10	6.5	93.5	29.5	70.5
	47	6.6	93.4	30.6	69.4
	146	12.3	87.5	34.2	65.8
18.6	0	8.3	91.7	31.2	68.8
	5	5.9	94.1	30.5	69.5
	10	7.0	93.0	30.1	69.9
	47	12.3	87.5	35.8	64.2
	146	8.1	91.9	38.3	61.7
27.5	0	7.4	92.6	30.9	69.1
	5	5.9	94.1	31.4	68.6
	10	8.7	91.3	34.2	65.8
	47	7.0	93.0	36.2	63.8
	146	14.0	86.0	36.6	63.4

[a] The n-C$_7$ asphaltenes content in the feed was adjusted by mixing bitumen, maltenes, and asphaltenes. The 0% feed consisted of just maltenes (deasphalted oil) and the 18.6 wt% feed consistent of just bitumen.
[b] The reaction time indicated excludes the heat up and cool down time periods. These time periods are, on average, 58 minutes.
[c] Analysis performed on a single sample.

5.3.3. ^{1}H and ^{13}C NMR analysis of narrow cut hydroprocessed distillates

Hydroprocessed distillates were included as a control group in this study. Most of the materials that were analyzed by Cookson, et al. [9] to develop **Equation (5-1)**, were distillate-range materials from different sources. In this study hydrocracked wax and hydrotreated kerosene were fractionated into narrow distillation cuts. Three cuts from each material were selected and were analyzed using ^{1}H and ^{13}C NMR spectrometry (**Table 5-6**). The ^{1}H and ^{13}C NMR spectra are shown in **Figure C-20** to **Figure C-25** in the **Appendix C**.

Table 5-6. Nature of hydrogen and carbon in narrow distillation cuts from hydroprocessed distillates, as determined by ^{1}H NMR and ^{13}C NMR, respectively.

Material Description	^{1}H NMR [a]		^{13}C NMR [a]	
	Aromatic (%)	Aliphatic (%)	Aromatic (%)	Aliphatic (%)
Hydrocracked wax				
140–145 ºC cut	0.3	99.7	5.7	94.3
230–235 ºC cut	0.3	99.7	3.8	96.2
315–320 ºC cut	0.1	99.9	2.6	97.4
Hydrotreated kerosene				
135–140 ºC cut	3.2	96.8	6.7	93.3
195–200 ºC cut	4.0	96.0	15.6	84.4
245–250 ºC cut	2.0	98.0	12.4	87.6

[a] Analysis performed on a single sample.

Cookson et al. [36] studied kerosene derived from different petroleum sources. It was reported that aromatic hydrogen content was typically between 0 and 6 %, whereas the aromatic carbon content ranged from 0 to 15 %. The materials in **Table 5-6** are broadly speaking within these ranges.

Usually, it is not expected to have an aromatic fraction in the hydrocracked paraffinic wax and Pillon [37] argued that the presence of an aromatic fraction detected by NMR may be due to contamination with other materials. However, the hydrocracked wax used in this study was obtained from hydrocracking at 2 MPa, and one of the consequences of reducing the hydrocracking pressure is that more cyclic material is formed [25].

5.4. Discussion

5.4.1. Relationship between aromatic hydrogen and carbon

Brown and Ladner's work [8] was focused on comparing the hydrogen distribution in coal-like materials using NMR and infrared spectrometry. Three structural parameters were estimated using both techniques: aromaticity (f_a), degree of substitution in aromatic systems (σ), and the atomic hydrogen to carbon ratio of hypothetical unsubstituted aromatic material $(H/C)_{Ar}$.

Cookson et al. [9] aimed to continue Brown and Ladner's work using only NMR spectroscopy. They noted that to make use of the relationship developed by Brown and Ladner, it was necessary to make an assumption about the nature of the material and additionally, to perform the elemental analysis. They articulated the desire to develop a relationship that were generally valid and that did not require any additional analyses beyond ^{1}H NMR analysis. Working towards this goal, they analysed 324 samples from a wide variety of origins by ^{1}H NMR or ^{13}C NMR and developed the relationship that was shown in **Equation (5-1)**. The parameter k is a proportionality constant between the atomic H/C ratio for hypothetically unsubstituted aromatic groups, $(H/C)_{Ar}$, and the atomic H/C ratio for hypothetical aliphatic groups, $(H/C)_{Al}$, in the sample (**Equation (5-2)**).

$$k = \frac{(H/C)_{Ar}}{(H/C)_{Al}} \qquad (5\text{-}2)$$

The goodness of fit and the seemingly regular relationship described by **Equation (5-1)** can be seen in **Figure 5-1**, which shows a re-plotting of all of the data from Cookson et al. [9].

The relationship was evaluated by using the absolute average relative deviation, AARD (%) as an indicator of agreement (**Equation (5-3)**), or disagreement, of the experimentally determined data. Additionally, the bias (%), **Equation (5-4)**, was consider as a metric for the under prediction of the relationship [38], or the opposite.

$$AARD\ (\%) = \frac{100}{N} \sum_{i}^{N} \left| \frac{X_{i,cal} - X_{i,exp}}{X_{i,exp}} \right| \tag{5-3}$$

$$Bias\ (\%) = \frac{100}{N} \sum_{i}^{N} \frac{X_{i,cal} - X_{i,exp}}{Xi_{i,exp}} \tag{5-4}$$

Where N is the number of points in the dataset, X is the variable of interest (C_{Ar}), and the subscripts *cal* and *exp* refer to the calculated and measured values. The results are summarized in **Table 5-7**.

While the AARD and Bias for the relationship in **Equation (5-2)** described by $k = 0.282$ are different for different types of materials analyzed by Cookson et al., the AARD is below 15 % and the Bias is below 11 % for all materials except for the crude oil and derived materials. This group of materials is described with slightly lower AARD and Bias by k=0.199, as Cookson et al. pointed out in their original publication.
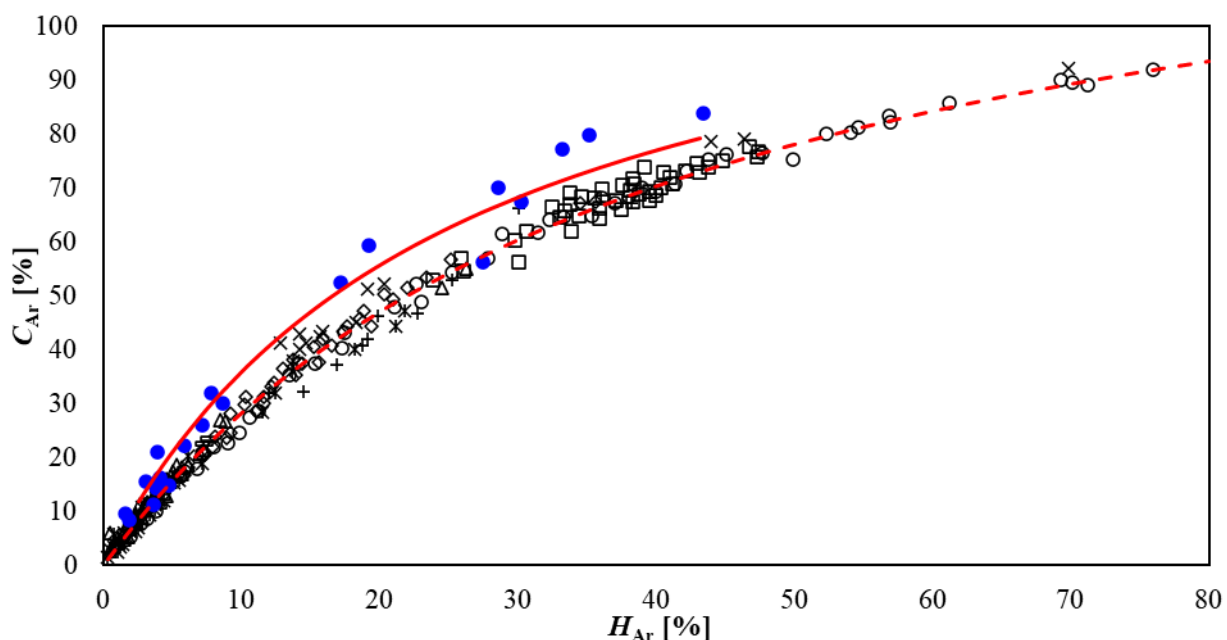
Figure 5-1. C_{Ar} against H_{Ar} from the 324 samples presented by Cookson et al. [9] The samples groups are Anthracene and Creosote Oil (○), Recycled Oil from Coal Hydrogenation (□), Hydrotreated products from Coal-Derived Syncrude (◊), Diesel Fuel (Δ), Kerosene Fuels (∗) Aromatic fractions from diesel and kerosene (x) and, gasoline (+), petroleum and synfuels (━). In blue, crude oil and derived materials (●). The solid line and dashed line in red were obtained using k as 0.199 and 0.282, respectively.

The main characteristic of these samples was that more than half of the samples had atmospheric equivalent boiling point temperature ranges below 320 °C. Only about one tenth of the samples could be classified as atmospheric residues and these samples included petroleum, shale, coal, and oilsands bitumen samples. It is noteworthy that the residua were better described using a different value for k than the bulk of the lower boiling materials, as can be seen in **Figure 5-1** or **Table 5-7** "crude oil and derived materials".

What was encouraging, was the regularity in **Figure 5-1**, despite the variance. It was reasoned that in petroleum the monotonic decrease in H/C ratio and monotonic increase in aromatic to aliphatic ratio with atmospheric equivalent boiling point noted by Altgelt and Boduszynski [39] could be largely responsible for changes in k and the variance seen in **Figure 5-1**.

With this in mind, the experimental ^{1}H NMR or ^{13}C NMR data collected in this study, as well as data from the literature, were divided into four groups for evaluation. The first three groups were defined based on their boiling point distribution, while the last group compared straight run with thermally converted materials. These groups are: (i) Data from wide-boiling materials with a median boiling point (i.e., T_{50}) below 320 °C (**Section 5.4.2**), (ii) Data from wide-boiling materials with a median boiling point above 320 °C (**Section 5.4.3**), (iii) Data from narrow boiling point cut materials (**Section 5.4.4**), and (iv) Data for oilsands bitumen before and after thermal conversion (**Section 5.4.5**).

Table 5-7. Absolute average relative deviation, AARD (%), and bias (%) of the datasets used in this study.

Dataset	$k = 0.282$		$k = 0.199$	
	AARD (%)	Bias (%)	AARD (%)	Bias (%)
Cookson [9]				
Anthracene oils and hydrogenated products	3.1	1.8	17.7	17.7
Creosote oil hydrogenated products	10.2	10.2	36.4	36.4
Recycle oils from coal hydrogenation	2.4	-0.9	9.7	9.7
Hydrotreated products from coal-derived syncrude	3.9	0.1	23.2	23.2
Diesel Fuels	11.7	-8.2	27.0	23.0
Kerosene	14.0	1.2	38.2	35.5
Diesel and Kerosene	7.9	-7.9	8.2	8.1
Gasoline	8.6	7.1	32.1	32.1
Petroleum and Synfuel	8.4	-1.1	31.0	31.0
Crude oil derived materials	18.6	-17.8	12.1	3.4
$T_{50} < 320$ °C				
Cookson [10]	7.5	-0.7	27.7	25.0
Awadalla [11]	5.4	5.3	26.2	26.2
Rodriguez [12]	15.1	-15.1	7.5	7.5
Hasan [13] – Saudi Arabian extra-light and light crude oils	20.4	12.2	39.6	39.6

Table 5-7. Absolute average relative deviation, AARD (%), and bias (%) of the datasets used in this study (continued).

Dataset	k = 0.282		k = 0.199	
	AARD (%)	Bias (%)	AARD (%)	Bias (%)
Hasan [14] – Saudi Arabian medium crude oil	13.5	4.8	29.7	29.7
Hasan [15] – Saudi Arabian heavy crude oil	16.2	5.9	32.6	32.6
Suzuki [16]	16.5	-10.0	14.8	5.7
Hiller [17]	2.0	-1.9	26.0	25.1
Collin [18]	12.7	-10.2	10.9	6.3
Adesanwo [19]	0.6	0.6	2.4	2.4
$T_{50} > 320\ °C$				
Cookson [10]	0.6	-0.4	4.3	4.3
Rodriguez [12]	3.3	-3.3	3.4	3.4
Hasan [13] – Saudi Arabian extra-light and light crude oils	10.3	-10.3	4.1	-2.9
Hasan [14] – Saudi Arabian medium crude oil	7.3	-7.3	4.6	0.5
Hasan [15] – Saudi Arabian heavy crude oil	9.0	-9.0	2.7	-1.4
Suzuki [16]	8.8	-8.8	5.8	-5.8
Collin [18]	0.6	-0.6	0.3	0.3
Adesanwo [19]	1.0	1.0	2.1	2.1
Ali [20]	19.5	-8.0	21.6	15.6
Snape [21]	3.8	2.7	10.6	10.6
Diaz [22]	3.8	3.8	5.2	5.2
O'Donnell [23]	28.8	-27.8	17.5	-5.5
Poveda [24]	64.6	-64.6	54.0	-54.0
Narrow boiling cut materials				
Link [25]	80.5	-80.5	72.5	-72.5
Athabasca bitumen	60.2	39.2	91.4	89.5
Kerosene	39.9	-2.3	49.4	32.6
Thermally converted products				
Athabasca bitumen	77.2	31.1	20.6	-13.7

5.4.2. Aromatic carbon and hydrogen in wide-boiling materials with $T_{50} < 320$ °C

Despite the thoroughness of the evaluation by Cookson, et al. [9] it was of interest to verify the applicability of **Equation (5-1)** with $k = 0.282$ with ^{1}H and ^{13}C NMR data in the literature for materials with median boiling point temperatures below 320 °C. Some additional variation was anticipated, because not all investigators used exactly the same spectral ranges to denote aliphatic and aromatic compounds. In fact, it was pointed out by Cookson, et al. [9] that they deliberately did not include literature data in their study, because of perceived concerns about ^{13}C NMR quantification. It was therefore encouraging to see that the measurements for many of the materials that were reported in literature followed this relationship in spite of the increased variability (**Figure 5-2**) [10-19]. The AARD and Bias were comparable to Cookson's original data for a significant fraction of the samples, particularly those with a low distillation boiling range when using $k = 0.282$ (see **Table 5-7**).

Nevertheless, even though all different samples are complying with the requirement of $T_{50} < 320$ °C, not all of the samples are well described by **Equation (5-1)** with $k = 0.282$ (**Figure 5-2**). Staying within the formalism of that work, the solubility fractions from bitumens [16], and some of the products from Liddell coal,[18] had a higher aromatic carbon content than predicted from the aromatic hydrogen content and were better described by **Equation (5-1)** with $k = 0.199$ (see **Table 5-7**). A closer look was taken at both of these samples.

The solubility fractions from bitumens reported by Suzuki et al. [16] and that reportedly met the $T_{50} < 320$ °C criterion, were the first three solubility fractions from saturates-aromatics-resins-asphaltenes (SARA) separation. The bitumens considered were Athabasca and Cold Lake bitumens from Canada and Orinoco bitumen from Venezuela. These materials include a large vacuum residue (>525 °C) fraction and considering the typical properties [31], it is doubtful that the saturate, aromatic, and resin solubility fractions were indeed meeting the $T_{50} < 320$ °C criterion.

The coal liquids from the work by Collin et al. [18] displayed differing relationships between the aromatic hydrogen and carbon content and it was not possible to make any general statements based on the method of preparation. The samples included pyrolyzed coal, coal hydrogenated

using SnCl$_2$ as catalyst, coal hydrogenated using Ni/Mo as catalyst and tetralin as hydrogen-donor solvent, and coal hydrogenated using Ni/Mo as catalyst and a coal-derived oil as solvent.

The evaluation cast doubt on the postulate that variation in values of k was related to the atmospheric equivalent boiling point.
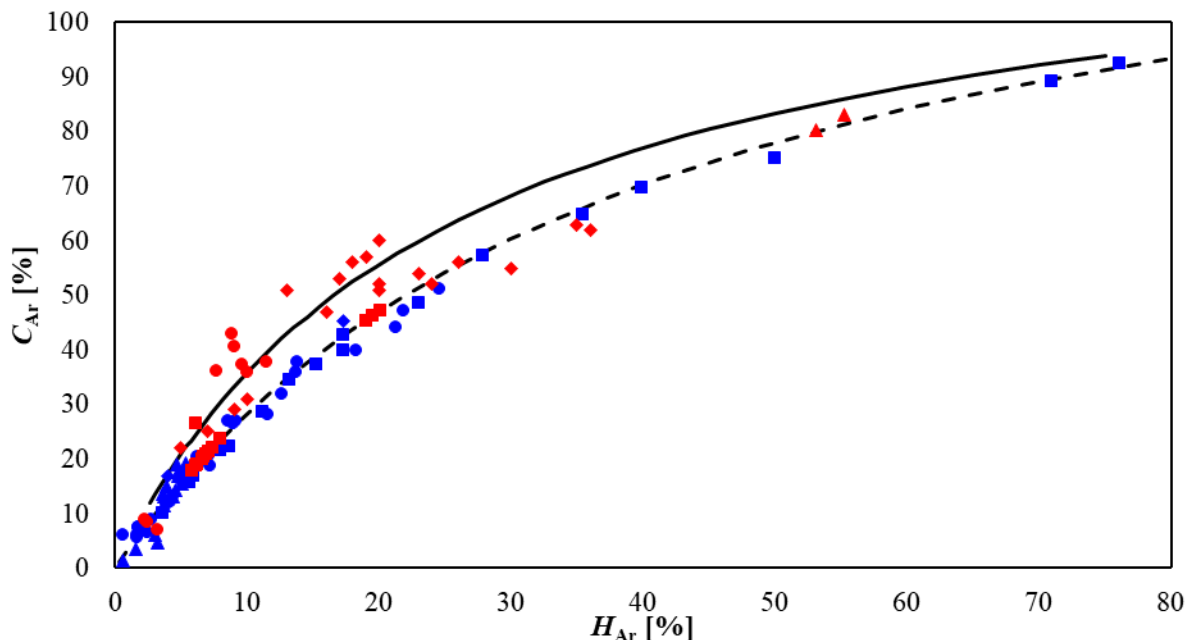
Figure 5-2. C$_{Ar}$ against H$_{Ar}$ from different materials and studies. The samples groups are diesel and kerosene fuels [10] (●), creosote and anthracene oils and their derived products [11] (■), FCC naphtha and distillate [12] (♦), fractions of extra-light and light, medium and heavy Arabian crude oils [13-15] (▲), solubility fractions from bitumens [16] (●), gasoline [17] (■), hydrogenated and pyrolyzed products from Liddell coal fractions [18] (♦), and liquid coal fractions [19] (▲). The solid line and dashed lines were obtained by Cookson [9] using k as 0.199 and 0.282, respectively.

5.4.3. Aromatic carbon and hydrogen in wide-boiling materials with $T_{50} > 320 \,°C$

For materials with median boiling point temperatures above 320 °C the same rationale as explained in **Section 5.4.2** was applied. In this case it was of interest to see the applicability of **Equation (5-1)** with $k = 0.199$ with ^{1}H and ^{13}C NMR data in the literature. The relationship between aromatic hydrogen and carbon content of materials for which such data was reported in the literature is shown in **Figure 5-3** [10,12,13-16,18,20-24,30].

The spread of values included samples that were better described using $k = 0.282$, even though T_{50} > 320 °C, as well as samples that were better described using $k = 0.199$. Generally, the AARD and Bias were significantly higher than for the samples with T50 < 320 °C (see **Table 5-7**). As was concluded from **Figure 5-2**, the data in **Figure 5-3** also indicated that the median boiling point was not a sufficient criterion to fix a value for k.

Three groups of samples appeared to have a different relationship between their aromatic hydrogen and carbon content. The most obvious group of samples in **Figure 5-3** is that of the n-C$_7$ asphaltenes from thermally cracked Colombian heavy crude oil.[24] Next is the n-C$_7$ asphaltenes from Athabasca, Cold Lake, and Orinoco bitumens.[16] The last group is Kuwaiti vacuum gas oils,[20] which spans a range of aromatic hydrogen to carbon values from 0.27 to 0.58, although most values were in the narrower range of 0.30–0.35.

The deviation of the asphaltenes from the predicted relationships (**Figure 5-3**) can to some extent be rationalised. Asphaltenes have a higher heteroatom content than the material it is derived from, since it is a solubility class that is defined by insolubility in an excess of n-alkane. Sulfur and oxygen, when present in multicyclic aromatic compounds, do not occupy ring-junction positions, which require a minimum of three covalent bonds. Nitrogen, when present in multicyclic compounds, seldom occupy a ring-junction position, although there are examples of neutral multinuclear aromatic compounds with nitrogen at a ring-junction position, such as indolizine (C_7N_7N). All of the heterocyclic aromatic compounds affect aromatic hydrogen and carbon accounting of a molecule. The accounting is affected either by having a smaller ring size (5-membered as opposed to 6-membered) with less chance of having a hydrogen substituted aromatic

carbon, or by heteroatom replacement of an aromatic carbon–hydrogen group and not aromatic carbon only (ring-edge as opposed to ring-junction). In both instances the presence of heteroatoms diminishes the probability of finding aromatic hydrogen in association with aromatic carbon.
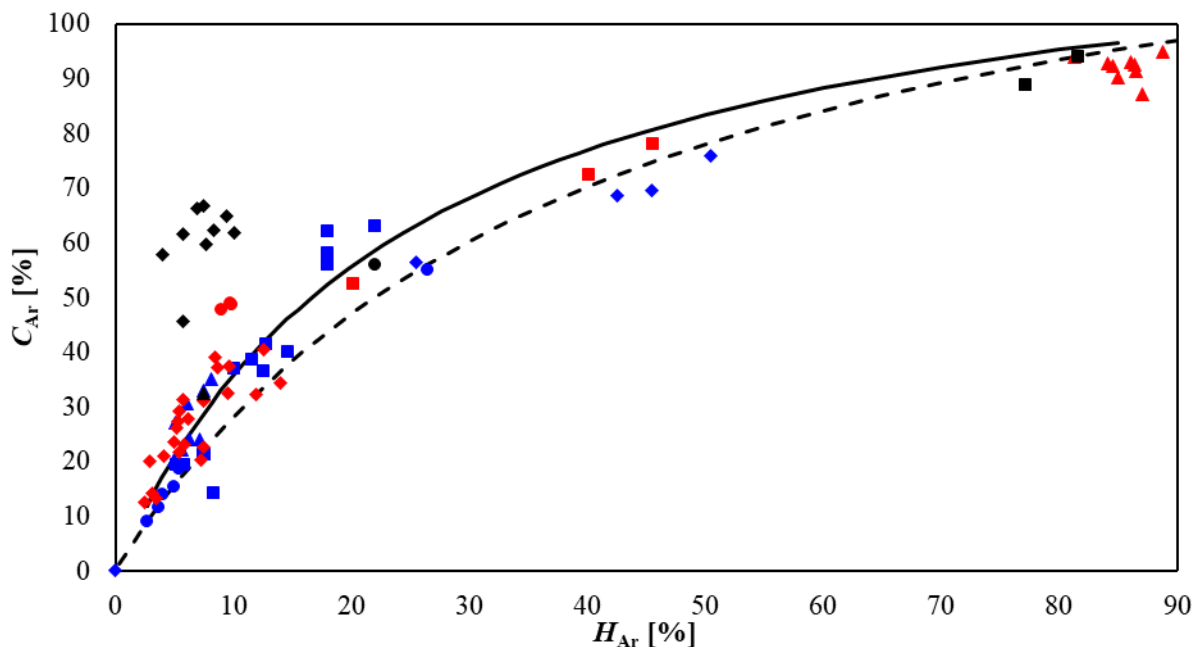
Figure 5-3. C_{Ar} against H_{Ar} from different materials and studies. The samples groups are heavy diesel fuels [10] (●), Kuwaiti vacuum gas oils [20] (■), hydrocracked coal extract fractions [21] (♦), fractions of extra-light and light, medium and heavy Arabian crude oils [13-15] (▲), asphaltene from bitumens [16] (●), FCC fractions [12] (■), 535–675 °C oil fractions [23] (♦), coal tar pitch extracts [22] (▲), hydrogenated and pyrolyzed products from Liddell coal [18] (●), liquid coal fractions [19] (■), asphaltenes from thermally cracked Colombian heavy crude oil [24] (♦), Vacuum Residue Deasphalted Oil from Athabasca bitumen [30] (▲). The solid line and dashed lines were obtained by Cookson [9] using k as 0.199 and 0.282, respectively.

The argument based on heterocyclic content is fundamental to aromatic hydrogen and carbon accounting in aromatic compounds. As a generally valid statement the probability of finding aromatic hydrogen in association with aromatic carbon is diminished by increased heteroatom content, or more specifically, heterocyclic aromatic content. Differently put, an increase in

heterocyclic aromatic content will decrease the atomic H/C ratio for hypothetical unsubstituted aromatic groups and thereby k (**Equation (5-2)**).

This was a potentially useful observation, because it indicated that within a specific boiling point range, materials with a high heteroatom content were likely to have a different k-value.

5.4.4. *Petroleum narrow-boiling fractions*

The relationship between the aromatic hydrogen and carbon content of the straight run narrow-boiling fractions distilled from bitumen (**Table 5-4**) and hydroprocessed refined kerosenes (**Table 5-6**) are shown in **Figure 5-4**. There was no orderly progression of the aromatic hydrogen and carbon content with boiling point. The experimental values in some instances had a very different relationship between aromatic hydrogen and carbon and indicated that narrow-boiling fractions (**Figure 5-4**) as opposed to wide-boiling fractions (**Figure 5-2** and **Figure 5-3**) had no obvious bias or difference in the scatter of its distribution. This is confirmed by the calculated AARD and Bias (see **Table 5-7**).
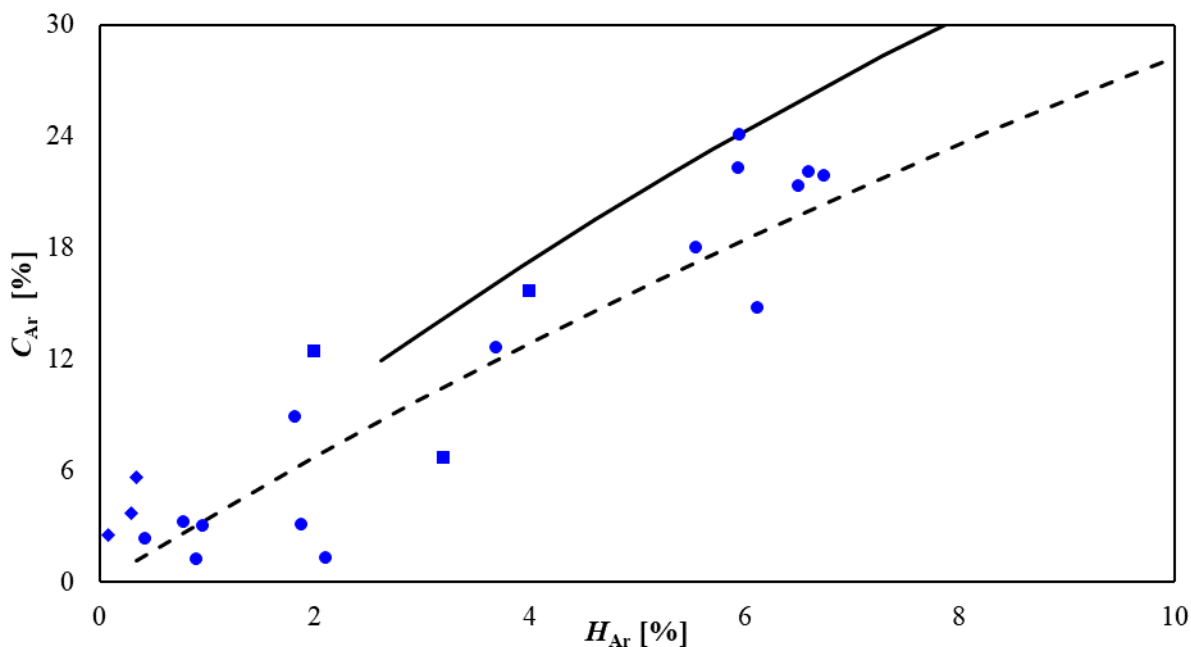
Figure 5-4. C_{Ar} against H_{Ar} for petroleum fractions. The data corresponds to: Athabasca bitumen cuts (●), kerosene (■), and hydrocracked paraffinic wax [25] (◆). The solid line and dashed lines were obtained by Cookson, et al. [9] using k as 0.199 (solid line) and 0.282 (dashed line), respectively.

The reason for the seemingly irregular relationship between aromatic hydrogen and carbon between narrow-boiling fractions was explored further.

When the relationship is explored in the context of **Equation (5-1)**, part of the variation seen in the narrow cuts from bitumen can be explained by reference to the *k*-value. The *k* value is defined as the aromatic H/C divided by the aliphatic H/C as shown in **Equation (5-2)**. Since the narrow boiling cut materials in the distillate and vacuum gas oil range are free of unsaturated aliphatic compounds, $(H/C)_{Al} \sim 2$ and have a low heteroatom content. This means that variations in the *k*-value is describing the variation in $(H/C)_{Ar}$. The $(H/C)_{Ar}$ is essentially a function of the degree of substitution of aromatic rings. The more substituents that are located on an aromatic ring, the lower the aromatic $(H/C)_{Ar}$ ratio becomes, as aromatic hydrogen is replaced by substituents.

A further clue is provided by the progression of the aromatic carbon content as percentage of the total carbon in each distillation cut. There is a noticeable oscillation in the aromatic content with successive cuts from the 150–170 °C to 250–270 °C (**Table 5-4**). This type of behavior was also observed by Muller, et al. [40] in work where they compared their ^{13}C NMR results with the data obtained using Haverly Crude Assay and Management Software (H/CAMS).

It seems that the periodic decrease in aromatic carbon content might be related to the change in the number of aromatic rings a structure may present. This is illustrated by **Figure 5-5** showing the data from this study and that from the study by Muller, et al. [40] in relation to the homologous series of alkyl substituted aromatics.
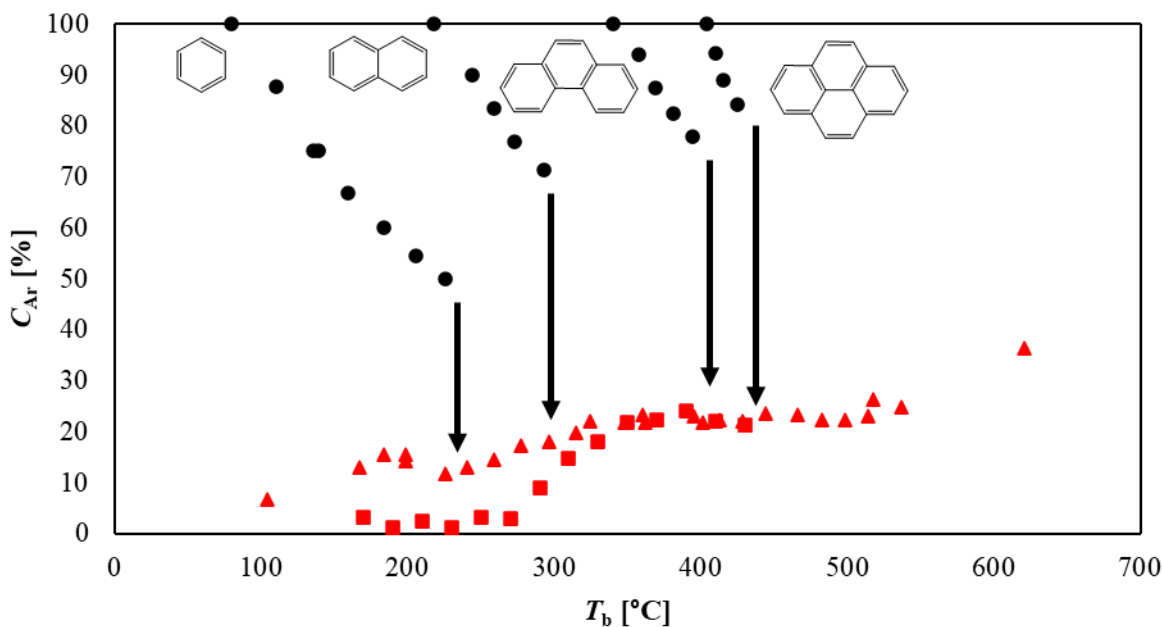
Figure 5-5. ^{13}C NMR Carbon Aromatic Content as a function of the boiling temperature of Athabasca bitumen distillation cut (■). Muller et al. [40] (▲) data has also been included to show the effect of the number of rings in the homologous series of alkyl substituted aromatics.

In **Figure 5-5**, it can be seen that the boiling point transition from aromatic species that have only one aromatic ring (benzene-derivatives) to include species with two aromatic rings (naphthalene-

derivatives) is accompanied by a decrease in the overall aromatic content. Similar observations can be made for the boiling range where three or four ring aromatics can be present in the product.

Directionally the observed change in aromatic content (**Figure 5-5**) is counter to what one would have anticipated, since the unsubstituted aromatics have the highest aromatic carbon content per molecule and the opposite is observed. Unalkylated aromatics, such as benzene and naphthalene, tend to be less abundant in straight run oils and products from refining than in processes operated at temperatures >600 °C, during which dealkylation of alkyl aromatics becomes increasingly important as temperature is increased [41]. The counter intuitive observation in **Figure 5-5**, namely, that the aromatic carbon content decreases at distillation temperatures where a new aromatic series starts, is tentatively ascribed due to the lower abundance of unalkylated aromatics than alkylated aromatics unless the material originates from a high temperature (>600 °C) process.

5.4.5. *Oilsand bitumen before and after thermal conversion*

The preceding data sets represented straight run and converted materials, but the data in **Table 5-5** was the only large data set that provided information on the relative changes caused by thermal conversion of material derived from a single source. The reaction progression of any one of the feed materials prepared from oilsands bitumen solubility fractions would show to what extent thermal conversion caused not only a change in aromatic content, but also the nature of the relationship between aromatic hydrogen and carbon.

As explained in the **Introduction**, there was the hope that ^{1}H NMR could be used to track changes both in aromatic hydrogen and carbon through **Equation (5-1)**. For this specific purpose the *k*-value could be determined experimentally for the feed material specifically and then used for subsequent prediction of changes in thermally converted products.

However, the relationship between aromatic hydrogen and carbon for the feed and products at different severity of thermally conversion (**Figure 5-6**) was not described by **Equation (5-1)** with a single *k*-value. This is confirmed by AARD and Bias, which were above 13 % for all of the

samples. The change in aromatic hydrogen and carbon content caused by thermal conversion did not have a fixed relationship.
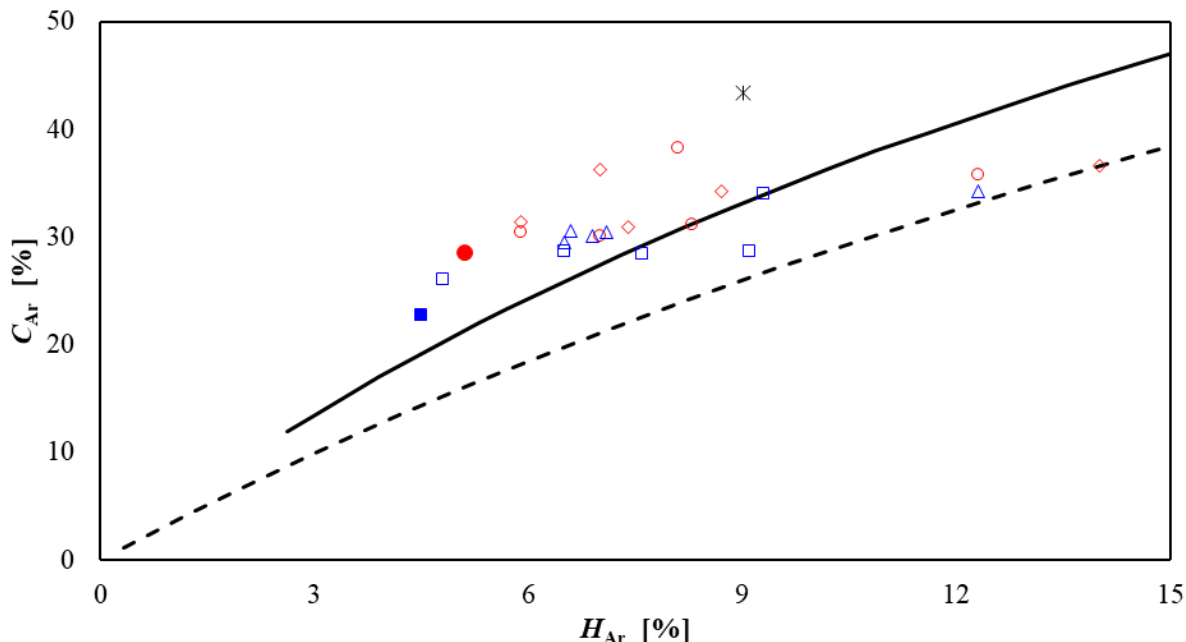
Figure 5-6. C_{Ar} against H_{Ar} of thermally converted products. The data corresponds to: visbroken products from Athabasca bitumen (□), visbroken products from a mixture of Athabasca bitumen and asphaltenes (△), visbroken products from Athabasca maltenes (○), visbroken products from Athabasca maltenes and asphaltenes (◇). Athabasca bitumen (●), Athabasca bitumen maltenes (■), Athabasca asphaltenes (✶). The solid line and dashed lines were obtained by Cookson [9] using k as 0.199 and 0.282, respectively.

5.4.6. *Prognosis for aromatic carbon content prediction from aromatic hydrogen content*

So far it was shown that the relationship in **Equation (5-1)** was broadly indicative of the relationship between aromatic hydrogen content and aromatic carbon content (**Section 5.4.1**). The relationship has only one parameter, k (**Equation (5-2)**). The original work by Cookson et al. [9] was thorough and made use of an extensive range of materials. There was some uncertainty in predictions, but by using different values from k selected based on median boiling point

temperature (T_{50}), the uncertainty with predictions could be reduced and a standard deviation of 1.8% was reported [9].

The prognosis for general applicability was good. Following on the original work by Cookson et al. [9] and rationalising it with reference to Altgelt and Boduszynski [39], it was initially postulated that variations in k was due to differences in atmospheric equivalent boiling point. Yet, using both experimentally collected ^{1}H and ^{13}C NMR data in combination with data from literature, it was convincingly shown that the variation in k could not be explained just in terms of boiling range (**Sections 5.4.2 - 5.4.4**).

Three other observations emerged from the work. It was shown that some narrow close-boiling cuts had quite different ratios of aromatic hydrogen and carbon due to the natural progression of the alkyl aromatic homologous series (**Section 5.4.4**). It was also observed and explained that an increase in heterocyclic aromatic content would inherently decrease the ratio of aromatic hydrogen content to the aromatic carbon content for otherwise comparable materials (**Section 5.4.3**). Thermal conversion of a material did not progress in such a way that the change in aromatic hydrogen and carbon content had a fixed relationship (**Section 5.4.5**).

Considering the above mentioned evidence, it was concluded that the relationship in **Equation (5-1)** had a larger uncertainty than suggested by Cookson et al. [9] **Equation (5-1)** had some use for estimation in the broad sense, since there appeared to be a band within which aromatic hydrogen content was related to aromatic carbon content (**Figure 5-1** to **Figure 5-4**), that is $C_{Ar} \sim f(H_{Ar})$. One could also directionally bias predicted values if it was known that a material had a high heteroatom content. However, for individual oil samples with no further *a priori* knowledge, the aromatic hydrogen content determined by ^{1}H NMR analysis could not be considered an adequate estimate for the aromatic carbon content determined by ^{13}C NMR analysis.

5.5. Conclusions

The ability to calculate the aromatic carbon content of petroleum and coal derived materials from the aromatic hydrogen content was evaluated. The main outcomes from the evaluation of the relationship between ^{1}H and ^{13}C NMR measured aromatic hydrogen and carbon content were:

a. Petroleum and coal derived materials displayed a range of values of aromatic carbon content, C_{Ar}, for any given value of aromatic hydrogen content, H_{Ar}. As a consequence, the relationship between these two values represented a band, or broadly related relationship, instead of a narrowly defined relationship as suggested in the work of Brown and Ladner [8] and Cookson, et al. [9].

b. The median atmospheric equivalent boiling point temperature (T_{50}) was not a parameter with good predictive value for adjusting the relationship between C_{Ar} and H_{Ar}. The usefulness of T_{50} was not improved when considering narrow distillation fractions as opposed to wide distillation fractions. In fact, in narrow distillation fractions it was possible to discern the impact of the transition in ring count of homologous series of alkyl aromatics, which affected the C_{Ar} of the narrow distillation fractions.

c. An increase in the heterocyclic aromatic content caused a decrease in the $(H/C)_{Ar}$ ratio. This is a generally valid observation, since heteroatoms are predominantly found in ring-edge positions instead of aromatic C–H instead of ring-junction position instead of aromatic C.

d. The change in H_{Ar} and C_{Ar} of a material that is thermally converted was monitored for oilsands bitumen at different levels of conversion severity. It was found that conversion affected changes in H_{Ar} and C_{Ar} differently, and no fixed relationship could be discerned.

References

[1]   Gray, M.R. Fundamentals of Partial Upgrading of Bitumen. *Energy and Fuels* **2019**, *33*: p. 6843 - 6856.

[2]   Kaiser, M.J.; de Klerk, A.; Gary, J.H.; Handwerk G.E. *Petroleum refining: technology, economics, and markets*. Sixth edit. CRC Press: Boca Raton, FL, 2020.

[3]   Riazi, M. R.; Gupta R. *Coal Production and Processing Technology*. CRC Press: Boca Raton, FL, 2016.

[4]   Rosendahl, L. *Direct Thermochemical Liquefaction for Energy Applications*. Woodhead Publishing: Duxford, UK, 2018.

[5]   Dente, M.; Bozzano, G.; Faravelli, T.; Marongiu, A.; Pierucci, S.; Ranzi, E. Kinetic Modelling of Pyrolysis Processes in Gas and Condensed Phase. *Advances in Chemical Engineering* **2007**, *32*: p. 51 - 166.

[6]   Stock, L. M. Hydrogen-transfer reactions. In *Chemistry of Coal Conversion*; Schlosberg, R. H., Ed.; Plenum Press: New York, 1985; p. 253−316.

[7]   Rahimi, P.M.; Teclemariam, A.; Taylor, E.; DeBruijn, T.; Wiehe, I.A. Thermal Processing Limits of Athabasca Bitumen during Visbreaking Using Solubility Parameters. *ACS Symposium Series* **2005**, *895*: p. 183 - 196.

[8]   Brown, J.K.; Ladner, W.R. A Study of the Hydrogen Distribution in Coal-like Materials by High-resolution Nuclear Magnetic Resonance Spectroscopy. II - A Comparison with Infra-red Measurement and the Conversion to Carbon Structure. *Fuel* **1967**, *39*: p. 87 - 96.

[9]   Cookson, D.J.; Lloyd, C.O.; Smith B. E. A Novel Semi-Empirical Relationship between Aromaticities Measured from ^{1}H and ^{13}C N.M.R. Spectra. *Fuel* **1986**, *65*: p. 1247 - 1253.

[10]   Cookson, D.J.; Latten, J.L.; Shaw, I.M.; Smith, B. E. Property-Composition Relationship for Diesel and Kerosene Fuels. *Fuel* **1985**, *64*: p. 509 - 519.

[11]   Awadalla, A.A.; Cookson, D.J.; Smith, B.E. Coal Hydrogenation: Quality of Start-up Solvents and Partially Process-derived Recycle Solvents. *Fuel* **1985**, *64*: p. 1097 - 1107.

[12]   Rodriguez, J.; Tierney, J.W.; Wender I. Evaluation of a Delayed Coking Process by ^{1}H and ^{13}C N.M.R Spectroscopy: 2. Detailed Interpretation of Liquid N.M.R Spectra. *Fuel* **1994**, *73*: p. 1870 - 1875.

[13]   Hasan, M.U.; Ali, M.F.; Arab, M. Structural Characterization of Saudi Arabian Extra Light and Light Crudes by ^{1}H and [13]C N.M.R. Spectroscopy. *Fuel* **1989**, *68*: p. 801 - 803.

[14]   Hasan, M.U.; Bukhari, A.; Ali, M.F. Structural Characterization of Saudi Arabian Medium Crude Oil by N.M.R. Spectroscopy. *Fuel* **1985**, *64*: p. 839 - 841.

[15]   Hasan, M.U.; Ali, M.F.; Bukhari, A. Structural Characterization of Saudi Arabian Heavy Crude Oil by N.M.R. Spectroscopy. *Fuel* **1983**, *62*: p. 518 - 523.

[16]   Suzuki, T.; Itoh, M.; Takegami, Y.; Watanabe, Y. Chemical Structure of Tar-sand Bitumens by ^{13}C and [1]H N.M.R. Spectroscopic Methods. *Fuel* **1982**, *61*: p. 402 - 410.

[17]   Hiller, W.G.; Abu-Dagga, F.; Al-Tahou, B. Determination of Gasoline Octane Numbers by ^{1}H and ^{13}C-NMR Spectroscopy. *Journal für Praktische Chemie* **1992**, *334*: p. 691 - 695.

[18]   Collin, P.J.; Gilbert, T.D.; Philp, P.; Wilson, M.A. Structures of the Distillates Obtained from Hydrogenation and Pyrolysis of Liddell Coal. *Fuel* **1983**, *62*: p. 450 - 458.

[19]   Adesanwo, T.; Rahman, M.; Gupta, R.; De Klerk A. Characterization and Refining Pathways of Straight-Run Heavy Naphtha and Distillate from the Solvent Extraction of Lignite. *Energy and Fuels* **2014**, *28*: p. 4486 - 4495.

[20]   Ali, F.; Khan, Z.H.; Ghaloum, N. Structural Studies of Vacuum Gas Oil Distillate Fractions of Kuwaiti Crude Oil by Nuclear Magnetic Resonance. *Energy and Fuels* **2004**, *18*: p. 1798 - 1805.

[21]   Snape, C.E.; Ladner, W.R.; Bartle, K.D. Structural Characterization of Coal Extracts by NMR. In: *Coal Liquefaction Products*; Schultz, H.D., editor. John Wiley & Sons, Inc.: New York, NY, 1983; Vol 1, p. 70 - 84.

[22]   Diaz, C.; Blanco C.G. NMR: A Powerful Tool in the Characterization of Coal Tar Pitch. *Energy and Fuels* **2003**, *17*: p. 907 - 913.

[23]   O'Donnell, D.J.; Sigle, S.O.; Berlin, D.K.; Sturm, G.P.; Vogh, J.W. Characterization of High-boiling Petroleum Distillate Fractions by Proton and [13]C Nuclear Magnetic Resonance Spectroscopy. *Fuel* **1980**, *59*: p. 166 - 174.

[24]   Poveda, J.C.; Molina, D.R.; Pantoja-Agreda E.F. ^{1}H- and ^{13}C-NMR Structural Characterization of Asphaltenes from Vacuum Residua Modified by Thermal Cracking. *CT&F - Ciencia, Tecnología y Futuro* **2014**, *5*: p. 49 - 60.

[25] Link, F.; Halmenschlager, C.; Chauhan, G.; De Klerk, A. Wax Hydrocracking over Pt/SiO2-Al2O3 at 2 MPa: Product Characterization and its Implications for Catalysis. *Energy and Fuels* **2021**, *35*: p. 5252 - 5263.

[26] *ASTM D3279: Standard Test Method for n-Heptane Insolubles*, ASTM International: West Conshohocken, PA, 2019.

[27] Castillo, J.; de Klerk, A. Visbreaking of Deasphalted Oil from Bitumen at 280−400 °C. *Energy and Fuels* **2019**, *33*: p. 159 - 175.

[28] Tulegenova, D. Physical Properties of Bitumen Distillation Fractions and Solvent Effect on Free Radical Content. MSc Thesis, University of Alberta, 2021.

[29] Chen, B. Introduction to NMR. In *Fundamentals of Recoupling and Decoupling Techniques in Solid State NMR*. AIP Publishing LLC: Melville, N.Y, 2020, p. 1 - 16.

[30] Tannous, J. H. Heavy Products Formation in Free Radical Systems during Thermal Conversion of Heavy Oil. PhD Thesis, University of Alberta, 2019.

[31] Gray, M. R. *Upgrading Oilsands Bitumen and Heavy Oil.* University of Alberta Press: Edmonton, Canada, 2015.

[32] Ancheyta Juárez, J.; Trejo, F.; Rana, M.S. *Asphaltenes: Chemical Transformation during Hydroprocessing of Heavy Oils*. CRC Press: Boca Raton, FL, 2009.

[33] Shafiee Neistanak, M. Kinetics of Asphaltene Precipitation and Flocculation from Diluted Bitumen. MSc Thesis, University of Calgary, 2014.

[34] Girdler RB. Constitution of Asphaltenes and Related Studies. Proceedings of Technical Sessions by the Association of Asphalt Paving Technologies, Philadelphia: 1965, p. 45 - 79.

[35] Rahimi, P.M.; Gentzis, T. The Chemistry of Bitumen and Heavy Oil Processing. In: *Practical Advances in Petroleum Processing*; Hsu C.S.; Robinson, P, R., editors. Springer: New York, NY, 2006, p. 597 - 634.

[36] Cookson, D.J.; Lloyd, C.O.; Smith, B. E. Investigation of the Chemical Basis of Kerosene (Jet Fuel) Specification Properties. *Energy and Fuels* **1987**, *1*: p. 438 - 447.

[37] Pillon, L.Z. Use of NMR Spectroscopy to Study the Effect of Hydrocracking on the Chemistry of Hydrocarbons. *Petroleum Science and Technology* **2002**, *20*: p. 357 - 365.

[38] Altgelt, K.H., Boduszynski, M.M. *Composition and Analysis of Heavy Petroleum Fractions*. Marcel Dekker: New York, NY, 1994.

[39]   Montoya-Sanchez, N.; de Klerk, A. Viscosity Mixing Rules for Bitumen at 1-10 wt %
         Solvent Dilution When Only Viscosity and Density Are Known. *Energy and Fuels* **2020**,
         34: p. 8227 - 8238.

[40]   Muller, H.; Saleem, Q.; Alawi, E.A.; Alsewdan, D.A.; Naqvi, I.A.S.; Saleh, A.;
         Rowaished. T.A. Narrow Distillation Cuts for an Improved Characterisation of Crude Oil:
         an Insight on Heteroatoms in Heavy Fraction Molecules. *International Journal of Oil, Gas
         and Coal Technology* **2021**, *26*: p. 40 - 59.

[41]   Kubicka, D.; Lederer, J.; Hanika, J.; Kolena, J. Kinetics of Thermal Hydrodealkylation of
         C_7 and C_8 Aromatics. *Petroleum and Coal* **2002**, *44*: p. 192 - 194.

6. Is Solubility Classification a Meaningful Measure in Thermal Conversion?

6.1. Introduction

Solubility classification is ubiquitous in disciplines dealing with macromolecules. Solubility classifications range from simple binary classifications, such as differentiating oil from wax using methyl ethyl ketone solubility [1], to more complex solubility classification trees, such as those found in solvent extraction of coal [2]. Due to the challenges associated with the characterization of macromolecules found in high-boiling petroleum fractions, solubility classification remains an important technique [3]. The most commonly encountered petroleum solubility classification is in terms of saturates, aromatics, resins, and asphaltenes (SARA) [4-6].

Of these solubility fractions, the asphaltenes fraction has direct practical significance. It has direct bearing on flow assurance of petroleum, and in petroleum refining, it is a product from solvent deasphalting [7]. The asphaltenes fraction is the material that is insoluble in light n-alkanes (usually either n-pentane, or n-heptane) and soluble in light aromatics (usually toluene). Phase separation, as well as the physical and chemical description of asphaltenes is therefore a topic of broad relevance, with significant recent reviews [8,9].

Another solubility class relevant to petroleum conversion is the carbonaceous material formed during thermal conversion and is often referred to as 'coke'. The coke content of thermally processed material is defined as the toluene insoluble fraction [10,11]. It is possible to further sub-classify the coke into carbenes and carboids based on solubility, where carbenes are CS_2 soluble material and the carboids are CS_2 insoluble material (pyridine is also used as solvent for this classification) [12].

The development of the carbonaceous material during thermal conversion is relevant, since it could affect the proper operation of a processing unit and lead to its premature shutdown. In literature, a possible link between coke and asphaltenes was investigated [10,13], since both are solubility classes and going from asphaltenes to coke appears to represent progression of increasing

insolubility. At the same time, there are also investigations that indicate that the asphaltenes content is not a good predictor of coke formation during thermal conversion [14].

Nevertheless, it stands to reason that if a second condensed phase forms during the transport or processing of petroleum, it will affect rheology, transport processes, and reactions. Consequently, there is the anticipation that solubility and solubility classes would be relevant to petroleum conversion.

The onset of the formation of a second condensed phase is of particular relevance, since it must be prevented during petroleum transport and storage. It must similarly be prevented in some process units, such as in furnaces preheating petroleum for distillation and in furnaces associated with conversion processes. Several approaches have been suggested to describe the relationship between a change in bulk liquid composition and second condensed phase formation [15]. Conceptually, the easiest description of phase separation is that involving the absolute difference in solubility parameters ($\Delta\delta = |\delta_i - \delta_j|$) between species, or phases i and j when a threshold value for $\Delta\delta$ is exceeded [16,17]. Since petroleum is a mixture of many species, it is more appropriate to refer to the range of solubility parameters between the lowest (δ_{min}) and highest (δ_{max}), rather than just a single value [18]. The threshold for $\Delta\delta$ can be exceeded with respect to either δ_{min}, or δ_{max}, depending on the direction of the change in the solubility parameter. In the case of asphaltenes, the separation follows on changing the bulk liquid solubility parameter to a lower value, and it is the material at δ_{max} that would first exceed the threshold $\Delta\delta$.

During thermal conversion, it is the formation of a second condensed phase at the operating conditions that is relevant to the description of coke formation. The assumption that was questioned was whether the asphaltenes, which is a solubility class separated at a temperature well below that of the thermal conversion process, would be descriptive of phase separation at reaction conditions. To probe this, a more general question was posed: Is solubility classification of the feed a meaningful measure in the description of thermal conversion?

In this study, both n-heptane and CS_2 solubility classification was employed, with Athabasca bitumen as the petroleum of interest. The solubility parameters of n-heptane and CS_2 are 15.3 and

20.3 MPa$^{0.5}$, respectively [16], which straddle the reported solubility parameter of 18.25 MPa$^{0.5}$ for Athabasca bitumen, as determined by titration [19]. These solvents were selected to probe solubility from either side of the solubility parameter range and because these solvents are used to determine asphaltenes and coke content.

The paper is in honor of Oliver Mullins. It is difficult to read the literature on solubility classification and petroleum asphaltenes without coming across his name [8,20-23]. It is our hope that this work is a fitting contribution to his continuing quest and continuing inspiration to researchers to better understand petroleum asphaltenes.

6.2. Experimental

6.2.1. Materials

A sample of Athabasca bitumen was obtained as bitumen-and-water emulsion produced at the Long Lake SAGD (Steam-Assisted Gravity Drainage) facility, located near Anzac, Alberta, in the Athabasca oilsands region. The water was removed from the bitumen by heating the bitumen-and-water emulsion in a rotary evaporator with the heating bath temperature set at 110 °C and the pressure controlled at 40 kPa absolute. The separation process took 82 hours to remove 99.4 wt% of the water in the emulsion, which was determined by Karl Fischer titration. Characterization of the Athabasca bitumen recovered from the emulsion is presented in **Table 6-1**.

Table 6-1. Characterization of Athabasca bitumen obtained from bitumen-and-water emulsion produced at Long Lake SAGD facility.

Property	Athabasca bitumen [a]
Solubility classes (wt%)	
n-heptane insolubles	18.6 ± 0.6
CS_2 insolubles	0.8 ± 0.6
Elemental composition (wt%)	
carbon	83.0 ± 0.1
hydrogen	10.3 ± 0.1
nitrogen	0.5 ± 0.1
sulfur	5.2 ± 0.3
oxygen (by difference)	1.0
Aromatic hydrogen content (%)	5.3
Aromatic carbon content (%)	28.4
Refractive index, n	
20 °C	1.5791 ± 0.0001
30 °C	1.5753 ± 0.0002
40 °C	1.5716 ± 0.0002
60 °C	1.5641 ± 0.0002
dn/dT (1/K)	-3.74×10^{-4}
Density, ρ (kg/m³)	
20 °C	1014.2 ± 2.1
30 °C	1008.0 ± 2.1
40 °C	1001.6 ± 2.2
60 °C	988.6 ± 2.6
$d\rho/dT$ (kg/m³K)	-0.643
Viscosity at 20 °C (Pa.s)	2461 ± 26
Free radical content (spins/g)	1.58×10^{18}
Cumulative amount distilled (wt%)	
360 °C	13.5
525 °C	43.5

[a] Average ± sample standard deviation from analyses in triplicate.

Other materials employed in the study were the solvents *n*-heptane (99.7%), carbon disulfide (99.99%), tetrahydrofuran (99.9%) and toluene (99.8%), all commercially obtained from Fisher Scientific and used without further purification. Hydranal® composites 1 used for Karl Fischer titration was obtained from Fluka. Samples for nuclear magnetic resonance analyses were prepared in deuterated chloroform (99.8% deuterium) obtained from Arcos Organic, and the relaxing agent used was chromium (III) acetylacetonate (99.9%) obtained from Aldrich.

6.2.2. *Equipment and procedure*

6.2.2.1. Solvent classification

Bitumen feed and conversion products were separated into solvent-soluble and solvent insoluble fractions based on the standard test method described in ASTM D3279 [24].

The *n*-heptane insoluble material was obtained by mixing the sample with *n*-heptane in a ratio equal to 1:60 (wt/vol) in a glass flask. The mixture was stirred for 1 h at 250 rpm using a magnetic stirrer. After this, the mixture was left for a period of 24 h. Then, the sample was filtered using a 0.22 μm Millipore nitrocellulose membrane filter. The filter with solvent insoluble material was transferred to an aluminum pan of known mass. The solids were left to dry for 48 h and were weighed after this period. The *n*-heptane soluble material was collected, and the *n*-heptane solvent was removed using a rotary evaporator, Heidolph Hei-VAP advantage, over a period of 4 h at 50 °C and 12 kPa absolute pressure. The vapor pressure of *n*-heptane at 50 °C is 19 kPa.

A similar procedure was followed in order to obtain carbon disulfide (CS_2) soluble and insoluble fractions. The CS_2 was removed at 30 °C and 40 kPa absolute pressure. **Safety note**: CS_2 has a flashpoint of -30 °C and autoignition temperature of 100 °C [25]. Appropriate care must be taken to control temperature and keep CS_2 away from potential ignition sources.

6.2.2.2. Preparation of materials

Bitumen-derived materials were prepared with different amounts of *n*-heptane insoluble asphaltenes. This was achieved by preparing *n*-heptane soluble and *n*-heptane insoluble fractions from the Athabasca bitumen and then blending those in different ratios to obtain bitumen-derived materials with different asphaltenes content. Four different materials were employed (**Table 6-2**) for the thermal conversion experiments, bitumen and three bitumen-derived mixtures. For the mixtures that were prepared, after adding the components together, the mixture was placed in an ultrasonic bath and sonicated for 30 min to facilitate mixing.

Table 6-2. Bitumen-derived materials with different levels of *n*-heptane insoluble asphaltenes.

Asphaltenes content (wt%)	Amount in blended material (wt%)		
	bitumen	**maltenes** [a]	**asphaltenes** [a]
0	0	100	0
9	0	91	9
18.6	100	0	0
28	89	0	11

[a] Maltenes and asphaltenes were the *n*-heptane soluble and the *n*-heptane insoluble fractions separated from the bitumen.

Despite the effort to efficiently mix the materials, the resulting mixtures were in fact dispersions and not true solutions in the thermodynamic sense. Although the mixtures visually appeared to be homogenous, when the mixtures were viewed under a stereomicroscope, it was clear that the mixtures were dispersions (**Figure 6-1**). It was anticipated that as temperature was increased for thermal conversion, the viscosity would decrease, and the dispersed phase will become a fluid to facilitate better dissolution. This was a point that was resolved by comparing the feed materials that did not have dispersions with those that did.
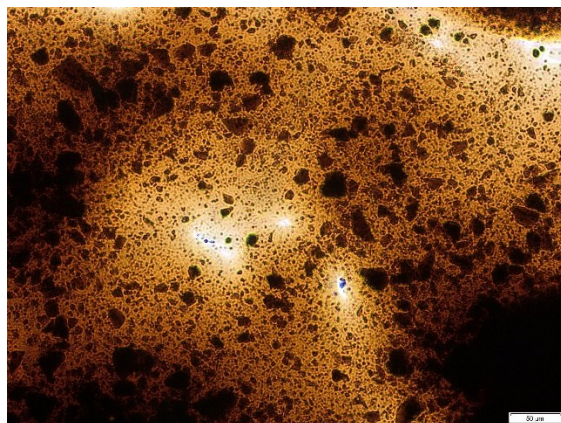
Figure 6-1. Stereo microscope image of bitumen and asphaltenes mixture (28 wt% asphaltenes content) at ambient conditions. The scale bar is 50 μm.

6.2.2.3. Thermal conversion

Thermal conversion was performed in microbatch reactors at 380 °C and an initial pressure of 2 MPa N_2 atmosphere. Reaction time at 380 °C was varied over a range; the longest time that was considered was around 3 h. At 380 °C the rate of thermal conversion is sufficiently high to achieve measurable thermal conversion, but at the same time sufficiently slow to limit gas and coke formation over the reaction period studied [26].

The microbatch reactors employed for thermal conversion were manufactured from Swagelok 316 stainless steel tubing and fittings with a diameter of 2.5 cm and length of 16.0 cm. The feed material was placed in a glass vial with an outside diameter of 2.0 cm and 15.0 cm long. For a typical experiment, approximately 12 g of material was employed, while the exact mass was recorded. To reduce the amount of air in the reactor, the sequence of pressurizing the reactor to 2 MPa with N_2 and releasing the pressure was repeated three times before final pressurization.

To carry out the reactions, the pressurized reactor was placed inside a fluidized sand-bath heater, Omega fluidized sand-bath FSB-3, that was preheated to the reaction temperature. At reaction temperature, the pressure was around 4 MPa. The temperature inside the reactor was monitored using a thermocouple. A temperature profile during the reaction was obtained by recording the temperature in the thermocouple reader with an interval of 30 seconds. The start of the indicated

reaction time was when the reaction temperature inside the reactor reached 380 °C. Different reaction times at 380 °C were evaluated. Once the planned reaction time was completed, the reactor was taken out from the sand-bath and cooled down to room temperature. Accounting for the total temperature-time history was shown to be necessary, even for microbatch reactors, despite their temperature responsiveness [27]. The contribution of the heat-up, reaction, and cool-down periods to the actual equivalent residence time (ERT) at 380 °C was calculated by method of Yan [28]. This method works well for most visbreaking studies, but it was recognized that its use in this study was at the limit of its validity [29]. In the absence of a better strategy to account for heat-up and cool-down periods, it was nevertheless decided to use the equivalent residence time method of Yan [28].

Once the reactor was cold, the reactor was depressurized and opened to collect the thermally converted product. The sample was recovered using 100 mL of CS_2. The mixture of the reaction products and CS_2 was separated into a CS_2 soluble and CS_2 insoluble fraction as described in **Section 6.2.2.1**. Material balance was performed, and the products were characterized.

6.2.3. Analyses

The water content of the emulsion and the bitumen were determined using a Mettler Toledo V20S Karl Fischer titrator. A modified version of the method that was developed by Carbognani et al. [30] to quantify the water content in vacuum residue and bitumen using tetrahydrofuran as solvent was used.

CHNS elemental analyses were performed by the Analytical and Instrumentation Laboratory of the University of Alberta's Chemistry Department. The equipment used was a Thermo Flash CHNS-O analyzer.

Proton nuclear magnetic resonance (^{1}H NMR) and carbon-13 nuclear magnetic resonance (^{13}C NMR) analyses were performed by the NMR facility of the University of Alberta's Chemistry Department. The spectra were collected using an Agilent/Varian Innova 400 MHz spectrometer, which was operated at 100.6 MHz in the case of ^{13}C NMR analyses. Sample preparation for ^{1}H

NMR analysis involved dissolving 0.15 g sample in 0.7 mL deuterated chloroform, which was then placed in a 5 mm NMR tube. For the ^{1}H NMR analysis, each spectrum was obtained by performing 16 scans within the -1 to 11 ppm range. Hydrogen was classified as 'aromatic hydrogen' if it was in the 6–9 ppm range [31], otherwise it was considered 'non-aromatic hydrogen'. Sample preparation for ^{13}C NMR analysis involved dissolving 0.35 mL sample in 0.35 mL of a 0.2 M chromium (III) acetylacetonate in deuterated chloroform solution. Once the sample was completely dissolved, it was placed in a 5 mm NMR tube. For the ^{13}C NMR analysis, each spectrum was obtained by performing 2000 scans within the -10 to 270 ppm range. The acquisition time was 0.5 s and the relaxation time was 2 s. Carbon was classified as 'aromatic carbon' if it was in the 110–160 ppm range [31], otherwise it was considered 'non-aromatic carbon'.

Refractive index and liquid density measurements were performed using an Anton Paar Abemat 200 (sodium D-line, 589 nm) and Anton Paar DMA 4500M respectively.

The free radical content was quantified by electron spin resonance (ESR) measurements using an Active Spectrum Micro-ESR. The samples were prepared by diluting 20 mg of sample in 600 μL of toluene, which was then transferred to 5 mm diameter PQ quartz tubes for analysis. The measurements were performed using the microwave X-band at 15 mW power, 1.2 Gauss coil amplitude, and digital gain of 12 dB. For quantification the ESR was calibrated using 2,2-diphenyl-1-picrylhydrazyl (DPPH) in toluene.

Simulated distillation analysis was performed according to the ASTM D7169 standard test method [32], using an Agilent 7890B high temperature gas chromatograph.

Thermogravimetric analysis (TGA) was performed to determine the mineral content of materials by combusting the organic matter under air at 600 °C. The instrument used was a Mettler Toledo TGA/DSC1 with MX5 microbalance.

6.3. Results

6.3.1. n-Heptane solubility fractions

The two main solubility fractions in this study are the *n*-heptane soluble fraction (maltenes) and the *n*-heptane insoluble fraction (asphaltenes). On initial characterization, it was found that the maltenes were not *n*-heptane free. The maltenes were dissolved in CS_2 and recovered from CS_2, while at the same time determining the CS_2 insoluble content. The CS_2 insoluble content was very low, 0.2 ± 0.2 wt%, and the procedure had the added benefit of removing residual *n*-heptane. The maltenes and asphaltenes were characterized (**Table 6-3**) and as an internal consistency check, a balance was performed and compared with the bitumen characterization in **Table 6-1**.

Table 6-3. Characterization of *n*-heptane soluble maltenes and *n*-heptane insoluble asphaltenes fractions separated from the Athabasca bitumen.

Property	Maltenes	Asphaltenes	Balance (%)[a]
Solubility classes (wt%)			
CS$_2$ insolubles	0.2 ± 0.2	1.9 ± 0.9	65
Elemental composition (wt%)			
carbon	83.7 ± 0.1	79.6 ± 1.4	100
hydrogen	10.8 ± 0.1	8.0 ± 0.2	100
nitrogen	0.4 ± 0.1	1.2 ± 0.1	110
sulfur	4.7 ± 0.1	8.6 ± 0.1	104
oxygen (by difference)	0.5	2.6	-
Aromatic hydrogen content (%)[b]	4.5	7.2	94
Aromatic carbon content (%)[b]	23.3	43.4	95
Refractive index, n			
20 °C	1.5520	1.9210 [c]	102
30 °C	1.5472	1.8397 [c]	102
40 °C	1.5434	1.7839 [c]	101
60 °C	1.5363	1.7104 [c]	100
dn/dT (1/K)	-3.87×10^{-4}	-51.1×10^{-4}	-
Density, ρ (kg/m^3)			
20 °C	984.3	1145.0 [c]	100
30 °C	977.8	1139.7 [c]	100
40 °C	971.6	1134.8 [c]	100
60 °C	958.8	1125.4 [c]	100
d$ρ$/dT (kg/m^{3}K)	-0.637	-0.487	-
Free radical content (spins/g)[c]	1.12×10^{18}	3.38×10^{18}	98
Cumulative amount distilled (wt%)			
360 °C	16	0	96
525 °C	52	2	98

[a] Balance = (weighted contributions of maltenes + asphaltenes)/(bitumen)x100.
[b] Nature of hydrogen by 1H NMR analysis and nature of carbon by 13C NMR analysis.
[c] Free radical concentration from quantitative electron spin resonance (ESR) spectrometry.

Near-perfect elemental balance was found for carbon and hydrogen. The uncertainty associated with the sulfur balances was of the order 5%, which is comparable to that reported for the bitumen

analysis. The uncertainty associated with the nitrogen balance was 10%, which was more than suggested by the variability of repeat analyses. The uncertainty associated with the CS_2 insoluble material was high, and this was also evident from the variance of repeat analyses.

The ^{1}H NMR values for aromatic hydrogen balanced within 6%, and the ^{13}C NMR values for aromatic carbon balanced within 5%.

When interpreting the results dealing with aromatic hydrogen, some caution is needed. Unlike the ^{13}C NMR spectral range of aromatic carbon that is far removed from non-aromatic carbon and is free of overlap, the same is not true for aromatic hydrogen. The ^{1}H NMR spectral range used to identify aromatic hydrogen in this study, 6–9 ppm [31], is affected by overlap with non-aromatic hydrogen from functional groups such as olefinic hydrogen conjugated with other unsaturated groups such as aromatics and carbonyls [33]. In straight run petroleum products this is seldom a necessary qualification to make. However, in thermally converted material, the label 'aromatic hydrogen' does not guarantee that all of the hydrogen that is so labeled is indeed attached to an aromatic carbon, it only signifies that the hydrogen appears in the indicated spectral range.

The asphaltenes are solids at ambient conditions, and to determine their refractive index and density, the asphaltenes were dissolved in toluene. By measuring the refractive index and density of the toluene, and that of the asphaltenes in toluene mixture, it was possible to calculate the values for the asphaltenes shown in **Table 6-3** under the assumption of conservation of volume. It was reported that volume was additive for mixtures of bitumen with aromatic solvents [34], and that the excess volume was zero, with the implication that regular solution theory can be used in the description. This was consistent with what Yarranton and co-workers reported for mixtures up to 7% asphaltenes [35], but with a cautionary note that this might not hold true for higher concentrations. The present study provides no supporting evidence for this assumption and the reported values for asphaltenes density are therefore subject to this unresolved uncertainty.

The density values of the maltenes and asphaltenes were in balance with that of bitumen (**Table 6-1**) and the results appeared internally consistent. The refractive index values balanced within

2%, but unlike in other measures, for refractive index 2% is a large deviation. The refractive index values that were calculated for the asphaltenes from the experimental measurements were too high.

The persistent free radical content measured for the maltenes and asphaltenes balanced within 2% with that of the bitumen from which the fractions were derived.

The simulated distillation curves for the Athabasca bitumen, maltenes, and asphaltenes are shown in **Figure 6-2**. The results reflect the type of boiling point distribution anticipated for bitumen, with about half of the material being in the vacuum residue and almost no naphtha and kerosene [19]. The cumulative distillation amounts at the atmospheric residue (360 °C) and vacuum residue (525 °C) cut-points balanced within 4% and 2% respectively (**Table 6-3**).
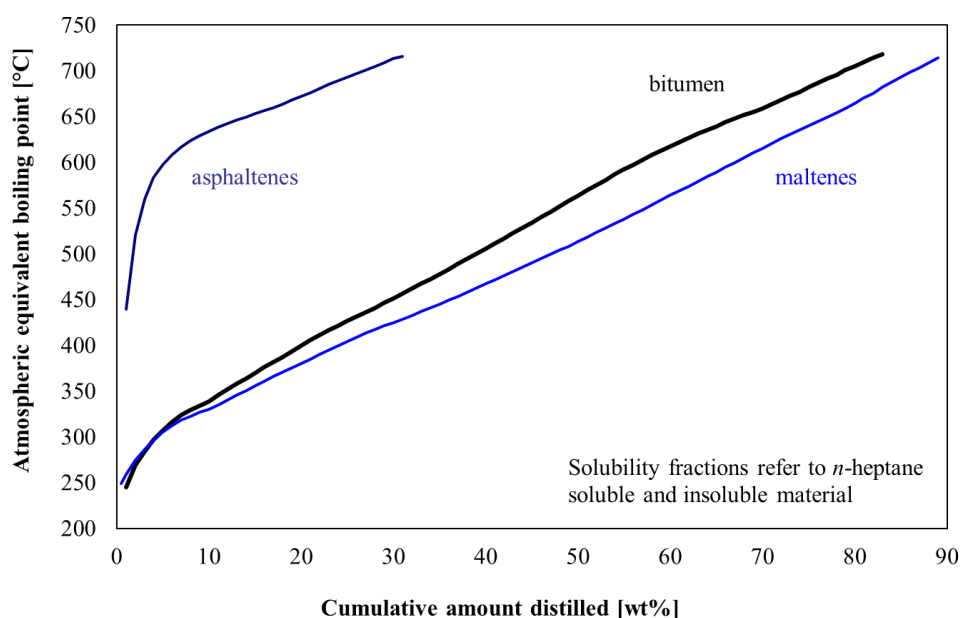
Figure 6-2. Simulated distillation curves of Athabasca bitumen, n-heptane soluble maltenes, and n-heptane insoluble asphaltenes.

Interpretation of these and subsequent results obtained by simulated distillation should consider the cautionary comments made about bitumen characterization by simulated distillation. It was reported that on-column cracking takes place when the column temperature in the gas

chromatograph exceeds 320 °C [36]. Due to the high content of polar and aromatic compounds in material with an atmospheric equivalent boiling point temperature >400 °C, there is also an impact on column polarization that can cause a deviation with respect to the inferred distillation temperature [37].

Finally, it should be pointed out that the *n*-heptane insoluble fraction of the Athabasca bitumen sample used in this study, 18.6 ± 0.6 wt%, was on the high side for oilsands bitumen from that region. The amount of *n*-heptane insoluble material was closer to that normally expected for *n*-pentane insoluble asphaltenes, which is in the range 14–20 wt% [38]. The reason for this high *n*-heptane insoluble content is not known, but it was consistently high for the batch of Athabasca bitumen used in this study. This topic is further discussed in **Section 6.4.1**.

This separation was performed many times, since it was employed to separate the maltenes and asphaltenes fractions used to prepare the feed materials in **Table 6-2**. By definition, it also determined the amount and composition of the maltenes and asphaltenes fractions, which were internally consistent (see balance column in **Table 6-3**) with the composition of the bitumen from which these fractions were derived. However, despite the good repeatability of this value, the high *n*-heptane insoluble content may have been a consequence of factors that affected the physical separation [27,39]. Thus, repeatability is not called into question, only the absolute amount that was separated with good repeatability. This topic is further discussed in **Section 6.4.2**.

6.3.2. CS₂ insoluble material

The CS_2 insoluble material that was separated from bitumen (**Table 6-1**) and the *n*-heptane solubility fractions (**Table 6-3**), likely comprised of two parts, organic and mineral matter. The organic matter in the CS_2 insoluble material was determined using thermogravimetric analysis under air atmosphere. Sufficient time was provided at 600 °C under air to reach constant mass, and in this way, the organic content and ash content of the CS_2 insoluble material was determined (**Table 6-4**).

Table 6-4. Organic and ash content present in CS_2 insoluble material.

Description	CS_2 insoluble material obtained from:		
	bitumen	**maltenes**	**asphaltenes**
organic matter (wt%)	71	90	76
ash content (wt%)	29	10	24

The values in **Table 6-4** are for single samples and are only indicative of composition. Of relevance for the investigation was that 70–90 wt% of the CS_2 insoluble material was organic in nature. The contribution of mineral matter could not be ignored, but mineral matter was not the major constituent in the CS_2 insoluble material.

6.3.3. *Thermal conversion of maltenes*

Thermal conversion of the maltenes fraction, which by definition contains no asphaltenes, was the first feed material in **Table 6-2** that was investigated. The maltenes fraction is interesting from the perspective that any material that subsequently becomes *n*-heptane insoluble must have been formed by reaction. The development of new *n*-heptane insoluble material during thermal conversion of maltenes forms the baseline against which the impact of asphaltenes in the feed on thermal conversion can be evaluated.

The results from the conversion of the feed with 0% asphaltenes are shown in **Table 6-5**. Material balance closure ranged from 96–101%. From the perspective of solubility classification there was little change in the CS_2 insoluble content, while the *n*-heptane insoluble content increased with increasing equivalent residence time at 380 °C.

Table 6-5. Material balance, product yields and characterization of 380 °C converted liquid products from maltenes, a feed material with no asphaltenes, at the indicated equivalent residence times.

Property	Products from conversion at indicated ERT[a]			
	24 min	31 min	75 min	189 min
Material balance closure (%)	97.8	96.0	98.5	100.5
Product yield (wt%)				
CS$_2$ soluble liquid	97.1	97.6	99.6	99.3
CS$_2$ insoluble solid	0.6	0.4	0.3	0.4
n-Heptane insoluble (wt%)[b]	1.5	1.5	3.1	5.2
Aromatic hydrogen content (%)[c]	4.8	9.1	6.5	9.3
Aromatic carbon content (%)[c]	26.0	28.7	28.7	34.0
Refractive index, n				
20 °C	1.5566	1.5586	1.5572	1.5624
30 °C	1.5521	1.5545	1.5529	1.5582
40 °C	1.5477	1.5500	1.5490	1.5545
60 °C	1.5395	1.5419	1.5413	1.5470
dn/dT (1/K)	-4.26×10^{-4}	-4.18×10^{-4}	-3.96×10^{-4}	-3.82×10^{-4}
Density, ρ (kg/m³)				
20 °C	997.9	1001.1	987.9	983.5
30 °C	991.3	994.2	981.1	976.8
40 °C	984.1	987.2	974.3	969.9
60 °C	970.1	973.2	960.6	956.6
dρ/dT (kg/m³K)	-0.696	-0.697	-0.683	-0.673
Free radical content (spins/g)[d]	1.18×10^{18}	1.21×10^{18}	1.23×10^{18}	1.33×10^{18}
Cumulative amount distilled (wt%)				
360 °C	20.5	22	21	30
525 °C	53.5	57	51	69

[a] Equivalent residence time (ERT) at 380 °C that considers heat-up, reaction, and cool-down temperature-time history.
[b] Amount in CS$_2$ soluble liquid product.
[c] Nature of hydrogen by ^{1}H NMR analysis and nature of carbon by ^{13}C NMR analysis.
[d] Free radical concentration from quantitative electron spin resonance (ESR) spectrometry.

Considering the high liquid yield, little difference in elemental composition was expected and CHNS analyses are not reported. Changes in the liquid product composition were additionally monitored using NMR, refractive index, density, and simulated distillation (**Table 6-5**).

Several general observations could be made based on the additional characterization of the thermally converted products. The product properties did not always change monotonically with an increase in equivalent residence time at 380 °C, but directionally several changes in **Table 6-5** with respect to the maltenes feed (**Table 6-3**) can be highlighted.

The aromatic carbon content increased from 23.3 % in the maltenes feed to 34.0%. This was not accompanied by a proportional change in the aromatic hydrogen content. The way in which the thermal conversion chemistry proceeded was such that the aromatic hydrogen-to-carbon ratio changed. To some extent this type of variation should have been anticipated, considering the cautionary comments about overlap in the spectral range of aromatic hydrogen (**Section 6.3.1**).

Several properties changed in such a way that they passed through a local maximum or minimum with increasing equivalent residence time compared to the value of the feed. This type of behavior was seen with the first derivative of refractive index with temperature (dn/dT), density, and the first derivative of density with temperature ($d\rho/dT$).

Both derivatives, dn/dT and $d\rho/dT$, contain information about composition. A systematic change in $d\rho/dT$ with molecular mass was found [40]. If the nature of the compounds remained similar, the $d\rho/dT$ of -0.637 (**Table 6-3**) for the maltenes feed that changed to -0.696 (**Table 6-5**) for the product after 24 min reaction, could be interpreted as a decrease in average molecular mass. Likewise, the directional change of $d\rho/dT$ on increasing from -0.697 after 31 min to -0.683 after 75 min reaction could be interpreted as an increase in average molecular mass. The same was also seen in the distillation profile, although it was unlikely that this change was as meaningful, due to the higher level of uncertainty in the simulated distillation results.

The relationship between refractive and density [41], would suggest that dn/dT and $d\rho/dT$ are two different ways to represent the same chemical information. However, dn/dT was reported to also correlate with properties, such as viscosity, aromatic content, and distillation curve [42].

6.3.4. Thermal conversion of feed containing 9% asphaltenes

Feed material containing 9% asphaltenes was prepared by mixing *n*-heptane soluble maltenes with *n*-heptane insoluble asphaltenes (**Table 6-2**). This material was thermally converted at 380 °C and the products were characterized using the same methods as applied for the maltenes. The results from these experiments are reported in **Table 6-6**.

Table 6-6. Material balance, product yields and characterization of 380 °C converted liquid products from a feed material with 9 wt% asphaltenes at the indicated equivalent residence times.

Property	Products from conversion at indicated ERT[a]				
	7 min	13 min	43 min	57 min	174 min
Material balance closure (%)	100.0	98.5	97.3	100.0	100.5
Product yield (wt%)					
CS$_2$ soluble liquid	99.2	98.7	96.2	98.5	98.0
CS$_2$ insoluble solid	0.8	1.3	1.7	1.5	1.8
n-Heptane insoluble (wt%)[b]	7.8	8.5	8.8	8.3	10.7
Aromatic hydrogen content (%)[c]	6.9	7.1	6.5	6.6	12.3
Aromatic carbon content (%)[c]	30.1	30.4	29.5	30.6	34.2
Refractive index, n					
20 °C	1.5680	1.5711	1.5711	1.5666	1.5740
30 °C	1.5637	1.5673	1.5671	1.5619	1.5703
40 °C	1.5591	1.5629	1.5626	1.5583	1.5663
60 °C	1.5518	1.5549	1.5546	1.5510	1.5586
dn/dT (1/K)	-4.05×10^{-4}	-4.08×10^{-4}	-4.14×10^{-4}	-3.84×10^{-4}	-3.85×10^{-4}
Density, ρ (kg/m^3)					
20 °C	1011.3	1016.4	1012.6	999.3	997.8
30 °C	1004.6	1009.6	1005.8	992.5	991.1
40 °C	997.8	1002.8	-[c]	986.0	984.4
60 °C	984.1	989.1	-[c]	971.2	970.8
d$ρ$/dT (kg/m^{3}K)	-0.680	-0.683	-[c]	-0.702	-0.675
Free radical content (spins/g)[d]	1.40×10^{18}	1.49×10^{18}	1.47×10^{18}	1.55×10^{18}	1.67×10^{18}
Cumulative amount distilled (wt%)					
360 °C	16	18	20	23	24
525 °C	47	51	53.5	57	66.5

[a] Equivalent residence time (ERT) at 380 °C that considers heat-up, reaction, and cool-down temperature-time history.
[b] Amount in CS$_2$ soluble liquid product.
[c] Nature of hydrogen by ^{1}H NMR analysis and nature of carbon by ^{13}C NMR analysis.
[d] Free radical concentration from quantitative electron spin resonance (ESR) spectrometry.

Directionally there was an increase in both the CS$_2$ and *n*-heptane insoluble content of the thermally converted products with an increase in equivalent residence time at 380 °C. Two

observations are noteworthy. First, there appears to have been an initial about 1% decrease in the *n*-heptane insoluble asphaltenes content, which is within the experimental uncertainty for the measurements. Second, the extent to which the *n*-heptane insoluble content increased over a period of about 3 h (**Table 6-6**), which was from 9 to 10.7 wt%, was less than the increase observed for maltenes (**Table 6-5**), which was from 0 to 5.2 wt%.

The aromatic carbon content remained in a narrow range of 29.5–30.6 % for the first 1 h of reaction, reaching 34.2 % after 3 h. The aromatic hydrogen-to-carbon ratio changed, but in the first 1 h of reaction the aromatic hydrogen content was also in a narrow range, 6.5–7.1 %.

Several properties passed through a local maximum or minimum with increasing equivalent residence time, namely, first derivative of refractive index with temperature (dn/dT), density, and the first derivative of density with temperature ($d\rho/dT$). These properties were also properties that had analogous behavior during thermal conversion of the maltenes (compare **Table 6-5** and **Table 6-6**).

6.3.5. *Thermal conversion of bitumen*

The Athabasca bitumen, which contains 18.6 ± 0.6 wt% *n*-heptane insoluble asphaltenes (**Table 6-1**), was thermally converted at 380 °C. The products were characterized, and the results are presented in **Table 6-7**.

Table 6-7. Material balance, product yields and characterization of 380 °C converted liquid products from Athabasca bitumen with 18.6% asphaltenes at the indicated equivalent residence times.

Property	Products from conversion at indicated ERT[a]				
	17 min	38 min[b]	39 min	60 min	178 min
Material balance closure (%)	99.8	100.0	99.7	104.5	102.8
Product yield (wt%)					
CS$_2$ soluble liquid	98.7	97.0	97.8	97.7	97.6
CS$_2$ insoluble solid	1.1	3.0	1.9	2.2	2.2
n-Heptane insoluble (wt%)[c]	13.2	13.3	12.4	13.1	15.1
Aromatic hydrogen content (%)[d]	5.9	8.3	7.0	12.3	8.1
Aromatic carbon content (%)[d]	30.5	31.2	30.1	35.8	38.3
Refractive index, n					
20 °C	1.5824	1.5812	1.5828	1.5817	1.5883
30 °C	1.5786	1.5773	1.5788	1.5777	1.5841
40 °C	1.5744	1.5731	1.5747	1.5732	1.5802
60 °C	1.5664	1.5650	1.5669	1.5656	1.5725
dn/dT (1/K)	-4.01×10^{-4}	-4.05×10^{-4}	-3.99×10^{-4}	-4.04×10^{-4}	-3.92×10^{-4}
Density, ρ (kg/m^3)					
20 °C	1027.1	1022.2	1028.7	1016.6	1019.5
30 °C	1020.3	1015.4	1021.9	1009.9	1012.7
40 °C	1014.2	1008.5	1015.2	1003.1	1005.6
60 °C	1000.5	994.0	1001.6	989.5	-[e]
dρ/dT (kg/m^{3}K)	-0.664	-0.704	-0.678	-0.678	-0.696
Free radical content (spins/g)[f]	1.69×10^{18}	1.69×10^{18}	1.67×10^{18}	1.88×10^{18}	2.09×10^{18}
Cumulative amount distilled (wt%)					
360 °C	16	17	18.5	20.5	25
525 °C	46	48	48.5	54.5	63

[a] Equivalent residence time (ERT) at 380 °C that considers heat-up, reaction, and cool-down temperature-time history.
[b] Material spent about 50 min in the temperature range 360-380 °C due to an issue with sand bath heater.
[c] Amount in CS$_2$ soluble liquid product.
[d] Nature of hydrogen by ^{1}H NMR analysis and nature of carbon by ^{13}C NMR analysis.
[e] Problem with analysis, results not trustworthy.
[f] Free radical concentration from quantitative electron spin resonance (ESR) spectrometry.

Two of the experiments had nearly the same equivalent residence times, 38 and 39 min. One would anticipate that these experiments had near similar results, but they did not. It raised a serious question, namely, was the difference in the results due to variability in the experimental results, or was the difference due to the equivalent residence time calculation?

As was explained in **Section 6.2.2.3**, the calculated equivalent residence time used the method of Yan [28], was at its limit of its validity. The reaction rate used for the equivalent residence time calculation is calculated using an average activation energy based on cracking conversion. In terms of reaction fundamentals, the reaction rate is proportional to the free radical concentration, and at temperatures below 380 °C, the calculation increasingly under-predicts the free radical concentration [29]. The experiment with equivalent residence time of 38 min had an uncommonly long heat-up period. It spent 50 min in the temperature range 360–380 °C due to an issue with the sand bath heater. Although this period was accounted for in the equivalent residence time calculation, free radical conversion, which is not the same as cracking conversion, is not adequately reflected. This needs to be considered in the interpretation of the results.

The values for the *n*-heptane insoluble asphaltenes content remained in the range 12.4–13.3 wt% for the first hour of reaction and then increased to 15.1 wt% after 3 h of reaction. These values are consistently lower than in the bitumen feed and highlighted an issue with the separation of *n*-heptane insoluble asphaltenes, previously noted in literature [27,39], and pointed out in **Section 6.3.1**.

There was no specific trend in the CS_2 insoluble content of the thermally converted products, which remained in the range 1.1–3.0 wt%.

For the first three time periods, the aromatic carbon content remained in the range 30.1–31.2 %, but by 1 h equivalent residence time it increased to 35.8 % and by 3 h to 38.3 %. The change in aromatic hydrogen content was more varied and did not follow the same pattern of change as the aromatic carbon content.

The cumulative amount distilled indicated an increase in cracking conversion with an increase in equivalent residence time. None of the other properties had a discernable pattern to their change. One observation worth pointing out is that in all instances the density of the liquid product after thermal conversion at 380 °C was higher than that of the bitumen feed (compare **Table 6-1** and **Table 6-7**), despite the increase in the cumulative amount of material distilled at 360 and 525 °C. The directional change of dρ/dT from -0.643 (**Table 6-1**) in the bitumen feed to -0.696 (**Table 6-7**) in the product after 178 min reaction also indicated that there was a decrease in average molecular mass. The feed material was bitumen and did not involve re-dispersion of asphaltenes. Without offering additional experimental support, it is speculated that steric constraints imposed by the high cycloalkane content of bitumen limits the packing density in the fluid phase, and that cracking reduces those steric constrains to increase packing density, despite a decrease in density of the individual cracked products.

6.3.6. *Thermal conversion of feed containing 28% asphaltenes*

Feed material containing 28% asphaltenes was prepared by mixing bitumen with *n*-heptane insoluble asphaltenes (**Table 6-2**). The results from the 380 °C thermal conversion at different equivalent residence times are presented in **Table 6-8**.

Table 6-8. Material balance, product yields and characterization of 380 °C converted liquid products from a feed material with 28 wt% asphaltenes at the indicated equivalent residence times.

Property	Products from conversion at indicated ERT[a]				
	13 min	30 min	36 min	68 min	107 min
Material balance closure (%)	102.6	100.0	99.1	100.6	98.1
Product yield (wt%)					
CS$_2$ soluble liquid	98.4	98.2	96.8	96.0	95.7
CS$_2$ insoluble solid	1.2	1.7	3.1	3.8	3.8
n-Heptane insoluble (wt%)[b]	19.6	18.0	17.3	18.1	23.0
Aromatic hydrogen content (%)[c]	7.4	5.9	8.7	7.0	14.0
Aromatic carbon content (%)[c]	30.9	31.4	34.2	36.2	36.6
Refractive index, n					
20 °C	1.5927	1.5932	1.5955	1.5933	1.6204
30 °C	1.5883	1.5895	1.5913	1.5892	1.6136
40 °C	1.5842	1.5854	1.5868	1.5850	1.6082
60 °C	1.5772	1.5774	1.5787	1.5764	1.5999
dn/dT (1/K)	-3.86×10^{-4}	-3.95×10^{-4}	-4.20×10^{-4}	-4.25×10^{-4}	-5.04×10^{-4}
Density, ρ (kg/m^3)					
20 °C	1033.7 [d]	1037.7	1046.0	1033.1	1050.1[d]
30 °C	1027.7 [d]	1030.9	1039.0	1026.2	1044.3[d]
40 °C	1021.7 [d]	1024.0	1031.6	1019.2	1038.5[d]
60 °C	1009.9 [d]	1010.2	- [e]	1005.4	1027.0[d]
dρ/dT (kg/m^{3}K)	-0.595	-0.687	-0.719	-0.694	-0.577
Free radical content (spins/g)[f]	1.98×10^{18}	2.04×10^{18}	2.03×10^{18}	2.03×10^{18}	2.20×10^{18}
Cumulative amount distilled (wt%)					
360 °C	11	17.5	17.5	18	13
525 °C	41	46	44.5	47	49

[a] Equivalent residence time (ERT) at 380 °C that considers heat-up, reaction, and cool-down temperature-time history.
[b] Amount of *n*-heptane insoluble material in CS$_2$ soluble liquid product.
[c] Nature of hydrogen by ^{1}H NMR analysis and nature of carbon by ^{13}C NMR analysis.
[d] Calculated from measurements performed on sample dissolved in toluene.
[e] Problem with analysis, results not trustworthy.
[f] Free radical concentration from quantitative electron spin resonance (ESR) spectrometry.

The CS$_2$ insoluble content of the thermally converted products increased with an increase in equivalent residence time. On the other hand, the n-heptane insoluble content passed through a local minimum, although the values for the equivalent residence time period up to one hour were all in a narrow range, 17.3–19.6 wt%. The n-heptane insoluble content increased to 23.0 wt% after 107 min, but all of the values were below the n-heptane insoluble asphaltenes content of the feed material.

As in previous experiments, the aromatic carbon content increased with increasing equivalent residence time, and there was apparently no relationship between the change in aromatic carbon and aromatic hydrogen content.

Directionally, refractive index, the first derivative of refractive index with temperature (dn/dT), and density increased with increasing equivalent residence time. Only the product after 68 min had a somewhat lower refractive index and density, with no indication from the experimental work that this was an outlier. The change in refractive index and density was therefore not monotonic. The first derivative of density with temperature ($d\rho/dT$) passed through a local minimum, -0.719 kg/m^{3}K.

The cumulative amount distilled at 360 °C passed through a local maximum, although the vacuum residue conversion expressed in terms of the cumulative amount distilled at 525 °C directionally increased with increase in equivalent residence time.

The products collected at the shortest and longest equivalent residence times, 13 and 103 min, had three features in common. Both were found to be very viscous and when the viscosity was measured, the viscosity values at 20 °C were 47 and 26 Pa.s, respectively. Both had high $d\rho/dT$ values, -0.595 and -0.577 kg/m^{3}K, respectively. Lastly, both samples had a low cumulative amount distilled at 360 °C, 11 and 13 wt%, despite having the lowest and highest cumulative amount distilled at 525 °C, 41 and 49 wt%, respectively.

6.4. Discussion

6.4.1. *Quantification of n-heptane insoluble asphaltenes*

A potential issue that was identified early on in this study, was that the *n*-heptane insoluble content of the Athabasca bitumen (**Table 6-1**) was consistently high, 18.6 ± 0.6 wt%. For comparison, other values for the *n*-heptane insoluble asphaltenes content of Athabasca bitumen that were reported are: 11.3 [11], 11.8 [43], 12.7–17.4 [39], 13 [44], 13.4 [45], 15 [46], and 16.5 [47]. This list is not exhaustive, but it is sufficiently clear that there is a spread in the reported values and that the value found in this study is unusually high.

There are several reasons for variability in the reported values, ranging from differences in origin of the bitumen in the Athabasca region to the exact procedure followed for separation. One of the most poignant illustrations of the impact is the work in Yarranton's group, which highlighted good repeatability for several specific test protocols, ± 0.2 wt%, but differences in the amount of *n*-heptane insoluble asphaltenes that were separated by each [39]. This point is emphasized, because it is a challenge in the description of asphaltenes as solubility class when dealing with conversion. The state of aggregation affects physical separation [9], which in turn affects the amount of material that is separated and classified as *n*-heptane insoluble asphaltenes. It should further be noted that the material in this study was not washed with the same rigor as in separation protocols [48] that required repeated washing, i.e. multi-step solid–liquid equilibrium separation. The entrapment of material that is *n*-heptane soluble in the material that is *n*-heptane insoluble is possible [49,50]. Throughout the study any reference to '*n*-heptane insoluble asphaltenes' should therefore be interpreted as material separated as insoluble in *n*-heptane using the specific experimental protocol described in **Section 6.2.2.1**.

Pertinent to this study, and the interpretation of results related to *n*-heptane insoluble asphaltenes, is that all of the values were determined using the same test protocol and using material from the same batch of bitumen. Despite this, it appears likely that asphaltenes separation from a viscous material, compared to a less viscous material after conversion, had an impact on the physical separation independently of conversion that caused the decrease in viscosity. No proof of this

147

assertion is provided and interpretation of the results would have to consider both possibilities, namely, that the feed asphaltenes content is consistent for the test protocol and that the asphaltenes separated included some *n*-heptane soluble material.

6.4.2. *Net asphaltenes conversion, or a separation artifact?*

It was shown that the solvent classification was repeatable and in **Table 6-3** it was shown that the characterization was internally consistent. When rejecting the postulate that a fraction of the *n*-heptane insoluble material was rendered soluble due to the reduced product viscosity before solvent addition independently of conversion, then the solubility classification in **Table 6-1** can be taken as absolute. What this means is that the fraction that was separated as *n*-heptane insoluble material, consisted only of *n*-heptane insoluble material.

By comparing the *n*-heptane insoluble content in the feed materials to that in the reaction products, it can be seen that the maltenes formed new *n*-heptane insoluble asphaltenes (**Table 6-5**). The feed material prepared using maltenes and asphaltenes to have a 9 wt% asphaltenes content at long time formed sufficient new *n*-heptane insoluble asphaltenes, 10.7 wt% after 3 h (**Table 6-6**), to exceed the asphaltenes content of the feed. However, with the bitumen feed (**Table 6-7**) and the asphaltenes enriched bitumen feed (**Table 6-8**), thermal conversion yielded a reduced amount of *n*-heptane insoluble asphaltenes over the whole equivalent residence time range studied.

It is likely that some asphaltenes were converted to maltenes, and it was demonstrated in **Table 6-5** that some maltenes were converted to asphaltenes. However, finding that feed asphaltenes are more readily converted to maltenes than maltenes to asphaltenes, appeared incongruous despite the reactivity of asphaltenes. More specifically, it meant that the conversion of asphaltenes to maltenes was close to 30% within 13–17 min at 380 °C (**Table 6-7** and **Table 6-8**), whereas only 1.5 wt% of maltenes were converted to asphaltenes within 24–31 min at 380 °C (**Table 6-5**). There is no precedent for this.

In a comprehensive study of Athabasca bitumen that evaluated the change in *n*-heptane insoluble content and oil phase stability criteria with increased severity of thermal conversion [11], the *n*-

heptane insoluble content was invariably higher after thermal conversion than in the bitumen feed. The same was found for the *n*-pentane insoluble content, which after thermal conversion always exceeded that of the bitumen feed over a wide time range spanning visbreaking and delayed coking periods [51].

The alternative is to consider the postulate that a fraction of the *n*-heptane insoluble material was rendered soluble due to the reduced product viscosity before solvent addition, independent of conversion. Accepting this postulate has some implications. Not only does it mean that the bitumen has a lower *n*-heptane insoluble content in the thermodynamic sense, but also that a portion of the asphaltenes fraction that was separated, is actually *n*-heptane soluble. There may have been several contributing factors to cause more material to be separated as *n*-heptane insoluble asphaltenes, such as aggregation, physical entrapment, and rate phenomena that affected separation [9,43-44,52].

In a practical sense the solvent separation is a process facing a transport limitation. After mixing the bitumen and solvent, it is the *n*-heptane rich phase that separates from the bitumen–solvent mixture, leaving the *n*-heptane insoluble phase behind. To quote [53]: "... at the conditions for phase separation, the solvent, rather than the asphaltenes, nucleate as a (nearly) pure phase." Thus, the solvent classification relies solvent extraction to remove all of the *n*-heptane soluble material from the bitumen–solvent mixture. Although the initial viscosity of the bitumen–solvent mixture is low, as the solvent-rich phase separates, the viscosity of the remaining phase increases and eventually exceeds that of the material before solvent addition. The description of the actual process of separation makes it easier to explain how the solvent classification from a viscous material like bitumen (**Table 6-1**) can be repeatable, but incomplete. At the same time it also explains how the same separation could be more complete with a less viscous material, such as solvent classification after thermal conversion.

The limiting bitumen *n*-heptane insoluble content was calculated that would not result in a net decrease in *n*-heptane insoluble material during thermal conversion. It was found that if the bitumen had about 11.5 wt% asphaltenes, which were *n*-heptane insoluble in the thermodynamic sense of solubility, then none of the experiments (**Table 6-5** to **Table 6-8**) would lead to a net

conversion of asphaltenes to maltenes. Using a revised bitumen *n*-heptane insoluble asphaltenes content of 11.5 wt%, the change in asphaltenes content over time during thermal conversion is shown in **Figure 6-3**.
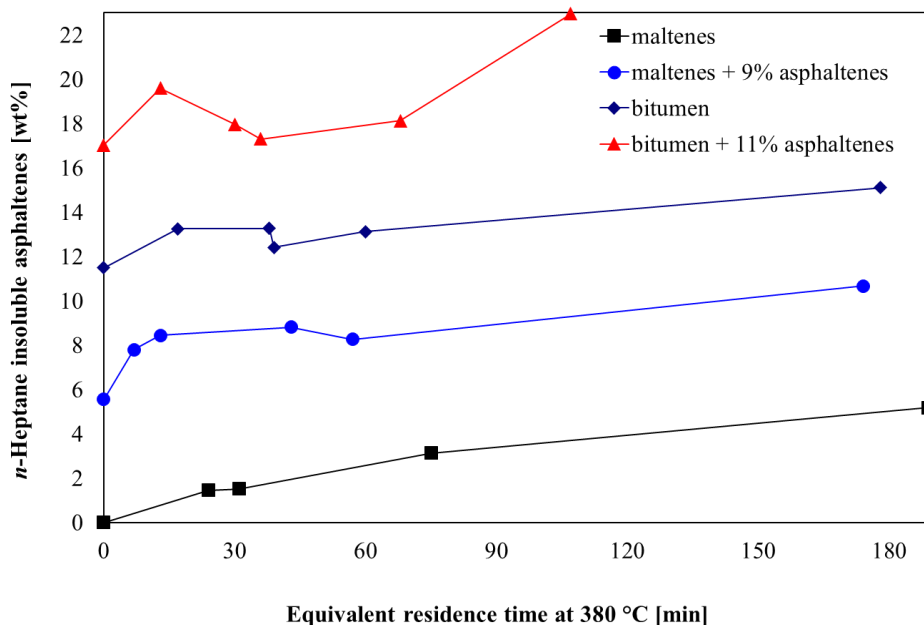
Figure 6-3. Amount of n-heptane insoluble asphaltenes as function of equivalent residence time at 380 °C for 11.5 wt% asphaltenes in the bitumen feed. Lines are shown for readability and not to suggest trends.

The results shown in **Figure 6-3**, with the exception of the calculated *n*-heptane insoluble content of the bitumen, are not changed by the assumption that was made. Directionally, all products showed an eventual increase in asphaltenes content with time. Additionally, there appeared to be a time period where the *n*-heptane insoluble content passed through a local minimum.

Two of the feed materials were prepared by asphaltenes addition (**Table 6-2**), which was shown to be a fine dispersion (**Figure 6-1**) rather than homogenous solution at ambient conditions. It was an assumption that at higher temperature this dissolution would become homogenous. No direct evidence in support of this was provided, but **Figure 6-3** showed a comparable progression of the

n-heptane insoluble content of the feed with increasing equivalent residence time for all feed materials. This served as indirect support that the dispersed feeds (9% and 28% asphaltenes content) were converted in a comparable way to the homogeneous feed materials (maltenes and bitumen).

6.4.3.   *Asphaltenes as measure of thermal conversion leading to coke*

Conversion on a molecular level refers to a change from one species to another. Applying this simple concept to a bitumen-derived material is not as simple. Our ability to detect conversion is restricted to macroscopic property measurements, because it is difficult to keep track of changes at species level in such a complex mixture. This means that conversion becomes a macroscopic measure too. Species level changes that do not result in a change in macroscopic measurements are not detected. The absence of conversion in terms of any macroscopic measurement is therefore not a guarantee that there is no conversion at species level.

Viewing solubility classification in this context, and using a description based on solubility parameters, the increase in *n*-heptane insoluble content with increasing equivalent residence time as observed in **Figure 6-3** can be interpreted. It means that on average there is an increase in the population of species that exceeds the threshold $\Delta\delta$ with respect to 15.3 MPa$^{0.5}$, the solubility parameter of *n*-heptane. Since the solubility parameter of *n*-heptane is on the low-end of the δ-scale, material that exceeds the threshold $\Delta\delta$, exceeds the threshold by having a high solubility parameter. However, it should be kept in mind that the method of separation employed in this study was filtration, which imposes a second criterion, namely, that the insoluble material must be filterable at ambient temperature.

The same approach can now be used for solvent classification based on CS$_2$ insolubility. The solubility parameter of CS$_2$, 20.3 MPa$^{0.5}$, is intermediate on the δ-scale. The threshold $\Delta\delta$ can in principle be exceeded by material that has a solubility parameter that is either higher or lower than that of CS$_2$. Filterable material on the low-end of the δ-scale would be species such as petroleum waxes. However, at ambient conditions CS$_2$ is a better solvent for waxes than either toluene or *n*-heptane [54]. In fact, when petroleum waxes are present, for ambient temperature separation the

waxes may report as part of the asphaltenes fraction [55]. Nevertheless, the material that is separated as CS_2 insoluble from thermally converted bitumen is more likely to exceed the threshold $\Delta\delta$ on the high-end and be more carbonaceous in nature.

The relationship between the change in CS_2 insolubility and change in n-heptane insolubility with conversion is shown in **Figure 6-4**. There was no observable relationship between the change in CS_2 and n-heptane insolubility. There was also no indication that the two feed materials prepared by asphaltenes addition behaved differently to either maltenes or bitumen. The variability in **Figure 6-4** exceeded the uncertainty in mineral matter content indicated in **Table 6-4** and could not be attributed by variability in mineral matter. In essence **Figure 6-4** indicated that n-heptane insoluble asphaltenes content was a poor predictor for the formation of CS_2 insoluble coke-like material during thermal conversion.
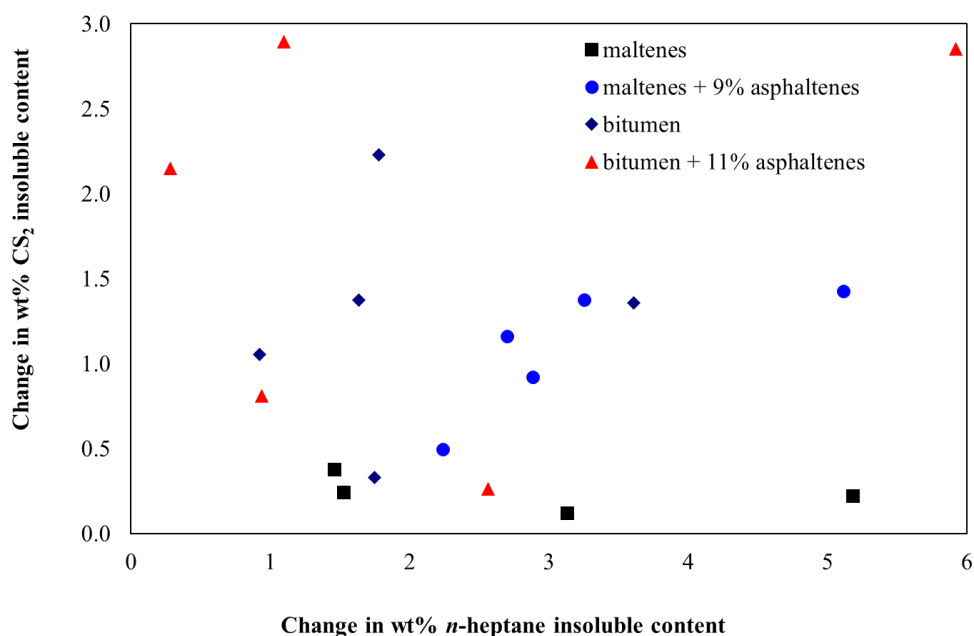
Figure 6-4. Change in CS_2 insoluble content with respect to the change in n-heptane insoluble content due to thermal conversion.

The absence of a relationship in **Figure 6-4** was incongruous with the description of thermal conversion by the sequential evolution of solubility classes [56]. It was also incongruous with the description of coking as a process whereby phase separation takes place to form a second fluid phase, which proceeds to be thermally converted to coke [10]. In that work [10], the change in *n*-heptane insoluble asphaltenes content and coking products formed during thermal conversion at 400 °C in an open system (mimicking a delayed coker) was monitored. It was shown how coke appeared at the point of maximum asphaltenes content and through modelling it was shown that the coke-forming reaction rate was phase equilibrium controlled.

At this point it is worthwhile taking a step back and to look more broadly at the use of solvent classification in the petroleum industry.

The main application of solvent classification in the petroleum industry is to serve as predictive measure for phase stability, either during changing conditions as petroleum is recovered and transported from a reservoir, or during crude oil blending. Solvent classification is described in terms of second *fluid* phase formation, as was done in the preceding discussion making reference to solubility parameters, instead of second phase formation per se. Experimental measurement requires the solvent insoluble phase to be *solid* and of sufficient particle size to be separable by filtration.

Directional changes in properties with increasing equivalent residence time at 380 °C, such as the increase in aromatic carbon content and free radical content (**Table 6-5** to **Table 6-8**), are in agreement with the general observations of Wiehe [56] about the change in properties with thermal conversion. There was also a directional increase in material that could be separated as solids by solvent classification, as was also observed by Wiehe [10]. However, in this study there was no evidence for the progression of thermal conversion to coke with asphaltenes as a necessary intermediate.

153

6.4.4. *Properties related to solubility classification*

The question that remained was whether solubility classification was a meaningful measure for thermal conversion. To pursue this further, the results were scoured for possible relationships between the amount of *n*-heptane insoluble asphaltenes and the measured physical and chemical properties of the thermally converted products.

There appeared to be a relationship between the amount of *n*-heptane insoluble asphaltenes and the amount of persistent free radicals present in the thermally converted material (**Figure 6-5**). The general relationship equally applied to the feed materials and was not a measure of thermal transformation. The asphaltenes content was just an indicator of an increase in the amount of heavier species that on average contain higher concentrations of free radicals [57,58].
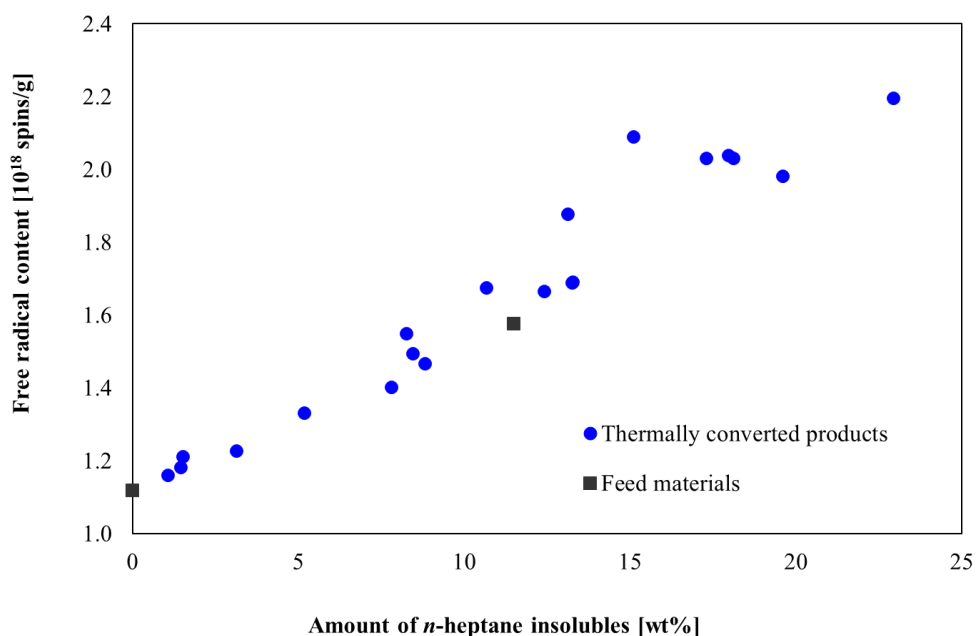
Figure 6-5. Free radical content in relation to n-heptane insoluble asphaltenes content. As a linear correlation, the r^2 = 0.944.

Interestingly, *n*-heptane insoluble asphaltenes and aromatic carbon had a weak relationship that appeared as a broad band (**Figure 6-6**). Various large aromatic core structures have been identified in asphaltenes [59]. Despite the anticipated compositional variations in asphaltenes from different sources, it was suggested that aromatic core structures are an important aspect leading to its solubility classification [60]. **Figure 6-6** does not provide evidence to the contrary, but if it is interpreted in the context conversion, then the increase in *n*-heptane insolubility during conversion is only weakly related to an increase in aromatic carbon content. It also follows from the relationship between free radical and asphaltenes content (**Figure 6-5**) that the increase in free radical content is not strongly related to an increase in aromatic carbon content either.
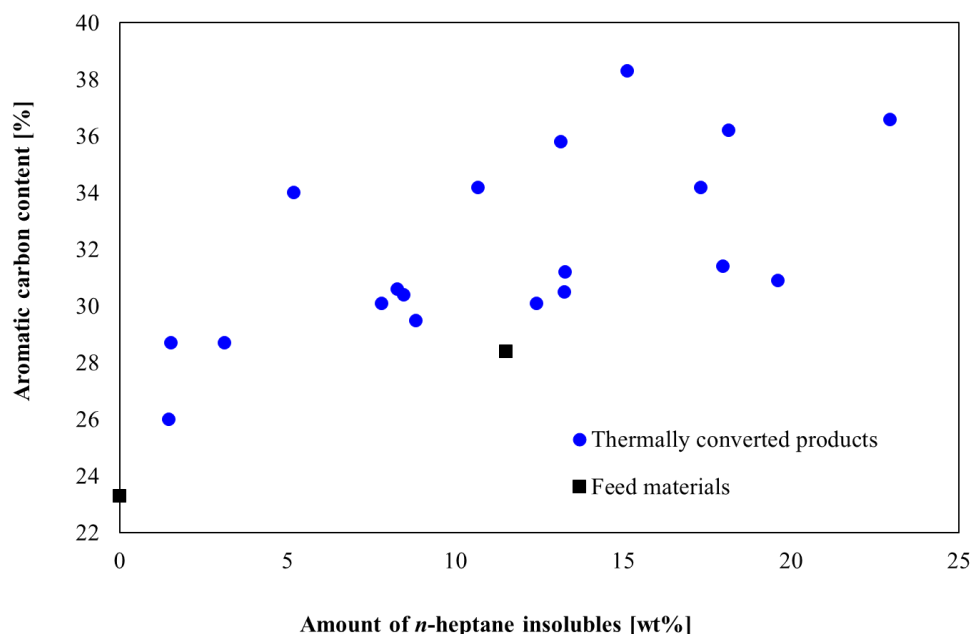
Figure 6-6. Aromatic carbon content in relation to n-heptane insoluble asphaltenes content. It had a poor linear correlation with $r^2 = 0.421$.

The only other property that was changed by thermal conversion and that had a strong relationship with the *n*-heptane insoluble content, was the refractive index (**Figure 6-7**). This was anticipated, since it was reported that refractive index could be used as a method to predict onset of phase instability due to phase separation of asphaltenes [61-64]. The relationship in **Figure 6-7**

suggested that the refractive index method may apply equally to determine the onset of phase instability of thermally converted material.
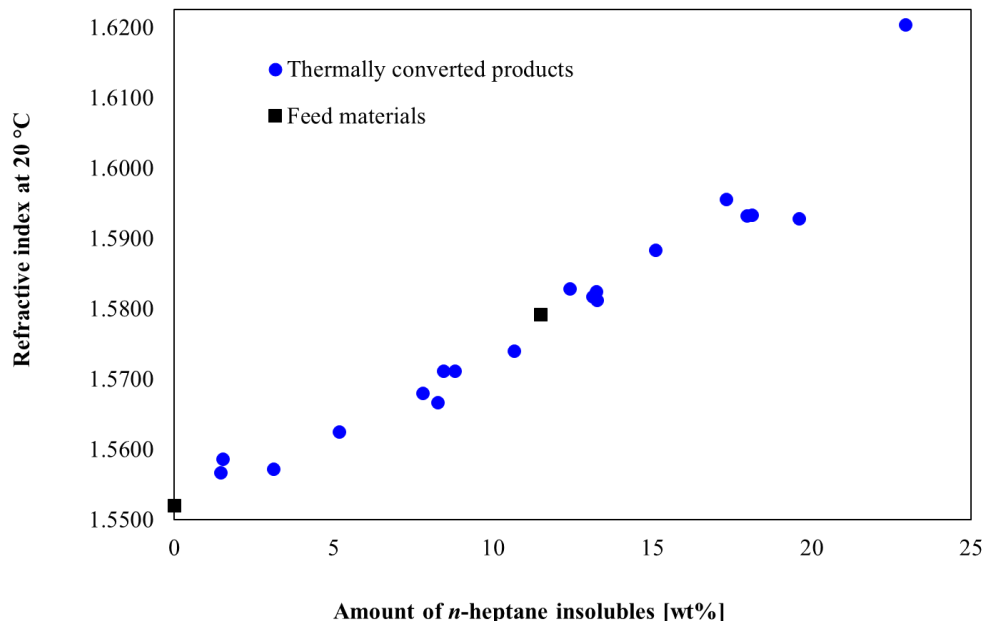
Figure 6-7. Refractive index at 20 °C in relation to n-heptane insoluble asphaltenes content. As a linear correlation, the $r^2 = 0.940$.

The rather limited relationships found between product properties and the amount of asphaltenes was to some extent anticipated. It is known that the chemical nature of the asphaltenes fraction changes during thermal conversion, for example, the hydrogen-to-carbon ratio in *n*-pentane insoluble asphaltenes was found to decrease from 1.2 to 0.8–0.9, while the free radical content increased from 10^{18} to 10^{19} spins/g [27]. The amount of asphaltenes in a thermally converted product is therefore an amount of material with a variable composition.

In conclusion, solubility classification was not a meaningful measure in thermal conversion. It was poorly related to properties with chemical meaning that could serve as predictors for the reaction chemistry. Solvent classification of thermally converted products remains a useful

measurement to assess phase stability, and oil compatibility, but not to describe the reaction progress of the conversion process itself.

6.5. Conclusions

The importance of solvent classification for flow assurance and phase stability was not disputed, but the study questioned whether solvent classification was a meaningful measure in thermal conversion. A range of feed materials was prepared by solvent classification of bitumen and the thermally converted products were characterized. The development of new *n*-heptane insoluble material during thermal conversion of maltenes was the baseline against which the impact of asphaltenes originally in the feed was evaluated. It was found that:

a. The formation of CS_2 insoluble coke was unrelated to the formation or amount of *n*-heptane insoluble asphaltenes. The progression of thermal conversion to form CS_2 insoluble material did not necessarily require the formation of *n*-heptane insoluble material first. It was unlikely that coke formed exclusively by the conversion of asphaltenes.

b. Few physical and chemical properties of the thermally converted products were related to the amount of *n*-heptane insoluble asphaltenes. There was a relationship with free radical content that was directionally related to the increase in heavier material suggested by the increased amount of asphaltenes. At the same time the relationship to aromatic carbon content was poor. There was also a relationship with refractive index, which was anticipated from the reported use of refractive index to predict onset of asphaltenes separation.

c. Solubility classification was not found to be meaningful measure in thermal conversion and it was poorly related to properties that could serve as predictors for the reaction chemistry.

References

[1] *ASTM D721: Standard Test Method for Oil Content of Petroleum Waxes*. ASTM International: West Conshohocken, PA, 2017.

[2]   Van Krevelen, D. W. *Coal. Typology–Physics–Chemistry–Constitution.* 3ed; Elsevier: Amsterdam, 1993.

[3]   Stratiev, D.; Shishkova, I.; Tankov, I.; Pavlova, A. Challenges in Characterization of Residual Oils. A Review. *Journal of Petroleum Science and Engineering* **2019**, *178:* p. 227 - 250.

[4]   *ASTM D2007: Standard Test Method for Characteristic Groups in Rubber Extender and Processing Oils and Other Petroleum-Derived Oils by the Clay-Gel Absorption Chromatographic Method*. ASTM International: West Conshohocken, PA, 2020.

[5]   *ASTM D4124, Standard Test Method for Separation of Asphalt into Four Fractions*. ASTM International: West Conshohocken, PA, 2018.

[6]   *ASTM D6560: Standard Test Method for Determination of Asphaltenes (Heptane Insolubles) in Crude Petroleum and Petroleum Products*. ASTM International: West Conshohocken, PA, 2022.

[7]   Ramirez-Corredores, M.M. *The Science and Technology of Unconventional Oils*. Academic Press: London, UK, 2017.

[8]   Schuler, B.; Zhang, Y.; Liu, F.; Pomerantz, A. E.; Andrews, A. B.; Gross, L.; Pauchard, V.; Banerjee, S.; Mullins, O. C. Overview of Asphaltene Nanostructures and Thermodynamic Applications. *Energy and Fuels* **2020**, *34*: p. 15082 - 15105.

[9]   Gray, M. R.; Yarranton, H. W.; Chacón-Patiño, M. L.; Rodgers, R. P.; Bouyssiere, B.; Giusti, P. Distributed Properties of Asphaltene Nanoaggregates in Crude Oils: A Review. *Energy and Fuels* **2021**, *35*: p. 18078 - 18103.

[10]   Wiehe, I.A. A Phase-Separation Kinetic Model for Coke Formation. *Industrial and Engineering Chemistry Research* **1993**, *32*: p. 2447 – 2454.

[11]   Rahimi, P.M.; Teclemariam, A.; Taylor, E.; DeBruijn, T.; Wiehe, I.A. Thermal Processing Limits of Athabasca Bitumen during Visbreaking Using Solubility Parameters. *ACS Symposium Series* **2005**, *895*: p. 183 – 196.

[12]   Speight, J. G.; Özüm, B. *Petroleum Refining Processes*. Marcel Dekker: New York, NY, 2002.

[13]   Rahimi, P.; Gentzis, T.; Dawson, W.H.; Fairbridge, C.; Khulbe, C.; Chung, K.; Nowlan, V.; DelBianco, A. Investigation of Coking Propensity of Narrow Cut Fractions from

Athabasca Bitumen using Hot-Stage Microscopy. *Energy and Fuels* **1998**, *12*: p. 1020 - 1030.

[14]   Brauch, R.; Fainberg, V.; Kalchouck, H.; Hetsroni, G. Correlations between Properties of Various Feedstocks and Products of Visbreaking. *Fuel Science and Technology International* **1996**, *14*: p. 753 - 765.

[15]   Subramanian, S.; Simon, S.; Sjöblom, J. Asphaltene Precipitation Models: A Review. *Journal of Dispersion Science and Technology* **2016**, *37*: p. 1027 - 1049.

[16]   Wiehe, I. A. *Process Chemistry of Petroleum Macromolecules.* CRC Press: Boca Raton, FL, 2008.

[17]   Louwerse, M. J.; Maldonado, A.; Rousseau, S.; Moreau-Masselon, C.; Roux, B.; Rothenberg, G. Revisiting Hansen Solubility Parameters by Including Thermodynamics. *ChemPhysChem* **2017**, *18*: p. 2999 - 3006.

[18]   Ramos-Pallares, F.; Santos, D.; Yarranton, H. W. Application of the Modified Regular Solution Model to Crude Oils Characterized from a Distillation Assay. *Energy and Fuels* **2020**, *34*: p. 15270 - 15284.

[19]   Gray, M. R. *Upgrading Oilsands Bitumen and Heavy Oil.* University of Alberta Press: Edmonton, Canada, 2015.

[20]   Mullins, O. C.; Pomerantz, A. E.; Andrews, B.; Majumdar, R. D.; Hazendonk, P.; Ruiz-Morales, Y.; Goual, L.; Zare, R. N. Asphaltenes. In *Springer Handbook of Petroleum Technology*; Hsu, C. S., Robinson, P. R. Eds.; Springer: Cham, 2017, p. 221 - 250.

[21]   *Asphaltenes, Heavy Oils, and Petroleomics*; Mullins, O. C., Sheu, E. Y., Hammami, A., Marshall, A. G. Eds.; Springer: New York, 2010.

[22]   *Structures and Dynamics of Asphaltenes;* Mullins, O.C., Sheu, E.Y., Eds.; Springer Science+Business Media: New York, 1998.

[23]   *Asphaltenes. Fundamentals and Applications*; Sheu, E. Y., Mullins, O. C. Eds.; Plenum Press: New York, 1995.

[24]   *ASTM D3279: Standard Test Method for n-Heptane Insolubles*. ASTM International: West Conshohocken, PA, 2019

[25]   Hawley, G.G. *The Condensed Chemical Dictionary*. 8th Edition. Van Nostrands Reinhold: New York, NY, 1971.

[26]   Wang, L.; Zachariah, A.; Yang, S.; Prasad, V.; De Klerk, A. Visbreaking Oilsands-Derived Bitumen in the Temperature Range of 340–400 °C. *Energy and Fuels* **2014**, *28*: p. 5014 - 5022.

[27]   Yan, Y.; De Klerk, A.; Prado, G. H. C. Visbreaking of Vacuum Residue Deasphalted Oil: New Asphaltenes Formation. *Energy and Fuels* **2020**, *34*: p. 5135 - 5147.

[28]   Yan, T. Y. Characterization of Visbreaker Feeds. *Fuel* **1990**, *69*: p. 1062 - 1064.

[29]   De Klerk, A. Thermal Conversion Modeling of Visbreaking at Temperatures below 400 °C. *Energy and Fuels* **2020**, *34*: p. 15285 – 15298.

[30]   Carbognani, L.; Roa-Fuentes, L.C.; Diaz, L.; Berezinski, J.; Carbognani-Arambarri, L.; Pereira-Almao, P. Reliable Determination of Water Contents of Bitumen and Vacuum Residua via Coulometric Karl Fischer Titration using Tetrahydrofuran. *Petroleum Science and Technology* **2014**, *32*: p. 602 - 609

[31]   Cookson, D. J.; Lloyd, C. O.; Smith, B. A Novel Semi-Empirical Relationship between Aromaticities Measured from ^{1}H and [13]C N.M.R. Spectra. *Fuel* **1986**, *65*: p. 1247 - 1253.

[32]   *ASTM D7169: Standard Test Method for Boiling Point Distribution of Samples with Residues such as Crude Oils and Atmospheric and Vacuum Residues by High Temperature Gas Chromatography.* ASTM International: West Conshohocken, PA, 2020.

[33]   Chamberlain, N. F. *The Practice of NMR Spectroscopy With Spectra-Structure Correlations for Hydrogen-1*. Plenum Press: New York, 1974.

[34]   Guan, J. G.; Kariznovi, M.; Nourozieh, H.; Abedi, J. Density and Viscosity for Mixtures of Athabasca Bitumen and Aromatic Solvents. *Journal of Chemical Engineering Data* **2013**, *58*: p. 611 - 624.

[35]   Barrera, D. M.; Ortiz, D. P.; Yarranton, H. W. Molecular Weight and Density Distributions of Asphaltenes from Crude Oils. *Energy and Fuels* **2013**, *27*: p. 2474 - 2487.

[36]   Carbognani, L.; Lubkowitz, J.; Gonzalez, M.F.; Pereira-Almao, P. High Temperature Simulated Distillation of Athabasca Vacuum Residue Fractions. Bimodal Distributions and Evidence for Secondary "On-Column" Cracking of Heavy Hydrocarbons. *Energy and Fuels* **2007**, *21*: p. 2831 - 2839.

[37]   Castellanos Diaz, O.; Yarranton, H. W. Applicability of Simulated Distillation for Heavy Oils. *Energy and Fuels* **2019**, *33*: p. 6083 - 6087.

[38]   Strausz, O. P. Lown, E. M. *The Chemistry of Alberta Oil Sands, Bitumens and Heavy Oils*. Alberta Energy Research Institute: Calgary, AB, 2003.

[39]   Alboudwarej, H.; Beck, J.; Svrcek, W. Y.; Yarranton, H. W. Sensitivity of Asphaltene Properties to Separation Techniques. *Energy and Fuels* **2002**, *16*: p. 462 - 469.

[40]   Lipkin M.R; Kurtz, S.S. Temperature Coefficient of Density and Refractive Index for Hydrocarbons in the Liquid State. *Industrial and Engineering Chemistry – Analytical Edition* **1941**, *13*: p. 291 – 295.

[41]   Ward, A. L.; Kurtz, S. S. Jr. Refraction, Dispersion, and Related Properties of Pure Hydrocarbons. Arranged for Use in the Analysis of Hydrocarbon Mixtures. *Industrial and Engineering Chemistry, Analytical Edition* **1938**, *10*: p. 559 - 576.

[42]   Shen, J.; Astrath, N. G. C.; Pedreira, P. R. B.; Guimarães, F. B.; Gieleciak, R.; Wen, Q.; Michaelian, K. H.; Fairbridge, C.; Malacarne, L. C.; Rohling, J. H.; Baesso, M. L. Correlations among Thermophysical Properties, Ignition Quality, Volatility, Chemical Composition, and Kinematic Viscosity of Petroleum Distillates. *Fuel* **2016**, *163*: p. 324 - 333.

[43]   Beck, J.; Svrcek, W. Y.; Yarranton, H. W. Hysteresis in Asphaltene Precipitation and Redissolution. *Energy and Fuels* **2005**, *19*: p. 944 - 947.

[44]   Bjorøy, Ø.; Fotland, P.; Gilje, E.; Høiland, H. Asphaltene Precipitation from Athabasca Bitumen using an Aromatic Diluent: A Comparison to Standard *n*-Alkane Liquid Precipitants at Different Temperatures. *Energy and Fuels* **2012**, *26*: p. 2648 - 2654.

[45]   Peramanu, S.; Singh, C.; Agrawala, M.; Yarranton, H. W. Investigation on the Reversibility of Asphaltene Precipitation. *Energy and Fuels* **2001**, *15*: p. 910 - 917.

[46]   Clarke, P.F.; Pruden, B.B. Asphaltene Precipitation from Cold Lake and Athabasca Bitumen. *Petroleum Science and Technology* **1998**, *16*: p. 287 – 305.

[47]   Suzuki, T.; Itoh, M.; Takegami, Y.; Watanabe, Y. Chemical Structure of Tar-sand Bitumens by ^{13}C and ^{1}H N.M.R. Spectroscopic Methods. *Fuel* **1982**, *61*: p. 402 – 410.

[48]   Ramos-Pallares, F.; Yarranton, H. W. Extending the Modified Regular Solution Model to Predict Component Partitioning to the Asphaltene-Rich Phase. *Energy and Fuels* **2020**, *34*: p. 5213 - 5230.

[49]   Chacón-Patiño, M. L.; Vesga-Martínez, S. J.; Blanco-Tirado, C.; Orrego-Ruiz, J. A.; Gómez-Escudero, A.; Combariza, M. Y. Exploring Occluded Compounds and their Interactions with Asphaltene Networks using High-Resolution Mass Spectrometry. *Energy and Fuels* **2016**, *30:* p. 4550 - 4561.

[50]   Ganeeva, Y. M.; Barskaya, E. E.; Okhotnikova, E. S.; Yusupova, T. N. Features of the Composition of Compounds Trapped in Asphaltenes of Oils and Bitumens of the Bavly Oil Field. *Energy and Fuels* **2021**, *35*: p. 2493 - 2505.

[51]   Zachariah, A.; De Klerk, A. Thermal Conversion Regimes for Oilsands Bitumen. *Energy and Fuels* **2016**, *30*: p. 239 - 248.

[52]   Andersen, S. I.; Lindeloff, N.; Stenby, E. H. Investigation of Asphaltenes Precipitation at Elevated Temperature. *Petroleum Science and Technology* **1998**, *16*: p. 323 - 334.

[53]   Cimino, R.; Correra, S.; Del Bianco, A.; Lockhart, T. P. Solubility and Phase Behavior of Asphaltenes in Hydrocarbon Media. In *Asphaltenes. Fundamentals and applications*; Sheu, E. Y., Mullins, O. C. Eds.; Plenum Press: New York, 1995, p. 97 - 130.

[54]   Jennings, D. W.; Weispfennig, K. Experimental Solubility Data of Various *n*-Alkane Waxes: Effects of Alkane Chain Length, Alkane Odd versus Even Carbon Number Structures, and Solvent Chemistry on Solubility. *Fluid Phase Equilibria* **2005**, *227*: p. 27 - 35.

[55]   Andersen, S. I.; Stenby, E. H. Thermodynamics of Asphaltene Precipitation and Dissolution Investigation of Temperature and Solvent Effects. *International Journal of Petroleum Science and Technology* **1996**, *14*: p. 261 - 287.

[56]   Wiehe, I. A. A Solvent-Resid Phase Diagram for Tracking Resid Conversion. *Industrial and Engineering Chemistry Research* **1992**, *31*: p. 530 - 536.

[57]   Tannous, J. H.; De Klerk, A. Quantification of the Free Radical Content of Oilsands Bitumen Fractions. *Energy and Fuels* **2019**, *33*: p. 7083 - 7093.

[58]   Chang, H-L.; Wong, G. K.; Lin, J-R.; Yen, T. F. Electron Spin Resonance Study of Bituminous Substances and Asphaltenes. In *Asphaltenes And asphalts. Vol. 2* (Developments in Petroleum Science Vol. 40 B); Yen, T. F., Chilingarian, G. V. Eds.; Elsevier: Amsterdam, 2000, p. 229 - 280.

[59]   Schuler, B.; Meyer, G.; Peña, D.; Mullins, O. C.; Gross, L. Unraveling the Molecular Structures of Asphaltenes by Atomic Force Microscopy. *Journal American Chemical Society* **2015**, *137*: p. 9870 - 9876.

[60]   Bake, K. D.; Craddock, P. R.; Bolin, T. B.; Abdallah, W.; Mitra-Kirtley, S.; Andrews, A. B.; Mullins, O. C.; Pomerantz, A. E. Structure-Solubility Relationships in Coal, Petroleum, and Immature Source-Rock-Derived Asphaltenes. *Energy and Fuels* **2020**, *34*: p. 10825 - 10836.

[61]   Buckley, J. S.; Hirasaki, G. J.; Liu, Y.; Von Drasek, S.; Wang, J-X., Gill, B. S. Asphaltene Precipitation and Solvent Properties of Crude Oils. *Petroleum Science and Technology* **1998**, *16*: p. 251 - 285.

[62]   Buckley, J. S. Predicting the Onset of Asphaltene Precipitation from Refractive Index Measurements. *Energy and Fuels* **1999**, *13*: p. 328 - 332.

[63]   Angle, C. W.; Long, Y.; Hamza, H.; Lue, L. Precipitation of Asphaltenes from Solvent-Diluted Heavy Oil and Thermodynamic Properties of Solvent-Diluted Heavy Oil Solutions. *Fuel* **2006**, *85*: p. 492 - 506.

[64]   Wattana, P.; Wojciechowski, D. J.; Bolaños, G.; Fogler, H. S. Study of Asphaltene Precipitation using Refractive Index Measurement. *Petroleum Science and Technology* **2003**, *21*: p. 591 - 613.

7. Relationship between free radical concentration and petroleum properties

7.1. Introduction

Free radicals are inherently present in raw materials like oilsands bitumen, and coals, even before conversion processes take place [1,2]. It was believed that due to the high viscosity of bitumen under ambient conditions, it was possible for free radicals to be stabilized by steric shielding [3]. This was related to a decrease in the probability of species undergoing free radical recombination because high viscosity slows the diffusion rate [4]. However, the work of Alili et al. [5] showed that viscosity, caging, and steric effects were not able to explain the existence of persistent free radicals. Instead, it was postulated that the persistence of the free radicals was a dynamic process that could be described as analogous to the ionic dissociation of water. Such a description does not require the longevity of any individual radical species and describes the persistence in terms of the relative rates of dissociation and association reactions.

If the description of free radical persistence in terms dynamic reaction equilibrium is valid, then it is anticipated that free radical concentration would depend on (i) the bulk properties of the material affecting the equilibrium, (ii) temperature, and (iii) the nature of the species involved in radical formation.

It was indeed noted that the quantification of the persistent free radical concentration of petroleum in solution was dependent on the bulk liquid properties that could affect the dissociation equilibrium [1,6].   The work of Barry et al. [4,7] explored the effect of different solvents in the "cage" effect and discussed the impact of the viscosity, and the polarity of those solvents in the recombination efficiency of reactions. It was also reported that the concentration of free radicals in petroleum varies with temperature [8,9], which can be interpreted in terms of the combined effect temperature has on both reaction rate (association and dissociate rate) and viscosity. Since the material in petroleum that is responsible for its free radical concentration is the product of transformation over geological time, yet, near instantaneously responsive to changes in temperature and bulk properties, the evidence points to a dynamic reaction equilibrium.

The persistent free radical concentration of straight run petroleum is therefore a property of the petroleum that can be used to characterize petroleum, just like physical and chemical properties such as density, distillation profile, and elemental composition. The question that was of interest in this work was whether the persistent free radical concentration of straight run petroleum is a property that describes an independent aspect of the nature of the petroleum? Differently put, can the persistent free radical concentration of straight run petroleum be related to other properties of the material?

Rudnick and Tueting [10] investigated the relationship between the free radical content in two different feedstocks with the molecular weight of different distillation fractions. They found that the concentration of free radical species increased with the average molecular weight. Rudnick et al. [10,11] also mentioned the relationship of free radical concentration with coke formation tendency, sulfur content, and mesophase formation. Of these, the relationship between free radical concentration and sulfur content may be a consequence of the relationship between sulfur content and boiling range in petroleum [12]. The same relationship between free radical concentration and molecular weight is implied by the increase in free radical concentration with increasing boiling range of petroleum from the same source [1]. Likewise, Gutowsky et al. [13] reported that free radical species were concentrated in the heaviest material collected from prolonged centrifugation of petroleum.

In work [2,14] that spanned different materials, including straight run petroleum, it was proposed that there is a relationship between the free radical concentration and aromatic content. The relationship appeared linear over limited regions for specific materials but was by no means a single proportionality. In the same work, many different relationships between free radical concentration and other properties were explored and at best some directional trends were noted with properties such as burial depth of the deposit and carbon content.

It appears that there is a relationship between the boiling range of straight run petroleum and its free radical concentration. This suggests that there are other attributes more readily found in heavier molecules that enable them to participate in the type of interactions that give rise to free radical persistence. Elucidating those relationships would not only be of fundamental value, but

165

also of practical value. For example, one would then be able to measure the free radical concentration of a petroleum sample, which is an easily measurable macroscopic property, and thereby be able to infer additional information about the nature of the petroleum.

Persistent free radical content can also be developed in heavy products produced by pyrolysis of lighter feed materials [15-17]. However, in these cases the material is no longer straight run petroleum and the argument that the persistent free radical concentration is not a transient property, cannot be applied. In fact, there is direct evidence that the free radical concentration of heavy products from pyrolysis is not constant over time [18,19].

This study made use of straight run petroleum fractions developed in this work (**Chapter 5** and **6**), as well as characterization data reported in the literature. The aim was to determine whether there are relationships between free radical concentration and other physical and chemical properties.

7.2. Data sources

The study drew on the published literature to obtain experimentally measured properties of straight run petroleum and sub-fractions of petroleum, as well as thermally converted products that also include measurement of the free radical concentration. Additionally, data from coal and carbon black was included to check whether any of the observed relationships were generally applicable, or just valid for petroleum. **Table 7-1** shows the materials considered from the literature along with the additional properties that were reported in each of the references.

Table 7-1. Materials and corresponding data sources considered in this study. Available properties are indicated.

| Sample	No. of samples	Refractive Index [nD]	N [wt.%]	S [wt.%]	H/C	Aromaticity	Asphaltenes [wt.%]	Free Radicals [spins/g]	Refs.
Straight run petroleum samples									
Athabasca bitumen (Ab)	3	✓	✓	✓	✓	✓	✓	✓	[18,20,21]
Bitumen	15		✓	✓				✓	[14]
Asphaltenes (Ab)	2	✓	✓	✓	✓	✓	✓	✓	[21]
Asphaltenes	31		✓	✓	✓	✓		✓	[14,22,23]
Maltenes (Ab)	1	✓	✓	✓	✓	✓	✓	✓	[21]
Resins	4				✓	✓		✓	[22]
Maltenes	8					✓		✓	[22]
Distillation fractions	4	✓	✓	✓	✓			✓	[1,24]

7.3. Discussion

7.3.1. *Relationship between free radical concentration and boiling point*

One of the most powerful concepts in the characterization of petroleum is the concept of the compositional continuum. To quote from Altgelt and Boduszynski [12]: "... compositional trends in fractions of increasing boiling point are continuous and that this continuity extends even to nondistillable residues." This continuity was demonstrated for many properties such as aromaticity and heteroatom content as the presence of such compounds will increase intermolecular interactions which will be reflected in higher boiling points; but the work did not include quantification of the free radical content. Nevertheless, the expectation is that the compositional features giving rise to the persistent free radical nature of petroleum would also follow the continuum.

The persistent organic free radicals can easily be distinguished from other paramagnetic species present in petroleum, such as the vanadyl ion. The quantification of free radical content has several pitfalls [25], which may introduce discrepancies in the absolute numbers reported. For this reason, the data collected from different sources are considered independently, instead of collating all of the measurements into a single data set. This is an approach that was employed throughout this study.

Using the information provided by Rudnick and Tueting [10], it is possible to plot the molecular weight fractions against the free radical concentration as it is shown in **Figure 7-1**. The measurement uncertainty reported in that study was 8% relative.
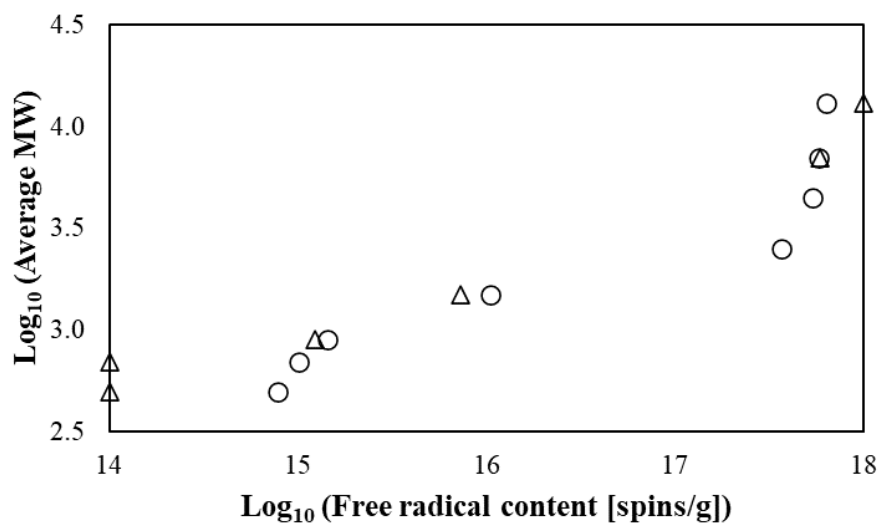
Figure 7-1. Average molecular weight (MW) and free radical content of Arabian (○) and Sheng Li (△) Oils reported by Rudnick and Tueting [10].

The average molecular weight used in **Figure 7-1** corresponded to the fractions collected by preparative size exclusion chromatography and the electron spin resonance (ESR) calibration was performed with 1,l-diphenyl-2-picryl-hydrazyl (DPPH) [10]. The free radical concentration was, however, related to the peak intensity and not the integral area as this was calculated based on the integration method described by Poole [26]. Based on current understanding [27] the molecular weights are likely over-estimated. This does not detract from the value of this study, which shows that the persistent free radical content has a regular relationship with molecular weight, which in turn is related to the boiling point of the petroleum.

The study by Rudnick and Tueting [10] is unfortunately the only one of its kind that I am aware of.

In a study that quantified the persistent free radical content in different petroleum fractions, the free radical concentration in light vacuum gas oil (LVGO), heavy vacuum gas oil (HVGO), and vacuum residue (VR) of Athabasca bitumen was determined (**Table 7-2**) [1]. The ESR calibration was performed using DPPH and the uncertainty was of the order 10% relative. The concentration of free radicals increased with increasing boiling point of straight run distillation fractions.

Table 7-2. Free radical content from distillation fractions of Athabasca bitumen reported in [1].

Sample	Free radical content [spins/g]
Light vacuum gas oil (LVGO), Nexen Long Lake	7.8×10^{17}
Heavy vacuum gas oil (HVGO), Nexen Long Lake	8.7×10^{17}
Cold Lake vacuum residue (VR), Imperial Oil	1.4×10^{18}
Athabasca vacuum residue (VR), Syncrude	1.4×10^{18}

In conclusion, the persistent free radical nature of straight run petroleum increases monotonically with an increase in boiling point. Based on the limited evidence presented, it appears that persistent free radical content is a property that follows the boiling point continuum.

7.3.2. *Relationship between free radical concentration and solubility fractions*

A commonly encountered solubility fraction is the asphaltenes. Asphaltenes is defined as a solubility class and different standard test methods have been developed to quantify asphaltenes and other solubility fractions, such as ASTM D3279 [28], ASTM D6560 [29], ASTM D893 [30], ASTM D4124 [31], and ASTM D2007 [32].

Defining asphaltenes in terms of chemical composition has as been a "quest" that many researchers have attempted. Macroscopic properties indicated that compared to the whole petroleum, asphaltenes have a lower hydrogen-to-carbon ratio, a higher heteroatom content, a higher density and a higher refractive index. This disproportionation of material by solvent partitioning formed the basis for the petroleum refining technology called solvent deasphalting [33]. Attempts to provide species level generalization, however, is controversial.

The free radical content in asphaltenes is higher compared to the whole petroleum, and therefore also the maltenes **Table 7-3** [1,21].

Table 7-3. Free radical content of whole petroleum and the asphaltenes and maltenes solubility fractions obtained by solvent deasphalting.

Sample	Mass Fraction [%][a]	Free radical content [spins/g]
Athabasca bitumen, Suncor [1]		
whole petroleum	100	1.1×10^{18}
asphaltenes [b]	16.8 ± 2.1	2.1×10^{18}
Athabasca bitumen, Nexen [21]		
whole petroleum	100	1.6×10^{18}
asphaltenes [c]	18.6 ± 0.6	3.4×10^{18}
maltenes	81.4	1.1×10^{18}

[a] Average ± sample standard deviation
[b] *n*-Pentane insoluble material
[c] *n*-Heptane insoluble material. It was explained in the source that the anomalous high value was repeatable, but that other measures indicated that a portion of this material should have partitioned to the *n*-heptane rich phase.

Both asphaltenes and its parent oil have a molecular weight distribution [34-42] and asphaltenes are usually associated with the heaviest part of the oil. In **Section 7.3.1**, it was concluded that the concentration of free radicals seem to increase with increasing boiling point (hence molecular weight), and so do asphaltenes content, suggesting an agreement with the Boduszynski compositional continuum.

However, while asphaltenes are considered to be the heaviest fraction in whole petroleum, the work of McKenna et al. [34] showed that this is not true for a topped-and-tailed distillation fraction. Within vacuum gas oil, the molecular weight distribution of the asphaltenes was on the low side of the overall molecular weight distribution. These two observations can be reconciled if the 'nondistillable' portion of the vacuum residue, the material with the highest molecular weight, is mostly solvent classified as asphaltenes. The implication for this study is that it would be tenuous to extend a conclusion derived only on the free radical content of whole petroleum and its solubility fractions (as in **Table 7-3**) to distillation fractions.

The results in **Table 7-3** make it clear that the persistent free radical content is not restricted to the asphaltenes alone. The question that remains is whether the higher concentration of free radicals in the asphaltenes is due to its molecular weight distribution, or whether the free radical content of the asphaltenes would be higher than that of the maltenes when the molecular weight is the same, or within the same narrow-cut distillation fraction?

To address the first part of the question, the study of Adams et al. [43] is useful. In that study the *n*-pentane insoluble asphaltenes fractions from different crude oils was further separated by size exclusion chromatography into different molecular weight fractions. The free radical concentration of each fraction as determined by ESR spectrometry is presented in **Figure 7-2.**
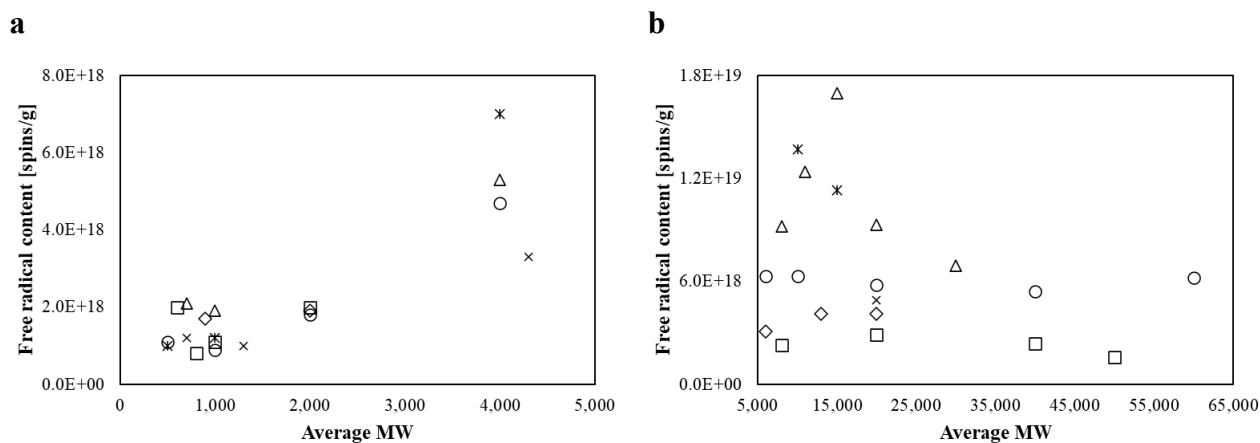
Figure 7-2. Free radical content and average molecular weight (MW) of different asphaltenes sub-fractions from size exclusion chromatography reported by Adams et al. [42]: a) Average molecular weight from 0 to 5,000; and b) Average molecular weight from 5,000 to 65,000. The symbols correspond to: Natural asphalt (○), Venezuela (□), California (Δ), Arabian I (◊), Arabian II (✕), and Sumatra (✳).

The calibration of the ESR was performed using a coal pitch standard and the calibration equation was based on both the intensity and line width of the second derivative curve [43]. As mentioned before, the molecular weights are likely over-estimated, but this does not detract from the value of the relationship shown in **Figure 7-2.**

Asphaltenes are also notoriously prone to aggregation at molecular level [44]. It is doubtful that the species in the highest molecular weight fractions of the asphaltenes are monomeric. It is more likely that the highest molecular weight fractions from size exclusion chromatography represent a higher extent of molecular-level aggregation [45]. If it is assumed that only the lower molecular weight species in **Figure 7-2a** are monomeric, then the conclusion drawn in **Section 7.3.1** may still be valid, namely, that free radical concentration in the asphaltenes increases with the boiling point continuum and therefore with molecular weight. However, it can be noticed from **Figure 7-2b** that the increase of free radical content with molecular weight was not monotonic, even for the lower molecular weight species, and it appears unlikely that free radical concentration in the asphaltenes increases with the boiling point continuum.

This does not address the second part of the question, which is whether the asphaltenes and maltenes would have comparable free radical content when they have comparable boiling point or molecular weight. To answer this, one must also address the uncertainty introduced by the change in bulk liquid composition that may affect the measured concentration of free radicals [6]. It may well be that association-dissociation equilibria of the free radical pairs in the individual solubility fractions are different to that in the whole petroleum.

From the data presented in **Table 7-3**, it is noteworthy that the free radical content in bitumen (1.6×10^{18} spins/g) and that calculated from its solubility fractions ($1.5 \times 10^{18} = 0.186 \times 3.4 \times 10^{18} + 0.814 \times 1.1 \times 10^{18}$ spins/g) are close, but not the same. Although the balance closes within experimental uncertainty, no strong conclusion can be drawn.

Based on the data presently available, it is not possible to determine whether the persistent free radical content of individual solubility fractions follows the boiling point continuum like that of the whole petroleum. Similarly, it was not possible to determine whether asphaltenes and maltenes in the same narrow boiling range would have the same free radical content. To answer the remaining questions, the use of different fractionated asphaltene samples to which free radical content could be determined will be fundamental. However, one should be cautious regarding higher molecular weight fractions as it should be kept in mind that it could be the result of asphaltene aggregation [46].

7.3.3. *Relationship between free radical concentration and composition related properties*

It was concluded in **Section 7.3.1** that free radical content increases with the boiling point continuum. From the work of Altgelt and Boduszynski [12], it is known that some compositional properties will increase with the increase in boiling point and molecular weight. This is true for individual oils, but, the relationship between properties and boiling point cannot be generalized amongst different crude oils. For example, knowing the relationship between sulfur content and boiling point for one crude oil does not imply that the sulfur content of a different crude oil can be predicted from its boiling point distribution. The compositional continuum is unique for each oil, although similarilties can be found between oils of comparable origin and nature.

In the petroleum industry, the Watson (UOP) K-factor is one of the powerful tools to reflect on the nature of the oil [47]. It employs information about density in relation to mean boiling point to infer information about composition. For instance, a high value in the K-factor will suggest that the studied oil is likely paraffinic, rather than aromatic/naphthenic, and vice versa. However, the K-factor cannot be used to generalize values for all of the properties that follow the compositional continuum.

It was nevertheless of interest to see whether there is a property relationship that allows the normalization of the impact of the measured compositional properties in relation to free radical content. If such property relationship exists, then the free radical concentration is related only to the increase in boiling point, otherwise, the free radical content is the result of a both the composition and the change in composition with boiling point, as is the case with other properties that follow the compositional continuum.

To answer whether the free radical content is only related to the boiling point distribution, the mean average boiling temperature (T_{50}) value and the K-factor were considered to illustrate "normalizing" factors. The calculated values are shown next to the free radical content from different bitumen samples from the Western Canadian Sedimentary Basin in **Table 7-4**. The comparison amongst the reported samples is valid as the free radical content was obtained

following the same sample protocol and analysis. This is relevant due to the uncertainty associated with quantitative ESR, which is dependent on the type of calibration substance, ESR tube type, and several other factors that could cause a difference in the absolute number of spins per gram reported [25].

Table 7-4. Mean average boiling temperature (T_{50}), K-factor and free radical content in different bitumen samples.

Sample	T_{50} [°C]	K-factor	Free radical content [spins/g]
Athabasca – 1[a]	554	11.2	1.6×10^{18}
Athabasca – 2[b]	535	11.2	$1.1 \times 10^{18} \pm 2.4 \times 10^{17}$
Athabasca – 3[c]	569	11.1	$9.3 \times 10^{17} \pm 1.2 \times 10^{17}$
Cold Lake[d]	577	11.2	$9.5 \times 10^{17} \pm 3.8 \times 10^{16}$

[a] Ref. [21]
[b] Ref. [1,18]
[c] Ref. [1,48]
[d] Ref. [1,49,50]

When it is assumed that the shape of the boiling point distribution with respect to volume distilled is similar for all straight run crude oils, then the mean boiling point (T_{50}) will also describe the curve. This can be understood through analogy, to describe a regular distribution like the normal distribution, all that needs to be known is the mean and standard deviation as measure of spread. In terms of the boiling point curve the mean is given by the T_{50} and the measure of spread is implied by the initial boiling point (IBP). The inherent assumption is that the IBP for oils being compared should be the same.

Under this assumption, when petroleum samples have similar values for T_{50} will suggest that the distillation profile is also similar. The points considered from the distillation curve tends to properly describe the distillation profile with a slight deviation at lower boiling points. This was pointed by Watson and Nelson [51] where a correction factor was suggested. Nevertheless, T_{50} has been widely used to predict different properties in the oil industry [52]. In addition, the UOP K-factor adds a compositional aspect to the mean average boiling temperature by involving the density of the samples. Watson and Nelson [51] initially proposed the use of this characterization

factor to estimate what they called molar properties (i.e., molecular weight, specific heat, among other) but it does not seem to account for heteroatom concentration. The implication of the two illustrative "normalizing" parameters is that a similarity in both parameters between the two oils can indicate that the nature of the oil and the boiling point distribution of both oils are similar.

The Athabasca bitumen samples reported in **Table 7-4** showed that the T_{50} of the samples is fairly similar as well as the K-factor. However, to guarantee that they are of comparable nature, the molar refractivity (intrinsic property independent of temperature or pressure) of the four samples was calculated. The finding of Rivolta [53] suggested that the refractive index expression developed by Eykman to relate molar volume to molar refractivity is more accurate for hydrocarbon systems, compared to others, such as Lorentz–Lorentz. The values obtained for Athabasca – 1 and Athabasca – 2 bitumen samples are 674 and 645 cm³/mol, respectively. For the Athabasca – 3 and the Cold Lake bitumen, the values were equal (~ 710 cm³/mol), indicating that the two bitumen samples are of comparable nature based on molar refractivity. This is of significance, because the molar refractivity can be expressed as the sum of the fractional molar refractivity contributions of all of the chemical bonds in a sample. Although it is possible to have two dissimilar sets of fractional contributions adding to the same total molar refractivity of the sample, the comparable origin of the oilsands bitumen samples suggest that molar refractivity may in this specific case be a reasonable measure of chemical similarity.

To be able to answer the question whether the free radical concentration only depends on the boiling point distribution, Athabasca – 3 and Cold Lake bitumen samples, reported in **Table 7-4**, are considered. The values show a difference in the free radical content in the two samples. However, due to the standard deviation of the measurement, the results fell within the same range. As a consequence, and due to the limited amount of available data, it is not possible to conclude at this point whether the free radical concentration is only related to the boiling point distribution of the samples or if there is a compositional contribution to it.

If additional information becomes available, and it is found that free radical concentration is not only dependent on the boiling point distribution, only then, it will be of interest to explore the

impact of compositional properties such as heteroatom content and aromaticity (both shown to agree with the Boduszynski continuum [12,40]) on the free radical content of the samples.

Nevertheless, it can be mentioned that coal literature has explored the relationship of heteroatom content, particularly oxygen content, and characteristics of the free radical spectra (i.e., the g-value [22] and shape [54]). While Yen and Sprang [22] found a relationship between the oxygen content in aromatic systems and g-value, Uebersfeld et al. [54] discarded any influence of the oxygen content on the ESR spectra. Retcofsky et al. [55], to the best of the authors' knowledge, evaluated the relationship of nitrogen content and free radical concentration in coal samples without finding any trend. For petroleum, Tannous et al. [6] found a relationship between the shift in g-value and sulfur content in the solvent used to dilute a bitumen sample which could be attributed to the dipole moment of the sample. In regard to free radical concentration, Rudnick et al. [11] presented preliminary results of a potential relationship with sulfur content study in different types of coker feed.

If in future it is found that free radical content does not only depend on boiling point distribution, then it would make sense to return to these studies to evaluate whether a directional change in change in free radical concentration is related to heteroatom content.

Several studies [13,15,56] reported that the free radical concentration in their studies was the result of "incomplete" or "broken bonds" in condensed aromatic systems (e.g., graphite-like structures). This explanation encounters the same challenge as previously mentioned relationships when the probability of finding "incomplete" or "broken bonds" increases with molecular weight of the species. It could then be suggested that if the free radical content of a sample is not only dependent on the boiling point distribution, a study the relationship of aromaticity, or a measure of it (e.g., aromatic carbon content, H/C ratio, or double bond equivalent) with the free radical concentration would make sense.

The results obtained in this section do not seem to provide enough information to conclude whether the free radical content in the bitumen samples reported in **Table 7-4** was a consequence of the

compositional continuum proposed by Boduszynski, or whether it could be attributed to specific compositional properties.

7.4. Conclusions

This work aimed to investigate the relationship of free radical content with different bulk properties in straight-run materials. The study was hampered by the limited information available in literature for these materials, which cause the conclusions to be more tentative in nature. Within these constraints, the following conclusions were drawn:

a. The monotonous increase of free radical content with the increase in molecular weight and by extension boiling point, suggests that free radical concentration may be a property consistent with the compositional continuum proposed by Boduszynski.

b. There was insufficient information available to determine whether the free radical content of individual solubility fractions followed the compositional continuum, or if asphaltenes and maltenes in the same narrow boiling range would have the same free radical content.

c. There was insufficient information available to determine whether the apparent continuum of free radical concentration with increase in boiling point temperature could be attributed to specific compositional properties other than boiling point temperature.

References

[1]   Tannous, J. H.; De Klerk, A. Quantification of the Free Radical Content of Oilsands Bitumen Fractions. *Energy and Fuels* **2019**, *33*: p. 7083 - 7093.

[2]   Chang, H-L.; Wong, G. K.; Lin, J-R.; Yen, T. F. Electron spin resonance study of bituminous substances and asphaltenes. In *Asphaltenes and asphalts. Vol. 2* (Developments in Petroleum Science Vol. 40 B); Yen, T. F., Chilingarian, G. V. Eds.; Elsevier: Amsterdam, 2000, p. 229 - 280.

[3]   Grossman, R.B. Free-Radical Reactions. In: *The Art of Writing Reasonable Organic Reaction Mechanisms*, 3rd Ed., Springer: Switzerland, 2019, p. 283 - 339.

[4]   Barry, J.T.; Berg, D.J.; Tyler, D.R. Radical Cage Effects: The Prediction of Radical Cage Pair Recombination Efficiencies Using Microviscosity Across a Range of Solvent Types. *Journal of the American Chemical Society* **2017,** *139*: p. 14399 - 14405.

[5]   Alili, A.S.; Siddiquee, M.N.; De Klerk, A. Origin of Free Radical Persistence in Asphaltenes: Cage Effect and Steric Protection. *Energy and Fuels* **2020**, *34*: p. 348 - 359.

[6]   Tannous, J.H.; Tulegenova, D.; De Klerk, A. Effect of Solvents on Persistent Free Radical Content in the Absence of Reactions. *Energy and Fuels* **2022**, *36*: p. 5253 - 5266.

[7]   Barry, J.T., Berg, D.J., Tyler, D.R. Radical Cage Effects: Comparison of Solvent Bulk Viscosity and Microviscosity in Predicting the Recombination Efficiencies of Radical Cage Pairs. *Journal of the American Chemical Society* **2016**, *138*: p. 9389 - 9392.

[8]   Yokono, T.; Obara, T.; Sanada, Y.; Shimomura, S.; Imamura, T. Characterization of Carbonization Reaction of Petroleum Residues by Means of High-Temperature ESR and Transferable Hydrogen. *Carbon* **1986**, *24*: p. 29 - 32.

[9]   Dappe, V.; Ben Tayeb, K.; Vezin, H.; Mariette, S.; Serve, O.; Livadaris, V. Effect of Thermal Treatment of Different Petroleum Fractions: Characterization by in situ EPR Spectroscopy. *Energy and Fuels* **2020**, *34*: p. 12026 - 12032.

[10]   Rudnick, L.R.; Tueting, D.R. Variation of Free Radical Concentration with Molecular Weight in Petroleum Feedstocks. *Fuel Science and Technology International* **1989**, *7*: p. 57 - 68.

[11]   Rudnick, L.R.; Tueting, D.R.; Sinclair, J.L. ESR Investigation Related to Carbonization Tendency. In: *Extended Abstracts of the 17th Biennial Conference on Carbon*, American Carbon Society: Lexington, KY, 1985, p. 403 - 404.

[12]   Altgelt, K.H.; Boduszynski, M.M. *Composition and Analysis of Heavy Petroleum Fractions*. Marcel Dekker: New York, NY, 1994.

[13]   Gutowski, H.S.; Ray, B.R.; Rutledge, R.L. Carbonaceous Free Radicals in Crude Petroleum. *Journal of Chemical Physics* **1958**, *28*: p. 744.

[14]   Yen, T.F.; Erdman, J.G.; Saraceno, A.J. Investigation of the Nature of Free Radicals in Petroleum Asphaltenes and Related Substances by Electron Spin Resonance. *Analytical Chemistry* **1962**, *34*: p. 694 - 700.

[15]   Bennett, J.E.; Ingram, D.J.; Tapley, J.G. Paramagnetic Resonance from Broken Carbon Bonds. *Journal of Chemical Physics* **1954**, *23*: p. 215.

[16]   Pastor, R.C.; Weil, J.A.; Brown, T.H.; Turkevich, J. Narrow Electron Spin Resonance in Charred Dextrose. *Physical Review* **1956**, *102*: p. 918 - 919.

[17]   Tannous, J.H.; De Klerk, A. Asphaltenes Formation during Thermal Conversion of Deasphalted Oil. *Fuel* **2019**, *255*: p. 115786.

[18]   Yan, Y.; Prado, G.H.C.; De Klerk, A. Storage Stability of Products from Visbreaking of Oilsands Bitumen. *Energy and Fuels* **2020**, *34*: p. 9585 - 9598.

[19]   Zhang, N.; Zhao, S.; Sun, X.; Xu, Z.; Xu, C. Storage Stability of the Visbreaking Product from Venezuela Heavy Oil. *Energy and Fuels* **2010**, *24*: p. 3970 - 3976.

[20]   Sivaramakrishnan, K.; De Klerk, A. Viscosity of Canadian Oilsands Bitumen and Its Modification by Thermal Conversion. In: *Chemistry Solutions to Challenges in the Petroleum Industry*, Rahimi, P., Ovalles, C., Zhang, Y., Adams, J.J., editor.; ACS Symposium, American Chemical Society: Washington, DC, 2019, p. 115 - 199.

[21]   Yañez Jaramillo, L.M.; de Klerk, A. Is Solubility Classification a Meaningful Measure in Thermal Conversion? *Energy & Fuels* **2022**, *36*: p. 8649 - 8662.

[22]   Yen, T.F.; Sprang, S.R. ESR g-Values of Bituminous Materials. In: *ACS Meeting, Petroleum Chemistry*, Chicago, IL, 1970, p. A65 - A76.

[23]   Scotti, R.; Montanari, L. Molecular Structure and Intermolecular Interaction of Asphaltenes by FT-IR, NMR and EPR. In: *Structures and Dynamics of Asphaltenes*, Mullins, O.C., et al., editor.; Springer Science + Business Media: New York, NY, 1998.

[24]   Halmenschlager, C.M.; Brar, M.; Apan, I.T., De Klerk, A. Hydrocracking Vacuum Gas Oil with Wax. *Catalysis Today* **2020**, *353*: p. 187 - 196.

[25]   Eaton, G.R.; Eaton, S.S.; Barr, D.P.; Weber, R.T. *Quantitative EPR*. Springer: New York, NY, 2010.

[26]   Poole, C.P. Electron Spin Resonance: A Comprenhensive Treatise in Experimental Techniques. Interscience Publishers: New York, NY, 1967.

[27]   Podgorski, D.C.; Corilo, Y.E.; Nyadong, L.; Lobodin, V.V.; Bythell, B.J.; Robbins, W.K.; McKenna, A.M.; Marshall, A.G.; Rodgers, R.P. Heavy Petroleum Composition. 5. Compositional and Structural Continuum of Petroleum Revealed. *Energy and Fuels* **2013**, *27*: p. 1268 - 1276.

[28]   *ASTM D3279: Standard Test Method for n-Heptane Insolubles*. ASTM International: West Conshohocken, PA, 2019.

[29]   *ASTM D6560: Standard Test Method for Determination of Asphaltenes (Heptane Insolubles) in Crude Petroleum and Petroleum Products*. ASTM International: West Conshohocken, PA, 2022.

[30]   *ASTM D893: Standard Test Method for Insolubles in Used Lubricating Oils.* ASTM International: West Conshohocken, PA, 2018.

[31]   *ASTM D4124: Standard Test Method for Separation of Asphalt into Four Fractions*. ASTM International: West Conshohocken, PA, 2018.

[32]   *ASTM D2007: Standard Test Method for Characteristic Groups in Rubber Extender and Processing Oils and Other Petroleum-Derived Oils by the Clay-Gel Absorption Chromatographic Method*. ASTM International: West Conshohocken, PA, 2020.

[33]   Ramirez-Corredores, M.M. *The Science and Technology of Unconventional Oils*. Academic Press: London, UK, 2017.

[34]   McKenna, A.M.; Chacón-Patino, M.L.; Weisbrod, C.R.; Blakney, G.T.; Rodgers, R.P. Molecular-Level Characterization of Asphaltenes Isolated from Distillation Cuts. *Energy and Fuels* **2019**, *33*, p. 2018 - 2029.

[35]   Acevedo, S.; Gutierrez, L.B.; Negrin, G.; Pereira, J.C. Molecular Weight of Petroleum Asphaltenes: A Comparison between Mass Spectrometry and Vapor Pressure Osmometry. *Energy and Fuels* **2005**, *19*: p. 1548 - 1560.

[36]   Pomerantz, A.E.; Hammond, M.R.; Morrow, A.L.; Mullins, O.C.; Zare, R.N. Asphaltene Molecular-Mass Distribution Determined by Two-Step Laser Mass Spectrometry. *Energy and Fuels* **2009**, *23*: p. 1162 - 1168.

[37]   Pomerantz, A.E.; Hammond, M.R.; Morrow, A.L.; Mullins, O.C.; Zare, R.N. Two-Step Laser Mass Spectrometry of Asphaltenes. *Journal of the American Chemical Society* **2008**, *130*: p. 7216 - 7217.

[38]   Tanaka, R.; Sato, S.; Takanohashi, T.; Hunt, J.E.; Winans, R. Analysis of the Molecular Weight Distribution of Petroleum Asphaltenes Using Laser Desorption-Mass Spectrometry. *Energy and Fuels* **2004**, *18*: p. 1405 - 1413.

[39]   Hayes, M.H.B.; Stacey, M.; Standley, J. Studies on Bitumen: Part 1. Characterization of Bitumen by Use of Physical Methods. *Fuel* **1972**, *51*: p. 27 - 31.

[40]   Boduszynski, M.M. Composition of Heavy Petroleums. 1. Molecular Weight, Hydrogen Deficiency, and Heteroatom Concentration as a Function of Atmospheric Equivalent Boiling Point up to 1400 ºF (760 ºC). *Energy and Fuels* **1987**, *1*: p. 2 - 11.

[41]   Acevedo, S.; Méndez, B.; Rojas, A.; Layrisse, I.; Rivas, H. Asphaltenes and Resins from the Orinoco Basin. *Fuel* **1985**, *64*: p. 1741 - 1747.

[42]   Becker, C.; Qian, K.; Russell, D.H. Molecular Weight Distributions of Asphaltenes and Deasphaltened Oils Studied by Laser Desorption Ionization and Ion Mobility Mass Spectrometry. *Analytical Chemistry* **2008**, *80*: p. 8592 - 8597.

[43]   Adams, J.Q.; Altgelt, K.H.; LeTourneau, R.L.; Lindeman, L.P. Free Radical Concentrations in Gel Permeation Fraction of Asphaltenes from Different Crude Oils. In: *Symposium on Characterization and Processing of Heavy Ends of Petroleum, Division of Petroleum Chemistry*, American Chemical Society: Pittsburgh, PA 1966, p. B140 - B144.

[44]   Zhang, Y.; Siskin, M.; Gray, M.R.; Walters, C.C.; Rodgers, R.P. Mechanisms of Asphaltene Aggregation: Puzzles and a New Hypothesis. *Energy and Fuels* **2020**, *34*: p. 9094 - 9107.

[45]   Andersen, S.I. Effect of Precipitation Temperature on the Composition of n-Heptane Asphaltenes. *Fuel Science and Technology International* **1994,** *12*: p. 51 - 74.

[46]   Chacón-Patiño, M.L.; Gray, M.R.; Rüger, C.; Smith, D.F.; Glattke, T.J.; Niles, S.F.; Neumann, A.; Weisbrod, C.R.; Yen, A.; McKenna, A.M.; Giusti, P.; Bouyssiere, B.; Barrere-Mangote, C.;Yarranton, H.; Hendrickson, C.L.; Marshall, A.G.; Rodgers, R.P. Lessons Learned from a Decade-Long Assessment of Asphaltenes by Ultrahigh-Resolution Mass Spectrometry and Implications for Complex Mixture Analysis. *Energy and Fuels* **2021**, *35*: p. 16335 - 16376.

[47]   Kaiser, M.J.; de Klerk, A.; Gary, J.H.; Handwerk G.E. *Petroleum refining: technology, economics, and markets*. Sixth edit. CRC Press: Boca Raton, FL, 2020.

[48]   Turuga, A.S.S. Effect of Solvent Deasphalting Process on the Properties of Deasphalted Oil and Asphaltenes from Bitumen. MSc Thesis, University of Alberta, 2017.

[49]   Wang, L.; Zachariah, A.; Yang, S.; Prasad, V.; De Klerk, A. Visbreaking Oilsands-Derived Bitumen in the Temperature Range of 340−400 °C. *Energy and Fuels* **2014**, *28*: p. 5014 - 5022.

[50]   Yañez Jaramillo, L.M. Visbreaking of Oilsands Bitumen between 150 and 300 ºC. MSc Thesis, University of Alberta, 2016.

[51]   Watson, K.M.; Nelson, E.F. Improved Methods for Approximating Critical and Thermal Properties of Petroleum Fractions. *Industrial and Engineering Chemistry* **1933**, *25*: p. 880 - 887.

[52]   Riazi, M.R. *Characterization and Properties of Petroleum Fractions*. ASTM International: West Conshohocken, PA, 2005.

[53]   Rivolta, A.A. Molar Refractivity and Oxygen Solubility. MSc Thesis, University of Alberta, 2020.

[54]   Uebersfeld, J.; Etienne, A.; Combrisson, J. Paramagnetic Resonance, a New Property of Coal-like Materials. *Nature* **1954**, *174*: p. 614.

[55]   Retcofsky, H.L., Hough, M.R., Maguire, M.M., Clarkson, R.B. Nature of the Free Radicals in Coals, Pyrolyzed Coals, Solvent-Refined Coal, and Coal Liquefaction Products. In: *Coal Structure*, Gorbaty and Ouchi., editor.; Advances, American Chemical Society: Washington, D.C., 1981.

[56]   Ingram, D.J.; Tapley, J.G.; Jackson, R.; Bond, R.L.; Murnaghan, A.R. Paramagnetic Resonance in Carbonaceous Solids. *Nature* **1954**, *174*: p. 797 - 798.

8. Conclusions

8.1. Introduction

The objective of the work presented in this thesis was to better understand the change in bitumen and bitumen-related materials as consequence of thermal conversion from the perspective of the change in the nature of the species. To place the conclusions in context, current thinking about coke formation during thermal conversion is summarized before presenting the conclusions.

The formation of undesirable carbonaceous materials (coke) during upgrading processes, specifically but not limited to thermal conversion, can affect the proper unit operation due to fouling (defined as deposition or scaling [1]). In the case of visbreaking, the conversion (often referred to as the amount of converted material from a heavy distillation fraction) is limited by the coke formation. The study therefore has practical application.

To provide context for the conclusions from this study, it is useful to summarize the concepts in literature that are at the core of the description of coke formation.

The development of coke has been described as a process in which planar aromatic structures stack and form sphere-shaped materials that will grow within the liquid phase to become an ordered liquid (mesophase) and eventually precipitate [2-4]. The formation of the mesophase and the formation of coke result from reactions taking place during thermal conversion [5]. As free radical reactions occur, aromatic molecules required for coke to develop are formed [6]. However, the formation of coke has also been explained as the result of asphaltenes association as thermal conversion progresses. In this case, asphaltenes are considered as coke precursors [7-10] and the formation of coke is explained by self-association. This leads to formation of aggregates and eventually to phase separation, resulting in coke formation [9]. These two descriptions are not mutually exclusive but have a different emphasis and a different sequence of events leading to coke, namely, (i) aromatization leading to phase separation as mesophase, as opposed to (ii) asphaltenes causing phase separation leading to an increase in aromatics.

Aspects of the above mentioned two descriptions to explain coke formation were challenged.

This thesis investigated unconverted materials and used the results as baseline for changes in aromaticity, solubility classification and free radical concentration of thermally converted products. The major conclusions and findings are presented in the next section.

8.2. Major conclusions and significance

The formation of aromatics during thermal conversion is one potential pathway to the formation of coke. The change in aromatic carbon content as result of thermal conversion could be obtained through ^{13}C Nuclear Magnetic Resonance (NMR). However, since this analysis is time intensive, ^{1}H NMR can be used instead in conjunction with correlation developed by Cookson et al. [11] (derived from Brown and Ladner [12]) to estimate aromatic carbon content in fossil fuels. The ^{1}H NMR is also useful for tracking these changes by studying variations in the types of hydrogen (e.g., aromatic) concentration as hydrogen transfer reactions take place. During hydrogen transfer some species will get hydrogen enriched whereas other species will be hydrogen depleted (e.g., aromatic), allowing one to infer to some information about the associated changes in the nature of the carbon (e.g., aliphatic to aromatic nature).

This work concluded that for bitumen and bitumen-derived systems, the relationship between aromatic carbon content (C_{Ar}) and aromatic hydrogen content (H_{Ar}) as given by Cookson et al. [11] applies poorly. In other words, estimating aromatic carbon content from aromatic hydrogen content can be inaccurate. Additionally, the results in thermally converted products of bitumen and bitumen-related systems did not show a fixed relationship between the aromatic carbon content and the aromatic hydrogen content.

The changes in aromatic hydrogen content do not necessarily describe the changes in aromatic carbon content after visbreaking; in fact, the changes in the nature of both hydrogen and carbon are not monotonic. While this corroborated the findings of previous work (e.g., [14,15]) about the occurrence of both hydrogen and methyl transfer reactions during thermal conversion, it also

implied that the typical description of hydrogen transfer leading to aromatics formation is an oversimplification.

Furthermore, the formation of aromatic structures as an early step of coke formation would imply an increase in the aromaticity of the visbroken products with an increase in the amount of coke. In contrast, it was found that the aromatic carbon and coke content of the thermally converted products only had a weak relationship. This does not provide evidence of the absence of a relationship between the coke and the aromatic carbon content, but it suggests that aromaticity changes might not be an adequate description for coke formation.

The formation and aggregation of asphaltenes during thermal conversion was another potential pathway to coke. This explanation suggests an increase in the degree of insolubility as both asphaltenes and coke can be described in terms of their insolubility in a solvent, n-heptane for asphaltenes and carbon disulfide for coke in this study. Wiehe's model [9,13] [9,13] presents asphaltenes as an intermediate step for coke formation. Contrary to the usually accepted notion in the literature (i.e., Wiehe's model), the results of this thesis showed that coke formation (defined as CS_2 insolubles) was unrelated to the amount of asphaltenes (n-heptane insolubles) present in the feed or change after reaction. More importantly, it did not provide evidence for asphaltenes as a required intermediate step for coke formation in thermal conversion.

This raised the question whether a solubility class could be used as a descriptor for the changes that take place during thermal conversion. For instance, asphaltenes are often associated with heavier species such as multinuclear aromatic cores, hence an increase in n-heptane insoluble (i.e., asphaltenes) might reflect an increase in the aromatic carbon content (aromaticity). Contrary to what was expected, asphaltenes and aromaticity only showed a poor relationship.

The lack of asphaltene's relationships with macroscopic properties, with the exception of free radical content and refractive index, shows that solubility classification is not a good descriptor for the reaction progress as it is unable to provide information about the reaction chemistry taking place during thermal conversion that leads to coke formation. More importantly, the two pathways (i.e., mesophase formation and asphaltenes) described in the literature to explain coke formation

were evaluated after a thermal conversion process in bitumen and bitumen-related products. The findings of this work did not show a strong relationship between coke formation and either aromaticity or asphaltene content, suggesting that neither of them are necessary steps in their respective pathways for coke formation. This has direct implications in the understanding of processes leading to coke as it will impact the modelling of thermal conversion reactions. The results of this work highlighted potential misconceptions within this field, providing a different perspective within this field. In addition, this Ph.D. study provides a different perspective about coke formation and suggests that the aromatic carbon and asphaltenes content are inadequate descriptors for the process of coke formation during thermal conversion.

8.3. Minor conclusions and significance

Although the main objective of this work was related to provide a better understanding about the nature of the changes that species undergo during thermal conversion, and more specifically with the pathways to coke formation, a few aspects related to the thermal conversion of bitumen and bitumen-related systems were explored.

The first aspect relates to the removal of water from a SAGD emulsion to obtain the bitumen used in this study and the estimation of water content in the emulsion and the resulted bitumen. The strength of the emulsion was such that centrifugation was inefficient and the analyses that could be affected by mass transport, such as thermogravimetric analysis, experienced a delayed release of water under dynamic heating conditions. Water could only effectively be removed when the removal rate was low, for example, 99 % of the water in the emulsion could be removed by rotary evaporation at 110 ºC and 400 mbar for 82 hours.

The second aspect is related to the postulate that free radical concentration in straight run petroleum materials (i.e., unconverted) may be consistent with the composition continuum proposed by Boduszynski as free radical content monotonously increases with molecular weight. Despite an indication that this may be the case, the evidence was insufficient to draw a conclusion. The fractionation of additional bitumen samples to which free radical content is determined could provide the necessary evidence to conclude about an agreement of free radicals with the

compositional continuum. This work has opened the possibility to not only address some of the hypotheses postulated in this work but also evaluate the role of free radicals in coke formation during thermal conversion.

8.4. Recommended future work

8.4.1. Characteristics of carbon disulfide insoluble

The formation of coke described via mesophase is described in terms of the formation of a sphere-like structure that coalesces and grows (mesophase) until it is not able to remain in the solution. Based on this definition, the resulting solid material (coke) should appear as round shaped solids. However, coke material from thermal conversion in this study had sharp edges rather than the sphere-like shape. This observation is in complete disagreement with the mesophase description of coke formation. It suggests that coke formed during the onset of coking in thermal conversion, formed through a different mechanism other than via mesophase.

To understand this process, it is required to consider two aspects:

a. Physical: The morphology of coke has been studied previously in the literature, particularly from delayed coking [16,17]. Two types of structure have been commonly referred to as shot coke (fine-grained mosaic) and sponge coke (optical texture domains). In both cases these coke products are products from prolonged and severe thermal conversion and not coke formed during the initial stages at the onset of coking.

b. Chemical: During thermal conversion, the feed material will undergo changes that could be tracked (e.g., aromatic carbon content), the same can be applied to the resulted coke. The composition of coke at the onset of coking is likely different to coke from prolonged and severe thermal conversion.

Feed composition and reaction severity [18,19] have been reported in the literature as affecting factors for coke's morphology. While the morphology of coke gives optical information (physical aspect) about the processes that led to coke (e.g., mesophase), the chemical properties of the resulted coke will provide insights about the molecules involved (e.g., heteroatom-containing molecules). In the context of bitumen and bitumen-related materials, this can be studied by focusing on the resulted coke of thermal conversion reactions performed using different feed materials (e.g., the feeds used in this study) at different reaction severities (e.g., different reaction temperatures and reaction times). The morphological study of coke can be completed by analyzing the resultant coke samples using polarized light optical microscopy and scanning electron microscopy (SEM). On the other hand, chemical characteristics of coke can be determined by analyzing the samples with ^{1}H and ^{13}C NMR, elemental analysis (CHNS), and Fourier-Transformed Infrared (FTIR) microscope.

The findings resulting from this type of investigation could offer a more complete overview about the changes that took place during thermal conversion. In addition, it will provide information to help elucidate the mechanism involved at the onset of coke formation.

8.4.2. *Relationship between free radical concentration and other compositional properties in straight-run materials*

Although the foundations for this work have been established, it is necessary to answer the question whether the free radical concentration in a sample is only dependent on the boiling point distribution or if other compositional properties play a role. The limited available amount of data and the limitations of the technique to provide comparable results within studies, makes this task more complicated. However, the answer to this question could provide answers in regard to the characteristics of the compounds associated to the free radical content and potentially the chemistry involving these radical species.

To evaluate whether the free radical concentration in straight-run materials is exclusively dependent in boiling point distribution, samples of comparable crude oils (i.e., similar distillation

profile and/or molar refractivity) should be analyzed to quantify the free radical concentration. After analyzing the samples, two outcomes are possible:

a. The free radical content is the same for all the comparable oils. Therefore, free radical concentration is only dependent on the boiling point distribution;

b. The free radical content is different for all the comparable oils. This would be an indication that there are other compositional properties involved in the relationship between free radical concentration and molecular weight. Some compositional properties to be considered are heteroatom content (nitrogen, sulfur and oxygen), aromatic carbon content, and H/C ratio.

The development of a correlation involving the boiling point distribution could provide significant practical advantages for estimating the free radical content.

8.4.3. *Relationship between free radical concentration and solubility classification*

Asphaltenes were shown to have a high concentration of free radical species in comparison with other solubility classes, i.e., maltenes [20]. In addition, the work of Yan et al. [21] as well as this thesis, provided evidence about an apparent relationship between free radical content and asphaltene content. However, the causality of this relationship is yet to be established.

To test the causality of this relationship, it should be determined whether asphaltenes follow the compositional continuum (i.e., molecular weight distribution). To achieve this, different asphaltene samples can be fractionated and the average molecular weight of each fraction determined. If asphaltenes agree with the compositional continuum and the answer to **Section 8.4.2** is that free radical concentration is only dependent on the boiling point distribution, then it could be speculated that the relationship between free radical content and asphaltene concentration is a consequence of the boiling point distribution. On the contrary, if there is no agreement between asphaltenes and the compositional continuum, the nature of this relationship may be related to other compositional

properties. Similar to what was done by Adams et al. [22], the free radical content should be estimated for each of the individual asphaltenes fractions.

This is of importance as it will provide a better understanding about the role of asphaltenes, a solubility class, in many reaction processes taking place in thermal conversion. Additionally, it could open a new line of questioning in regard to whether the solubility classification could impact the dynamic equilibrium of free radicals in bitumen.

References

[1]   Speight, J.G. *Fouling in Refineries*. Gulf Professional Publishing: Amsterdam, Netherlands, 2015.

[2]   Hurt, R.H.; Hu, Y. Thermodynamics of Carbonaceous Mesophase. *Carbon* **1999**, *37*: p. 281 - 292.

[3]   Marsh, H.; Walker, P.L. The Formation of Graphitizable Carbons via Mesophase: Chemical and Kinetic considerations. *Chemistry and Physics of Carbon* **1979**, *15*: p. 230 - 286.

[4]   Santamaría-Ramírez, R.; Romero-Palazón, E.; Gómez-de-Salazar, C.; Rodríguez-Reinoso, F.; Martínez-Saez, S.; Martínez-Escandell, M.; Marsh, H. Influence of Pressure Variations on the Formation and Development of Mesophase in a Petroleum Residue. *Carbon* **1999**, *37*: p. 445 - 455.

[5]   Greinke, R.A. Quantitative Influence of Dealkylation and Polymerization Reactions on Mesophase Formation. *Carbon* **1990**, *28*: p. 701 - 706.

[6]   Singer, L.S.; Lewis, I.C.; Greinke, R.A. Characterization of the Phases in Centrifuged Mesophase Pitches. *Molecular Crystals and Liquid Crystals* **1986**, *132*: p. 65 - 79.

[7]   Rahimi, P.; Gentzis, T.; Dawson, W.H.; Fairbridge, C.; Khulbe, C.; Chung, K.; Nowlan, V.; DelBianco, A. Investigation of Coking Propensity of Narrow Cut Fractions from Athabasca Bitumen using Hot-Stage Microscopy. *Energy and Fuels* **1998**, *12*: p. 1020 - 1030.

[8]   Rahimi, P.; Gentzis, T.; Taylor, E.; Carson, D.; Nowlan, V.; Cotté, E. The Impact of Cut Point on the Processability of Athabasca Bitumen. *Fuel* **2001**, *80*: p. 1147 - 1154.

[9]   Wiehe, I. A. A Solvent-Resid Phase Diagram for Tracking Resid Conversion. *Industrial and Engineering Chemistry Research* **1992**, *31*: p. 530 - 536.

[10]   Wiehe, I.A.; Kennedy, R.J. Oil compatibility model and crude oil incompatibility. *Energy and Fuels* **2000**, *14*: p. 56 - 59.

[11]   Cookson, D.J.; Lloyd, C.O.; Smith B. E. A Novel Semi-Empirical Relationship between Aromaticities Measured from ^{1}H and [13]C N.M.R. Spectra. *Fuel* **1986**, *65*: p. 1247 - 1253.

[12]   Brown, J.K., Ladner, W.R. A Study of the Hydrogen Distribution in Coal-like Materials by High-resolution Nuclear Magnetic Resonance Spectroscopy. II - A Comparison with Infra-red Measurement and the Conversion to Carbon Structure. *Fuel* **1967**, *39*: p. 87 - 96.

[13]   Wiehe, I. A. *Process Chemistry of Petroleum Macromolecules.* CRC Press: Boca Raton, FL, 2008.

[14]   Barrera, D. M.; Ortiz, D. P.; Yarranton, H. W. Molecular Weight and Density Distributions of Asphaltenes from Crude Oils. *Energy and Fuels* **2013**, *27*: p. 2474 - 2487.

[14]   Zachariah, A.; Wang, L.; Yang, S.; Prasad, V.; De Klerk, A. Suppression of Coke Formation during Bitumen Pyrolysis. *Energy and Fuels* **2013,** *27*: p. 3061 - 3070.

[15]   Tannous, J.H.; De Klerk, A. Methyl and Hydrogen Transfer in Free Radical Reactions. *Energy and Fuels* **2020**, *34*: p. 1698 - 1709.

[16]   Siskin, M.; Kelemen, S.R.; Gorbaty, M.L.; Ferrughelli, D.T.; Brown, L.D.; Eppig, C.P.; Kennedy, R.J. Chemical Approach to Control Morphology of Coke Produced in Delayed Coking. *Energy and Fuels* **2006**, *20*: p. 2117 - 2124.

[17]   Ovalles, C.; Rogel, E.; Hajdu, P.; Rea, T.; Chaudhuri, K.; Hench, K.; Cuspar, D.; Moir, M.E. Predicting Coke Morphology in Delayed Coking from Feed Characteristics. *Fuel* **2020**, *263*: p. 116739.

[18]   Legin-Kolar, M.; Ugarkovic, D. Petroleum Coke Structure: Influence of Feedstock Composition. *Carbon* **2000**, *31*: p. 383 - 390.

[19]   Picón-Hernández, H.J.; Centeno-Hurtado, A.; Pantoja-Agreda, E.F. Morphological Classification of Coke formed from the Castilla and Jazmín Crude Oils. *CT & F - Ciencia, Tecnologia y Futuro* **2008**, *3*: p. 169 - 183.

[20]   Tannous, J. H.; De Klerk, A. Quantification of the Free Radical Content of Oilsands Bitumen Fractions. *Energy and Fuels* **2019**, *33*: p. 7083 - 7093.

[21]   Yan, Y.; Prado, G.H.C.; De Klerk, A. Storage Stability of Products from Visbreaking of Oilsands Bitumen. *Energy and Fuels* **2020**, *34*: p. 9585 - 9598.

[22]   Adams, J.Q.; Altgelt, K.H.; LeTourneau, R.L.; Lindeman, L.P. Free Radical Concentrations in Gel Permeation Fraction of Asphaltenes from Different Crude Oils. In: *Symposium on Characterization and Processing of Heavy Ends of Petroleum, Division of Petroleum Chemistry*, American Chemical Society: Pittsburgh, PA 1966, p. B140 - B144.

Bibliography

Acevedo, S.; Gutierrez, L.B.; Negrin, G.; Pereira, J.C. Molecular Weight of Petroleum Asphaltenes: A Comparison between Mass Spectrometry and Vapor Pressure Osmometry. *Energy and Fuels* **2005**, *19*: p. 1548 – 1560.

Acevedo, S.; Mendez, B.; Rojas, A.; Layrisse, I.; Rivas, H. Asphaltenes and Resins from the Orinoco Basin. *Fuel* **1985**, *64*: p. 1741 - 1747.

Acevedo, S.; Méndez, B.; Rojas, A.; Layrisse, I.; Rivas, H. Asphaltenes and Resins from the Orinoco Basin. *Fuel* **1985**, *64*: p. 1741 – 1747.

Acree, W.E. Jr.; Chickos, J.S. Phase Transition Enthalpy Measurements of Organic and Organometallic Compounds. In: *NIST Chemistry WebBook, NIST Standard Reference Database Number 69*, Linstrom, P.J.; Mallard, W.G., editor.; National Institute of Standards and Technology: Gaithersburg, MD,

Adams, J.Q.; Altgelt, K.H.; LeTourneau, R.L.; Lindeman, L.P. Free Radical Concentrations in Gel Permeation Fraction of Asphaltenes from Different Crude Oils. In: *Symposium on Characterization and Processing of Heavy Ends of Petroleum, Division of Petroleum Chemistry*, American Chemical Society: Pittsburgh, PA 1966, p. B140 – B144.

Adesanwo, T.; Rahman, M.; Gupta, R.; De Klerk A. Characterization and Refining Pathways of Straight-Run Heavy Naphtha and Distillate from the Solvent Extraction of Lignite. *Energy and Fuels* **2014**, *28*: p. 4486 – 4495.

Albahlani, A.M., Babadagli, T. A Critical Review of the Status of SAGD: Where Are We and What Is Next? In: *SPE Western Regional and Pacific Section AAPG Joint Meeting*, Bakersfield, CA, March 29 – April 2, 2008; p. SPE 113283.

Alboudwarej, H.; Akbarzadeh, K.; Beck, J.; Svrcek, W.Y.; Yarranton, H.W. Regular Solution Model for Asphaltene Precipitation from Bitumens and Solvents. *AIChE Journal* **2003**, *49*: p. 2948 - 2956.

Alboudwarej, H.; Beck, J.; Svrcek, W. Y.; Yarranton, H. W. Sensitivity of Asphaltene Properties to Separation Techniques. *Energy and Fuels* **2002**, *16*: p. 462 - 469.

Ali, F.; Khan, Z.H.; Ghaloum, N. Structural Studies of Vacuum Gas Oil Distillate Fractions of Kuwaiti Crude Oil by Nuclear Magnetic Resonance. *Energy and Fuels* **2004**, *18*: p. 1798 - 1805.

Alili, A.S.; Siddiquee, M.N.; De Klerk, A. Origin of Free Radical Persistence in Asphaltenes: Cage Effect and Steric Protection. *Energy and Fuels* **2020**, *34*: p. 348 - 359.

Altgelt, K.H.; Boduszynski, M.M. *Composition and Analysis of Heavy Petroleum Fractions*. Marcel Dekker: New York, NY, 1994.

Ancheyta Juárez, J. *Modeling of processes and reactors for upgrading of heavy petroleum*. CRC Press: Boca Raton, FL, 2013.

Ancheyta Juárez, J.; Speight, J.G. *Hydroprocessing of Heavy Oils and Residua*. CRC Press: Boca Raton, FL, 2007.

Ancheyta Juárez, J.; Trejo, F.; Rana, M.S. *Asphaltenes: Chemical Transformation during Hydroprocessing of Heavy Oils*. CRC Press: Boca Raton, FL, 2009.

Andersen, S.I. Effect of Precipitation Temperature on the Composition of n-Heptane Asphaltenes. *Fuel Science and Technology International* **1994,** *12*: p. 51 - 74.

Andersen, S. I.; Stenby, E. H. Thermodynamics of Asphaltene Precipitation and Dissolution Investigation of Temperature and Solvent Effects. *International Journal of Petroleum Science and Technology* **1996**, *14*: p. 261 - 287.

Andersen, S. I.; Lindeloff, N.; Stenby, E. H. Investigation of Asphaltenes Precipitation at Elevated Temperature. *Petroleum Science and Technology* **1998**, *16*: p. 323 - 334.

Angle, C. W.; Long, Y.; Hamza, H.; Lue, L. Precipitation of Asphaltenes from Solvent-Diluted Heavy Oil and Thermodynamic Properties of Solvent-Diluted Heavy Oil Solutions. *Fuel* **2006**, *85*: p. 492 - 506.

Ansari, S., Sabbagh, R., Yusuf, Y., Nobes, D.S. The Role of Emulsions in Steam-Assisted-Gravity-Drainage (SAGD) Oil Production Process: A Review. *SPE Journal*, **2020**, *25*: p. 969 - 989.

Aranberri, I.; Beverly, K.J.; Binks, B.P.; Clint, J.H.; Fletcher, P.D.I. How Do Emulsions Evaporate? *Langmuir* **2002**, *18*: p. 3471 - 3475.

Asphaltenes, Heavy Oils, and Petroleomics; Mullins, O. C., Sheu, E. Y., Hammami, A., Marshall, A. G. Eds.; Springer: New York, 2010.

Asphaltenes. Fundamentals and Applications; Sheu, E. Y., Mullins, O. C. Eds.; Plenum Press: New York, 1995.

ASTM D2007: Standard Test Method for Characteristic Groups in Rubber Extender and Processing Oils and Other Petroleum-Derived Oils by the Clay-Gel Absorption Chromatographic Method. ASTM International: West Conshohocken, PA, 2020.

ASTM D3279: Standard Test Method for n-Heptane Insolubles, ASTM International: West Conshohocken, PA, 2019.

ASTM D3279: Standard Test Method for n-Heptane Insolubles. ASTM International: West Conshohocken, PA, 2019.

ASTM D4124, Standard Test Method for Separation of Asphalt into Four Fractions. ASTM International: West Conshohocken, PA, 2018.

ASTM D4124: Standard Test Method for Separation of Asphalt into Four Fractions. ASTM International: West Conshohocken, PA, 2018.

ASTM D6560: Standard Test Method for Determination of Asphaltenes (Heptane Insolubles) in Crude Petroleum and Petroleum Products. ASTM International: West Conshohocken, PA, 2022.

ASTM D7169: Standard test method for boiling point distribution of samples with residues such as crude oils and atmospheric and vacuum residues by high temperature gas chromatography; ASTM International: West Conshohocken, PA, 2020.

ASTM D721: Standard Test Method for Oil Content of Petroleum Waxes. ASTM International: West Conshohocken, PA, 2017.

ASTM D893: Standard Test Method for Insolubles in Used Lubricating Oils. ASTM International: West Conshohocken, PA, 2018.

ASTM E1131: Standard Test Method for Compositional Analysis by Thermogravimetry. ASTM International. West Conshohocken, PA, 2020.

ASTM E203: Standard Test Method for Water Using Volumetric Karl Fischer Titration. ASTM International. West Conshohocken, PA 2018.

Awadalla, A.A.; Cookson, D.J.; Smith, B.E. Coal Hydrogenation: Quality of Start-up Solvents and Partially Process-derived Recycle Solvents. *Fuel* **1985**, *64*: p. 1097 - 1107.

Bake, K. D.; Craddock, P. R.; Bolin, T. B.; Abdallah, W.; Mitra-Kirtley, S.; Andrews, A. B.; Mullins, O. C.; Pomerantz, A. E. Structure-Solubility Relationships in Coal, Petroleum, and Immature Source-Rock-Derived Asphaltenes. *Energy and Fuels* **2020**, *34*: p. 10825 - 10836.

Barrera, D. M.; Ortiz, D. P.; Yarranton, H. W. Molecular Weight and Density Distributions of Asphaltenes from Crude Oils. *Energy and Fuels* **2013**, *27*: p. 2474 - 2487.

Barry, J.T., Berg, D.J., Tyler, D.R. Radical Cage Effects: Comparison of Solvent Bulk Viscosity and Microviscosity in Predicting the Recombination Efficiencies of Radical Cage Pairs. *Journal of the American Chemical Society* **2016**, *138*: p. 9389 - 9392.

Barry, J.T.; Berg, D.J.; Tyler, D.R. Radical Cage Effects: The Prediction of Radical Cage Pair Recombination Efficiencies Using Microviscosity Across a Range of Solvent Types. *Journal of the American Chemical Society* **2017,** *139*: p. 14399 - 14405.

Bartle, K.D.; Martin, T.G.; Williams, D.F. Chemical Nature of a Supercritical-Gas Extract of Coal at 350 ºC. *Fuel* **1975**, *54*, p. 226 - 235.

Beck, J.; Svrcek, W. Y.; Yarranton, H. W. Hysteresis in Asphaltene Precipitation and Redissolution. *Energy and Fuels* **2005**, *19*: p. 944 - 947.

Becker, C.; Qian, K.; Russell, D.H. Molecular Weight Distributions of Asphaltenes and Deasphaltened Oils Studied by Laser Desorption Ionization and Ion Mobility Mass Spectrometry. *Analytical Chemistry* **2008**, *80*: p. 8592 - 8597.

Bennett, J.E.; Ingram, D.J.; Tapley, J.G. Paramagnetic Resonance from Broken Carbon Bonds. *Journal of Chemical Physics* **1954**, *23*: p. 215.

Billaud, F.; Chaverot, P.; Berthelin, M.; Freund, E. Thermal Decomposition of Aromatics Substituted by a Long Aliphatic Chain. *Industrial and Engineering Chemistry Research* **1988**, *27*: p. 1529 - 1536.

Bitumen, Asphalts and Tar Sands. Chilingarian, G.V.; Yen, T.F., Eds.; Elsevier Scientific Publishing Company: Amsterdam, Netherlands,1978.

Bjorøy, Ø.; Fotland, P.; Gilje, E.; Høiland, H. Asphaltene Precipitation from Athabasca Bitumen using an Aromatic Diluent: A Comparison to Standard *n*-Alkane Liquid Precipitants at Different Temperatures. *Energy and Fuels* **2012**, *26*: p. 2648 - 2654.

Boduszynski, M.M. Composition of Heavy Petroleums. 1. Molecular Weight, Hydrogen Deficiency, and Heteroatom Concentration as a Function of Atmospheric Equivalent Boiling Point up to 1400 ºF (760 ºC). *Energy and Fuels* **1987**, *1*: p. 2 - 11.

Brauch, R.; Fainberg, V.; Kalchouck, H.; Hetsroni, G. Correlations between Properties of Various Feedstocks and Products of Visbreaking. *Fuel Science and Technology International* **1996**, *14*: p. 753 - 765.

Brezonik, P.L.; Arnold, W.L. *Water Chemistry: An Introduction to the Chemistry of Natural and Engineered Aquatic Systems*. Oxford University Press: Oxford, UK, 2011.

Brooks, J. D.; Taylor, G.H. The Formation of some Graphitizing Carbons. *Chemistry and Physics of Carbon* **1969**, *4*: p. 243 - 286.

Brooks, J.D.; Taylor, G.H. The Formation of Graphitizing Carbons from the Liquid Phase. *Carbon* **1965**, *3*: p. 185 - 193.

Brown, J.K., Ladner, W.R. A Study of the Hydrogen Distribution in Coal-like Materials by High-resolution Nuclear Magnetic Resonance Spectroscopy. II - A Comparison with Infra-red Measurement and the Conversion to Carbon Structure. *Fuel* **1967**, *39*: p. 87 - 96.

Bruttel, P.; Schlink, R. *Water Determination by Karl Fischer Titration*. Herisan, Switzerland, 2006.

Buckley, J. S. Predicting the Onset of Asphaltene Precipitation from Refractive Index Measurements. *Energy and Fuels* **1999**, *13*: p. 328 - 332.

Buckley, J. S.; Hirasaki, G. J.; Liu, Y.; Von Drasek, S.; Wang, J-X., Gill, B. S. Asphaltene Precipitation and Solvent Properties of Crude Oils. *Petroleum Science and Technology* **1998**, *16*: p. 251 - 285.

Bunger, J.W.; Thomas, K.P.; Dorrence, S.M. Compounds Types and Properties of Utah and Athabasca Tar Sand Bitumens. *Fuel* **1979**, *58*: p. 183 -195.

Butler, R.M. SAGD Comes of Age! *Journal of Canadian Petroleum Technology* **1998**, *37*: p. 9 - 12.

Butler, R.M., Stephens, D.J. The Gravity Drainage of Steam-Heated Heavy Oil to Parallel Horizontal Wells. *Journal of Canadian Petroleum Technology* **1981**, *April-June*, p. 90 - 96.

Canadian Association of Petroleum Producers. Uses for Oil. https://www.capp.ca/oil/uses-for-oil/ (accessed March 23, 2021).

Carbognani, L.; Lubkowitz, J.; Gonzalez, M.F.; Pereira-Almao, P. High Temperature Simulated Distillation of Athabasca Vacuum Residue Fractions. Bimodal Distributions and Evidence for Secondary "On-Column" Cracking of Heavy Hydrocarbons. *Energy and Fuels* **2007**, *21*: p. 2831 - 2839.

Carbognani, L.; Roa-Fuentes, L.C.; Diaz, L.; Berezinski, J.; Carbognani-Arambarri, L.; Pereira-Almao, P. Reliable Determination of Water Contents of Bitumen and Vacuum Residua via Coulometric Karl Fischer Titration using Tetrahydrofuran. *Petroleum Science and Technology* **2014**, *32*: p. 602 - 609

Castellanos Diaz, O.; Yarranton, H. W. Applicability of Simulated Distillation for Heavy Oils. *Energy and Fuels* **2019**, *33*: p. 6083 - 6087.

Castillo, J.; de Klerk, A. Visbreaking of Deasphalted Oil from Bitumen at 280−400 °C. *Energy and Fuels* **2019**, *33*: p. 159 - 175.

Chacón-Patiño, M. L.; Vesga-Martínez, S. J.; Blanco-Tirado, C.; Orrego-Ruiz, J. A.; Gómez-Escudero, A.; Combariza, M. Y. Exploring Occluded Compounds and their Interactions with Asphaltene Networks using High-Resolution Mass Spectrometry. *Energy and Fuels* **2016**, *30:* p. 4550 - 4561.

Chacón-Patiño, M.L.; Gray, M.R.; Rüger, C.; Smith, D.F.; Glattke, T.J.; Niles, S.F.; Neumann, A.; Weisbrod, C.R.; Yen, A.; McKenna, A.M.; Giusti, P.; Bouyssiere, B.; Barrere-Mangote, C.;Yarranton, H.; Hendrickson, C.L.; Marshall, A.G.; Rodgers, R.P. Lessons Learned from a Decade-Long Assessment of Asphaltenes by Ultrahigh-Resolution Mass Spectrometry and Implications for Complex Mixture Analysis. *Energy and Fuels* **2021**, *35*: p. 16335 - 16376.

Chacón-Patino, M.L.; Rowland, S.M.; Rodgers, R.P. Advances in Asphaltene Petroleomics. Part 2: Selective Separation Method That Reveals Fractions Enriched in Island and Archipelago Structural Motifs by Mass Spectrometry. *Energy and Fuels* **2018**, *32*: p.314 - 328.

Chamberlain, N. F. *The Practice of NMR Spectroscopy With Spectra-Structure Correlations for Hydrogen-1*. Plenum Press: New York, 1974.

Chang, H-L.; Wong, G. K.; Lin, J-R.; Yen, T. F. Electron Spin Resonance Study of Bituminous Substances and Asphaltenes. In *Asphaltenes And asphalts. Vol. 2* (Developments in Petroleum Science Vol. 40 B); Yen, T. F., Chilingarian, G. V. Eds.; Elsevier: Amsterdam, 2000, p. 229 - 280.

Chen, B. Introduction to NMR. In *Fundamentals of Recoupling and Decoupling Techniques in Solid State NMR*. AIP Publishing LLC: Melville, N.Y, 2020, p. 1 - 16.

Chen, Q.; Wang, Y. Challenges in the Determination of Water Content by Karl Fischer Titration during In-Process Control. *American Pharmaceutical Review* **2009**, *12*: p. 48 - 54.

Cimino, R.; Correra, S.; Del Bianco, A.; Lockhart, T. P. Solubility and Phase Behavior of Asphaltenes in Hydrocarbon Media. In *Asphaltenes. Fundamentals and applications*; Sheu, E. Y., Mullins, O. C. Eds.; Plenum Press: New York, 1995, p. 97 - 130.

Clarke, P.F.; Pruden, B.B. Asphaltene Precipitation from Cold Lake and Athabasca Bitumen. *Petroleum Science and Technology* **1998**, *16*, p. 287 - 305.

Clint, J.H.; Fletcher, P.D.I.; Todorov, I.T. Evaporation Rates of Water from Water-in-Oil Microemulsions. *Physical Chemistry Chemical Physics* **1991**, *1*: p. 5005 - 5009.

Collin, P.J.; Gilbert, T.D.; Philp, P.; Wilson, M.A. Structures of the Distillates Obtained from Hydrogenation and Pyrolysis of Liddell Coal. *Fuel* **1983**, *62*: p. 450 - 458.

Collings, P.J.; Hird, M. *Introduction to Liquid Crystals: Chemistry and Physics*. Taylor & Francis Group: Boca Raton, FL, 2009.

Cookson, D.J.; Latten, J.L.; Shaw, I.M.; Smith, B. E. Property-Composition Relationship for Diesel and Kerosene Fuels. *Fuel* **1985**, *64*: p. 509 - 519.

Cookson, D.J.; Lloyd, C.O.; Smith B. E. A Novel Semi-Empirical Relationship between Aromaticities Measured from ^{1}H and [13]C N.M.R. Spectra. *Fuel* **1986**, *65*: p. 1247 - 1253.

Cookson, D.J.; Lloyd, C.O.; Smith, B. E. Investigation of the Chemical Basis of Kerosene (Jet Fuel) Specification Properties. *Energy and Fuels* **1987**, *1*: p. 438 - 447.

Czajka, K.M. The Impact of the Thermal Lag on the Interpretation of Cellulose Pyrolysis. *Energy* **2021**, *236*: p. 121497.

Czarnecki, J. Water-in-Oil Emulsions in Recovery of Hydrocarbons from Oil Sands. In *Encyclopedic Handbook of Emulsion Technology*; Sjöblom, J.; editor, Marcel Dekker: NY, NY 2001, p. 497 - 514.

Czarnecki, J., Moran, K., Yang, X. On the "Rag Layer" and Diluted Bitumen Froth Dewatering. *The Canadian Journal of Chemical Engineering* **2007**, *85*: p. 748 - 755.

Dappe, V.; Ben Tayeb, K.; Vezin, H.; Mariette, S.; Serve, O.; Livadaris, V. Effect of Thermal Treatment of Different Petroleum Fractions: Characterization by in situ EPR Spectroscopy. *Energy and Fuels* **2020**, *34*: p. 12026 - 12032.

Davis, M.C.; Fedick, P.W.; Lupton, D.V.; Ostrom, G.S.; Quintana, R.; Woodroffe, J.D. Solubility of Hydrocarbon Oils in Alcohols (< C_6) and Synthesis of Diesel Carbonate for Degreasing. *RSC Advances* **2019**, *9*: p. 22891 - 22899.

De Klerk A. Unconventional Oil: Oilsands. In *Future Energy: Improved, Sustainable and Clean Options for our Planet*; Letcher, T. M., Ed.; Elsevier: Amsterdam; 2020; 3ed, p. 49 - 65.

De Klerk, A. Processing Unconventional Oil: Partial Upgrading of Oilsands Bitumen. *Energy and Fuels* **2021**, *35*: p. 14343 - 14360.

De Klerk, A. Thermal Conversion Modeling of Visbreaking at Temperatures below 400 °C. *Energy and Fuels* **2020**, *34*: p. 15285 - 15298.

De Klerk, A.; Zerpa Reques, N. G.; Xia, Y.; Omer, A.A. Integrated Central Processing Facility (CPF) in Oil Field Upgrading (OFU). CA2837345A1, 2014.

Dente, M.; Bozzano, G.; Faravelli, T.; Marongiu, A.; Pierucci, S.; Ranzi, E. Kinetic Modelling of Pyrolysis Processes in Gas and Condensed Phase. *Advances in Chemical Engineering* **2007**, *32*: p. 51 - 166.

Diaz, C.; Blanco C.G. NMR: A Powerful Tool in the Characterization of Coal Tar Pitch. *Energy and Fuels* **2003**, *17*: p. 907 - 913.

Dunstan, A.E. *The Science of Petroleum*. Oxford University Press: London, UK, 1938.

Eaton, G.R.; Eaton, S.S.; Barr, D.P.; Weber, R.T. *Quantitative EPR*. Springer: New York, NY, 2010.

EIA. Oil and Petroleum Products Explained, Use of Oil. https://www.eia.gov/energyexplained/oil-and-petroleum-products/use-of-oil.php (accessed October 18, 2022).

Escobedo, J.; Mansoori, G.A. Viscometric Determination of the Onset of Asphaltene Flocculation: A Novel Method. *SPE Production and Facilities* **1995**, *10*: p. 115 - 118.

Escobedo, J.; Mansoori, G.A. Viscometric Principles of Onsets of Colloidal Asphaltene Flocculation in Paraffinic Oils and Asphaltene Micellization in Aromatics. *SPE Production and Facilities* **1997**, *12*: p. 116 - 122.

Evans, S.; Marsh, H. The Chemistry of Formation of Semi-Cokes from Aromatic Systems using Mass Spectrometer - I. *Carbon* **1971**, *9*: p. 733 - 746.

Fakher, S.; Ahdaya, M.; Elturki, M.; Imqam, A. Critical Review of Asphaltene Properties and Factors impacting its Stability in Crude Oil. *Journal of Petroleum Exploration and Production Technology* **2020**, *10*: p. 1183 - 1200.

Fingas, M. F., Fieldhouse, B. Studies of Water-in-Oil Emulsions and Techniques to Measure Emulsion Treating Agents. In: *Proceedings of the 17th Arctic and Marine Oil Spill Program (AMOP)Technical Seminar*, Environment Canada: Ottawa, CA, 1994, p. 213 - 244.

Friberg, S.E.; Langlois, B. Evaporation from Emulsions. *Journal of Dispersion Science and Technology* **1993**, *13*: p. 223 - 243.

Gabbott, P. *Principles and Applications of Thermal Analysi*s. Blackwell Publications: Oxford, UK, 2008.

Gafonova, O.; Yarranton, H.W. The Stabilization of Water-in-Hydrocarbon Emulsions by Asphaltenes and Resins. *Journal Colloidal and Interface Science* **2001**, *241*: p. 469 - 478.

Ganeeva, Y. M.; Barskaya, E. E.; Okhotnikova, E. S.; Yusupova, T. N. Features of the Composition of Compounds Trapped in Asphaltenes of Oils and Bitumens of the Bavly Oil Field. *Energy and Fuels* **2021**, *35*: p. 2493 - 2505.

Gary, J.H.; Handwerk, G.E.; Kaiser, M.J. *Petroleum Refining: Technology and Economics*. 5th ed. CRC Press: Boca Ratón, FL, 2007.

Gasparoux, H. Carbonaceous Mesophase and Disc-like Nematic Liquid Crystals. *Molecular Crystals and Liquid Crystals* **1981**, *63*: p. 213 - 248.

Gholami, R.; Alvarez-Majmutov, A.; Ali, M.; Chen, J. Understanding Bitumen Partial Upgrading through Process Modelling and Simulation. *The Canadian Journal of Chemical Engineering* **2021**, *99:* p. 222 - 234.

Girdler RB. Constitution of Asphaltenes and Related Studies. Proceedings of Technical Sessions by the Association of Asphalt Paving Technologies, Philadelphia: 1965, p. 45 - 79.

Gonçalves, M.L.A.; Ribeiro, D.A.; Teixeira, A.M.R.F.; Teixeira, M.A.G. Influence of Asphaltenes on Coke Formation during the Thermal Cracking of Different Brazilian Distillation Residues. *Fuel* **2007**, *86*: p. 619 - 623.

Gray, M.R.; Ayasse, A.R. Kinetics of Hydrodesulfurization of Thiophenic and Sulfide Sulfur in Athabasca Bitumen. *Energy and Fuels* **1995**, *9*: p. 500 - 506.

Gray, M. R.; McCaffrey, W. Role of Chain Reactions and Olefin Formation in Cracking, Hydroconversion, and Coking of Petroleum and Bitumen Fractions. *Energy and Fuels* **2002**, *16*: p.756 - 766.

Gray, M.R.; Tykwinski, R.; Stryker, J.; Tan, A. Supramolecular Assembly Model for Aggregation of Petroleum Asphaltenes. *Energy and Fuels* **2011**, *25*: p. 3125 - 3134.

Gray, M. R. *Upgrading Oilsands Bitumen and Heavy Oil.* University of Alberta Press: Edmonton, Canada, 2015.

Gray, M.R. Fundamentals of Partial Upgrading of Bitumen. *Energy and Fuels* **2019**, *33*, p. 6843 - 6856.

Gray, M. R.; Yarranton, H. W.; Chacón-Patiño, M. L.; Rodgers, R. P.; Bouyssiere, B.; Giusti, P. Distributed Properties of Asphaltene Nanoaggregates in Crude Oils: A Review. *Energy and Fuels* **2021**, *35*: p. 18078 - 18103.

Graziano, G. Solvation thermodynamics of cyclohexane. *The Canadian Journal of Chemistry* **2000**, *78*: p. 1233 – 1241.

Greinke, R.A. Kinetics of Petroleum Pitch Polymerization by Gel Permeation Chromatography. *Carbon* **1986**, *24*: p. 677 - 686.

Greinke, R.A. Quantitative Influence of Dealkylation and Polymerization Reactions on Mesophase Formation. *Carbon* **1990**, *28*: p.701 - 706.

Greinke, R.A.; Singer, L.S. Constitution of Coexisting Phases in Mesophase Pitch during Heat Treatment: Mechanism of Mesophase Formation. *Carbon* **1988**, *26*: p. 665 - 670.

Grossman, R.B. Free-Radical Reactions. In: *The Art of Writing Reasonable Organic Reaction Mechanisms*, 3rd Ed., Springer: Switzerland, 2019, p. 283 - 339.

Gruse, W.A.; Stevens, D.R. *Chemical Technology of Petroleum*. McGraw-Hill: New York,NY, 1960.

Guan, J. G.; Kariznovi, M.; Nourozieh, H.; Abedi, J. Density and Viscosity for Mixtures of Athabasca Bitumen and Aromatic Solvents. *Journal of Chemical Engineering Data* **2013**, *58*: p. 611 - 624.

Guisnet, M.; Magnoux, P. Organic Chemistry of Coke Formation. *Applied Catalysis A: General* **2001**, *212*: p. 83 - 96.

Gutowski, H.S.; Ray, B.R.; Rutledge, R.L. Carbonaceous Free Radicals in Crude Petroleum. *Journal of Chemical Physics* **1958**, *28*: p. 744.

Ha, E-S.; Lee, S-K.; Choi, D.H.; Jeong, S.H.; Hwang, S-J.; Kim, M.-S. Application of Diethylene Glycol Monoethyl Ether in Solubilization of Poorly Water-Soluble Drugs. *Journal of Pharmaceutical Investigation* **2020**, *50*: p. 231 - 250.

Halmenschlager, C.M.; Brar, M.; Apan, I.T., De Klerk, A. Hydrocracking Vacuum Gas Oil with Wax. *Catalysis Today* **2020**, *353*: p. 187 - 196.

Hamza, H. Effect of Solvent Selection on Froth Treatment for Mining Operations. In: *Proceedings of the 3rd NCUT Meeting on Upgrading and Refining of Heavy Oil, Bitumen and Synthetic Crude Oil*, Edmonton, Alberta, 2003.

Hasan, M.U.; Ali, M.F.; Bukhari, A. Structural Characterization of Saudi Arabian Heavy Crude Oil by N.M.R. Spectroscopy. *Fuel* **1983**, *62*: p. 518 - 523.

Hasan, M.U.; Bukhari, A.; Ali, M.F. Structural Characterization of Saudi Arabian Medium Crude Oil by N.M.R. Spectroscopy. *Fuel* **1985**, *64*: p. 839 – 841.

Hasan, M.U.; Ali, M.F.; Arab, M. Structural Characterization of Saudi Arabian Extra Light and Light Crudes by ^{1}H and [13]C N.M.R. Spectroscopy. *Fuel* **1989**, *68*: p. 801 - 803.

Hawley, G.G. *The Condensed Chemical Dictionary*. 8th Edition. Van Nostrands Reinhold: New York, NY, 1971.

Hayes, M.H.B.; Stacey, M.; Standley, J. Studies on Bitumen: Part 1. Characterization of Bitumen by Use of Physical Methods. *Fuel* **1972**, *51*: p. 27 - 31.

He, G-H; Chen, G.-H. Determination of Water in W/O Emulsion by TG. *Petrochemical Technology* **2000**, *7*: p. 526 - 529.

He, L.; Li, X.; Du, Y.; Wu, G.; Li, H.; Sui, H. Parameters of Solvent Extraction for Bitumen Recovery from Oil Sands. *Advanced Materials Research* **2012**, *347 - 353*: p. 3728 - 3731.

Heithaus, J.J. Measurement and Significance of Asphaltene Peptization. *Journal of the Institute of Petroleum* **1962**, *48*: p. 45.

Hiller, W.G.; Abu-Dagga, F.; Al-Tahou, B. Determination of Gasoline Octane Numbers by ^{1}H and ^{13}C-NMR Spectroscopy. *Journal für Praktische Chemie* **1992**, *334*: p. 691 - 695.

Hirschberg, A.; de Jong, L.N.J.; Schipper, B.A.; Meijer, J.G. Influence of Temperature and Pressure on Asphaltene Flocculation. *Society of Petroleum Engineers Journal* **1984**, *24*: p. 283 - 293.

Honda, H.; Kimura, H.; Sanada, Y.; Sugawara, S.; Furuta, T. Optical Mesophase Texture and X-ray Diffraction Pattern of the Early-Stage Carbonization of Pitches. *Carbon* **1970**, *8*: p. 181 - 182.

Hurt, R.H.; Hu, Y. Thermodynamics of Carbonaceous Mesophase. *Carbon* **1999**, *37*: p. 281 - 292.

Ihnatowicz, M.; Chiche, P.; Deduit, J.; Pregermain, S.; Tournant, R. Formation de la Texture des Cokes de Houilles et de Brais Etudiée par Solubilité et par Microscopie. *Carbon* **1966**, *4:* p. 41 - 50.

Ingram, D.J.; Tapley, J.G.; Jackson, R.; Bond, R.L.; Murnaghan, A.R. Paramagnetic Resonance in Carbonaceous Solids. *Nature* **1954**, *174*: p. 797 - 798.

International Union of Pure and Applied Chemistry. *Alcohols with Water*, vol. 15. Pergamon Press: Oxford, UK, 1984.

International Union of Pure and Applied Chemistry. *Hydrocarbons with Water and Seawater*, vol. 37. Pergamon Press: Oxford, UK, 1989.

Jacobs Consultancy. Bitumen Partial Upgrading (Whitepaper). Calgary, Canada, 2018.

Jacobs, F.S.; Filby, R.H. Solvent Extraction of Oil-Sand Components for Determination of Trace Elements by Neutron Activation Analysis. *Analytical Chemistry* **1983**, *55*: p. 74 - 77.

Jennings, D. W.; Weispfennig, K. Experimental Solubility Data of Various *n*-Alkane Waxes: Effects of Alkane Chain Length, Alkane Odd versus Even Carbon Number Structures, and Solvent Chemistry on Solubility. *Fluid Phase Equilibria* **2005**, *227*: p. 27 - 35.

Jha, K.N.; Montgomery, D.S.; Strausz, O.P. Chemical Composition of Gases in Alberta Bitumens and in Low-Temperature Thermolysis of Oil Sand Asphaltenes and Maltenes. In: *Symposium on Oil Sand and Oil Shale Chemistry*, Strausz, O.P.; Lown, E.M., editor.; Verlag Chemie International: 1977, p. 33 - 54.

Kaiser, M.J.; de Klerk, A.; Gary, J.H.; Handwerk G.E. *Petroleum refining: technology, economics, and markets*. Sixth edit. CRC Press: Boca Raton, FL, 2020.

Kar, T. Analysis of Saturates, Aromatics, Resins, Asphaltenes (SARA), Water, and Clays in Water-Oil Emulsions for Steam-Assisted Gravity Drainage (SAGD)and Expanding Solvent - SAGD (ES-SAGD). MSc Thesis, Texas A&M University, 2015.

Kato, H. *Karl Fischer Reagents: Technical Manual*. 2004.

Khatri, N.L.; Andrade, J.; Baydak, E.N.; Yarranton, H.W. Emulsion Layer Growth in Continuous Oil-Water Separation. *Colloids and Surfaces A: Physicochemical and Engineering Aspects* **2011**, *384*: p. 630 - 642.

Kilpatrick, P.K. Water-in-Crude Oil Emulsion Stabilization: Review and Unanswered Questions. *Energy and Fuels* **2012**, *26*: p. 4017 - 4026.

Kokal, S. Crude-Oil Emulsions: A State-of-the-Art Review. *SPE Production and Facilities* **2005**, *20*: p. 5 - 13.

Korošec, R.C.; Bukovec, P. Thermal Methods of Analysis as a Tool for Quantitative Composition Determination of Water-in-Oil Emulsions. In: *Explosive Materials: Classification, Composition and Properties*, Janssen, T.J., editor.; Nova Science Publishers: Hauppauge, NY, 2011, p. 125 - 144.

Kubicka, D.; Lederer, J.; Hanika, J.; Kolena, J. Kinetics of Thermal Hydrodealkylation of C_7 and C_8 Aromatics. *Petroleum and Coal* **2002**, *44*: p. 192 - 194.

Kucora, I.; Paunjoric, P.; Tolmac, J.; Vulovic, M.; Speight, J.G.; Radovanović, L.Z. Coke Formation in Pyrolysis Furnaces in the Petrochemical Industry. *Petroleum Science and Technology* **2017**, *35*: p. 213 - 221.

Kurtz, S.S.; Ward, A.L. The Refractivity Intercept and the Specific Refraction Equation of Newton. I. Development of the Refractivity Intercept and Comparison with Specific Refraction Equations. *Journal of the Franklin Institute* **1936**, *222*: p. 563 - 592.

Legin-Kolar, M.; Ugarkovic, D. Petroleum Coke Structure: Influence of Feedstock Composition. *Carbon* **2000**, *31*: p. 383 - 390.

Leprince, P. *Petroleum Refining.* Leprince, P., Ed.; Editions Technip: Paris, France, 2001; Vol. 3, Conversion Processes.

Lewis, I.C.; Edstrom, T. Thermal Reactivity of Polynuclear Aromatic Hydrocarbons. *The Journal of Organic Chemistry* **1963**, *28*: p. 2050 - 2057.

Lewis, I.C.; Singer, L.S. Electron Spin Resonance of Stable Aromatic Radical Intermediates in Pyrolysis. *Carbon* **1969**, *7*: p. 93 - 99.

Lewis, I.C.; Kovac, C.A. The Role of Free Radicals and Molecular Size in Mesophase Pitch. *Carbon* **1978**, *16*: p. 425 – 429.

Lewis, I.C.; Singer, L.S. Electron Spin Resonance and the Mechanism of Carbonization. *Chemistry and Physics of Carbon* **1984**, *17*: p. 1 - 79.

Link, F.; Halmenschlager, C.; Chauhan, G.; De Klerk, A. Wax Hydrocracking over Pt/SiO2-Al2O3 at 2 MPa: Product Characterization and its Implications for Catalysis. *Energy and Fuels* **2021**, *35*: p. 5252 - 5263.

Lipkin M.R; Kurtz, S.S. Temperature Coefficient of Density and Refractive Index for Hydrocarbons in the Liquid State. *Industrial and Engineering Chemistry – Analytical Edition* **1941**, *13*: p. 291 - 295.

Liu, Y.; Daum, P.H. Relationship of Refractive Index to Mass Density and Self-Consistency of Mixing Rules for Multicomponent Mixtures like Ambient Aerosols. *Journal of Aerosol Science* **2008**, *39*: p. 974 - 986.

Loison, R.; Foch, P.; Boyer, A. *Coke: Quality and Production.* 2nd Edition; Butterworth & Co: London, UK, 1989.

Long, Y.; Dabros, T.; Hamza, H. Selective Solvent Deasphaltene for Heavy Oil Emulsion Treatment. In: *Asphaltenes, Heavy Oils and Petroleomics*, Mullins, O., editor., Springer: New York, NJ, 2007, p. 511 - 547.

Long, Y.; Dabros, T.; Hamza, H. Stability and Settling Characteristics of Solvent-Diluted Bitumen Emulsions. *Fuel* **2002**, *81*: p. 1945 - 1952.

Louwerse, M. J.; Maldonado, A.; Rousseau, S.; Moreau-Masselon, C.; Roux, B.; Rothenberg, G. Revisiting Hansen Solubility Parameters by Including Thermodynamics. *ChemPhysChem* **2017**, *18*: p. 2999 - 3006.

MacKay, P.; Pedersen, P.K. The Western Canada Sedimentary Basin: A confluence of science, technology, and ideas. *AAPG Bulletin* **2022**, *106*: p. 655 - 676.

MacLeod, S.K. Moisture Determination using Karl Fischer Titrations. *Analytical Chemistry* **1991**, *63*: p. 557A - 566A.

Magaril, R.Z.; Aksenova, E.I. Study of the Mechanism of Coke Formation in the Cracking of Petroleum Resins. *International Chemical Engineering* **1968**, *8*: p. 727 - 729.

Magaril, R.Z.; Ramazaeva, L.F.; Aksenova, E.I. Kinetics of the Formation of Coke in Thermal Processing of Crude Oil. *International Chemical Engineering* **1971**, *11*: p. 250 - 251.

Maity, S.K.; Centeno, G.; Ancheyta, J. Experimentation with Heavy Oil in Batch Reactors. In *Experimental Methods for Evaluation of Hydrotreating Catalysts*; Ancheyta, J., Ed; Wiley: Hoboken, NJ, 2020, p. 97 - 119.

Marafi, M.; Stanislaus, A.; Furimsky, E. Spent Unconventional Hydroprocessing Catalysts. In: *Handbook of Spent Hydroprocessing Catalysts*; Elsevier B.V: Amsterdam, Netherlands, 2017, p. 357 - 374.

Marsh, H.; Latham, C.S. The Chemistry of Mesophase Formation. In: *Petroleum-Derived Carbons;* ACS Symposium Series: Washington, DC, 1986; p. 1 - 27.

Marsh, H.; Menendez, R. Mechanisms of Formation of Isotropic and Anisotropic Carbons. In: *Introduction to Carbon Science*; Marsh, H., Ed.; Butterworths: London, UK, 1989; p. 37 - 73.

Marsh, H.; Walker, P.L. The Formation of Graphitizable Carbons via Mesophase: Chemical and Kinetic considerations. In: *Chemistry and Physics of Carbon*; Walker, P.L.; Thrower, P.A., Eds.; Marcel Dekker Inc: New York, NY, 1979; vol. 15, p. 230 - 286.

McKenna, A.M.; Chacón-Patino, M.L.; Weisbrod, C.R.; Blakney, G.T.; Rodgers, R.P. Molecular-Level Characterization of Asphaltenes Isolated from Distillation Cuts. *Energy and Fuels* **2019**, *33*: p. 2018 - 2029.

McKenna, A.M.; Marshall, A.G.; Rodgers, R.P. Heavy Petroleum Composition. 4. Asphaltene Compositional Space. *Energy & Fuels* **2013**, *27*: p. 1257 - 1267.

Mitchell, J.; Smith, D.M. Aquametry: *A Treatise on Methods for the Determination of Water (Part III)*. Vol. 5. John Wiley & Sons, Inc., New York, NY, 1980.

Mitchell, J.; Smith, D.M.; Ashby, E.C.; Bryant, W.M.D. Analytical Procedures employing Karl Fischer Reagent. IX. Reactions with Inorganic Oxides and Related Compounds. Oxidation and Reduction Reactions. *Journal of the American Chemical Society* **1941**, *63*: p. 2927 - 2930.

Mochida, I.; Inoue, S.-I.; Maeda, K.; Takeshita, K. Carbonization of Aromatic Hydrocarbons VI. Carbonization of Heterocyclic Compounds Catalyzed by Aluminum Chloride. *Carbon* **1977**, *15*: p. 9 - 16.

Mochida, I.; Nakamura, E.-I.; Maeda, K.; Takeshita, K. Carbonization of Aromatic Hydrocarbons IV. Reaction Path of Carbonization Catalyzed by Alkali Metals. *Carbon* **1976**, *14*: p. 123 - 129.

Mochida, I.; Inoue, S.-I.; Maeda, K.; Takeshita, K. Carbonization of Aromatic Hydrocarbons VI. Carbonization of Heterocyclic Compounds Catalyzed by Aluminum Chloride. *Carbon* **1977**, *15*: p. 9 – 16.

Monthioux, M.; Oberlin, M.; Oberlin, A.; Bourrat, X.; Boulet, R. Heavy Petroleum Products: Microtexture and Ability to Graphitize. *Carbon* **1982**, *20*: p. 167 - 176.

Montoya-Sanchez, N.; de Klerk, A. Viscosity Mixing Rules for Bitumen at 1-10 wt % Solvent Dilution When Only Viscosity and Density Are Known. *Energy and Fuels* **2020**, *34*: p. 8227 - 8238.

Muller, H.; Saleem, Q.; Alawi, E.A.; Alsewdan, D.A.; Naqvi, I.A.S.; Saleh, A.; Rowaished. T.A. Narrow Distillation Cuts for an Improved Characterisation of Crude Oil: an Insight on Heteroatoms in Heavy Fraction Molecules. *International Journal of Oil, Gas and Coal Technology* **2021**, *26*: p. 40 - 59.

Mullins, O. C.; Pomerantz, A. E.; Andrews, B.; Majumdar, R. D.; Hazendonk, P.; Ruiz-Morales, Y.; Goual, L.; Zare, R. N. Asphaltenes. In *Springer Handbook of Petroleum Technology*; Hsu, C. S., Robinson, P. R. Eds.; Springer: Cham, 2017, p. 221 - 250.

Mullins, O.; Sabbah, H.; Pomerantz, A.E; Andrews, A.B.; Ruiz-Morales, Y.; Mostow, F.; Mcfarlane, R.; Goual, L.; Lepkowicz, R.; Cooper, T.; Orbulescu, J.; Leblanc, R.M.; Edwards, J.; Zare, R.N. Advances in Asphaltene Science and the Yen − Mullins Model. *Energy and Fuels* **2012**, *26*: p. 3986 - 4003.

Mullins, O.C. The Modified Yen Model. *Energy and Fuels* **2010**, *24*: p. 2179 - 2207.

Mura, E.; Josset, C.; Loubar, K.; Bellettre, J.; Massoli, P. Experimental Study of the Water in Oil Emulsions Features by Differential Scanning Calorimetry Analysis. *Applied Energy* **2012**, *97*: p. 834 - 840.

Murugan, P.; Mani, T.; Mahinpey, N.; Dong, M. Pyrolysis Kinetics of Athabasca Bitumen using a TGA under the Influence of Reservoir Sand. *The Canadian Journal of Chemical Engineering* **2012**, *90*: p. 315 - 319.

Nellesteyn, F.J. The Constitution of Asphalt. *Journal of the Institute of Petroleum* **1924**, *10*: p. 311 - 325.

Ng, A., Ovalles, C, Benson, I.P. Asphaltenes Contribution in Emulsion Formation During Solvent-Steam Processes. In: *SPE Western Regional Meeting*, Garden Grove, CA, 2018, p. SPE-190057-MS.

O'Donnell, D.J.; Sigle, S.O.; Berlin, D.K.; Sturm, G.P.; Vogh, J.W. Characterization of High-boiling Petroleum Distillate Fractions by Proton and ^{13}C Nuclear Magnetic Resonance Spectroscopy. *Fuel* **1980**, *59*: p. 166 - 174.

Ovalles, C.; Rogel, E.; Hajdu, P.; Rea, T.; Chaudhuri, K.; Hench, K.; Cuspar, D.; Moir, M.E. Predicting Coke Morphology in Delayed Coking from Feed Characteristics. *Fuel* **2020**, *263*: p. 116739.

Park, S.J.; Mansoori, G.A. Aggregation and Deposition of Heavy Organics in Petroleum Crudes. *Energy Sources* **1988**, *10*: p. 109 - 125.

Parsons, A.F. Radical Reactions. In: *Introduction to Free Radical Chemistry.* Blackwell Science: Oxford, UK, 2000, p. 61 - 95.

Pastor, R.C.; Weil, J.A.; Brown, T.H.; Turkevich, J. Narrow Electron Spin Resonance in Charred Dextrose. *Physical Review* **1956**, *102*: p. 918 - 919.

Penaloza, I. Effect of Water Chemistry on Cold Lake and Athabasca bitumen. MSc Thesis, University of Alberta, 2018.

Peñaloza, I.M.; Chauhan, G.; De Klerk, A. Desalting Behavior of Bitumen. *Energy and Fuels* **2021**, *35*: p. 15618 - 15627.

Peramanu, S.; Singh, C.; Agrawala, M.; Yarranton, H. W. Investigation on the Reversibility of Asphaltene Precipitation. *Energy and Fuels* **2001**, *15*: p. 910 - 917.

Picón-Hernández, H.J.; Centeno-Hurtado, A.; Pantoja-Agreda, E.F. Morphological Classification of Coke formed from the Castilla and Jazmín Crude Oils. *CT & F - Ciencia, Tecnologia y Futuro* **2008**, *3*: p. 169 - 183.

Pillon, L.Z. Use of NMR Spectroscopy to Study the Effect of Hydrocracking on the Chemistry of Hydrocarbons. *Petroleum Science and Technology* **2002**, *20*: p. 357 - 365.

Podgorski, D.C.; Corilo, Y.E.; Nyadong, L.; Lobodin, V.V.; Bythell, B.J.; Robbins, W.K.; McKenna, A.M.; Marshall, A.G.; Rodgers, R.P. Heavy Petroleum Composition. 5. Compositional and Structural Continuum of Petroleum Revealed. *Energy and Fuels* **2013**, *27*: p. 1268 - 1276.

Pomerantz, A.E.; Hammond, M.R.; Morrow, A.L.; Mullins, O.C.; Zare, R.N. Asphaltene Molecular-Mass Distribution Determined by Two-Step Laser Mass Spectrometry. *Energy and Fuels* **2009**, *23*: p. 1162 - 1168.

Pomerantz, A.E.; Hammond, M.R.; Morrow, A.L.; Mullins, O.C.; Zare, R.N. Two-Step Laser Mass Spectrometry of Asphaltenes. *Journal of the American Chemical Society* **2008**, *130*: p. 7216 - 7217.

Poole, C.P. Electron Spin Resonance: A Comprenhensive Treatise in Experimental Techniques. Interscience Publishers: New York, NY, 1967.

Poveda, J.C.; Molina, D.R.; Pantoja-Agreda E.F. ^{1}H- and ^{13}C-NMR Structural Characterization of Asphaltenes from Vacuum Residua Modified by Thermal Cracking. *CT&F - Ciencia, Tecnología y Futuro* **2014**, *5*: p. 49 - 60.

Pugmire, R.J.; Grant, D.M.; Zilm, K.W.; Anderson, L.L.; Oblad, A.G.; Wood, R.E. Carbon-13 Magnetic Resonance of Coal-Derived Liquids. *Fuel* **1977**, *56*: p. 295 - 301.

Rahimi, P.; Gentzis, T.; Dawson, W.H.; Fairbridge, C.; Khulbe, C.; Chung, K.; Nowlan, V.; DelBianco, A. Investigation of Coking Propensity of Narrow Cut Fractions from Athabasca Bitumen using Hot-Stage Microscopy. *Energy and Fuels* **1998**, *12*: p. 1020 - 1030.

Rahimi, P.; Gentzis, T.; Taylor, E.; Carson, D.; Nowlan, V.; Cotté, E. The Impact of Cut Point on the Processability of Athabasca Bitumen. *Fuel* **2001**, *80*: p. 1147 - 1154.

Rahimi, P.M.; Gentzis, T. The Chemistry of Bitumen and Heavy Oil Processing. In: *Practical Advances in Petroleum Processing*; Hsu C.S.; Robinson, P, R., editors. Springer: New York, NY, 2006, p. 597 - 634.

Rahimi, P.M.; Teclemariam, A.; Taylor, E.; DeBruijn, T.; Wiehe, I.A. Thermal Processing Limits of Athabasca Bitumen during Visbreaking Using Solubility Parameters. *ACS Symposium Series* **2005**, *895*: p. 183 - 196.

Rahmani, S.; McCaffrey, W.; Gray, M.R. Kinetics of solvent interactions with asphaltenes during coke formation. *Energy and Fuels* **2002**, *16*: p. 148 - 154.

Ramirez-Corredores, M.M. *The Science and Technology of Unconventional Oils*. Academic Press: London, UK, 2017.

Ramos-Pallares, F.; Santos, D.; Yarranton, H. W. Application of the Modified Regular Solution Model to Crude Oils Characterized from a Distillation Assay. *Energy and Fuels* **2020**, *34*: p. 15270 - 15284.

Ramos-Pallares, F.; Yarranton, H. W. Extending the Modified Regular Solution Model to Predict Component Partitioning to the Asphaltene-Rich Phase. *Energy and Fuels* **2020**, *34*: p. 5213 - 5230.

Rand, B. The Pitch-Mesophase-Coke Transformation as Studied by Thermal Analytical and Rheological Techniques. In: *Petroleum Derived Carbons*; ACS Symposium Series: Washington, DC, 1986, p.45 - 61.

Rao, F.; Liu, Q. Froth Treatment in Athabasca Oil Sands Bitumen Recovery Process: A Review. *Energy and Fuels* **2013**, *27*: p. 7199 - 7207.

Retcofsky, H.L., Hough, M.R., Maguire, M.M., Clarkson, R.B. Nature of the Free Radicals in Coals, Pyrolyzed Coals, Solvent-Refined Coal, and Coal Liquefaction Products. In: *Coal Structure*, Gorbaty and Ouchi., editor.; Advances, American Chemical Society: Washington, D.C., 1981.

Reyniers, G.C.; Froment, G.F.; Kopinke, F.D.; Zimmermann, G. Coke Formation in the Thermal Cracking of Hydrocarbons. 4. Modeling of Coke Formation in Naphtha Cracking. *Industrial and Engineering Chemistry Research* **1994**, *33*: p. 2584 - 2590.

Riazi, M. R.; Gupta R. *Coal Production and Processing Technology*. CRC Press: Boca Raton, FL, 2016.

Riazi, M.R. *Characterization and Properties of Petroleum Fractions*. ASTM International: West Conshohocken, PA, 2005.

Riggs, D.M.; Diefendorf, R.J. Effect of Heat Treatment on the Molecular Characteristics of Mesophase Forming Material. In: *Extended Abstracts 14th Biennial Conference of Carbon* **1979**, p. 413 - 414.

Rivolta, A.A. Molar Refractivity and Oxygen Solubility. MSc Thesis, University of Alberta, 2020.

Rocha, J.A.; Baydak, E.N.; Yarranton, H.W. What Fraction of the Asphaltenes Stabilizes Water-in-Bitumen Emulsions? *Energy and Fuels* **2018**, *32*: p. 1440 - 1450.

Rodriguez Leon, S.L. The Stability of Visbroken Heavy Oil Against Asphaltene Precipitation. MSc Thesis, University of Calgary, 2018.

Rodriguez, J.; Tierney, J.W.; Wender I. Evaluation of a Delayed Coking Process by ^{1}H and [13]C N.M.R Spectroscopy: 2. Detailed Interpretation of Liquid N.M.R Spectra. *Fuel* **1994**, *73*: p. 1870 - 1875.

Rondón, M.; Pereira, J.C.; Bouriat, P.; Graciaa, A.; Lachaise, J.; Salager, J.L. Breaking of Water-in-Crude-Oil emulsions. 2. Influence of Asphaltene Concentration and Diluent Nature on Demulsifier Action. *Energy and Fuels* **2008**, *22*: p. 702 - 707.

Rosendahl, L. *Direct Thermochemical Liquefaction for Energy Applications*. Woodhead Publishing: Duxford, UK, 2018.

Rudnick, L.R.; Tueting, D.R. Variation of Free Radical Concentration with Molecular Weight in Petroleum Feedstocks. *Fuel Science and Technology International* **1989**, *7*: p. 57 - 68.

Rudnick, L.R.; Tueting, D.R.; Sinclair, J.L. ESR Investigation Related to Carbonization Tendency. In: *Extended Abstracts of the 17th Biennial Conference on Carbon*, American Carbon Society: Lexington, KY, 1985, p. 403 - 404.

Rueda-Velásquez, R.I.; Freund, H.; Qian, K.; Olmstead, W.N.; Gray, M.R. Characterization of Asphaltene Building Blocks by Cracking under Favorable Hydrogenation Conditions. *Energy and Fuels* **2013**, *27:* p. 1817 - 1829.

Rumble, J.R., editor. Physical Constants of Organic Compounds. In: *CRC Handbook of Chemistry and Physics*, 103rd ed., CRC Press/Taylor & Francis: Boca Raton, FL, 2022.

Sachanen, A.N. *The Chemical Constituents of Petroleum*. Reinhold Publishing Corporation: New York, NY, 1945.

Santamaría-Ramírez, R.; Romero-Palazón, E.; Gómez-de-Salazar, C.; Rodríguez-Reinoso, F.; Martínez-Saez, S.; Martínez-Escandell, M.; Marsh, H. Influence of Pressure Variations on the Formation and Development of Mesophase in a Petroleum Residue. *Carbon* **1999**, *37*: p. 445 - 455.

Scholz, E. *Karl Fischer Determination: Titration of Water*. Springer: Berlin, 1984.

Schramm, L.L., Isaacs, E.E. Development on in-situ Oil Sands and Heavy Oil Reservoirs in Canada. In: *Handbook on theory and practice of bitumen recovery from Athabasca oil sands. Vol. II. Industrial practice,* Masliyah, J.; Xu, Z.; Dabros, M., editor. Kingsley Knowledge Publishing, 2013, p. 603 - 635.

Schramm, L.L., Mikula, R.J. Froth Flotation of Oil Sand Bitumen. In: *Foam Engineering: Fundamentals and Applications*, Stevenson, P., Ed.; Wiley-Blackwell: Chichester, UK, 2012; p. 530.

Schuler, B.; Meyer, G.; Peña, D.; Mullins, O. C.; Gross, L. Unraveling the Molecular Structures of Asphaltenes by Atomic Force Microscopy. *Journal American Chemical Society* **2015**, *137*: p. 9870 - 9876.

Schuler, B.; Zhang, Y.; Liu, F.; Pomerantz, A. E.; Andrews, A. B.; Gross, L.; Pauchard, V.; Banerjee, S.; Mullins, O. C. Overview of Asphaltene Nanostructures and Thermodynamic Applications. *Energy and Fuels* **2020**, *34*: p. 15082 - 15105.

Scotti, R.; Montanari, L. Molecular Structure and Intermolecular Interaction of Asphaltenes by FT-IR, NMR and EPR. In: *Structures and Dynamics of Asphaltenes*, Mullins, O.C., et al., editor.; Springer Science + Business Media: New York, NY, 1998.

Selucky, M.L.; Chu, Y.; Ruo, T.; Strausz, O.P. Chemical Composition of Athabasca Bitumen. *Fuel* **1977**, *56*: p. 369 - 381.

Shafiee Neistanak, M. Kinetics of Asphaltene Precipitation and Flocculation from Diluted Bitumen. MSc Thesis, University of Calgary, 2014.

Shen, J.; Astrath, N. G. C.; Pedreira, P. R. B.; Guimarães, F. B.; Gieleciak, R.; Wen, Q.; Michaelian, K. H.; Fairbridge, C.; Malacarne, L. C.; Rohling, J. H.; Baesso, M. L. Correlations among Thermophysical Properties, Ignition Quality, Volatility, Chemical Composition, and Kinematic Viscosity of Petroleum Distillates. *Fuel* **2016**, *163*: p. 324 - 333.

Sheremata, J.M.; Gray, M.R.; Dettman, H.D.; McCaffrey, W.C. Quantitative Molecular Representation and Sequential Optimization of Athabasca Asphaltenes. *Energy and Fuels* **2004**, *18*: p. 1377 - 1384.

Shoolery, J.N. Some Quantitative Applications of ^{13}C NMR Spectroscopy. *Progress in Nuclear Magnetic Resonance Spectroscopy* **1977**, *11*: p. 79 - 93.

Silverstein, R.M.; Webster, F.X.; Kiemle, D.J. *Spectrometric identification of organic compounds.* 7th Edition; John Wiley & Sons: Hoboken, NJ, 2005.

Singer, L.S.; Lewis, R.T. Orientation of Mesophase in a Magnetic Field: Optical and Electron Spin Resonance Studies. *Carbon* **1973**, *11*: p. 675.

Singer, L.S.; Lewis, I.C. ESR Study of the Kinetics of Carbonization. *Carbon* **1978**, *16*: p. 417 - 423.

Singer, L.S.; Lewis, I.C.; Greinke, R.A. Characterization of the Phases in Centrifuged Mesophase Pitches. *Molecular Crystals and Liquid Crystals* **1986**, *132*: p. 65 - 79.

Siskin, M.; Kelemen, S.R.; Gorbaty, M.L.; Ferrughelli, D.T.; Brown, L.D.; Eppig, C.P.; Kennedy, R.J. Chemical Approach to Control Morphology of Coke Produced in Delayed Coking. *Energy and Fuels* **2006**, *20*: p. 2117 - 2124.

Sivaramakrishnan, K.; De Klerk, A. Viscosity of Canadian Oilsands Bitumen and Its Modification by Thermal Conversion. In: *Chemistry Solutions to Challenges in the Petroleum Industry*, Rahimi, P., Ovalles, C., Zhang, Y., Adams, J.J., editor.; ACS Symposium, American Chemical Society: Washington, DC, 2019, p. 115 - 199.

Snape, C.E.; Ladner, W.R.; Bartle, K.D. Structural Characterization of Coal Extracts by NMR. In: *Coal Liquefaction Products*; Schultz, H.D., editor. John Wiley & Sons, Inc.: New York, NY, 1983; Vol 1, p. 70 - 84.

Sneed, R.W.; Altman, R.W.; Mosteller, J.C. Effect of Aviation Fuel Components on the Accuracy of the Karl Fischer Electrometric Titration. *Analytical Chemistry* **1954**, *26*: p. 1018 - 1020.

Speight, J. G.; Özüm, B. *Petroleum Refining Processes*. Marcel Dekker: New York, NY, 2002.

Speight, J.G. *Fouling in Refineries*. Gulf Professional Publishing: Amsterdam, Netherlands, 2015.

Speight, J.G. Resids. In: *Handbook of Alternative Fuel Technologies*, 1st. ed.; S., Lee; Speight, J.G.; Loyalka, S.K., Eds.; Taylor & Francis Group: Boca Raton, FL, p. 171 - 196.

Speight, J.G. *The Chemistry and Technology of Petroleum*. 5th ed. CRC Press: Boca Raton, FL, 2014.

Speight, J.G. Visbreaking: A technology of the past and the future. *Scientia Iranica* **2012**, *19*: p. 569 - 573.

Stenseng, M; Jensen, A.; Dam-Johansen, K. Investigation of Biomass Pyrolysis by Thermogravimetric Analysis and Differential Scanning Calorimetry. *Journal of Analytical and Applied Pyrolysis* **2001**, *58 - 59*: p. 765 - 780.

Stock, L.M. Hydrogen Transfer Reactions. In. *Chemistry of Coal Conversion*; Scholsber, R.H. Plenum Press: New York, NY, 1985, p. 253 - 316.

Stratiev, D.; Shishkova, I.; Tankov, I.; Pavlova, A. Challenges in Characterization of Residual Oils. A Review. *Journal of Petroleum Science and Engineering* **2019**, *178:* p. 227 - 250.

Strausz, O. P. Lown, E. M. *The Chemistry of Alberta Oil Sands, Bitumens and Heavy Oils*. Alberta Energy Research Institute: Calgary, AB, 2003.

Structures and Dynamics of Asphaltenes; Mullins, O.C., Sheu, E.Y., Eds.; Springer Science+Business Media: New York, 1998.

Subramanian, S.; Simon, S.; Sjöblom, J. Asphaltene Precipitation Models: A Review. *Journal of Dispersion Science and Technology* **2016**, *37*: p. 1027 - 1049.

Suzuki, T.; Itoh, M.; Takegami, Y.; Watanabe, Y. Chemical Structure of Tar-sand Bitumens by ^{13}C and [1]H N.M.R. Spectroscopic Methods. *Fuel* **1982**, *61*: p. 402 - 410.

Tanaka, R.; Sato, S.; Takanohashi, T.; Hunt, J.E.; Winans, R. Analysis of the Molecular Weight Distribution of Petroleum Asphaltenes Using Laser Desorption-Mass Spectrometry. *Energy and Fuels* **2004**, *18*: p. 1405 - 1413.

Tannous, J. H. Heavy Products Formation in Free Radical Systems during Thermal Conversion of Heavy Oil. PhD Thesis, University of Alberta, 2019.

Tannous, J. H.; De Klerk, A. Quantification of the Free Radical Content of Oilsands Bitumen Fractions. *Energy and Fuels* **2019**, *33*: p. 7083 - 7093.

Tannous, J.H.; De Klerk, A. Asphaltenes Formation during Thermal Conversion of Deasphalted Oil. *Fuel* **2019**, *255*: p. 115786.

Tannous, J.H.; De Klerk, A. Methyl and Hydrogen Transfer in Free Radical Reactions. *Energy and Fuels* **2020**, *34*: p. 1698 - 1709.

Tannous, J.H.; Tulegenova, D.; De Klerk, A. Effect of Solvents on Persistent Free Radical Content in the Absence of Reactions. *Energy and Fuels* **2022**, *36*: p. 5253 - 5266.

Taylor, S.D.; Czarnecki, J.; Masliyah, J. Refractive Index Measurements of Diluted Bitumen Solutions. *Fuel* **2001**, *80*: p. 2013 - 2018.

Tipman, R. Froth Treatment. In: *Handbook on theory and practice of bitumen recovery from Athabasca oil sands. Vol. II. Industrial practice*, Masliyah, J.; Xu, Z.; Dabros, M., editor. Kingsley Knowledge Publishing, 2013, p. 211 - 253.

Trejo, F.; Ancheyta, J.; Noyola, A.; Sámano, V. Cracking of Maya Crude Asphaltenes. *Petroleum Science and Technology* **2014**, *32*: p. 2592 - 2598.

Tulegenova, D. Physical Properties of Bitumen Distillation Fractions and Solvent Effect on Free Radical Content. MSc Thesis, University of Alberta, 2021.

Turuga, A.S.S. Effect of Solvent Deasphalting Process on the Properties of Deasphalted Oil and Asphaltenes from Bitumen. M.Sc. Thesis, University of Alberta, 2017.

Tye, R.C.; Gardner, R.L.; Maesono, A. Temperature Measurement and Control: Critical Parameters in Thermal Analysis Techniques. *Journal of Thermal Analysis* **1993**, *40*: p. 1009 - 1016.

Uebersfeld, J.; Etienne, A.; Combrisson, J. Paramagnetic Resonance, a New Property of Coal-like Materials. *Nature* **1954**, *174*: p. 614.

Umar, A.A.; Saaid, I.B.M.; Sulaimon, A.A.; Pilus, R.B.M. A Review of Petroleum Emulsions and Recent Progress on Water-in-crude Oil Emulsions Stabilized by Natural Surfactants and Solids. *Journal of Petroleum Science and Engineering* **2018** *165*: p. 673 - 690.

Van Krevelen, D. W. *Coal. Typology–Physics–Chemistry–Constitution.* 3ed; Elsevier: Amsterdam, 1993.

Velayati, A., Nouri, A. Emulsification and Emulsion Flow in Thermal Recovery Operations with a Focus on SAGD Operations: A Critical Review. *Fuel* **2020**, *267*: p. 117141.

Wang, L. Low temperature visbreaking. MSc Thesis, Edmonton: University of Alberta, 2013.

Wang, L. Low temperature visbreaking. MSc Thesis, University of Alberta, 2013.

Wang, L.; Zachariah, A.; Yang, S.; Prasad, V.; De Klerk, A. Visbreaking Oilsands-Derived Bitumen in the Temperature Range of 340−400 °C. *Energy and Fuels* **2014**, *28*: p. 5014 - 5022.

Wang, T.; Zhang, C.; Zhao, R.; Zhu, C.; Yang, C.; Liu, C. Solvent Extraction of Bitumen from Oil Sands. *Energy and Fuels* **2014**, *28*: p. 2297 - 2304.

Ward, A. L.; Kurtz, S. S. Jr. Refraction, Dispersion, and Related Properties of Pure Hydrocarbons. Arranged for Use in the Analysis of Hydrocarbon Mixtures. *Industrial and Engineering Chemistry, Analytical Edition* **1938**, *10*: p. 559 - 576.

Watson, K.M.; Nelson, E.F. Improved Methods for Approximating Critical and Thermal Properties of Petroleum Fractions. *Industrial and Engineering Chemistry* **1933**, *25*: p. 880 - 887.

Wattana, P.; Wojciechowski, D. J.; Bolaños, G.; Fogler, H. S. Study of Asphaltene Precipitation using Refractive Index Measurement. *Petroleum Science and Technology* **2003**, *21*: p. 591 - 613.

Wen, C.S.; Chilingarian, G. V.; Yen, T.F. Properties and Structure of Bitumens. In: *Bitumen, Asphalts and Tar Sands*. Chilingarian, G.V.; Yen, T.F., Eds.; Elsevier Scientific Publishing Company: Amsterdam, Netherlands,1978, p. 162.

Wen, Q.; Shen, J.; Gieleciak, R.; Michaelian, K.H.; Rohling, J.H.; Astrath, N.G.C.; Baesso, M.L. Temperature Coefficients of the Refractive Index for Complex Hydrocarbon Mixtures. *International Journal of Thermophysics: Journal of Thermophysical Properties and Thermophysics and its Applications* **2014**, *35*, p. 930 - 941.

Wiehe, I. A. A Solvent-Resid Phase Diagram for Tracking Resid Conversion. *Industrial and Engineering Chemistry Research* **1992**, *31*: p. 530 - 536.

Wiehe, I.A. A Phase-Separation Kinetic Model for Coke Formation. *Industrial and Engineering Chemistry Research* **1993**, *32*: p. 2447 - 2454.

Wiehe, I.A. The Pendant-Core Building Block Model of Petroleum Residua. *Energy and Fuels* **1994**, *8*: p. 536 - 544.

Wiehe, I.A. The Chemistry of Coke Formation from Petroleum: A Tutorial. In: *Preprint National Meeting - American Chemical Society Division of Petroleum Chemistry* **1998**, p. 612 - 615.

Wiehe, I.A.; Kennedy, R.J. Oil compatibility model and crude oil incompatibility. *Energy and Fuels* **2000**, *14*: p.56 - 59.

Wiehe, I.A. *Process Chemistry of Petroleum Macromolecules*. CRC Press: Boca Raton, FL, 2008.

Winter, J.; Goodday, V.; Fellows, K. Enabling Partial Upgrading in Alberta: A review of the Regulatory Framework and Opportunites for Improvement. *The School of Public Policy Publications* **2019**, *12:* p. 1 - 47.

Xu, R. Settling Behavior in the Dewatering Process for Bitumen Froth with Different Qualities. MSc Thesis, University of Alberta, 2018.

Yan, N.; Masliyah, J.H. Adsorption and Desorption of Clay Particles at the Oil-Water Interface. *Journal of Colloid and Interface Science* **1994**, *168*: p. 386 - 392.

Yan, T. Y. Characterization of Visbreaker Feeds. *Fuel* **1990**, *69*: p. 1062 - 1064.

Yan, Y.; De Klerk, A.; Prado, G. H. C. Visbreaking of Vacuum Residue Deasphalted Oil: New Asphaltenes Formation. *Energy and Fuels* **2020**, *34*: p. 5135 - 5147.

Yan, Y.; Prado, G.H.C.; De Klerk, A. Storage Stability of Products from Visbreaking of Oilsands Bitumen. *Energy and Fuels* **2020**, *34*: p. 9585 - 9598.

Yañez Jaramillo, L.M. Visbreaking of Oilsands Bitumen between 150 and 300 ºC. M.Sc. Thesis, University of Alberta, 2016.

Yañez Jaramillo, L.M. Visbreaking of Oilsands Bitumen between 150 and 300 ºC. MSc Thesis, University of Alberta, 2016.

Yañez Jaramillo, L.M.; de Klerk, A. Is Solubility Classification a Meaningful Measure in Thermal Conversion? *Energy & Fuels* **2022**, *36*: p. 8649 - 8662.

Yañez Jaramillo, L.M.; Link, F.; De Klerk, A. Relationship between Aromatic hydrogen and Aromatic Carbon in Straight Run and Converted Oils. *Fuel* **2022**, *327*: p. 124414.

Yarranton, H.; Baydak, E.N. Effect of Solvents on the Stability of Water-in-Bitumen Emulsions. *Energy and Fuels* **2022**, *36*: p. 6243 - 6260.

Yen, T.F.; Erdman, J.G.; Saraceno, A.J. Investigation of the Nature of Free Radicals in Petroleum Asphaltenes and Related Substances by Electron Spin Resonance. *Analytical Chemistry* **1962**, *34*: p. 694 - 700.

Yen, T.F.; Sprang, S.R. ESR g-Values of Bituminous Materials. In: *ACS Meeting, Petroleum Chemistry*, Chicago, IL, 1970, p. A65 - A76.

Yokono, T.; Obara, T.; Sanada, Y.; Shimomura, S.; Imamura, T. Characterization of Carbonization Reaction of Petroleum Residues by Means of High-Temperature ESR and Transferable Hydrogen. *Carbon* **1986**, *24*: p. 29 - 32.

Zachariah, A. Low temperature pyrolysis and its application in bitumen processing. MSc Thesis, University of Alberta, 2014.

Zachariah, A.; De Klerk, A. Thermal Conversion Regimes for Oilsands Bitumen. *Energy and Fuels* **2016**, *30*: p. 239 - 248.

Zachariah, A.; Wang, L.; Yang, S.; Prasad, V.; De Klerk, A. Suppression of Coke Formation during Bitumen Pyrolysis. *Energy and Fuels* **2013,** *27*: p. 3061 - 3070.

Zhang, N.; Zhao, S.; Sun, X.; Xu, Z.; Xu, C. Storage Stability of the Visbreaking Product from Venezuela Heavy Oil. *Energy and Fuels* **2010**, *24*: p. 3970 - 3976.

Zhang, Y.; Siskin, M.; Gray, M.R.; Walters, C.C.; Rodgers, R.P. Mechanisms of Asphaltene Aggregation: Puzzles and a New Hypothesis. *Energy and Fuels* **2020**, *34*: p. 9094 - 9107.

Zhou, S.; Huang, H.; Liu, Y. Biodegradation and Origin of Oil Sands in the Western Canada Sedimentary Basin. *Petroleum Science*, **2008**, *5*: p. 87 - 94.

Appendix A

Table A-1. Gas Chromatography analysis of gaseous fraction resulted from the thermal conversion reactions.

Asphaltenes concentration [wt.%][a]	Nominal reaction time [min]	Composition [%]								
		C_1	C_2	C_3	C_4	C_5	C_6	CO_2	N_2	CO
	0	0.5	0.6	0.1	0.0	0.0	2.7	0.0	87.8	8.3
	5	0.6	0.2	0.1	0.1	0.2	0.5	0.0	98.0	0.3
0	10	1.3	0.5	0.5	0.2	0.2	0.7	0.6	95.3	0.4
	47	3.9	1.5	1.4	0.7	0.9	1.0	0.0	90.0	0.5
	146	7.4	3.1	2.6	1.3	1.5	1.0	0.0	82.6	0.5
	0	0.0	0.0	0.0	0.0	0.0	0.3	0.0	80.8	0.6
	5	0.0	0.0	0.0	0.0	0.0	0.0	0.0	80.1	0.6
9	10	3.7	1.5	1.2	0.5	0.4	0.5	0.0	89.8	0.8
	47	3.9	1.5	1.2	0.5	0.4	0.7	0.0	91.0	0.9
	146	6.8	3.0	2.5	1.2	1.5	1.2	0.0	78.4	0.8
	0	4.8	1.9	1.9	1.2	2.1	0.3	2.1	84.7	0.7
	5	1.3	0.5	0.5	0.3	0.9	0.0	0.0	95.8	0.7
18.6	10	2.4	1.0	1.1	0.7	1.5	0.2	0.0	91.5	0.5
	47	3.9	0.0	1.4	0.8	1.1	0.8	0.0	91.0	0.5
	146	8.6	3.7	3.1	1.7	2.8	0.4	0.0	78.9	0.9
	0	0.8	0.3	0.3	0.2	0.0	1.5	0.0	94.5	1.2
	5	4.7	1.9	1.8	1.1	2.1	0.8	0.0	86.8	0.9
28	10	2.5	1.0	0.7	0.6	2.6	4.2	0.0	82.2	6.1
	47	7.5	3.2	3.0	1.9	4.0	0.6	0.1	77.8	0.7
	146	8.2	3.7	3.6	2.4	4.6	0.9	0.1	74.6	0.7

[a] Description presented in Chapter 3.

Appendix B

Table B-1. Material balance for thermal conversion.

Asphaltenes concentration [wt.%][a]	Nominal reaction time [min]	Initial			Final			Product separation	
		Feed [g]	N_2 [g]	Total [g]	Product [g]	Gas [g]	Total [g]	Liquid [g]	Solid [g]
	0	12.03	1.0	13.03	12.03	1.0	13.03	11.88	0.017
	5	12.02	1.3	13.32	11.94	1.0	12.94	11.78	0.053
0	10	12.02	1.0	13.02	12.37	1.0	13.37	11.77	0.069
	47	12.04	1.6	13.64	12.25	1.4	13.65	12.12	0.039
	146	12.05	1.3	13.35	11.79	1.4	13.19	11.64	0.051
	0	11.94	1.0	12.94	11.96	1.0	12.96	11.76	0.101
	5	11.96	1.3	13.26	11.96	1.1	13.06	11.75	0.152
9	10	11.97	1.0	12.97	12.34	0.9	13.24	12.02	0.207
	47	11.98	1.0	12.98	11.74	1.0	12.74	11.51	0.181
	146	12.01	1.0	13.01	11.72	1.1	12.82	11.42	0.214
	0	12.37	1.0	13.37	11.97	1.0	12.97	11.53	0.374
	5	11.98	1.5	13.48	12.42	1.5	13.92	12.18	0.135
18.6	10	12.00	1.0	13.00	12.04	1.0	13.04	11.74	0.222
	47	12.02	1.0	13.02	11.97	1.6	13.57	11.64	0.261
	146	12.03	1.2	13.23	12.00	1.6	13.6	11.65	0.260
	0	12.30	1.1	13.40	12.28	1.5	13.78	12.02	0.146
	5	12.35	1.2	13.55	12.01	1.2	13.21	11.73	0.214
28	10	12.44	1.0	13.44	11.98	0.9	12.88	11.54	0.382
	47	12.30	0.9	13.20	12.00	1.0	13.00	11.47	0.469
	146	12.45	1.2	13.65	12.38	1.0	13.38	11.82	0.470

[a] Description presented in Chapter 3.

Table B-2. Material balance closure.

Asphaltenes concentration [wt.%][a]	Nominal reaction time [min]	$m_{feed} + m_{nitrogen}$ [g]	$m_l + m_s + m_g$ [g]	Material balance closure [%]	Pressure during reaction [MPa]
0	0	13.03	12.90	99.0	4.0
	5	13.32	12.83	96.3	4.0
	10	13.02	12.84	98.6	4.0
	47	13.64	13.56	99.4	4.0
	146	13.35	13.09	98.1	4.8
9	0	12.94	12.86	99.4	3.8
	5	13.26	13.00	98.0	4.0
	10	12.97	13.13	101.2	4.0
	47	12.98	12.69	97.8	4.0
	146	13.01	12.74	97.9	4.5
18.6	0	13.37	12.90	96.5	4.0
	5	13.48	13.82	102.5	4.0
	10	13.00	12.96	99.7	4.0
	47	13.02	13.50	103.7	4.0
	146	13.23	13.51	102.1	4.5
28	0	13.40	13.67	102.0	4.0
	5	13.55	13.15	97.0	4.0
	10	13.44	12.82	95.4	4.0
	47	13.20	12.94	98.1	4.0
	146	13.65	13.29	97.4	4.5

[a] Description presented in Chapter 3.

Appendix C

To ensure proper quantitation, the following measures were taken during the ^{13}C NMR analysis: (i) Chromium (III) acetylacetonate as relaxation agent to reduce relaxation times; (ii) 30º Ernst angle pulse; (iii) a relaxation delay of 2.5 seconds determined by the NMR facility due to the characteristics of the sample [1]; (iv) the pulse sequence used was a 1-D sequence with inverse decoupling and the noise decoupler being on during the pulse, but off during the pulse delay. This represents a no nOe pulse sequence. The detailed sequence is shown in **Figure C-1**.
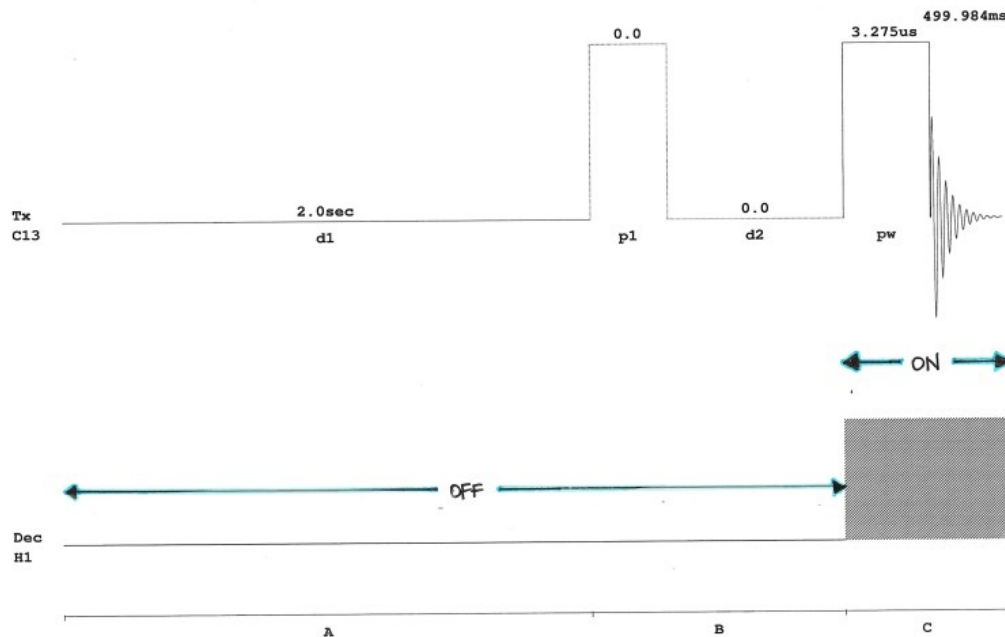
Figure C-1. Inverse Gated Coupling sequence

As was indicated in the manuscript, various straight run and thermally converted materials were analyzed by ^{1}H and ^{13}C NMR spectrometry. These materials supplemented the data that was

[1] Čuperlović-Culf M. Experimental methodology. In: *NMR Metabolomics in Cancer Research*. Woodhead Publishing Series in Biomedicine 63; Cambridge, U.K: Woodhead Publishing; 2013, p. 139 - 213.

obtained from literature. In the manuscript, only the integrated values are used and reported. The spectra contain more information and are included here. For each sample the ^{1}H and ^{13}C NMR spectra are provided, with details about the origin of the sample in the caption.

To assist with navigation, the following groups are identified:

(a) Unconverted oilsands bitumen and sub-fractions, and Straight run (Figures S2–S25).

(b) Thermally converted oilsands bitumen and bitumen-related products (Figures S26-S45).
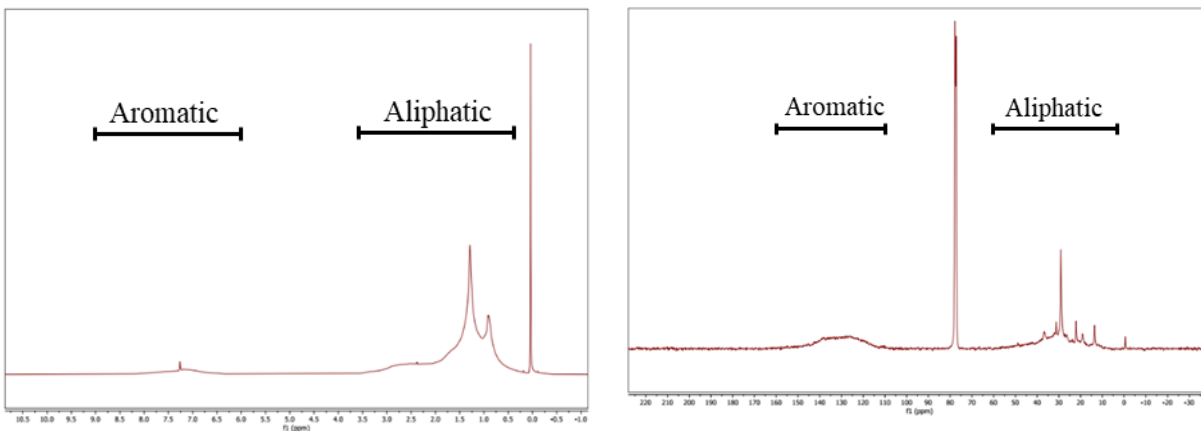
Figure C-2. ^{1}H and ^{13}C NMR spectra from *n*-heptane insolubles (asphaltenes) from Athabasca bitumen, respectively. Integration regions are indicated and correspond to what was used in this work.
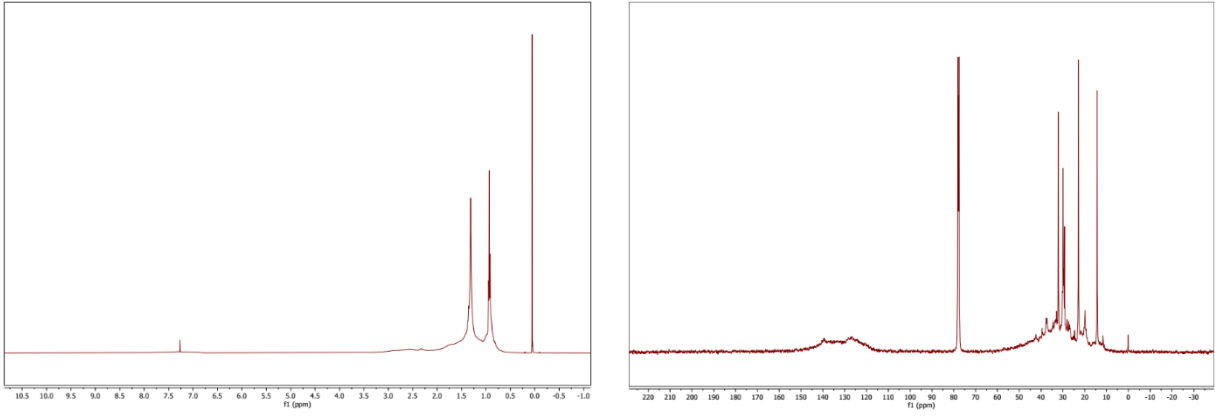
Figure C-3. ^{1}H and ^{13}C NMR spectra from *n*-heptane solubles (maltenes) from Athabasca bitumen, respectively.
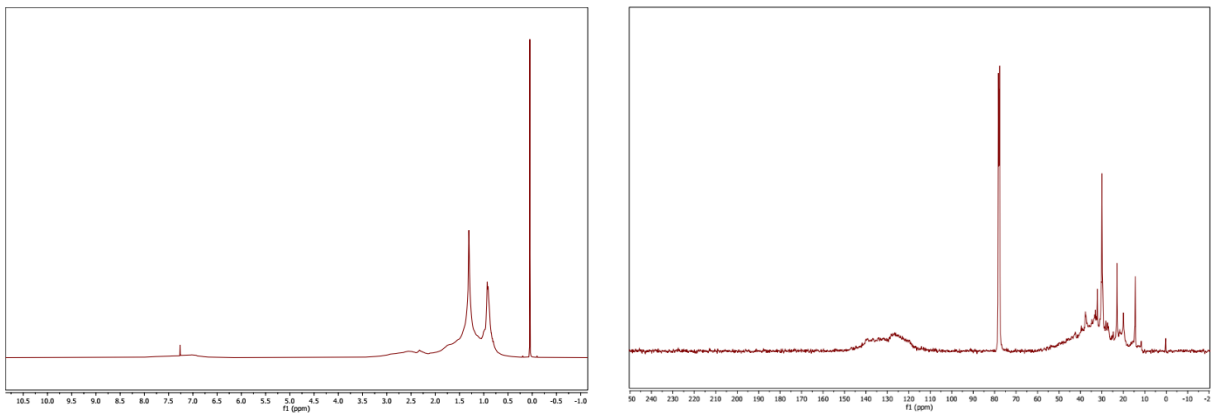
Figure C-4. ^{1}H and ^{13}C NMR spectra of Athabasca bitumen respectively.
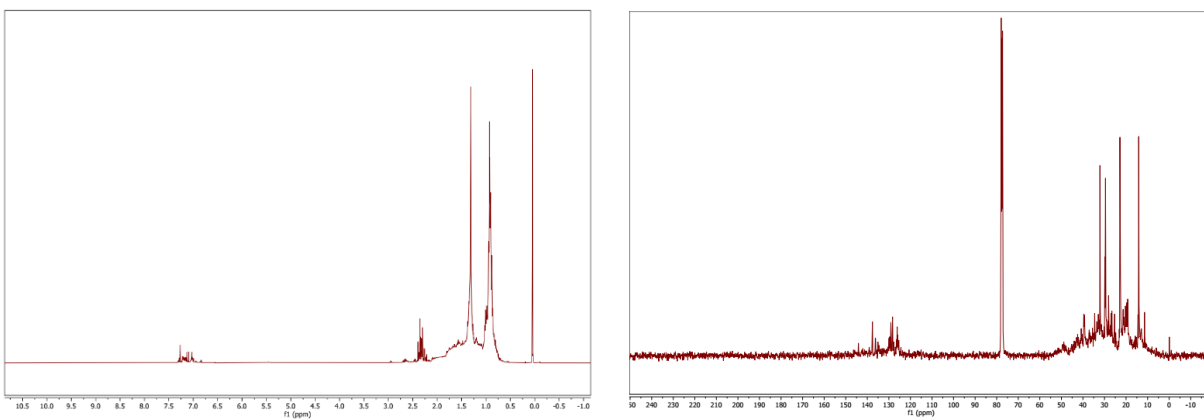
Figure C-5. ^{1}H and ^{13}C NMR spectra of the <150 ºC distillation fraction from vacuum distillation of Athabasca bitumen, respectively.
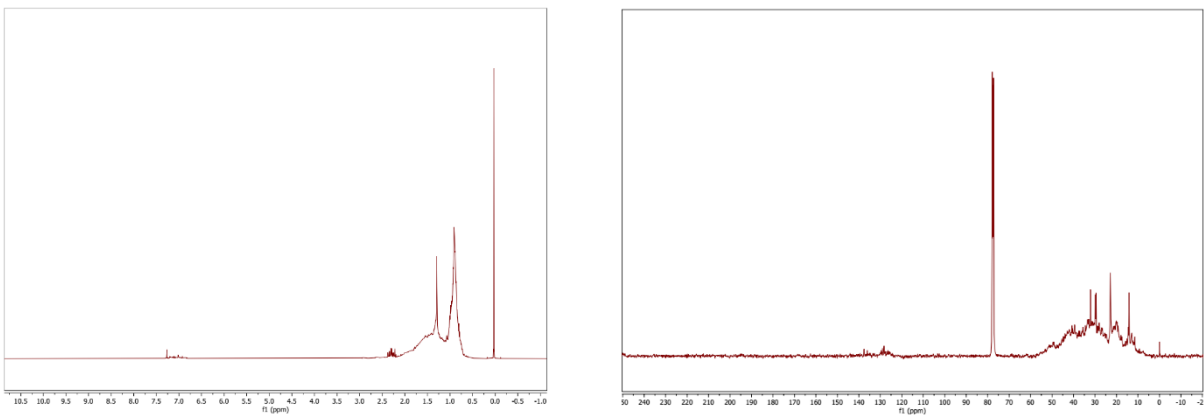
Figure C-6. ^{1}H and ^{13}C NMR spectra of the 150-170 ºC distillation fraction from vacuum distillation of Athabasca bitumen, respectively.
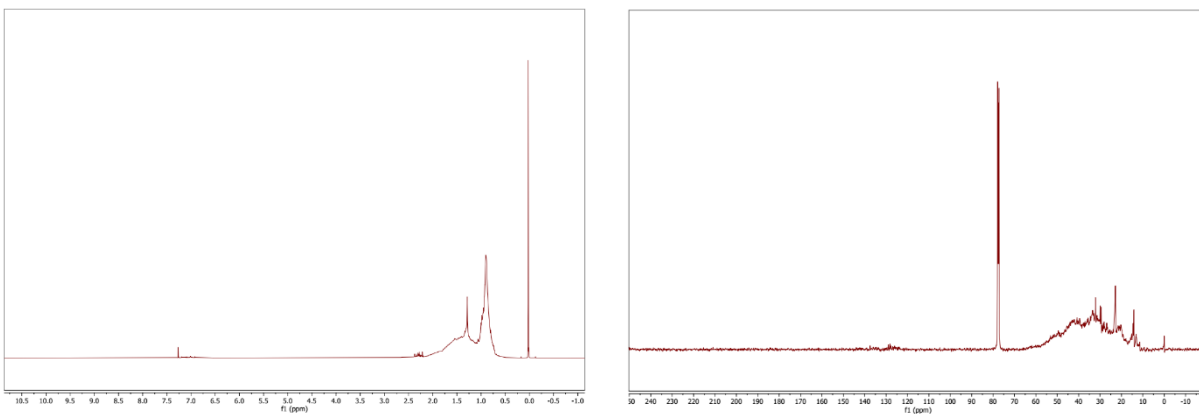
Figure C-7. ^{1}H and ^{13}C NMR spectra of the 170-190 ºC distillation fraction from vacuum distillation of Athabasca bitumen, respectively.
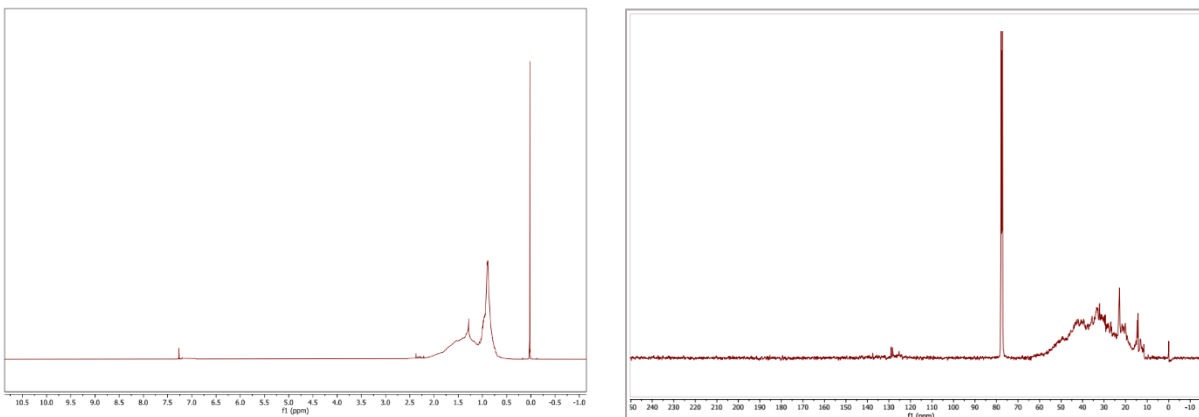
Figure C-8. ^{1}H and ^{13}C NMR spectra of the 190-210 ºC distillation fraction from vacuum distillation of Athabasca bitumen, respectively.

227
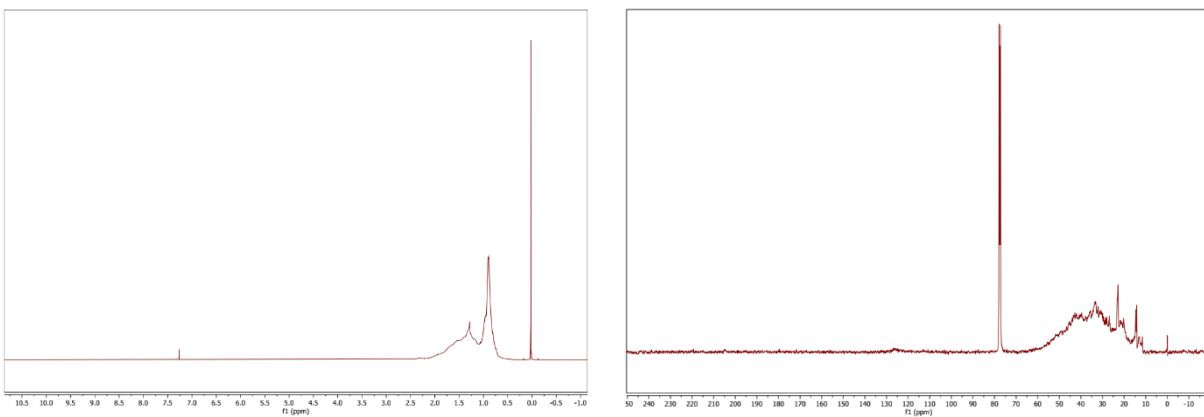
Figure C-9. ^{1}H and ^{13}C NMR spectra of the 210-230 ºC distillation fraction from vacuum distillation of Athabasca bitumen, respectively.
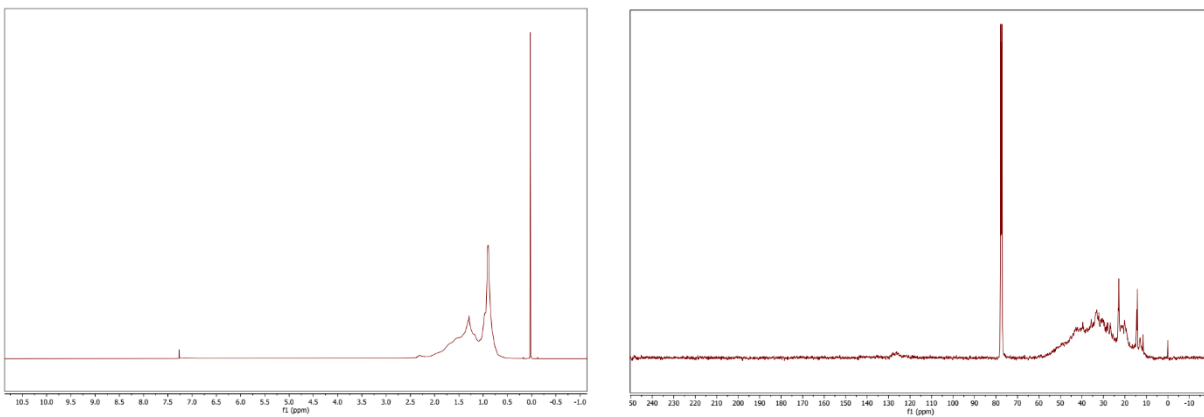
Figure C-10. ^{1}H and ^{13}C NMR spectra of the 230-250 ºC distillation fraction from vacuum distillation of Athabasca bitumen, respectively.
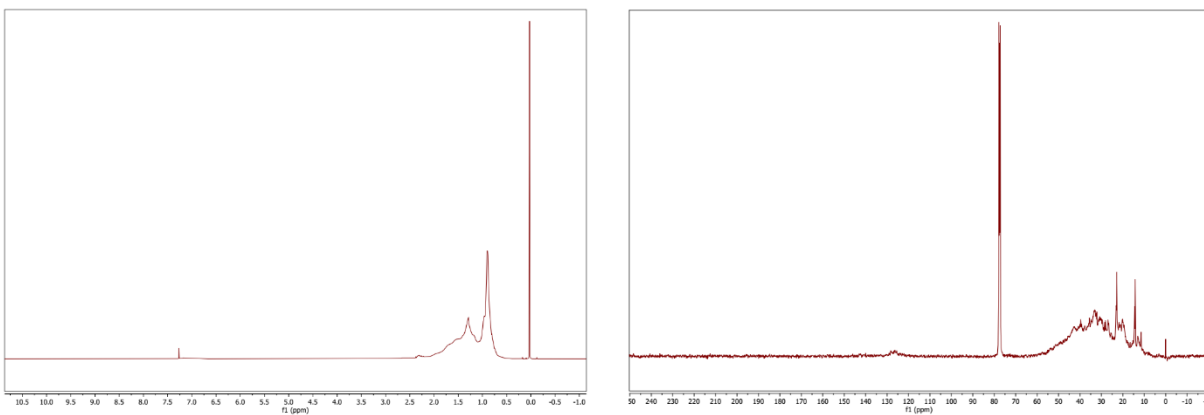
Figure C-11. ^{1}H and ^{13}C NMR spectra of the 250-270 ºC distillation fraction from vacuum distillation of Athabasca bitumen, respectively.
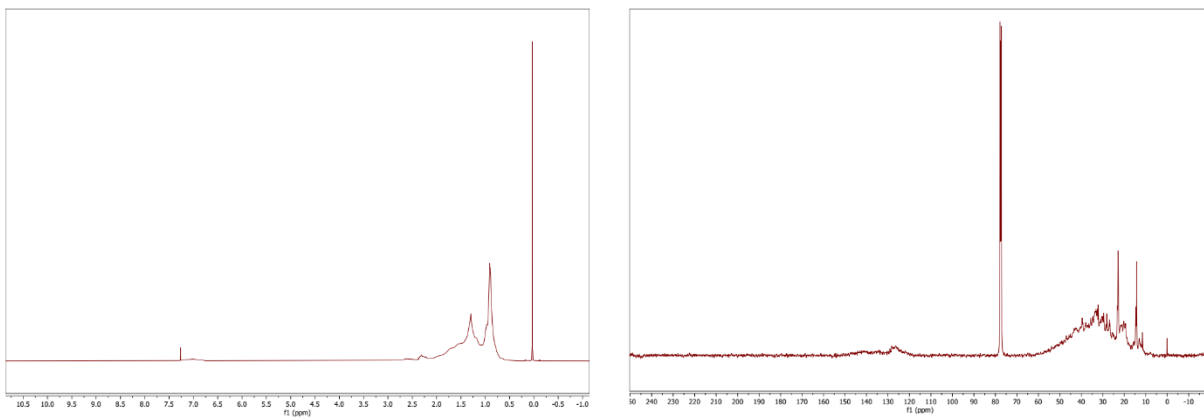
Figure C-12. ^{1}H and ^{13}C NMR spectra of the 270-290 ºC distillation fraction from vacuum distillation of Athabasca bitumen, respectively.
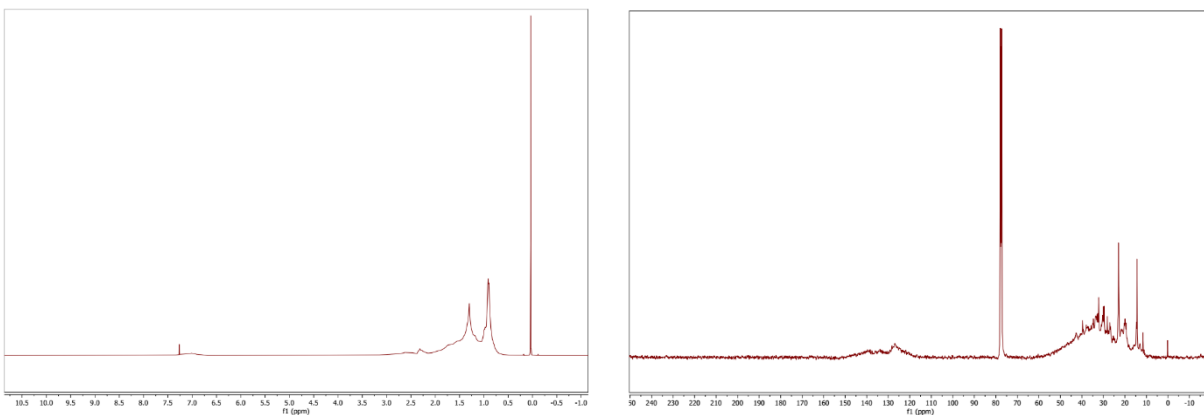
Figure C-13. ^{1}H and ^{13}C NMR spectra of the 290-310 ºC distillation fraction from vacuum distillation of Athabasca bitumen, respectively.
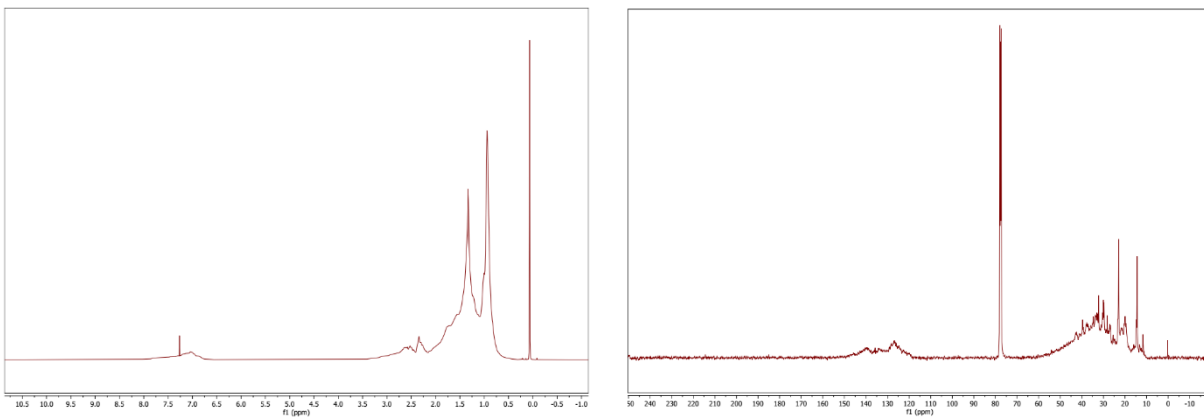
Figure C-14. ^{1}H and ^{13}C NMR spectra of the 310-330 ºC distillation fraction from vacuum distillation of Athabasca bitumen, respectively.
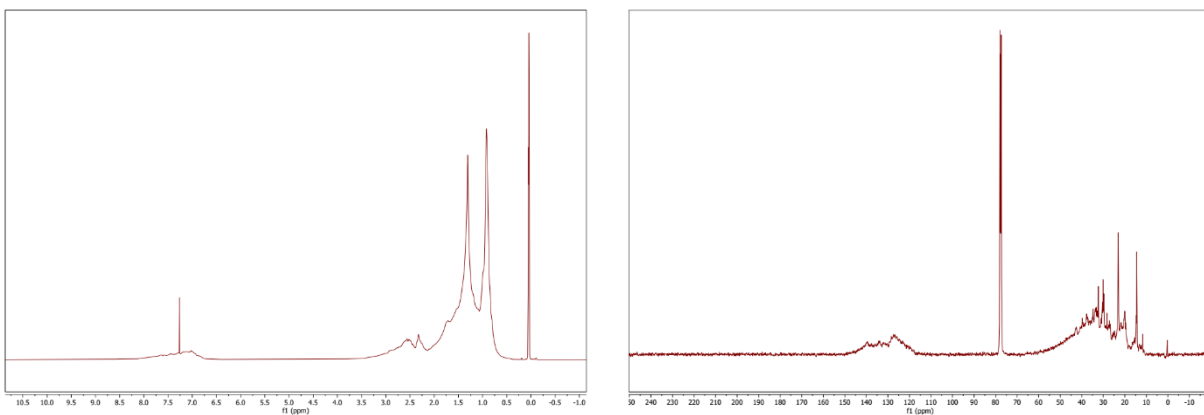
Figure C-15. ^{1}H and ^{13}C NMR spectra of the 330-350 ºC distillation fraction from vacuum distillation of Athabasca bitumen, respectively.
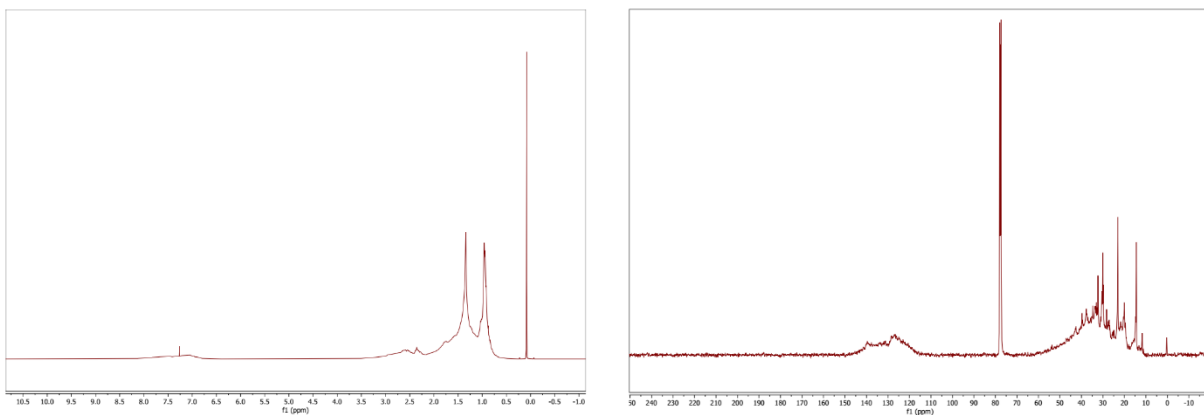
Figure C-16. ^{1}H and ^{13}C NMR spectra of the 350-370 ºC distillation fraction from vacuum distillation of Athabasca bitumen, respectively.
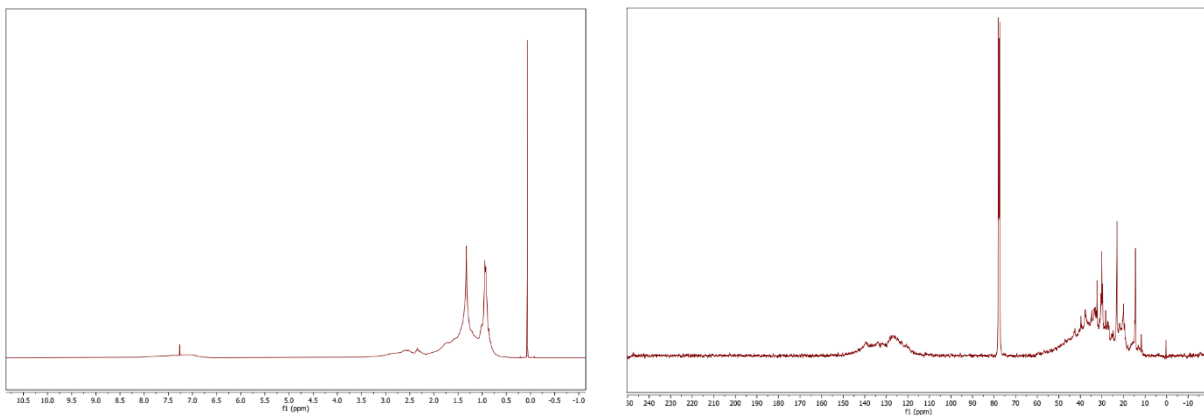
Figure C-17. ^{1}H and ^{13}C NMR spectra of the 370-390 ºC distillation fraction from vacuum distillation of Athabasca bitumen, respectively.
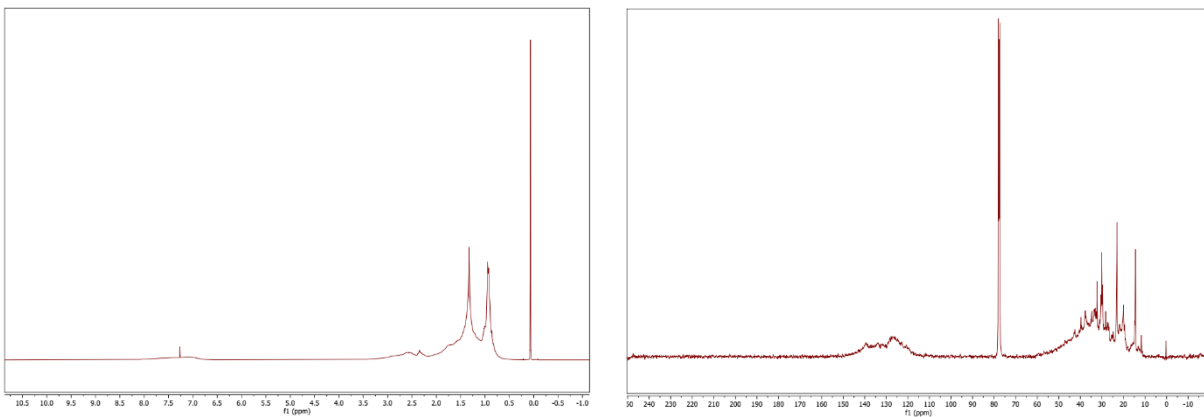
Figure C-18. ^{1}H and ^{13}C NMR spectra of the 390-410 ºC distillation fraction from vacuum distillation of Athabasca bitumen, respectively.
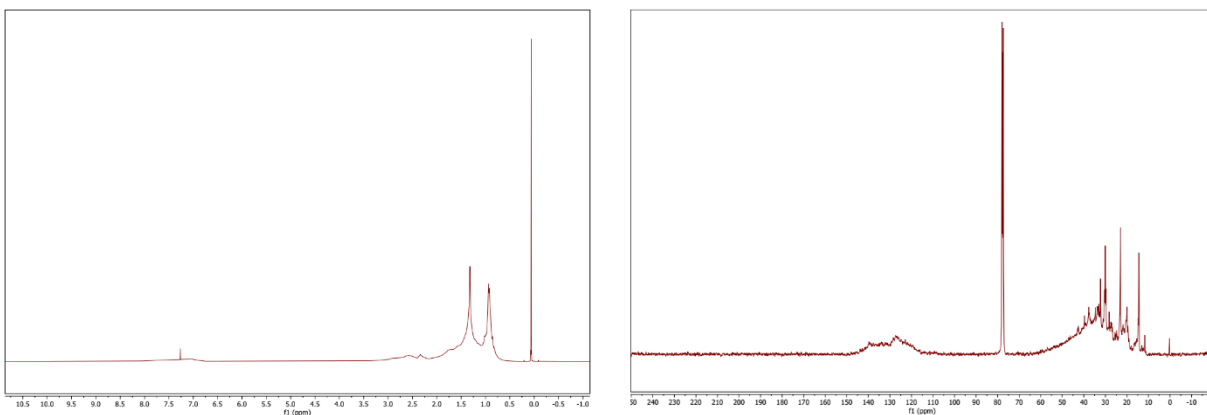
Figure C-19. ^{1}H and ^{13}C NMR spectra of the 410-430 ºC distillation fraction from vacuum distillation of Athabasca bitumen, respectively.
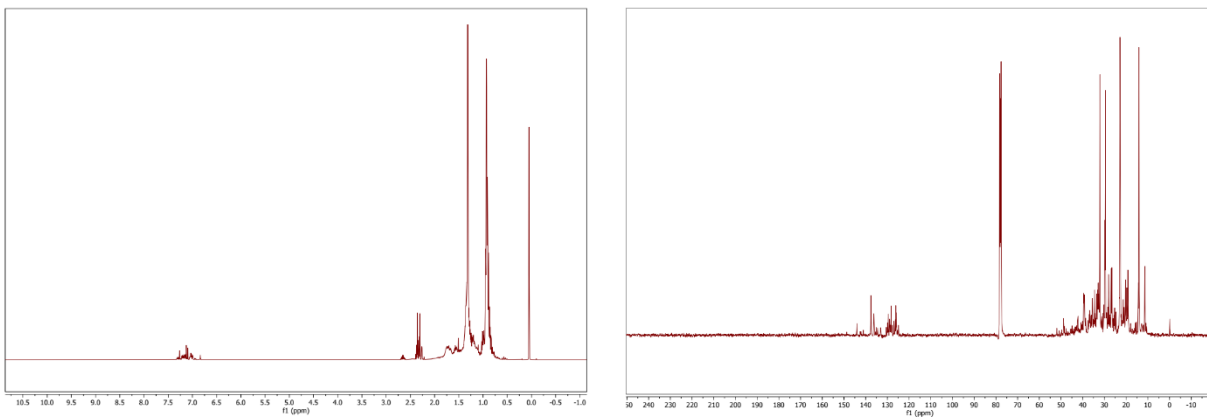
Figure C-20. ^{1}H and ^{13}C NMR spectra of the 135-140 ºC narrow distillation fraction from hydrotreated kerosene, respectively.
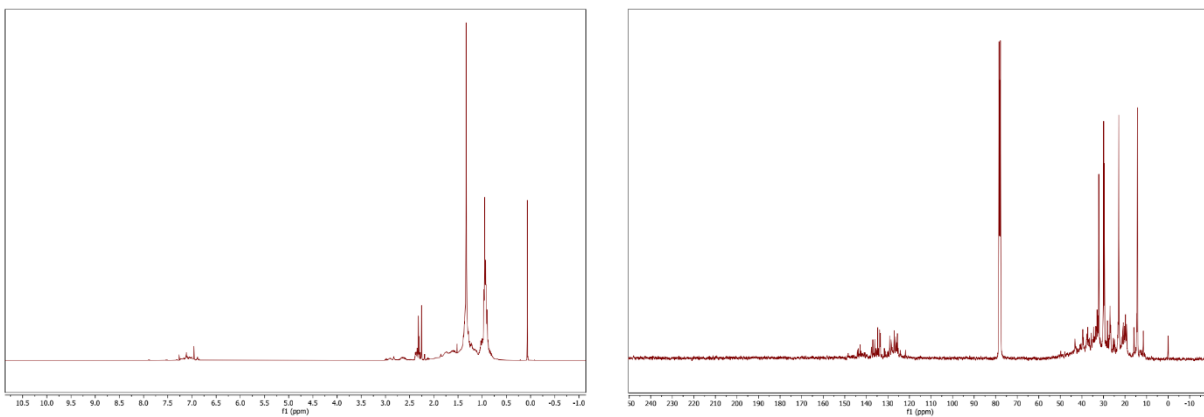
Figure C-21. ^{1}H and ^{13}C NMR spectra of the 195-200 ºC narrow distillation fraction from hydrotreated kerosene, respectively.
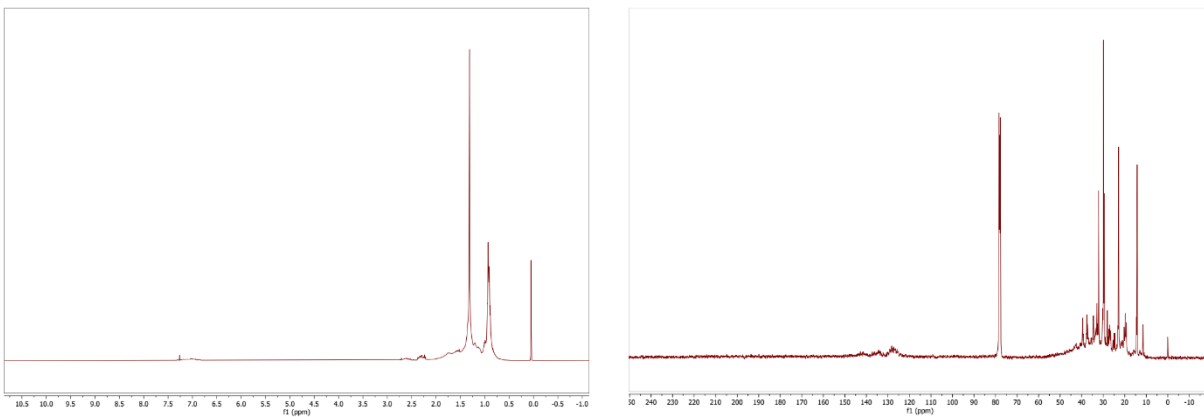
Figure C-22. ^{1}H and ^{13}C NMR spectra of the 245-250 ºC narrow distillation fraction from hydrotreated kerosene, respectively.
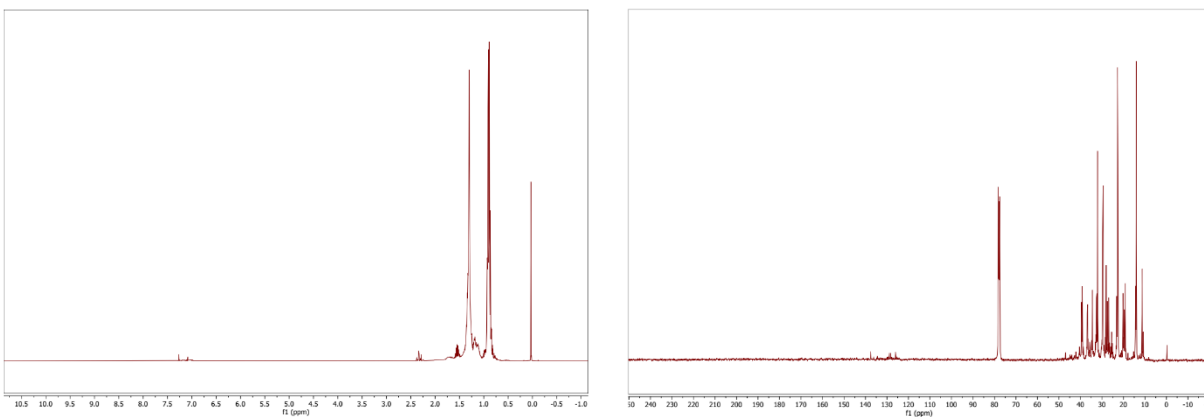
Figure C-23. ^{1}H and ^{13}C NMR spectra of the 140-145 °C narrow distillation fraction from hydrocracked wax, respectively.
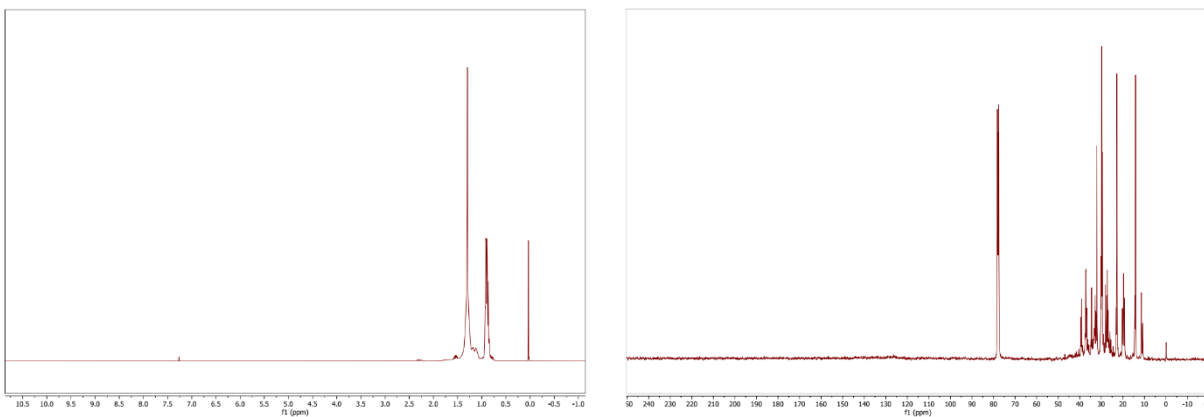
Figure C-24. ^{1}H and ^{13}C NMR spectra of the 230-235 °C narrow distillation fraction from hydrocracked wax, respectively.
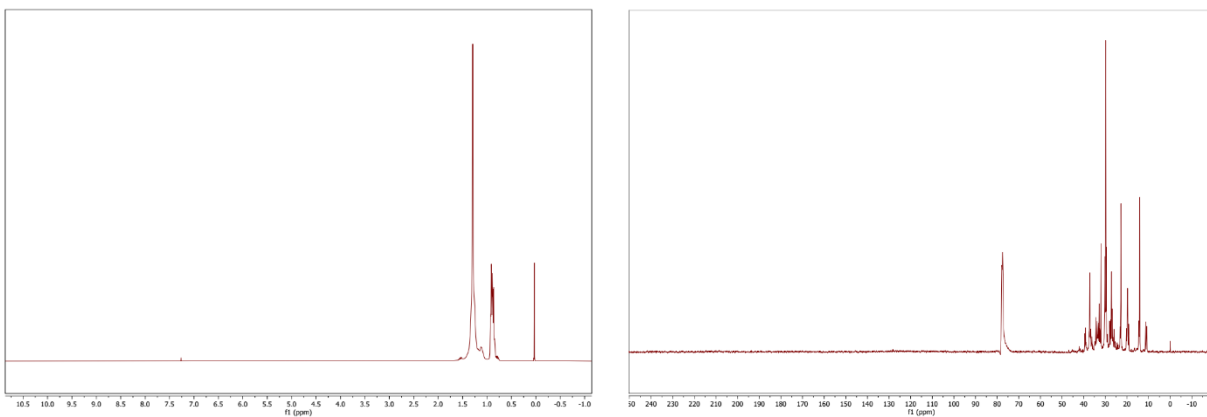
Figure C-25. ^{1}H and ^{13}C NMR spectra of the 315-320 °C narrow distillation fraction from hydrocracked wax, respectively.
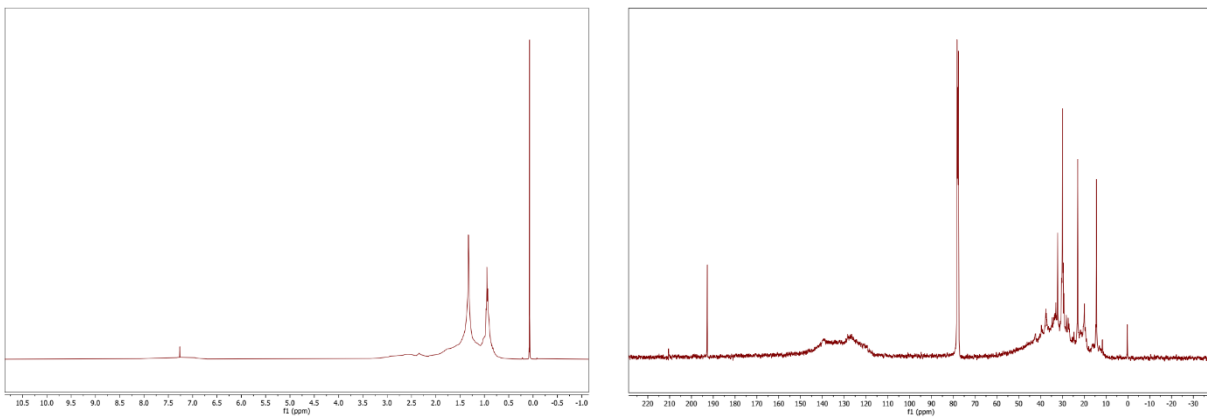
Figure C-26. ^{1}H and ^{13}C NMR spectra of maltenes thermally converted product after 0 minutes, respectively.
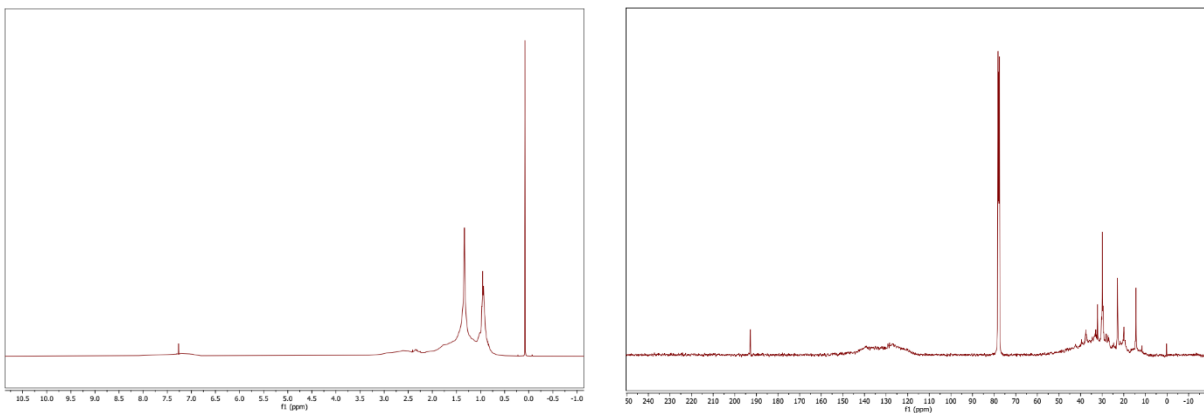
Figure C-27. ^{1}H and ^{13}C NMR spectra of maltenes thermally converted product after 5 minutes, respectively.
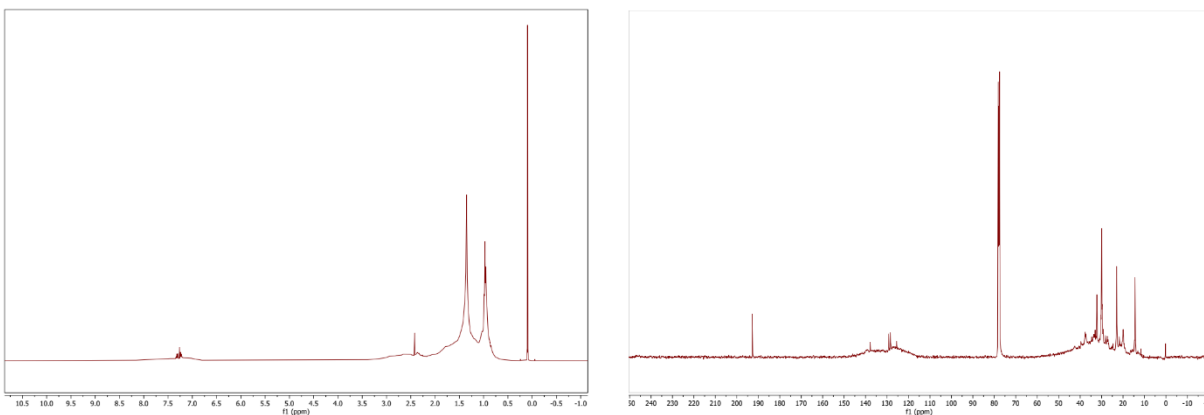
Figure C-28. ^{1}H and ^{13}C NMR spectra of maltenes thermally converted product after 10 minutes, respectively.
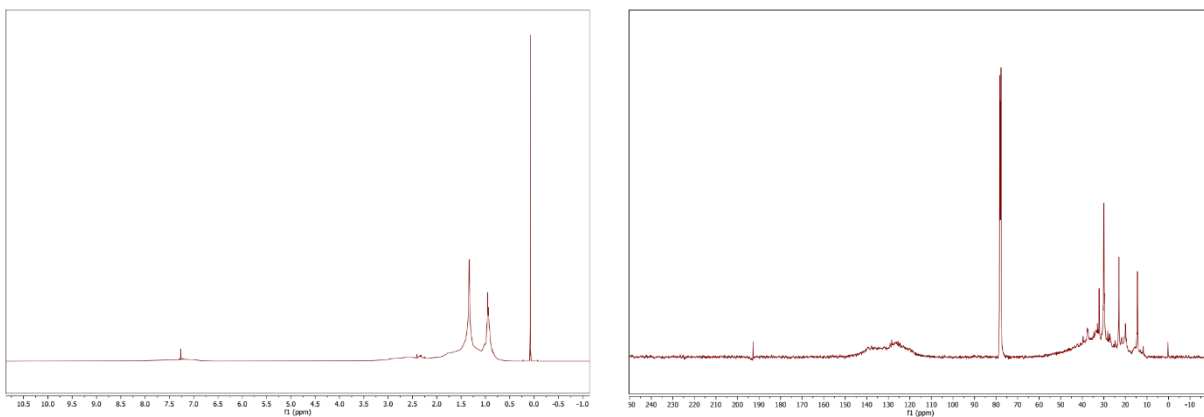
Figure C-29. ^{1}H and ^{13}C NMR spectra of maltenes thermally converted product after 47 minutes, respectively.
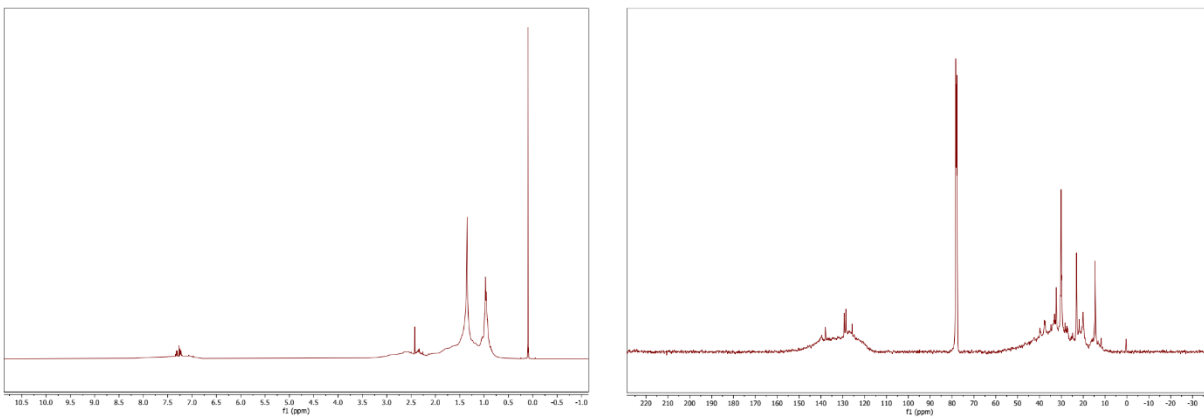
Figure C-30. ^{1}H and ^{13}C NMR spectra of maltenes thermally converted product after 146 minutes, respectively.
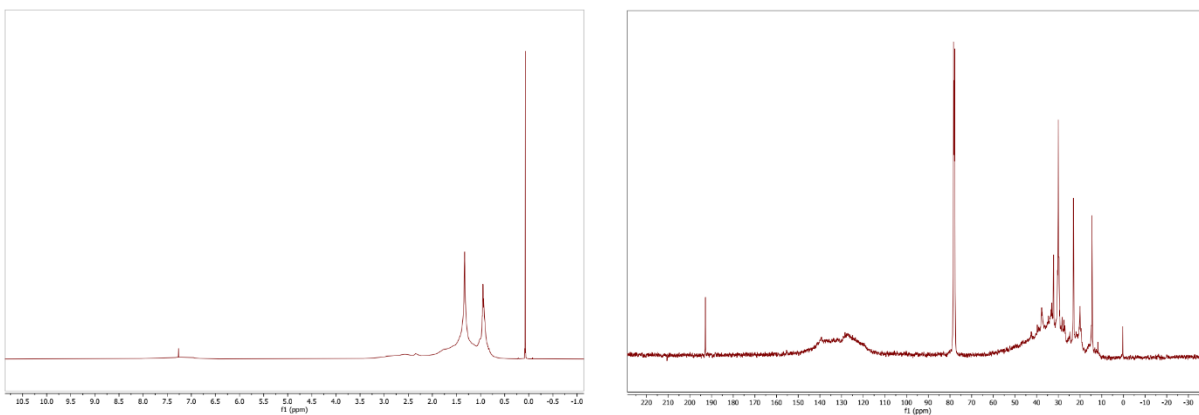
Figure C-31. ^{1}H and ^{13}C NMR spectra of maltenes and asphaltenes mixture thermally converted product after 0 minutes, respectively.
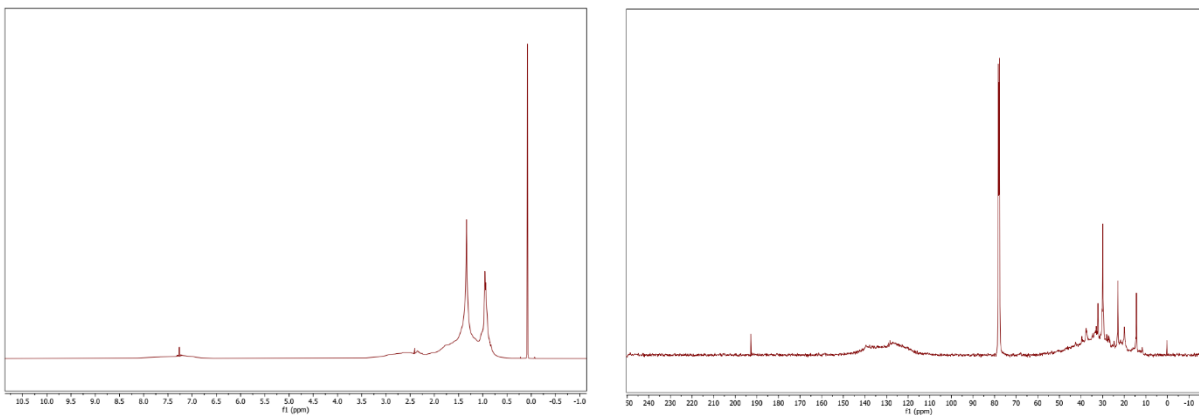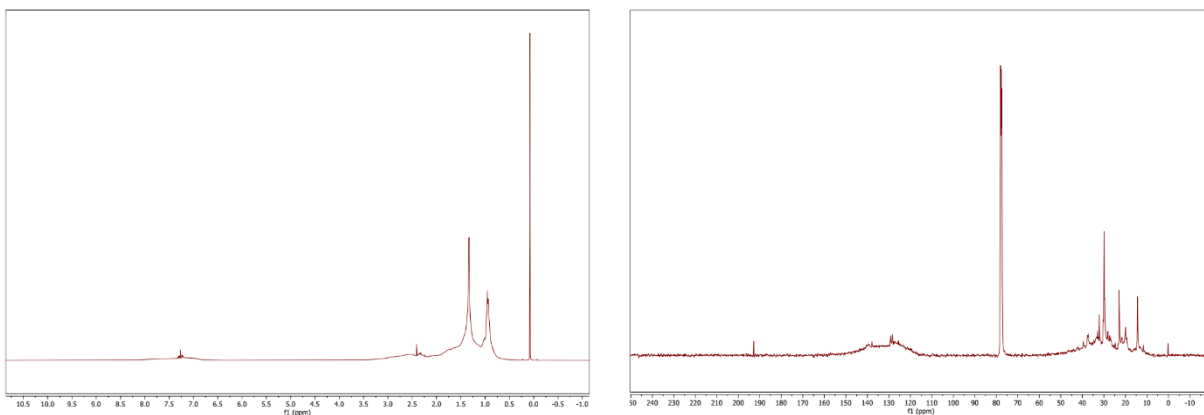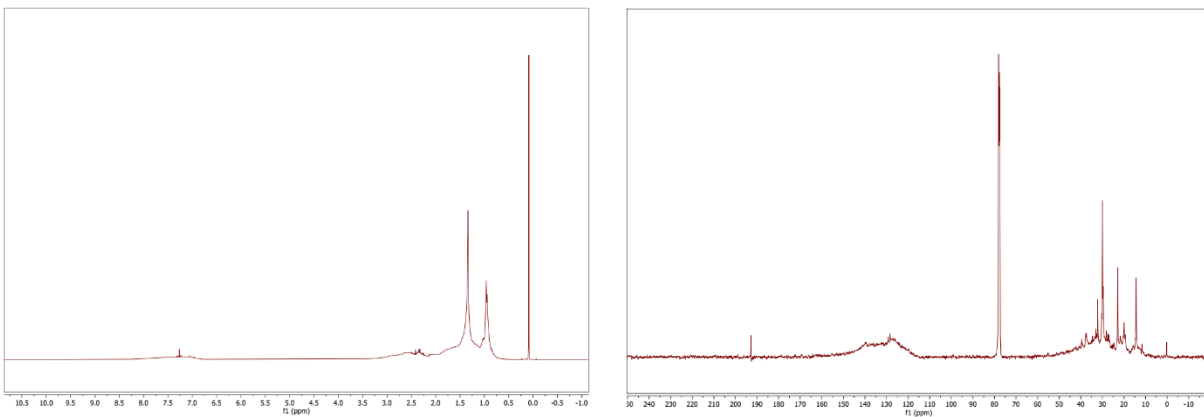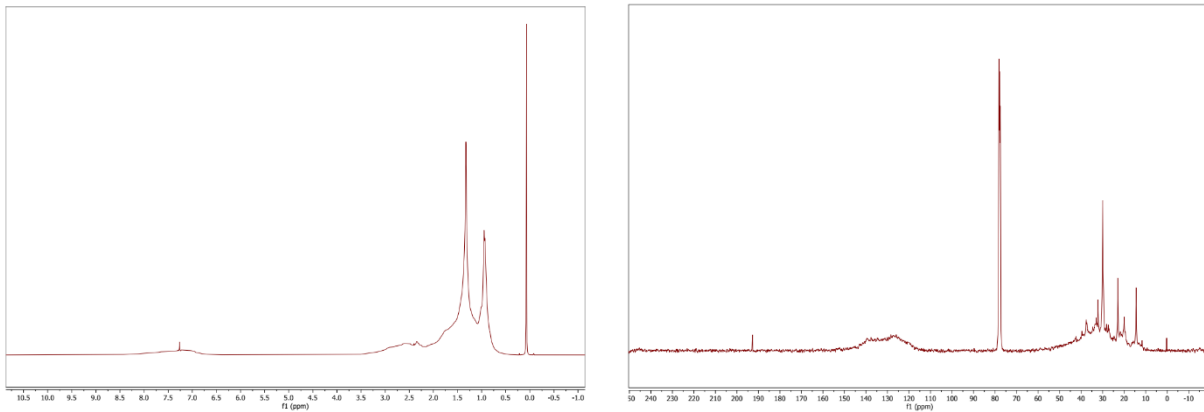

Figure C-32. ^{1}H and ^{13}C NMR spectra of maltenes and asphaltenes mixture thermally converted product after 5 minutes, respectively.
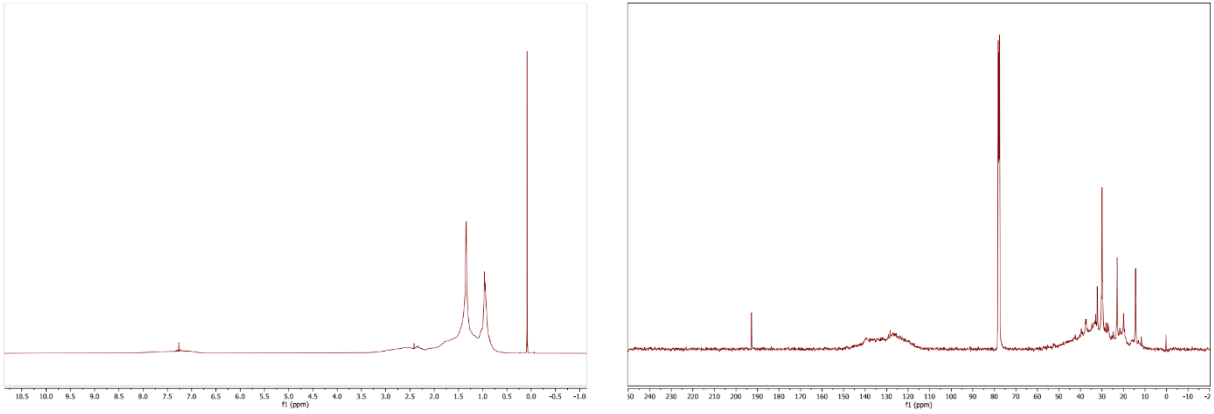
Figure C-33. ^{1}H and ^{13}C NMR spectra of maltenes and asphaltenes mixture thermally converted product after 10 minutes, respectively.
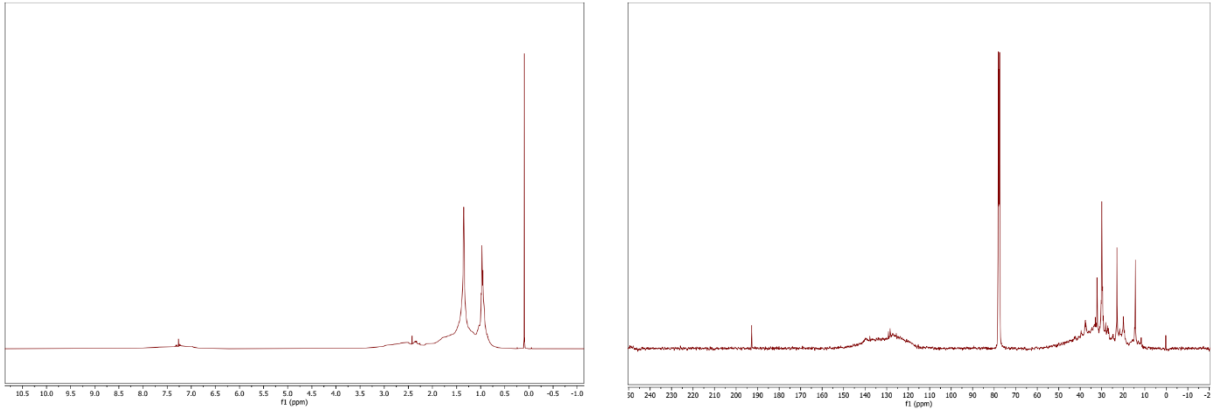
Figure C-34. ^{1}H and ^{13}C NMR spectra of maltenes and asphaltenes mixture thermally converted product after 47 minutes, respectively.
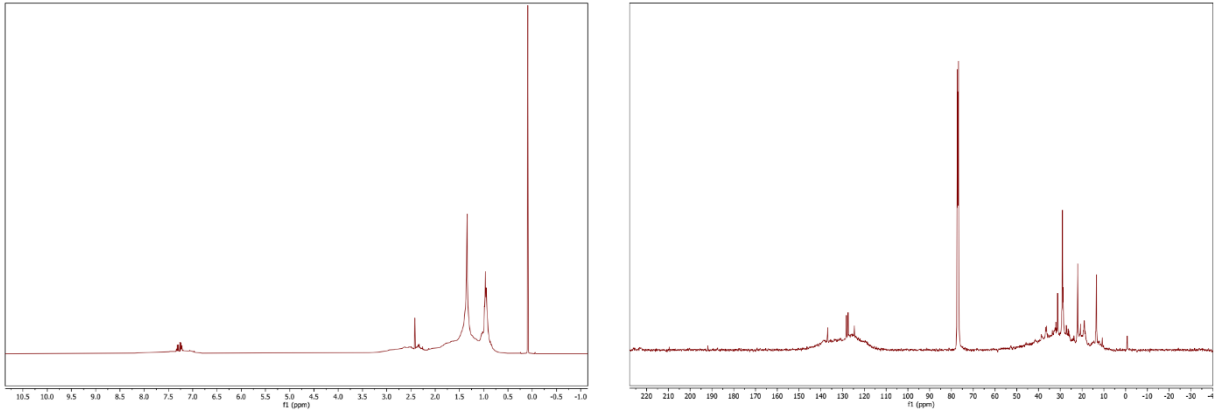
Figure C-35. ^{1}H and ^{13}C NMR spectra of maltenes and asphaltenes mixture thermally converted product after 146 minutes, respectively.
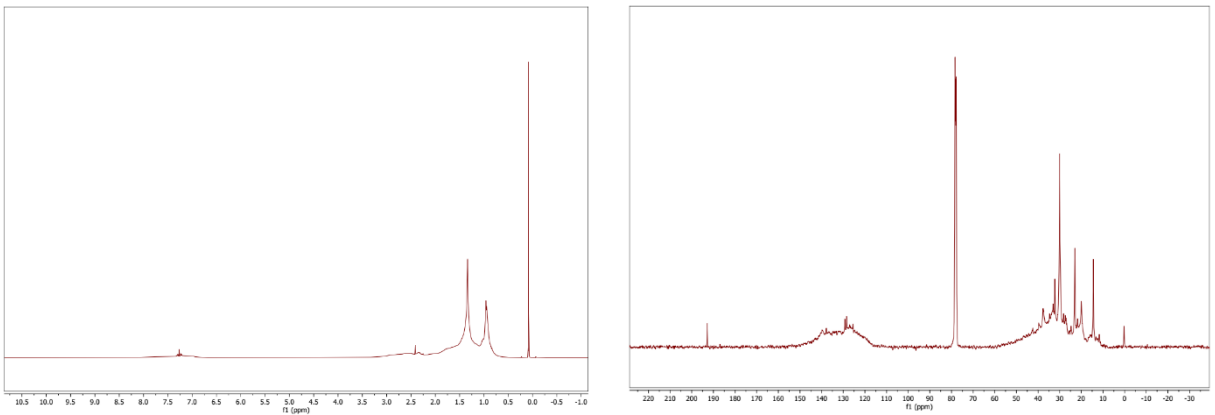
Figure C-36. ^{1}H and ^{13}C NMR spectra of bitumen thermally converted product after 0 minutes, respectively.
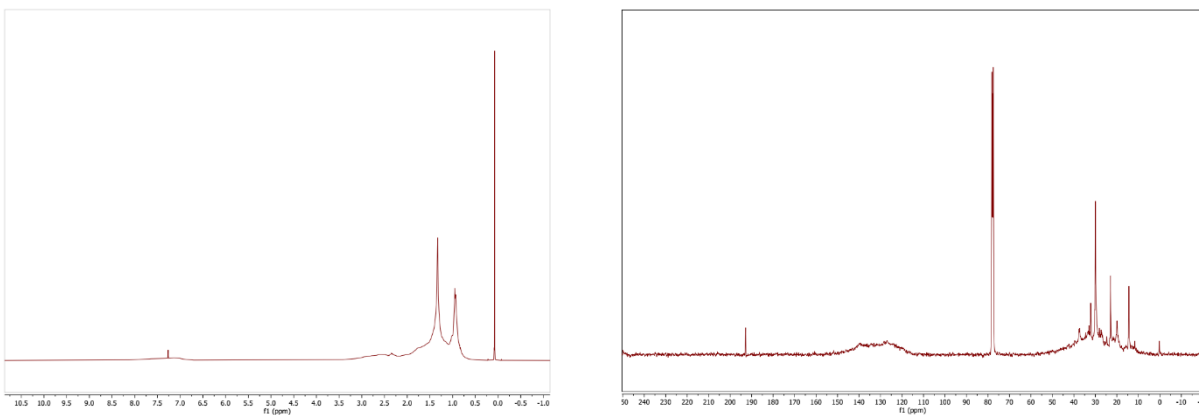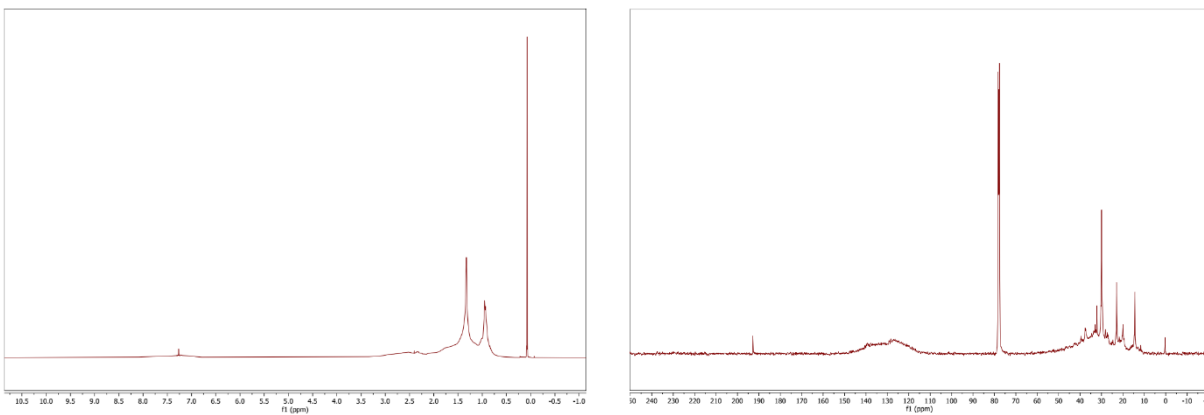
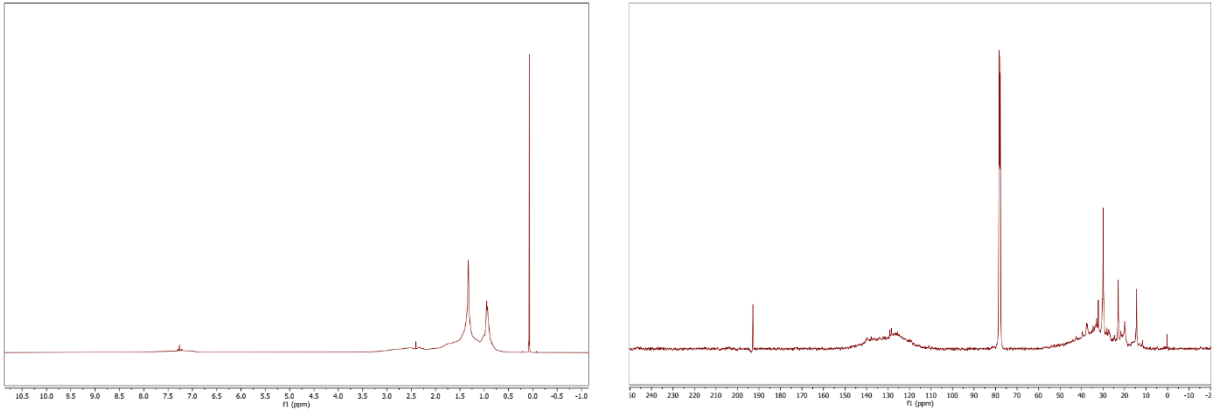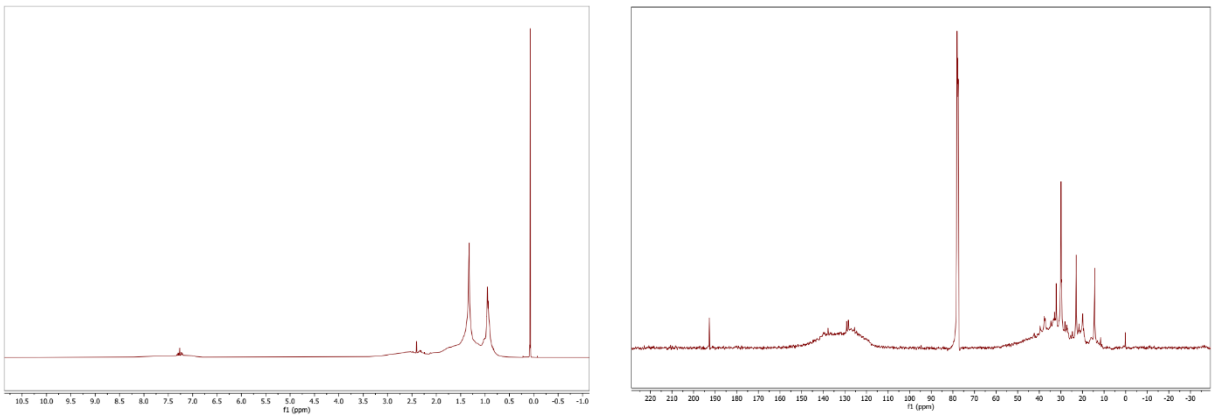**Figure C-37.** ^{1}H and ^{13}C NMR spectra of bitumen thermally converted product after 5 minutes, respectively.
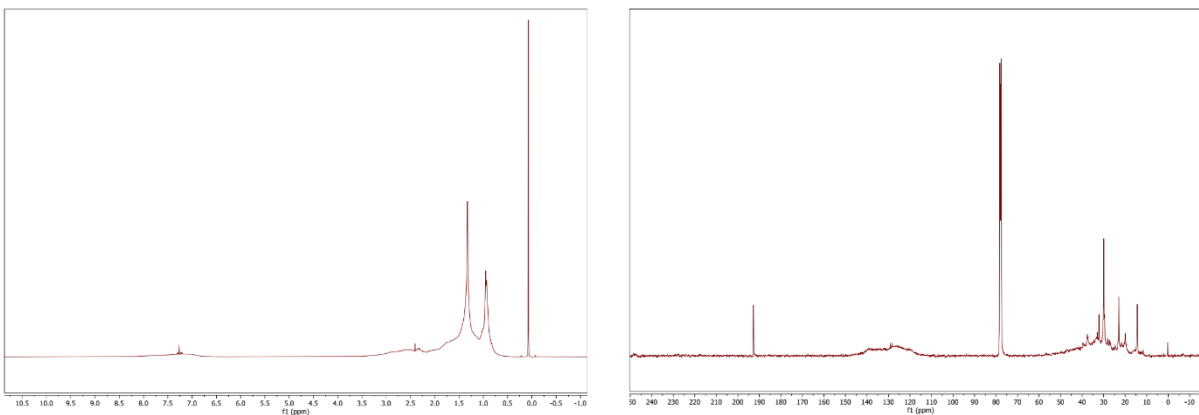
Figure C-38. ^{1}H and ^{13}C NMR spectra of bitumen thermally converted product after 10 minutes, respectively.

Figure C-39. ^{1}H and ^{13}C NMR spectra of bitumen thermally converted product after 47 minutes, respectively.

Figure C-40. ^{1}H and ^{13}C NMR spectra of bitumen thermally converted product after 146 minutes, respectively.

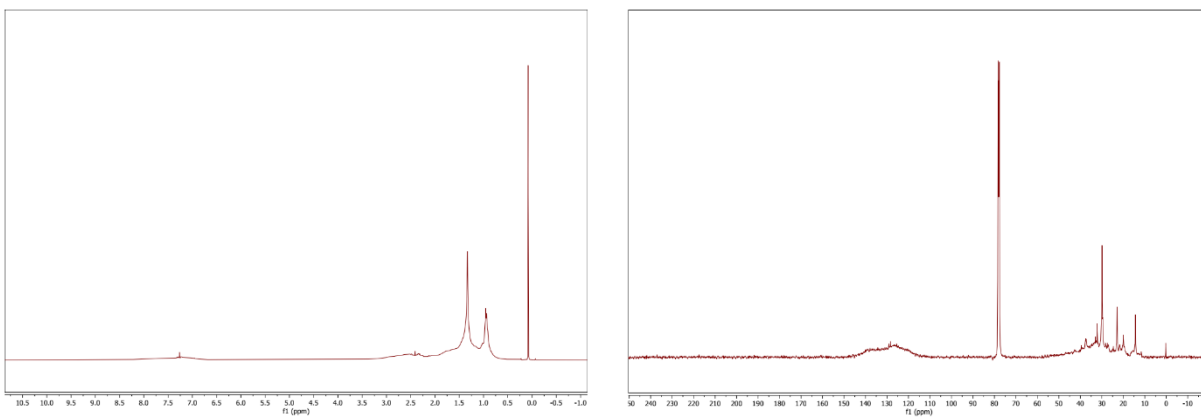**Figure C-41.** ^{1}H and ^{13}C NMR spectra of bitumen thermally converted product after 0 minutes, respectively.

Figure C-42. ^{1}H and ^{13}C NMR spectra of bitumen thermally converted product after 5 minutes, respectively.

Figure C-43. ^{1}H and ^{13}C NMR spectra of bitumen thermally converted product after 10 minutes, respectively.

Figure C-44. ^{1}H and ^{13}C NMR spectra of bitumen thermally converted product after 47 minutes, respectively.

Figure C-45. ^{1}H and ^{13}C NMR spectra of bitumen thermally converted product after 146 minutes, respectively.